Diss. ETH No 14429

Mantle evolution and magmatism in an evolving ocean-continent transition: The Platta nappe, eastern Switzerland

A dissertation submitted to the
Swiss Federal Institute of Technology Zurich

For the degree of
Doctor of natural sciences

Presented by

Laurent Desmurs
DEA UPMC-PARIS VI
Born November 1rst 1973
Citizen of France

Accepted on the recommendation of

Prof. Dr. D. Bernoulli	ETH Zürich	examiner
Prof. Dr. J. P. Burg	ETH Zürich	co-examiner
Prof. Dr. J. Girardeau	Univ. Nantes	co-examiner
Prof. Dr. U. Schaltegger	Univ. Geneva	co-examiner
Dr. G. Manatschal	Univ. Strasbourg	co-examiner
Dr. O. Müntener	Univ. Neuchatel	co-examiner

-2001-

Contents

Contents…….….I

Abstract……..…V

Résumé……...VII

Zusammenfassung……..….X

Chapter 1: Introduction

1.Evolution of the interpretation of the Alpine ophiolite.....….1

2. Geographic and tectonic overview.....2

3. Mesozoic evolution of the Ligurian Tethys passive margin.....4

4. Aims and organization of the thesis.....5

Chapter 2: The Steinmann Trinity revisited: Mantle exhumation and magmatism along an ancient ocean-continent transition: the Platta nappe, eastern Switzerland.

Abstract.....11

General situation.....13

The Platta nappe.....13
Alpine deformation.....14
Pre-Alpine situation and stratigraphy.....….....16

Mantle exhumation……17
Petrology and microstructure of the lower serpentinized peridotite.....18
Petrology and deformation of the upper serpentinized peridotite.....18
Mineral chemistry.....20
Retrograde metamorphism of mantle rocks.....21

Gabbroic Intrusion.....24
Field relationships.....24
Contact with mantle rocks.....25
Age.....25
Magmatic and deformational texture.....26
Mineral chemistry.....28
Condition of intrusion.....32
High-temperature deformation and hydration.....32

Low-temperature deformation.....33

Basalts and dolerites.....33
Discussion.....34
Mantle exhumation.....34
Gabbro intrusion and exhumation.....35
Basalt extrusion and related dykes.....35
Magmatic sources.....36
Timing of emplacement of different rock types.....36
Relationships between tectonic and magmatic processes.....37

Conclusion.....39

Chapter 3: Tectono-metamorphic and geochemical evolution of the mantle rocks of the Platta nappe.

1. Introduction.....49

2. Tectono-metamorphic evolution of the Platta mantle rocks.....50
2-1. Field relationships.....50
2-2. Petrography and microtexture.....53
2-3. Mineral chemistry.....57
2-4. Thermobarometry and mineral equilibria.....67
2-5. Discussion.....69

3. Chemical evolution of the Platta mantle rocks.....70
3-1. Whole rock chemistry.....71
3-2. Discussion.....77

4. Discussion.....79
4-1. Pre-rift location within the subcontinental mantle of the upper and lower serpentinite unit.....80
4.2. Rifting evolution of the upper and lower serpentinite unit.....81

5. Summary and conclusion.....82

Chapter 4: The Transition from rifting to sea-floor spreading within a magma-poor rifted margin: field and isotopic constraints

Abstract.....89

Introduction.....90

The geological framework.....92

U-Pb, Hf, Sr and Nd isotopic data.....93

Discussion.....94

Conclusion.....95

Chapter 5: Onset of magmatic accretion within a magma-poor rifted margin: A case study from the Platta ocean-continent transition, eastern Switzerland

Abstract.....99

Introduction.....100

Regional geology.....101

Gabbros.....103
Field relationships.....103
Petrography.....103
Mineral chemistry.....104
Whole rock composition.....109

Basalts and dolerites.....110
Field relationships.....110
Petrography.....111
Whole rock chemistry.....112

Discussion.....113
Primitive liquids in ocean-continent transition.....113
Gabbroic rocks: frozen liquids versus crystal fractionation.....115
Parental melts of the gabbros.....117
Modeling crystal fractionation.....117
Variation of degree and sources of melting.....118
Implication for magmatism in ocean-continent transitions.....119

Conclusions.....120

Chapter 6: Tectonic and magmatic evolution of the Jurassic Platta-ocean continent transition: summary and a conceptual model

1. Introduction.....125

2. Lithologies and structures in the Platta OCT.....125
2-1. Mantle rocks in the Platta OCT.....125

2-2. Chemistry, isotopes and age of the magmatic rocks in the Platta OCT..……...127
2-3. Extensional structures within the Platta OCT...…...……127
3. Tectonic model of Jurassic rifting……....128
3-1. Introduction..……128
3-2. A conceptual model for the transition from rifting to seafloor spreading……129
3-3. From mantle exhumation to seafloor spreading..……..……129
3-4. Mantle exhumation during rifting……130

4. Conclusions……..133

Appendix 1: Sample location……...…137

Appendix 2: Whole rock chemistry……139

Appendix 3: Curriculum Vitae……143

Abstract

The South-Pennine-Austroalpine boundary zone in the eastern Alps preserves the structural and petrological elements of an ancient ocean-continent transition (OCT). In this part of the Alpine nappe edifice, the lower Austroalpine Err nappe represents the distal, sediment-starved continental margin of the Adria plate. It consists of thinned continental crust, overlain by tilted blocks, slivers of shallow continental crust and pre-rift sediments, which were emplaced during the middle Jurassic along an oceanward-dipping low-angle detachment system. The nappe was thrust to the west and onto the underlying South-Pennine Platta nappe in late Cretaceous time. The Platta nappe represents a strip of transitional crust, formerly bordering the oceanic crust of the Liguria-Piemonte segment of the Tethyan ocean, and is the type-area of the Steinmann Trinity, the classical association of serpentinites, "variolithic" basalts and radiolarites. This classical "ophiolite" is distinguished from typical fast-spreading ridge associations by the scarcity of gabbroic rocks, the lack of a sheeted dike complex and the occurrence of continent-derived crustal blocks tectonically emplaced onto the exhumed mantle. In the Platta nappe, the "ophiolites" are preserved in two large thrust sheets, an upper and a lower serpentinite unit. Kinematic inversion of the alpine movement indicates that the upper serpentinite unit had an original position close to the distal margin whereas the lower one occurred nearer to the oceanic crust. Within both units the original geometrical and age relationships between mantle rocks, gabbroic intrusions, pillow lavas and oceanic sediments can be observed. Exhumed mantle rocks, extensional allochthons and pillow basalts are stratigraphically overlain by middle to upper Jurassic radiolarites. As temperatures never exceeded approximately 250°C during the Alpine orogeny, the pre-Alpine history of mantle deformation, gabbro intrusion and hydration during exhumation can be documented. The reconstruction of this OCT permits to track lithological and chemical changes of mantle and magmatic rocks along a profile from the distal margin towards the ocean and to describe the structural evolution of the OCT as a part of the evolution of the whole margin.

The mantle rocks preserved in the Platta nappe are serpentinized lherzolites preserving a high-temperature spinel foliation; because they are stratigraphically overlain by sediments, they must have been exhumed from the deep lithosphere to the sea floor. The mantle rocks of the upper serpentinite unit are spinel-lherzolite intruded by numerous garnet-pyroxenite dykes. They are characterized by a subsolidus temperature of equilibration (<800°C) at rather low pressure (7-12 kbars). These mantle rocks bear many similarities with those of the Malenco complex suggesting that they represent a shallow part of the subcontinental mantle, close to the pre-rift crust-mantle boundary. In contrast, the mantle rocks of the lower serpentinite do not contain any pyroxenite and show higher temperature of equilibration (>1000°C) in the plagioclase stability field. Geochemical investigations suggest that the mantle rocks of the lower serpentinite unit were impregnated by MORB-type melts after an earlier partial melting event, which probably started within the garnet stability field. Sm/Nd model ages suggest that these mantle rocks accreted the subcontinental mantle lithosphere during Permian times. These data indicate that the mantle rocks of the lower serpentinite unit represent deeper level of the pre-rift subcontinental mantle than the mantle rocks of the upper unit.

In contrast to their different high-temperature evolution, the mantle rocks of the upper and lower serpentinite unit have a similar evolution at lower temperatures. In both units, static hydration is documented in the mantle rocks by the growth of hornblende at the expense of pyroxene, which in turn was followed by further hydration at lower temperature as testified by the crystallization of tremolite. Serpentinization preceded or was contemporaneous with later deformation under decreasing temperatures. Low-temperature deformation produced serpentinite mylonites and tectonic breccias overprinting them, and was followed by the replacement of serpentinite minerals by calcite and the formation of breccias near or at the sea floor (ophicalcite). These tectono-sedimentary breccias form a more or less continuous layer along the surface of the serpentinites suggesting that these were brittlely deformed along extensional detachment faults. Extensional allochthons of continental crust locally overlying the serpentinites along gently inclined fault planes also demonstrate that final exhumation leading to exposure of the mantle rocks at the sea floor occurred along the low-angle detachment fault system cutting across the distal continental margin. Accordingly, the sense of shear found in the serpentinite mylonites is top-to-the-ocean as along the low-angle detachments. However, as this detachment system overprints upper crustal and mantle rocks exhumed from different level of the subcontinental mantle, it suggests that the different units were already juxtaposed during an extensional event prior to the activity of the detachment faults.

Magmatic rocks occur as basalts and dolerite in the upper and lower serpentinite unit. Gabbro intrusions are only observed in the lower serpentinite unit, which contains a larger volume of mafic rocks than the upper one. Gabbros form individual small intrusions ranging from olivine gabbros to apatite-rich ferrogabbros and diorites originating by fractional crystallization of the same parental magma. Field relationships, mineral-chemistry and U-Pb zircon age determinations show that they intruded already serpentinised mantle rocks at a shallow depth (< 8 km) 161 Ma ago. The gabbros were subsequently intruded by basaltic dikes, and finally exposed on the sea floor, as recorded by their occurrence as clasts in pillow- and sedimentary breccias stratigraphically overlying the exhumed mantle rocks. The microstructures in the gabbros indicate syn-magmatic deformation, followed by deformation under greenschist and lower temperature conditions during final exhumation. All gabbros show the same metamorphic evolution, i.e. intrusion at relatively low pressure, oceanic hydration at elevated temperature and a subsequent static oceanic alteration.

Chemical investigations of the gabbros and basalts indicate that they share similar parental melts, which are the products of low degree of melting (<10%) of two distinct sources. Magmatic rocks of the lower serpentinite unit have a typical N-MORB source as indicated by their REE concentration, Nd and Hf isotopic ratios determined on whole rock and zircons, respectively. In contrast, the REE concentrations of the basalts of the upper serpentinite unit indicate that they originated from a source enriched in incompatible elements. Our data show that magmatic rock from the Platta ocean-continent transition record increasing degrees of melting and decreasing contamination of their source by an enriched component as they crystallized oceanward. This process is probably related to the continuous thinning of the sub-continental mantle and the associated uplift of the underlying asthenosphere during a transitional stage between the crustal and the lithospheric break-up.

Our data show, that mantle and magmatic rocks of the transitional crust are related to different geodynamic processes. The serpentinites and associated ophicalcites document exhumation of sub-continental mantle and its exposure along the sea floor. It is characterized by the exhumation of deeper levels of the subcontinental mantle towards the ocean. Depending on their relative position in respect to the distal margin, the mantle rocks show a contrasting evolution during Mesozoic rifting. The mantle rocks exhumed close to the distal margin will record simply cooling and hydration whereas those exhumed in a more oceanward position will be impregnated by melts before subsequent cooling and hydration. Exhumation of the mantle rocks appears to occur in two different steps, first along continental-dipping shear zones juxtaposing the upper crust with shallow upper mantle rocks and those with deeper mantle rocks of the subcontinental lithosphere. In a second step, low angle detachment faults, affecting the distal Adriatic margin, with a possible concave downward geometry will lead to the final exhumation of the mantle rocks at the surface.
The final exhumation of the mantle rocks overlaps in time with intrusion and extrusion of MORB-type magmatic rocks reflecting the interplay between tectonic and magmatic processes in the transition from rifting to the evolution of a slow-spreading ridge. These magmatic rocks record the coeval thinning of the subcontinental mantle and rising of the asthenosphere, which will ultimately lead to the establishment of a spreading ridge system.

Résumé

Les éléments structuraux et pétrologiques d'une ancienne transition océan-continent (OCT) sont préservés à la limite des nappes pénninique du sud et des nappes austro-alpine dans les Alpes de l'est. Dans cette partie de l'édifice alpin, la nappe austro-alpine de l'Err représente la marge continentale distale de la plaque Adriatique. Cette nappe est constituée de croûte continentale amincie surmontée par des blocs basculés, des lentilles de croûte supérieure et de sédiments pré-rift, mises en place le long d'un système de détachement, faiblement penté en direction de l'océan. Cette nappe a chevauché vers l'ouest la nappe sud-pénninique de la Platta pendant la fin du Crétacé. La nappe de la Platta représente une partie de croûte transitionnelle originalement située à l'est de la croûte océanique du segment Piemont-Ligure de l'océan Téthysien. Elle contient les éléments types de la trinité de Steinmann, c'est à dire, l'association de serpentinites, de basaltes "variolithiques" et de radiolarites. Cette ophiolite classique se distingue des formations typiques des rides à expansion rapide par la rareté de roches gabbroiques, l'absence d'un complexe filonien et la présence de blocs de croûte continentale placés tectoniquement sur le manteau exhumé. Au sein de la nappe de la Platta, cette association ophiolitique est préservée dans deux larges écailles, les unités supérieure et inférieure des serpentinites. L'inversion cinématique des mouvements alpins indique que l'unité supérieure etait originellement située près de la marge distale, tandis que l'unité inférieure etait dans une position plus proche de la croûte océanique. Dans ces deux unités, les relations géométriques et chronologiques originales entre les roches mantélliques, les intrusions gabbroiques, les basaltes en coussins et les sédiments océaniques peuvent être observées. Comme la température n'a pas dépassé les 250°C durant l'orogenèse alpine, l'évolution pré-alpine de la déformation du manteau, de

l'intrusion des gabbros et de leur hydratation pendant leur exhumation peut être documentée. La reconstruction de OCT fossile permet de reconnaître les changements lithologiques et chimiques au sein des roches mantélliques et magmatiques le long d'un profil allant de la marge continentale distale en direction de l'océan et de décrire l'évolution structurale de l'OCT dans le contexte de l'évolution de la totalité de la marge Adriatique.

Les roches mantélliques de la nappe de la Platta sont majoritairement des lherzolites serpentinisées présentant une foliation à spinelle. Puisque ces roches sont stratigraphiquement recouvertes par des sédiments, elles ont du être exhumées de la lithosphere profonde sur le plancher océanique. Les roches mantélliques de l'unité supérieure des serpentinites sont des lherzolite à spinelle contenant de nombreux filons de pyroxenite à grenat. Elles se caractérisent par des températures d'équilibration sub-solidus (<800°C) sous des pressions plutôt faible (7-12 kbars). Ces roches mantélliques montrent de nombreux points communs avec celles du complexe de Malenco suggérant une position pré-rift superficielle au sein du manteau sous-continental, près de la limite croûte-manteau de la lithosphère continentale. Au contraire, les roches mantélliques de l'unité inférieures des serpentinites sont caractérisées par l'absence de pyroxenite et montrent des températures d'équilibration élevées (1000°C) dans le champ de stabilité du plagioclase. L'étude chimique de ces roches suggère que les lherzolites de cette unité ont été imprégné par des magmas de type MORB. Cette imprégnation postdate un événement de fusion partielle plus ancien, s'initiant probablement dans le champ de stabilité du spinelle. Des ages modèles Sm/Nd indiquent que ces roches mantélliques ont accrété le manteau lithosphérique sous-continental pendant le Permien. Ces données suggèrent que les lherzolites de l'unité inférieure des serpentinite représentent un niveau plus profond du manteau sous-continental que celles de l'unité supérieure. Ce niveau plus profond a été imprégné par des produits de fusions tholéiitiques lors de son exhumation sur le plancher océanique.

Contrairement à leur évolution à haute température très différente, les roches mantélliques des unités supérieure et inférieure ont une évolution similaire à des température plus basses. Dans les deux unités, l'hydratation des roches mantélliques est documentée par la croissance d'hornblende autour des clinopyroxènes, puis de tremolite autour des hornblendes. La serpentinisation précède ou est contemporaine d'une déformation tardive, active sous des températures décroissantes. Elle s'exprime par la formation de mylonites à serpentines et de brèches tectoniques et est suivie par la formation de brèche près du ou sur le plancher océanique (ophicalcites). Ces brèches tectono-sédimentaires forment un niveau plus ou moins continu à la surface des serpentinites suggérant une déformation fragile de leur surface par des failles de détachements extensives. La présence locale d'allochtones de croûte continentale surmontant les serpentinites le long de plans de faille légèrement inclinés démontre également que l'exhumation finale des roches mantélliques et leur exposition sur le plancher océanique s'est fait par le système de détachement affectant la marge continentale distale. En revanche, comme ce système extensif affecte des roches de la croûte continentale supérieure et de différents niveaux du manteau sous-continental, la juxtaposition de ces différentes unités a du avoir lieu lors d'un événement extensif plus ancien.

Les roches magmatiques se présentent sous la forme de basaltes et de dolérites dans les deux unités de serpentinites. Les intrusions de gabbros sont observées uniquement dans l'unité inférieure des serpentinites qui contient un volume de roches magmatiques plus important que l'unité supérieure. Les gabbros forment des affleurements isolés les uns des autres et leur composition va de Mg-gabbros à des ferrogabbros riches en apatites et des diorites qui se sont formés par cristallisation fractionnée d'un même magma. Les relations de terrain, la chimie des minéraux et les datations de zircons par la méthode U-Pb montrent que ces gabbros ont cristallisé à faible profondeur au sein d'un manteau déjà serpentinisé, il y a 161 Ma. Localement ces gabbros ont été recoupés par des filons de basaltes puis exposés sur le plancher océanique comme le prouve leur présence sous forme de clastes dans des brèches sédimentaires et basaltiques. Les microstructures observées dans les gabbros montrent des évidences pour une déformation syn-magmatique puis sous les conditions du faciès du schiste vert puis à température plus basse durant leur exhumation finale. Tous les gabbros montrent une évolution métamorphique commune, c'est-à-dire, une intrusion à basse pression suivie d'une hydratation à hautes températures suivie d'une altération océanique.

L'étude de la composition chimique des gabbros et de basaltes montrent qu'ils proviennent de la cristallisation de magmas parents similaires qui sont les produits de faibles taux de fusion (<10%) de deux sources distinctes. La composition en terres rares ainsi que les rapports isotopiques du Nd et de l'Hf des basaltes et gabbros de l'unité inférieure des serpentinites indiquent que leur source est un manteau appauvri similaire à ceux des N-MORB. Au contraire, la composition en terres rares des basaltes et dolérites de l'unité supérieure des serpentinites montre une source enrichie en éléments incompatibles. Ces données montrent que les roches magmatiques de l'OCT de la Platta enregistrent des taux de fusion plus important d'une source de moins en moins contaminée par une composante enrichie au fur et à mesure qu'ils cristallisent en direction de l'océan. Ce processus est probablement lié à l'amincissement continuel du manteau sous-continental associé à l'ascension de l'asthénosphère durant une phase transitionnelle entre la déchirure de la croûte continentale et celle de la lithosphère continentale.

Nos données montrent que les roches mantélliques et magmatiques de la nappe de la Platta sont liées à deux processus différents. Les serpentinites et ophicalcites documentent l'exhumation du manteau sous-continental et son exposition sur le plancher océanique. Cette exhumation se caractérise par l'exposition de niveau plus profond du manteau sous-continental en direction de l'océan. Les niveaux peu profonds du manteau sous-continental, exposés à proximité de la marge continentale distale, sont simplement hydratés et refroidis pendant leur exhumation alors que les niveaux plus profond, exposé dans une position plus océanique, sont imprégnés par des magmas durant leur exhumation avant d'être hydraté et refroidis. L'exhumation du manteau sous continental semble s'effectuer en deux phases. D'abord le long de zone de cisaillement extensive, pentées vers le continent qui juxtaposent la croûte continentale supérieure et le manteau sous-continental, qui sera exposé sur le plancher océanique lors d'une seconde phase caractérisé par l'activité de faille de détachement à faible pendage affectant la marge continentale distale. Pour etre en mesure d'exposer des parties profondes de la lithosphère, il est proposé que ces failles tardives aient une géométrie concave vers le bas.

L'exhumation finale du manteau sous-continental se superpose dans le temps à l'intrusion et l'extrusion de roches magmatiques de type MORB. Cela reflète l'interaction des processus tectoniques et magmatiques durant la transition entre l'amincissement de la lithosphère continentale et l'évolution vers un système d'expansion océanique. L'amincissement du manteau sous-continental associé a l'ascension simultanée de l'asthénosphère amènera finalement à l'établissement d'un système d'expansion océanique.

Zusammenfassung

Die Südpenninische-Austroalpine Grenzzone in den östlichen Alpen konserviert die strukturellen und petrologischen Elemente eines alten Ozean-Kontinent Überganges (OKT). In diesem Teil des alpinen Deckenbaus stellt die untere Austroalpine Err-Decke den distalen, an Sedimenten verarmten Kontinentalrand der adriatischen Platte dar. Sie besteht aus verdünnter kontinentaler Kruste, überlagert durch gekippte Blöcke, Splitter der flachen kontinentalen Kruste und Prärift-Sedimente, die während des mittleren Jura entlang einem ozeanwärts einfallenden flach-winkligen Abschiebungs-Systems („low-angle detachment"-System) plaziert wurden. Während der späten Kreide wurde die Decke gegen Westen und auf die darunterliegende südpenninische Platta-Decke überschoben. Die Platta-Decke stellt einen Streifen der Übergangskruste dar, der früher die ozeanische Kruste des Liguria-Piemont Segments der Tethys begrenzt hat. Es ist die Typlokalität der Steinmann Trinität, der klassischen Verbindung von Serpentiniten, „variolithischer" Basalte und Radiolarite. Dieser klassische „Ophiolith" unterscheidet sich von den typischen „fast-spreading ridge"-Assoziationen durch die Seltenheit der gabbroiden Gesteine, das Fehlen von einem „sheeted dike"-Komplex und das Auftreten der vom Kontinent stammenden krustalen Blöcke, die tektonisch auf dem exhumierten Mantel liegen. In der Platta-Decke werden die „Ophiolithe" in zwei großen Überschiebungsdecken konserviert: in einer oberen und einer unteren Serpentinit-Einheit. Die kinematische Inversion der alpinen Bewegung zeigt an, daß die obere Serpentinit-Einheit eine Ausgangsstellung nah am distalen Kontinentalrand hatte, während die untere Serpentinit-Einheit näher zur ozeanischen Kruste auftrat. Innerhalb der Einheiten können die ursprünglichen geometrischen Beziehungen und Altersverhältnisse zwischen Mantel, gabbroider Intrusionen, Kissenlavas und ozeanischer Sedimente beobachtet werden. Exhumierter Mantel, extensionale Allochthone und Kissenbasalte werden stratigraphisch durch Radiolarite des mittleren bis oberen Jura überlagert. Da die Temperaturen während der alpinen Orogenese nie ca. 250°C überstiegen, kann die prä-alpine Geschichte der Manteldeformation, die Intrusion der Gabbros und die Hydratation während der Exhumation dokumentiert werden. Die Rekonstruktion von diesem OKT ermöglicht es, die lithologischen und chemischen Umwandlungen des Mantels und der magmatischen Gesteine entlang einem Profil vom distalen Kontinentalrand in Richtung Ozean zu verfolgen und die strukturelle Entwicklung des OKT als Teil der Entwicklung eines vollständigen Kontinentalrandes zu beschreiben.

Die Mantelgesteine, die in der Platta-Decke konserviert sind, sind serpentinisierte Lherzolithe mit einer konservierten Hochtemperatur-Spinell-Foliation. Da sie stratigraphisch durch Sedimente überlagert werden, müssen sie von der tiefen Lithosphäre zum Meeresgrund exhumiert worden sein. Der Mantel der oberen

Serpentinit-Einheit ist ein Spinell-Lherzolith, der von zahlreichen Granat-Pyroxenit-Gängen intrudiert wurde. Das Equilibrium in den Mantelgesteinen wird durch eine Subsolidustemperatur (< 800°C) unter ziemlich niedrigen Druck gekennzeichnet (7-12 kbar). Sie weisen viele Ähnlichkeiten mit denen des Malenco-Komplexes auf und lassen darauf schließen, daß sie einen flachen Teil des subkontinentalen Mantels darstellen, der nah an der Prä-rift Kruste-Mantel-Grenze war. Demgegenüber enthalten die Mantelgesteine der unteren Serpentinite keine Pyroxenite und zeigen im Equilibrium eine höhere Temperatur (> 1000°C) im Plagioklas Stabilitätsfeld an. Geochemische Untersuchungen lassen darauf schließen, daß die Gesteine der unteren Serpentinit-Einheit nach einer früheren Teilaufschmelzung durch MORB-artige Schmelzen imprägniert wurden. Diese Imprägnation begann vermutlich innerhalb des Stabilitätsfeldes von Granat. Sm/Nd Modellalter deuten darauf hin, daß diese Mantelgesteine während des Perms an die subkontinentale Mantellithosphäre angeschweißt wurden. Diese Daten zeigen, daß die Mantelgesteine der unteren Serpentinit-Einheit tiefere Bereiche des prä-rift subkontinentalen Mantels darstellen als die Mantelgesteine der oberen Einheit.

Im Gegensatz zu ihrer unterschiedlichen Hochtemperaturentwicklung haben die Mantelgesteine der oberen und unteren Serpentinit-Einheit eine ähnliche Entwicklung bei niedrigeren Temperaturen. In beiden Einheiten wird die statische Hydratation in den Mantelgesteinen durch das Wachstum von Hornblende auf Kosten von Pyroxen dokumentiert, die von der weiteren Hydratation bei niedrigeren Temperaturen gefolgt wurde, wie durch die Kristallisation von Tremolit belegt ist. Die Serpentinisation erfolgte vor der späteren Deformation unter abnehmenden Temperaturen oder gleichzeitig. Die Niedrigtemperaturdeformation produzierte Serpentinitmylonite und diese überprägende tektonische Breccien. Nachfolgend wurden die Serpentinitminerale durch Kalzit ersetzt und es bildeten sich Breccien nahe oder am Meeresgrund (Ophikalzite). Diese tektono-sedimentären Breccien bilden eine mehr oder weniger ununterbrochene Schicht entlang der Oberfläche der Serpentinite. Dies deutet darauf hin, daß diese Breccien sich spröd entlang von extensionalen Störungen geformt haben. Die extensionalen Allochthone der kontinentalen Kruste überlagern lokal Serpentinite entlang leicht geneigten Störungsflächen. Daraus folgt, daß die zur Freilegung des Mantels führende abschließende Exhumation am Meeresgrund entlang dem über den distalen Kontinentalrand schneidende “low-angle detachment”-System auftrat. Dementsprechend spiegelt der Schersinn, den die Serpentinitmylonite anzeigen, eine Top zu Ozean Bewegungsrichtung entlang dem „low-angle detachment”-System wider. Dieses „low-angle detachment”-System überprägt jedoch die obere Krusten- und Mantelgesteine, die von den unterschiedlichen Bereiche des subkontinentalen Mantels exhumiert wurden. Folglich wurden die unterschiedlichen Einheiten bereits während einer extensionalen Phase vor der Aktivität des „low-angle detachment”-Systems nebeneinander gebracht.

Magmatische Gesteine treten als Basalte und Dolerite in der oberen und unteren Serpentinit-Einheit auf. Intrusionen von Gabbros werden nur in der unteren Serpentinit-Einheit beobachtet, die ein größeres Volumen an mafischen Gesteinen aufweist als die obere Einheit. Die Gabbros bilden einzelne kleine Intrusionen, die von Olivingabbros zu apatit-reichen Ferrogabbros und Dioriten reichen. Sie sind durch fraktionale Kristallisation der gleichen ursprünglichen Magmen entstanden. Geländebeziehungen, Mineral-Chemie und die Ermittlung von U-Pb Zirkonalter zeigen, daß sie in bereits

serpentinisierte Mantelgesteine in einer geringen Tiefe (< 8 Kilometer) vor 161 Ma intrudiert sind. Die Gabbros wurden nachfolgend von Basaltgängen geschnitten und schließlich am Meeresgrund freigelegt, wie ihr Vorkommen als Klasten in Breccien aus Kissenlavas und Sedimenten, die den exhumierten Mantel stratigraphisch überlagern, belegt. Die Mikrostrukturen in den Gabbros zeigen eine syn-magmatische Deformation an, gefolgt von einer Deformation unter grünschiefer-faziellen Bedingungen und niedrigeren Temperaturen während der abschließenden Exhumation. Alle untersuchten Gabbros zeigen die gleiche metamorphe Entwicklung, d.h. Intrusion unter verhältnismäßigen niedrigen Druck, ozeanische Hydratation bei erhöhten Temperaturen und einer nachfolgenden statischen ozeanischen Alteration.

Chemische Untersuchungen der Gabbros und der Basalte zeigen an, daß sie ähnliche ursprüngliche Schmelzen teilen, die das Produkt eines niedrigen Grads von Aufschmelzung (< 10%) zweier eindeutiger Quellen sind. Die magmatischen Gesteine der unteren Serpentinit-Einheit haben eine typische N-MORB Quelle, wie durch ihre REE-Konzentration und Nd- und Hf-Isotopischenverhältnisse aus Gesamtgesteinsanalysen beziehungsweise Zirkonanalysen nachgewiesen wird. Demgegenüber zeigen die REE-Konzentrationen der Basalte der oberen Serpentinit-Einheit an, daß sie von einer Quelle stammen, die an inkompatiblen Elementen angereichert wurde. Wie unsere Daten zeigen, haben die magmatische Gesteine vom Platta Ozean-Kontinent-Übergang einen zunehmenden Grad der Aufschmelzung und eine abnehmende Kontamination ihrer Quelle durch eine angereicherte Komponente, wie sie ozeanwärts kristallisierte, erfahren. Dieser Prozeß hängt vermutlich mit der ununterbrochenen Ausdünnung des subkontinentalen Mantels und der dazugehörigen Aufwölbung der darunterliegenden Asthenosphäre während eines Übergangsstadiums zwischen dem krustalen und lithosphärischen Aufbrechens zusammen.

Unsere Daten belegen, daß der Mantel und die magmatische Gesteine der Übergangskruste mit unterschiedlichen geodynamischen Prozessen zusammenhängen. Die Serpentinite und die dazugehörigen Ophikalzite dokumentieren die Exhumation des subkontinentalen Mantels und seine Freilegung am Meeresgrund. Dieser Prozess wird durch die Exhumation der tieferen Bereiche des subkontinentalen Mantels in Richtung zum Ozeanboden gekennzeichnet. Abhängig von ihrer relativen Position in bezug auf den distalen Kontinentalrand, zeigen die Mantelgesteine eine unterschiedliche Entwicklung während des mesozoischen Riftings. Die exhumierten Mantelgesteine nah am distalen Kontinentalrand überliefern einfach Abkühlung und Hydratation, während die mehr ozeanwärts exhumierten Mantelgesteine zuerst durch Schmelzen imprägniert wurden und dann erst Abkühlung und Hydratation folgte. Die Exhumation der Mantelgesteine scheint daher in zwei unterschiedlichen Schritten abzulaufen: 1) entlang den zum Kontinent einfallenden Scherzonen, welche die obere Kruste mit flachen oberen Mantelgestein mit den tieferen Mantelgesteinen der subkontinentalen Lithosphäre nebeneinander bringt und 2) der abschließenden Exhumation der Mantelgesteine an die Oberfläche entlang dem möglicherweise konkav-abwärts „low-angle detachment", das den distalen adriatischen Kontinentalrand beeinflußt.

Die abschließende Exhumation der Mantelgesteine überlappt zeitlich mit der Intrusion und der Extrusion von MORB-artigen magmatischen Gesteinen und spiegelt die Wechselwirkung zwischen tektonischen und magmatischen Prozessen im Übergang vom

Rifting hin zur Entwicklung eines „slow-spreading ridge“ wider. Die magmatischen Gesteine überliefern das gleichzeitige Ausdünnen des subkontinentalen Mantels und die Aufwölbung der Asthenosphäre, die schließlich zur Schaffung eines „spreading ridge“-Systems führt.

Chapter 1-Introduction

1. Evolution of the interpretation of the Alpine ophiolites

In 1905 Gustav Steinmann noted the close association of serpentinite, "diabase", and radiolarite and considered this "green rock" or ophiolitic association as characteristic for the axial part of the "geosyncline" and the deep ocean floor. Although Steinmann considered diabase, spilite and variolite (variolitic pillow lavas) as intrusive rocks distinctly younger than the associated sediments, he stressed their characteristic association with deep-sea sediments, notably radiolarian cherts but also deep-water limestones of Maiolica facies (Steinmann 1925, 1927). In his view, the "consanguineous" association of ultramafic and mafic material was characteristic for sub-oceanic environments from where these magmas ascended during folding of the oceanic sediments. A similar view was held by Argand (1911, 1916, his Fig. 1), and Staub (1922, 1924) who interpreted the ophiolites as intruded during the early phases of Alpine "folding". Staub (1922) stressed their occurrences in the "nappe synclines" in the back of the crystalline nappes of Adula, Suretta, and Margna, which seemed to him to confirm their intrusion into the "Bündnerschiefer" sequences "along the foredeeps of the embryonic nappes". Today we associate these ophiolite occurrences with the scarce ophiolites of the Valais basin (Misox zone, ex-Adula), the Avers (ex-Suretta), and the Platta nappe (ex-Margna).

Staub (1922) considered the serpentinites as resulting from the metamorphism of intrusive peridotites, however, many authors believed the serpentinites to be derived from "a hydrous ultrabasic magma" (Hess 1938), intruded during the early phases of orogeny (Hess 1955) or to represent even "serpentine lavas" (Bailey and McCallien 1950, 1953). Although Bowen (1927, 1928) experimentally demonstrated "that such magmas are not possible", most authors weighted the field evidence in favor of an intrusive or even extrusive origin of the serpentinites. In order to overcome the theoretical difficulties, other authors invoked solid-state intrusion of the peridotites (e.g. Peters & Niggli 1964).

With the advent of plate tectonics, the term ophiolite was redefined. A new concept of a stratified oceanic lithosphere was introduced, deduced from seismic refraction studies performed in present-day oceans (Raitt, 1963), and from observation in large ophiolitic complexes like Troodos (Moores & Vine 1971) or Semail (Glennie *et al.* 1974). This stratigraphy was codified during a Penrose Conference in 1972 (Anonymous 1972) in a four-layer model matching the geophysical structure of the oceanic lithosphere. According to this model, a completely developed ophiolite should be composed of the following stratigraphic terms (from top to bottom): the sedimentary cover (Layer 1) overlying a mafic volcanic complex, commonly pillowed, which together with the underlying sheeted dike complex represents the geophysical Layer 2 (1-2 km). Below this basaltic complex, a gabbroic complex occurs down to the Moho (Layer 3) overlying an ultramafic complex corresponding to the oceanic lithospheric mantle. This concept implies that ophiolites in Alpine-type mountain belts are part of oceanic basement nappes or of tectonic melanges associated with subduction complexes (e.g. Laubscher 1969; Dewey and Bird 1970).

Over the years, detailed fieldwork showed that the stratigraphy of the ophiolites of the Alps, and the Apennines did not match the classical ophiolite stratigraphy as defined by the Penrose Conference in 1972. No substantial relics of a sheeted dike complex were found, and gabbros appeared to play a subordinate role. Instead, oceanic sediments, radiolarian cherts, and pelagic limestones, were observed to

stratigraphically overlie (1) serpentinized mantle rocks, and tectono-sedimentary breccias ("ophicalcites") derived from them, and (2) pillow lavas which were extruded onto the serpentinites previously exposed along the ocean floor (Decandia & Elter 1972; Lagabrielle *et al.* 1984; Bernoulli & Weissert 1985; Weissert & Bernoulli 1985).

In the Alps, this peculiar stratigraphy indicating exposure of mantle rocks at the sea floor was, at an early stage, postulated to be associated with oceanic transform faults (Lemoine 1980; Bernoulli & Weissert 1985; Weissert & Bernoulli 1985) in analogy with serpentinite occurrences along such faults in present-day oceans (Bonnati *et al.* 1980). However, the data now available from the south-Pennine-Austroalpine margin suggest that in this area subcontinental mantle (Hermann *et al.* 1997; Müntener *et al.* 2000; for the Voltri Group see Rampone *et al.* 1998) was exhumed at the sea floor. Froitzheim & Manatschal (1996), and Manatschal & Nievergelt (1997) proposed that mantle rocks were exhumed by low-angle extensional detachment faults. Such an interpretation was first proposed by Lemoine *et al.* (1987) for the western Alps, however, their reasoning was based on circumstantial evidence, and analogies to the Iberian margin. Indeed, exhumation of mantle rocks, and their exposure at the sea floor is now well documented along undeformed, magma-poor margins where it occurred during the final stage of rifting and break-up of the continental crust (Boillot *et al.* 1987, 1988). However, it has been shown that mantle rocks can also be exhumed at the sea floor along slow-spreading ridges such as the mid-Atlantic ridge (e.g. Juteau *et al.* 1989) or along transform faults (Bonatti E. 1976). The question therefore arises whether the association of serpentinites, gabbros, and pillow lavas observed in the Platta nappe are part of an ocean-continent transition or represent oceanic lithosphere produced along a slow-spreading ridge as proposed by Lagabrielle & Lemoine (1997) for the ophiolites of the western Alps.

In any case, it appears today that the trinity of serpentinites, pillow lavas, and radiolarites Steinmann (1905, 1927) described from the Alps, and the Apennines corresponds, by and large, to the stratigraphy of ocean-continent transition, as observed along magma-poor continental margins (Manatschal & Bernoulli 1999) laterally grading into oceanic crust generated along a slow-spreading ridge (Lagabrielle & Lemoine 1997).

2. Geographic and tectonic overview

In the Alps, remnants of an ophiolitic suture can be traced along a discontinuous belt along the entire length of the chain from Corsica, and the Ligurian Apennines along the south-Pennine nappes to the eastern end of the Alps, and possibly beyond (Fig. 1-1). Most of these ophiolites (including the Platta nappe) belong to the Liguria-Piedmont segment of the Mesozoic Tethys ocean, which was eliminated by subduction and obduction during the late Cretaceous, and early Tertiary. Relics of this ophiolite zone can be followed from Val Malenco (Malenco complex) across the Engadin valley to the Sursés valley (Platta nappe), and across a number of imbricates (Arosa zone including the Totalp slice) to the northern margin of the Northern Calcareous Alps (Fig. 1-2). They occur between units derived from the European and Briançonnais margin, a possible promontory of Iberia (Stampfli 1993), below, and units derived from the Adriatic margin (Austroalpine) above.

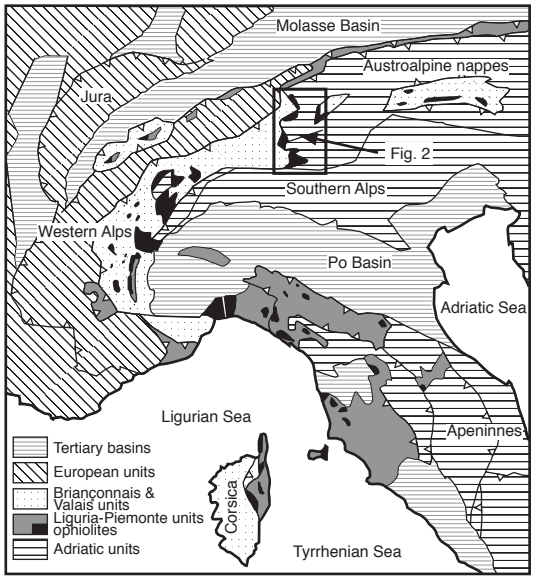

Figure 1.1: Liguria-Piemonte oceanic domain of the Alpine Tethys from Corsica to Platta.

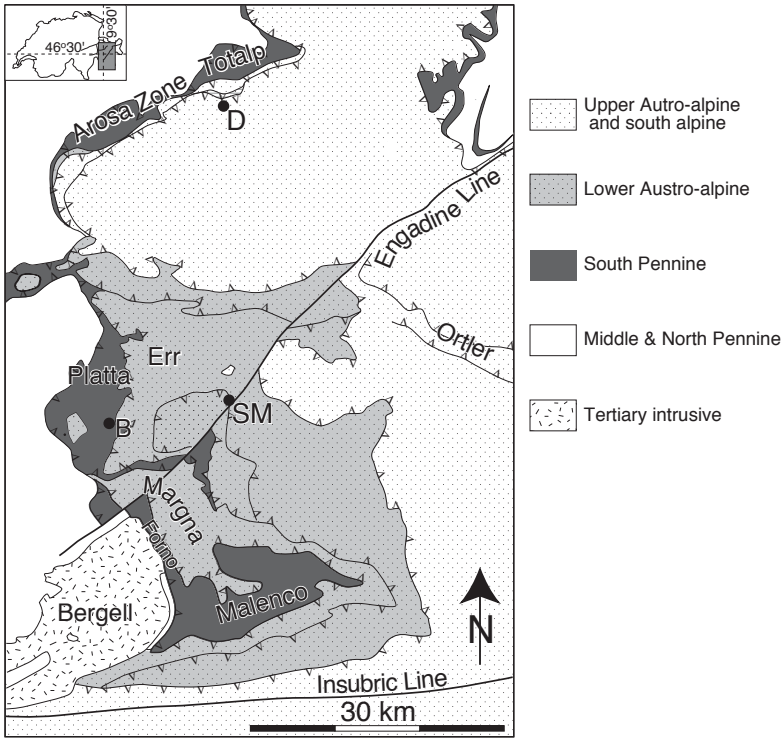

Figure 1-2: Simplified geological map and location of the study area. Bivio; D: Davos; B: SM: St. Moritz. Modified after Froitzheim et al. (1994).

Although the contact between the overlying Austroalpine units and the ophiolitic nappes is tectonised and the Alpine structures are more complicated in the ophiolites, recent investigations suggest that both continental and ophiolitic nappes derive from the same margin and show the same Alpine tectonic evolution. This is mainly supported by the same post-rift sedimentary evolution, the comparable Alpine and pre-Alpine tectonic evolution and the similar metamorphic overprint (Dietrich 1970, Trümpy 1975, Manatschal and Nievergelt 1997, Ferreiro-Mählmann 2001). In particular the lack of high-pressure metamorphism in the Platta and other ophiolites in eastern Switzerland supports the idea that these ophiolites belonged, together with the

Austroalpine units, to the upper plate beneath which the rest of the Liguria-Piemonte ocean and its distal European margin were subducted. The "relatively" simple Alpine tectonic situation allowed for a reconstruction of the former OCT (Manatschal & Nievergelt 1997). A more detailed reconstruction of the OCT preserved in the Platta nappe is presented for the first time in this work.

3. Mesozoic evolution of the Ligurian Tethys passive margin

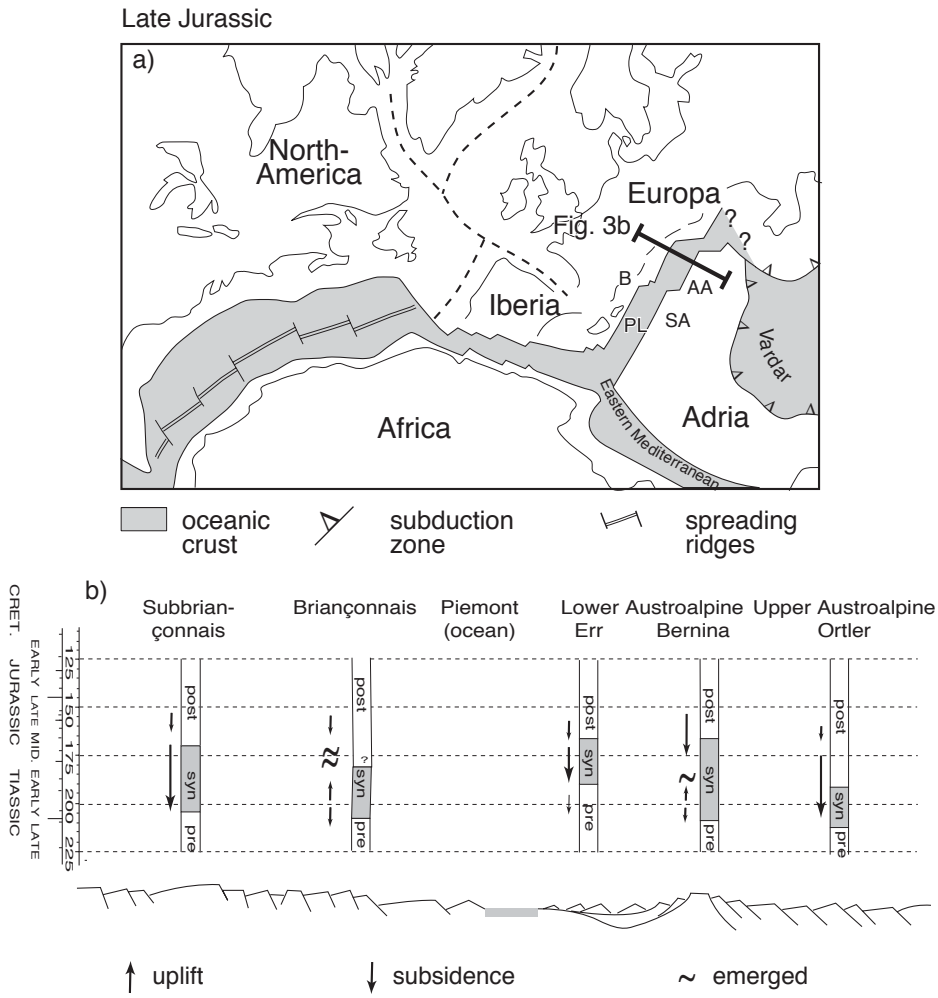

Figure 1-3: a) Paleogeographic reconstruction of the central Atlantic-Tethys ocean during Late Jurassic times. AA: Austroalpine; B: Briançonnais; LP: Liguria-Piemonte ocean; SA: Southern Alps. b) Subsidence history accompanying Mesozoic rifting and stratigraphic evolution of the pre-, syn- and post-rift sediments along the Alpine Tethyan margin. From Manatschal & Bernoulli (1998)

During Triassic times, shallow-water carbonate sedimentation prevailed along the evolving conjugate margins of the Liguria-Piedmont ocean (Briançonnais to the west, Austroalpine to the east). Highly subsiding basins formed in the proximal parts of the future passive margins (Briançonnais and upper Austroalpine domains Fig. 1-3b) during Late Triassic-Early Jurassic time, recording a first phase of rifting. During that time, the future distal Adriatic margin (Err domain) was not much affected by normal faulting. Rifting shifted to, and localized in the future distal margin (Err-domain) after Pliensbachian time. In this latest stage of rifting, the Austroalpine Bernina domain, separating the proximal, and the distal parts of the margin was uplifted. Now, extension was no longer accommodated by listric faults soling in the middle crust but

by a large-scale detachment system forming a break-away in the western Bernina zone, and dipping westward, towards the future ocean (Manatschal & Bernoulli 1999). Extension along this system of detachment faults eventually led to the final break-up of the continental crust, and the exposure of the sub-continental mantle at the sea floor. Emplacement of extensional allochthones onto the exhumed mantle rocks of the Platta nappe occurred at that time before the deposition of the middle-late Jurassic post-rift sediments, and the onset of sea-floor spreading.

4 Aims and organization of the thesis

Studies of ophiolites are commonly disconnected from that of the adjacent continental margin. This is mainly related to the fact that ophiolites do not preserve their primary contacts to continental units. Mapping in the Err and Platta nappes allowed to trace tectonic and stratigraphic elements from the continental Err nappe into the ophiolitic Platta nappe and a structural analysis of the Err-Platta nappes permits to propose a kinematic inversion of these nappes leading to a palinspastic reconstruction of the former ocean-continent transition (Fig. 1-4). Most of the "complicated" structures found in the Platta nappe turned out to be related to primary lateral thickness variations of oceanic basalt flows, pre-existing oceanic high-angle faults or the occurrence of extensional allochthones overlying detachment faults within the former OCT (Manatschal and Nievergelt 1997 and this work). A major result of the thesis is that it is possible to distinguish between two major serpentinite thrust sheets, an upper serpentinite unit and a lower serpentinite unit (Fig. 1-4a). Whereas the upper serpentinite unit is in a higher Alpine tectonic position and was originally located more continentwards, the lower serpentinite unit is in a deeper Alpine tectonic position and sampled portions of the OCT originally nearer to the future ocean (Fig. 1-4b). This discovery allows for the first time to study an ophiolite in terms of its position in a rifted margin and to track changes within mantle and igneous rocks in a profile from the continent towards the ocean. This makes the Platta nappe a suitable area for documenting processes related to the transition from continental rifting to exhumation of sub-continental mantle, break-up of the continental lithosphere and establishment of a slow-spreading system.

The thesis is subdivided into six chapters (including this introduction), which are in the form of three publications in press or submitted to international journals. In the second chapter, the field relationships between mantle rocks, gabbros, and basalts are presented, and the metamorphic retrograde evolution related to the exhumation of the mantle rocks, and the gabbros is described. The third chapter focuses on the tectono-metamorphic and chemical evolution of the mantle rocks in order to document their respective sub-continental origin and their evolution during rifting. The fourth chapter deals with the isotope geochemistry of the magmatic rocks including U/Pb dating of the gabbros, and the Sm/Nd ratios of the gabbros, and basalts, which characterize the sources of these magmatic rocks. In the fifth chapter, the geochemistry (major, and trace elements) of the gabbros is documented in order to reconstruct the differentiation processes, and to determine the parental melts of the gabbros and basalts. The final chapter gives a summary, and proposes a model for the tectonic and magmatic evolution of the Platta ocean-continent transition from continental rifting to the final break-up of the continental lithosphere and establishment of a slow-spreading system.

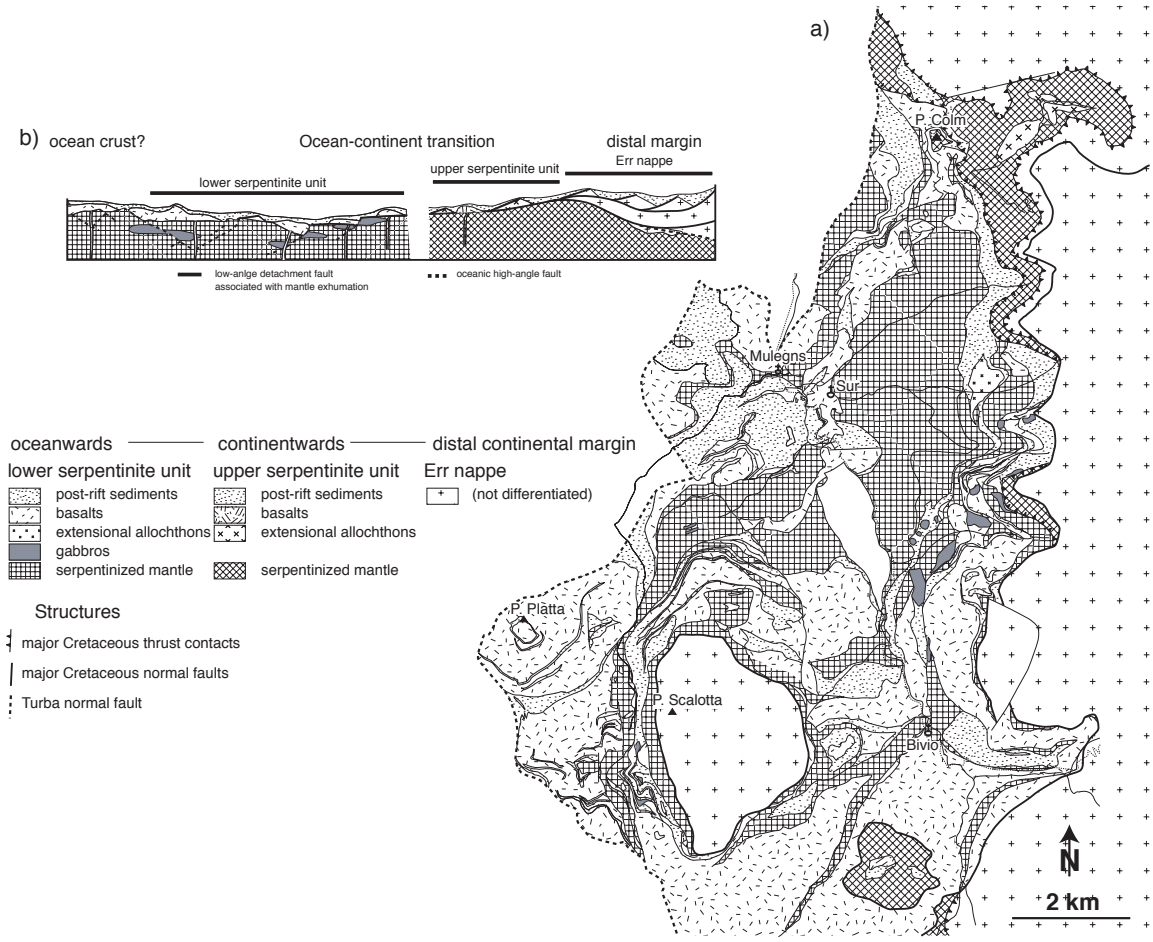

Figure 1-4: a) Tectonic map and b) palinspastic profile of the Platta nappe (after Dietrich 1969; Cornelius 1932, and own mapping).

References

ANONYMOUS 1972. Penrose Field Conference Ophiolites, Geotimes, **17**, 24-25.

ARGAND E. 1911. Sur la répartition des roches vertes mésozoiques dans les Alpes Pennines avant la formation des grands plis couchés, Proc. Verb. Soc. Vaudoise Sci. Nat.

ARGAND E. 1916. Sur l'arc des Alpes occidentales, Eclogae Geol. Helv. **14**, 145-191.

BAILEY E.B. & MCCALLIEN W.J. 1950. The Ankara mélange and the Anatolian thrust, Nature, **166**, 938-943.

BAILEY E.B. & MCCALLIEN W.J. 1953. Serpentine lavas, the Ankara mélange and the Anatolian thrust, Trans. R. Soc. Edinburgh, **62**, 2, 403-442.

BERNOULLI D. & WEISSERT H.J. 1985. Sedimentary fabrics in Alpine ophicalcites, South Pennine Arosa zone, Geology, **13**, 755-758.

BOILLOT G., RECQ M., WINTERER E.L., MEYER A.W., APPLEGATE J., BALTUCK M., BERGEN J.A., COMAS M.C., DAVIES T.A., DUNHAM K., EVANS C.A., GIRARDEAU J., GOLDBERG G., HAGGERTY J., JANSA L.F., JOHNSON J.A., KASAHARA J., LOREAU J.P., LUNA-SIERRA E., MOULLADE M., OGG J., SARTI M., THUROW J. & WILLIAMSON M. 1987. Tectonic denudation of the upper mantle along passive margin: a model based on drilling results (ODP Leg 103, Western Galicia Margin, Spain), Tectonophysics, **132**, 334-342.

BOILLOT G., COMAS M. C., GIRARDEAU J., KORNPROBST J., LOREAU J.-P., MALOD J., MOUGENOT D. & MOULLADE M. 1988. Preliminary results of the Galinaute cruise: dives of the submersible Nautile on the western Galicia margin, Spain, *In:* Boillot G., Winterer E. L. *et al.* (eds) Proc. ODP. Sci. Res., **103**, 37-51.

BONATTI E. 1976. Serpentinite intrusions in the oceanic crust, Earth. Planet. Sci. Lett., 32, 107-113.

BONATTI E., CHERMAK A. & HONNOREZ J. 1980. Tectonic and igneous emplacement of crust in oceanic transform zones. *In:* Talwani, M., Harrison, C.G. & Hayes, D. (eds) Deep Drilling Results in the Atlantic Ocean: Ocean crust, Am. Geophys. U., Maurice Ewing Series, **2**, 239-248.

BOWEN N.L. 1927. The origin of ultra-basic and related rocks, Amer. J. Sci., 5th ser., **14**, 89-108.

BOWEN N.L. 1928. The Evolution of Igneous Rocks, Princeton University Press.

CORNELIUS H.P. 1932. Geologische Karte der Err-Julier Gruppe 1:25'000, Schweizerische Geologische Kommission, Spezialkarte Nr. **115A**.

DECANDIA F.A. & ELTER P. 1972. La "zona" ofiolitifera del Bracco nel settore compreso tra Levanto e la Val Graveglia (Appennino ligure), Mem. Soc. Geolog. It., **11**, 503-530.

DESMURS L., MANATSCHAL G. & BERNOULLI D. 2001. The Steinmann trinity revisited: mantle exhumation and magmatism along an ocean-continent transition: the Platta nappe, eastern Switzerland, in: R.C.L. Wilson, R.B. Whitmarsh, B. Taylor & N. Froitzheim (Eds): Non-volcanic Rifting of Continental Margins: a Comparison of Evidence from Land and Sea, Geol. Soc. London Spec. Publ. (in press).

DEWEY J.F. & BIRD J.M. 1970. Mountain belts and the new global tectonics, J. Geophys. Res. **75**, 2625-2647.

DIETRICH V. 1969. Die Ophiolithe des Oberhalbsteins (Graubünden) und das Ophiolithmaterial der ostschweizerischen Molasseablagerungen, ein petrographischer Vergleich, Verlag Herbert Lang & Cie, Bern, 179 pp.

DIETRICH V. 1970. Vergleichende petrographische Untersuchungen zwischen den Ophiolithen der Platta-Decke und dem Ophiolithmaterial der ostschweizerischen Molasseablagerungen in Hinblick auf die regionale alpine Metamorphose im Oberhalbstein (Graubuenden), Fortschritte der Mineralogie., **47**, 10-15.

FERREIRO-MÄHLMANN R. 2001. Correlation of very low grade data to calibrate a thermal maturity model in a nappe tectonic setting, a case study from the Alps, Tectonophysics, **334**, 1-33.

FROITZHEIM N., SCHMID S.M. & CONTI P. 1994. Repeated change from crustal shortening to orogen-parallel extension in the Austroalpine units of Graubünden, Eclogae Geol. Helv., **87**, 559-612.

FROITZHEIM N. & MANATSCHAL G. 1996. Kinematics of Jurassic rifting, mantle exhumation, and passive-margin formation in the Austroalpine and Penninic nappes (eastern Switzerland), Geolog. Soc. Am. Bull., **108**, 1120-1133.

GLENNIE K.W., BOEUF M.G.A., HUGHES CLARKE M.W., MOODY STUART M., PILAAR W.F. & REINHARDT B.M. 1974. Geology of the Oman Mountains, Verhandelingen van het Koninklijk Nederlands Geologisch Mijnbouwkundig Genootschap, **31**, 1-423.

HERMANN J., MÜNTENER O., TROMMSDORFF V., HANSMANN W. & PICCARDO G.B. 1997. Fossil crust to mantle transition, Val Malenco (Italian Alps), J. Geophys. Res., **102**, B9, 20123-20132.

HESS H.H. 1938. A primary peridotite magma, Amer. J. Sci., 5th ser., 35, 321-344.

HESS H.H. 1955. Serpentines, orogeny, and epeirogeny, In: Poldervaart, A. (ed.), The Crust of the Earth, a Symposium, Geol. Soc. Amer. Spec. Paper, **62**, 391-407.

JUTEAU T., CANNAT M. & LAGABRIELLE Y. 1989. Peridotites in the upper oceanic crust away from transform zones: A comparison of the results of previous DSDP and ODP legs, *In*: Detrick,-R.S.; Honnorez, J.; Bryan, W.B.; Juteau, T.; et al (eds), Proc. ODP. Sc. Res., **109**, 303-308.

LAGABRIELLE Y., POLINO R., AUZENDE J.-M., BLANCHET R., CABY R., FUDRAL S., LEMOINE M., MEVEL C., OHNENSTETTER M., ROBERT D. & TRICART P. 1984. Les témoins d'une tectonique intra-océanique dans le domaine téthysien: Analyse des rapports entre les ophiolites et leur couverture métasédimentaire dans la zone piémontaise des Alpes franco-italiennes, Ofioliti, **9**, 67-88.

LAGABRIELLE Y. & LEMOINE M. 1997. Alpine, Corsican and Apennine ophiolites: the slow-spreading ridge model, C. R. Acad. Sci. Paris, II, **325**, 909-920.

LAUBSCHER H. 1969. Mountain building, Tectonophysics, **7**, 551-563.

LEMOINE M. 1980. Serpentinites, gabbros and ophicalcites in the Piemont-Ligurian domain of the Western Alps: Possible indicators of oceanic fracture zones and of associated serpentinite protrusions in the Jurassic-Cretaceous Tethys, Arch. Sci., Genève, **33**, 103-115.

LEMOINE M., TRICART P. & BOILLOT G. 1987. Ultramafic and gabbroic ocean floor of the Ligurian Tethys (Alps, Corsica, Apennines): In search of a genetic model, Geology, **15**, 622-625.

MANATSCHAL G. & NIEVERGELT P. 1997. A continent-ocean transition recorded in the Err and Platta nappes (Eastern Switzerland), Eclogae Geol. Helv, **90**, 3-27.

MANATSCHAL G. & BERNOULLI D. 1998. Rifting and early evolution of ancient ocean basins: the record of the Mesozoic Tethys and of the Galicia-Newfoundland margins, Mar. Geophys. Res., **20**, 371-381.

MANATSCHAL G. & BERNOULLI D. 1999. Architecture and tectonic evolution of non-volcanic margins: present-day Galicia and ancient Adria, Tectonics, **18**, 1099-1119.

MOORES E.M. & VINE F.J. 1971. The Troodos Massif, Cyprus and other ophiolites as oceanic crust: evaluations and implications, Phil. Trans. Royal Soc. London, A. **268**, 443-466.

MÜNTENER O., HERMANN J. & TROMMSDORFF V. 2000. Cooling history and exhumation of lower-crustal granulite and upper mantle (Malenco, Central Alps), J. Petrol., **41**, 1-25.

PETERS T. J. & NIGGLI E. 1964. Spinellfuehrende Pyroxenite ('Ariegite') in den Lherzolitkoerpern von Lherz und Umgebung (Ariege, Pyrenaeen) und der Totalp (Graubuenden, Schweiz), ein Vergleich, Schweiz. Mineral. Petrogr. Mitt. **44**, 513-517.

RAITT R. W. 1963. Seismic refraction studies of the Mendocino fracture zone, Mar. Phys. Lab. Scripps. Inst. Oceanogr., Rept. MPL-U-23/63.

RAMPONE E., HOFMANN A.E. & RACZECK I. 1998. Isotopic contrast within the Internal Liguride Ophiolite (N. Italy): the lack of a genetic mantle-crust link, Earth Planet. Sci. Lett., **163**, 175-189.

STAMPFLI G. M. 1993. Le Brianconnais, terrain exotique dans les Alpes?, Eclogae Geol. Helv. **86**, 1-45.

STAUB R. 1922. Über die Verteilung der Serpentine in den alpinen Ophiolithen, Schweiz. Mineral. Petrogr. Mitt. **2**, 78-149.

STAUB R .1924. Der Bau der Alpen, Beitr. Geol. Karte Schweiz, N.F. **52**.

STEINMANN G. 1905. Geologische Beobachtungen in den Alpen. II. Die Schardtsche Ueberfaltungstheorie und die geologische Bedeutung der Tiefseeabsätze und der ophiolitischen Massengesteine, Ber. Nat. Ges. Freiburg i.B., **16**, 18-67.

STEINMANN G. 1925. Gibt es fossile Tiefseeablagerungen von erdgeschichtlicher Bedeutung?, Geol. Rdsch., **14**, 435-468.

STEINMANN G. 1927. Die ophiolitischen Zonen in den mediterranen Kettengebirgen, Congrès Géol. Internat. XIV Sess, 1926, Madrid, **2**, 637-667.

TRÜMPY R. 1975. Penninic-Austroalpine boundary in the Swiss Alps; a presumed former continental margin and its problems. Am. J. Sci., **275**, 209-238.

WEISSERT H.J. & BERNOULLI D. 1985. A transform margin in the Mesozoic Tethys: Evidence from the Swiss Alps, Geol. Rdsch, **74**, 665-679.

Chapter 2-The Steinmann Trinity revisited: mantle exhumation and magmatism along an ocean-continent transition: the Platta nappe, eastern Switzerland

Laurent Desmurs[1], Gianreto Manatschal[1,2] & Daniel Bernoulli[1]

[1]*Geology Institute, ETH-Zentrum, CH-8092 Zürich, Switzerland*
[2]*EOST-UMR 7517 CNRS, Université Louis Pasteur, F-67084 Strasbourg, France*

(in press at Geological Society of London Special Publication)

Mapping the ophiolite group as a unit has often obscured critical relationships of its various members to the tectonic cycle (H.H. Hess 1955)

Abstract: The close association of serpentinites, basalts and radiolarites, later known as the Steinmann Trinity, was clearly described by Gustav Steinmann (1905) from the south-Pennine Arosa zone and its southern prolongation, the Platta nappe of the eastern Swiss Alps. This classical "ophiolite" is distinctly different from typical fast-spreading ridge associations and can be compared to the transitional crust occurring along non-volcanic passive continental margins in present-day oceans. It includes serpentinized peridotites which we interprete as subcontinental mantle rocks, which were exhumed along low-angle detachment faults and locally overlain by extensional allochthons of continental crust, minor gabbroic intrusions, tholeiitic pillow lavas and flows and a succession of oceanic sediments. The serpentinized peridotites record deformation under decreasing temperatures during extension leading to final exposure of the mantle rocks at the sea floor and their inclusion in tectono-sedimentary breccias (ophicalcites). Field relationships, mineral-chemical and radiometric data show that the gabbros intruded already serpentinized mantle rocks at shallow depth 161 Ma ago. They are Mg-gabbros, Fe-gabbros and Fe-Ti-gabbros, cut by dioritic pegmatoid veins and albitite dykes which originated by differentiation from the same parental magma. All gabbros show the same metamorphic evolution, i.e. intrusion at relatively low pressure, oceanic hydration at elevated temperature and a subsequent static oceanic alteration. The pillow lavas stratigraphically overlie the exhumed mantle rocks and the tectono-sedimentary breccias related to the exhumation of both mantle rocks and gabbros. However, both gabbros and pillow basalts are characterised by eNd values typical for an asthenospheric MOR-type source of the melts. They may be the products of a steady process which combined extensional deformation with magma generation and emplacement. They appear to document the onset of sea-floor spreading across an exhumed subcontinental mantle during the earliest phases of a slow spreading ridge.

In 1905, Gustav Steinmann noted the close association of serpentinites, "diabase" and radiolarite and considered this "green rock" or ophiolitic association as characteristic for the axial part of the "geosyncline" and the deep ocean floor. Although Steinmann considered diabase, spilite and variolite (variolitic pillow lavas) as intrusive rocks distinctly younger than the associated sediments, he stressed their characteristic association with deep-sea sediments, notably radiolarian cherts but also deep-water limestones of Maiolica facies (Steinmann 1925, 1927). In his view, the "consanguineous" association of ultramafic and mafic material was characteristic for suboceanic environments from where these magmas ascended during folding of the oceanic sediments. Eventually, the importance of Steinmann's discovery was recognised and the association of serpentinites, pillow lavas and radiolarites became known as the Steinmann Trinity: "Steinmann's realisation of this trinity as a world-wide, age-long characteristic of geosynclinal deposition ranks among the most exciting achievements of geological research" (Bailey & McCallien, 1950). With time, the Steinmann trinity became a synonym for ophiolitic associations in the sense of the 1972 Penrose Conference on ophiolites (Anonymous 1972). As a consequence, the examples described by Steinmann from the Alps and the Apennines were considered as tectonically dismembered ophiolites, incomplete equivalents of ancient oceanic lithosphere (e.g. Laubscher 1969; Dewey & Bird 1970).

In the nineteenseventies, detailed field work showed that the stratigraphy of the ophiolites of the Alps and the Apennines did not match the classical ophiolite stratigraphy as defined by the Penrose Conference in 1972 and observed in large ophiolitic complexes like Troodos (Moores & Vine 1971) or Semail (Glennie *et al.* 1974). No substantial relics of a sheeted dike complex were found, and gabbros appeared to play a subordinate role. Instead, oceanic sediments, radiolarian cherts and pelagic limestones, were observed to stratigraphically overlie (1) serpentinized mantle rocks and tectono-sedimentary breccias ("ophicalcites") derived from them, and (2) pillow lavas which were extruded onto the serpentinites previously exposed along the ocean floor (Fig. 2-1, Decandia & Elter 1972; Lagabrielle *et al.* 1984; Bernoulli & Weissert 1985; Weissert & Bernoulli 1985). At an early stage, exposure of mantle rocks at the sea floor was postulated to be associated with oceanic transform faults in analogy with serpentinite occurrences along such faults in present-day oceans (Lemoine 1980; Bernoulli & Weissert 1985; Weissert & Bernoulli 1985), however, the data now available from the south-Pennine-Austroalpine margin suggest that in this area subcontinental mantle was exhumed along a system of low-angle extensional detachment faults (Lemoine *et al.* 1987; Froitzheim & Manatschal 1996; Manatschal & Nievergelt 1997). It appears today that the trinity of serpentinites, pillow lavas and radiolarites Steinmann (1905, 1927) described from the Alps and the Apennines corresponds, by and large, to the stratigraphy of *transitional crust*, as observed along "non-volcanic" continental margins (Manatschal & Bernoulli 1999) laterally grading into that of oceanic crust generated along a slow-spreading ridge (Lagabrielle and Lemoine 1997). Indeed, exhumation of mantle rocks and their exposure at the sea-floor is now well documented along present-day margins where it occurred during the final stage of rifting and break-up of the continental lithosphere (Boillot *et al.* 1987, 1988). However, the origin and significance of the magmatic rocks associated with exhumation are still discussed.

In this contribution, we shall describe in detail the different stages of mantle exhumation and associated magmatic activity along the south-Pennine-Austroalpine margin of the Adria plate, the type area of the Steinmann Trinity. In an earlier paper, two of us described the extensional tectonic structures associated with rifting

(Manatschal & Bernoulli 1999), whereas here we deal with the retrograde metamorphism and the submarine alterations associated with mantle uplift and the magmatic processes associated with the latest phases of rifting at the turn to sea-floor spreading. Our argumentation is based on field relationships, petrological, geochemical, and geochronological data and will focus on: (1) The evolution of the mantle rocks during their exhumation to the sea floor; (2) the P-T conditions during the intrusion of the gabbros; and (3) the genetic and time relationships between the gabbros and the overlying pillow basalts and their relation to the rifting processes. From our data it will become clear that, in our study area, peridotites and mafic rocks are not a consanguineous association as originally conceived by Steinmann.

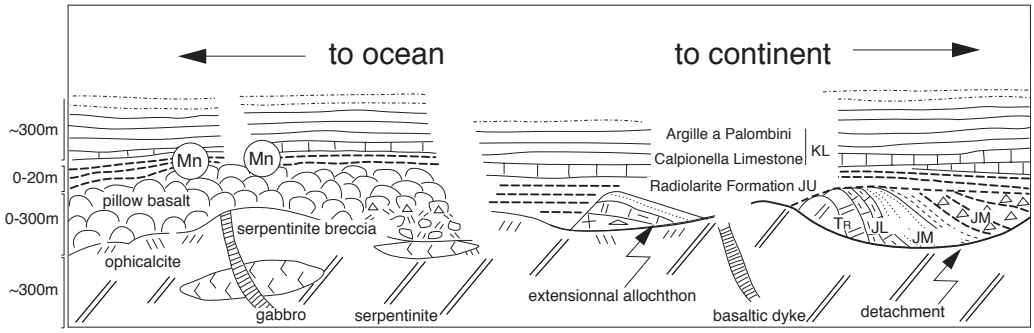

Figure 2-1: Generalised stratigraphy of transitional crust (ocean-continent transition) in the Platta nappe, eastern Switzerland. TR: Triassic, JL: Lower Jurassic, JM: Middle Jurassic, JU: Upper Jurassic, KL: Lower Cretaceous, Mn: Manganese deposits. After Manatschal & Nievergelt (1997).

General situation

Steinmann (1905) recognised that in the Alps his ophiolitic trinity always occurred in the same tectonic unit which he called the Rhetic nappe, a term which did not survive but included the ophiolite-bearing south-Pennine units of eastern Switzerland and the adjacent eastern Alps as well as the south-Pennine relics in the pre-Alpine nappes of western Switzerland (nappe des Gets). Remnants of this oceanic suture can be traced along the Alpine system from Corsica and the Apennines along the south-Pennine nappes to the eastern end of the Alps and possibly beyond. In eastern Switzerland and western Austria, the relics of this ophiolite zone can be followed below the Austroalpine nappes from Val Malenco (Malenco complex) across the Engadin valley to the Sursés valley (Platta nappe), and across a number of imbricates (Totalp slice) and local occurrences in tectonic melanges (Arosa zone) to the northern margin of the Northern Calcareous Alps (Fig. 2-2). It is, however, only in the area of the Platta and Err nappes of Sursés that the ocean-continent transition including the distal continental margin can be reconstructed with some confidence (Froitzheim & Manatschal 1996; Manatschal & Nievergelt 1997; Manatschal & Bernoulli 1999). In this area, the ophiolites were always part of the upper plate of the Alpine system and were never subducted to great depth. Here the Alpine nappe movements can be kinematically inverted and the pre-Alpine geometrical and age relationships between the exhumed mantle rocks, the gabbroic intrusions and the tholeiitic pillow lavas can be studied in detail. In many places, the primary contacts between plutonic, volcanic and sedimentary rocks are well exposed. Locally the pre-Alpine mineral parageneses are excellently preserved, and a complete sedimentary record of the late syn- and post-rift history is available. As temperatures, in our area, never exceeded

approximately 250°C during Alpine orogeny, the pre-Alpine history of mantle deformation and hydration during exhumation is well documented.

The Platta nappe

Together with the lower Austroalpine Err nappe, the Platta nappe preserves the remnants of the southeastern margin of the Liguria-Piedmont segment of the Alpine Tethys (Figs 2-2 & 2-3). The Err nappe includes the remnants of the distal Adriatic margin and was thrust onto the Platta nappe during late Cretaceous time. It consists of a thinned continental crust, overlain by a number of extensional allochthons, slivers of continental crust and pre-rift sediments which were tectonically emplaced during the middle Jurassic along an oceanward-dipping low-angle detachment system (Fig. 2-3; Froitzheim & Eberli 1990; Froitzheim & Manatschal 1996; Manatschal & Nievergelt 1997). The Platta nappe, originally situated oceanward of the Err nappe, represents the ocean-continent transition s.str. and exposes the Steinmann Trinity, i.e. serpentinized peridotites, basaltic volcanics and oceanic sediments. Far-travelled extensional allochthons, derived from the distal continental margin, were emplaced on the exhumed mantle rocks prior to the deposition of the basalts and sediments (Figs 2-1 & 2-3). Err and Platta nappes are now part of a late Cretaceous west-directed thrust wedge, which was probably associated with subduction along the eastern border of Adria (Froitzheim *et al*. 1996). Subduction of the Liguria-Piedmont ocean initiated later during the late Cretaceous and continued during the Tertiary as indicated by the early Tertiary ages of high-pressure metamorphism within the ophiolites of the western Alps (Rubatto *et al*. 1998). In contrast to these ophiolites, the south-Pennine ophiolites of the Arosa zone, the Platta nappe and the Malenco Complex lack a high-pressure metamorphic overprint, and show only a general increase of Alpine metamorphism from deep burial diagenesis in the north (Arosa zone) to epidote-amphibolite facies conditions in the south (Malenco complex, Ferreiro Mählmann 1995, and references therein). The serpentine mineral phases are lizardite-chrysotile north of Bivio and antigorite-lizardite-chrysotile south of this location, confirming the increase in Alpine metamorphism from north to south (Trommsdorff & Evans 1974; Trommsdorff 1983). Obviously, these nappes were part of the hanging wall of the south-directed subduction zone which apparently first developed within the ocean (Lagabrielle 1987; Avigad *et al*. 1993).

Alpine deformation

The occurrence of "middle" Cretaceous (Albian to ?Cenomanian; Dietrich 1970) hemipelagic and turbiditic sediments in the Platta nappe provides a lower age bracket for the Alpine deformation (Froitzheim et al. 1994) which is consistent with radiometric age data from the overlying Austroalpine nappes (Handy et al. 1993). The oldest structures related to Alpine convergence are localised thrust faults of late Cretaceous age with a top-to-the-west sense of shear. The occurrence of sediments and/or basalts stratigraphically overlying the exhumed mantle rocks suggests that decollement was near-surface and collected only the uppermost crust. The geometry of the thrust system is locally complicated by lateral thickness variations of the basalts, pre-existing basement topography, the occurrence of extensional allochthons of continental provenance overlying the serpentinites, and later, Tertiary, deformation. The resulting complex geometries probably led Ring *et al*. (1988, 1989) and Dürr (1992) to the conclusion that parts of the Platta ophiolites formed a tectonic mélange

generated during subduction of the upper Penninic below the Austroalpine units, an interpretation which is not supported by our field observations.

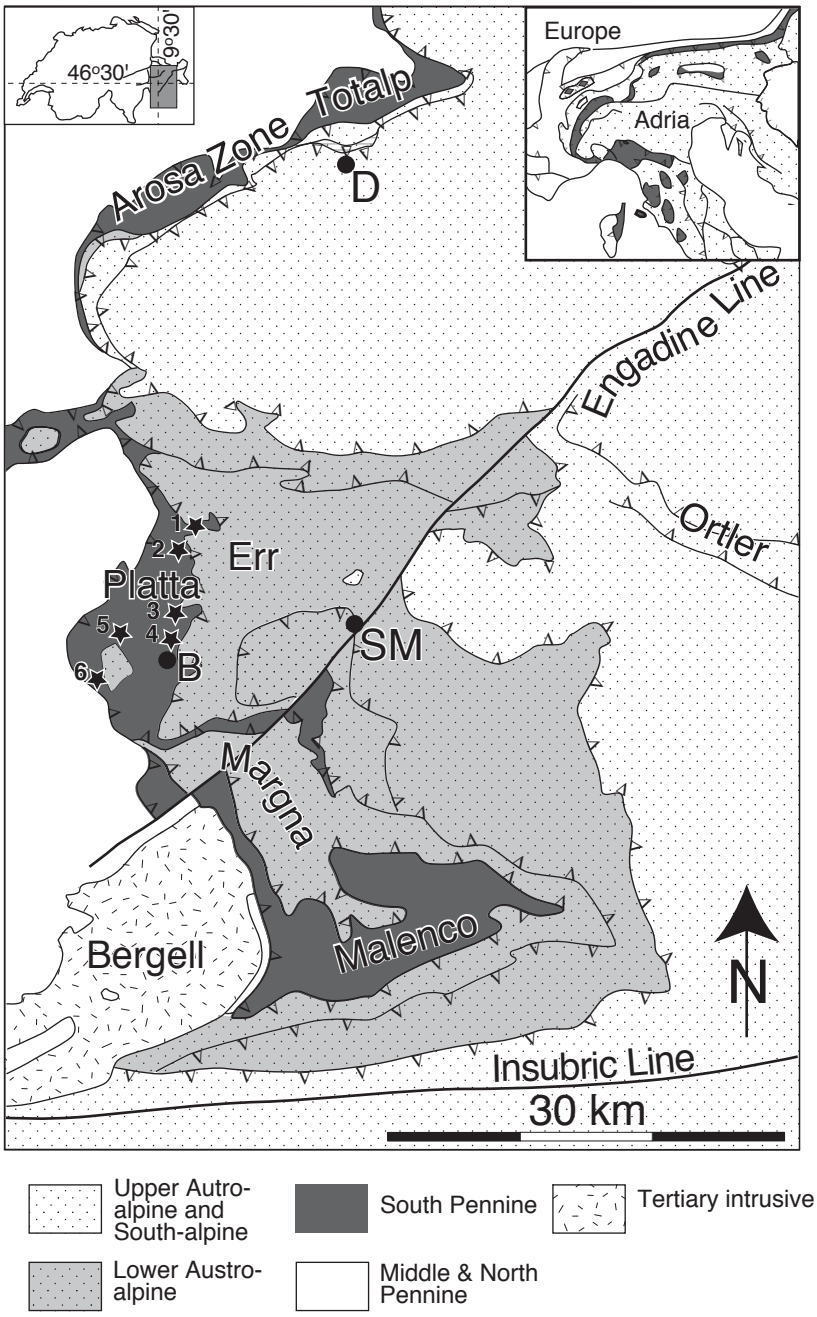

Figure 2-2: Simplified geological map and location of the study area. Bivio; D: Davos; B: SM: St. Moritz. 1: Val d'Err; 2: Falotta; 3: Val Savriez; 4: Val da Natons; 5: Starschagns; 6: Fuorcla da Faller; modified after Froitzheim et al. (1994).

By and large, the large-scale geometry of the Platta nappe is defined by two serpentinite thrust sheets which can be traced across the entire nappe and which are interleaved with imbricated cover sequences. This geometry resembles that of a large-scale duplex structure and is particularly well illustrated in the area of Falotta (for location see Fig. 2-2). In Falotta, the major tectonic units consist of massive, up to 300 m thick sheets of serpentinized peridotites (upper and lower serpentinites in Fig. 2-4a), which are floored by basal decollement horizons and are interleaved with basalts and post-rift sediments. Along the basement-cover contacts, i.e. between

serpentinites and massive pillow basalts, thrust faults occur, typically along ophicalcites, which eventually ramp across the basalts into the sediments leading to local repetitions in the cover sequence (Fig. 2-4b). Locally, isoclinal folds preserving preferentially the inverted limb are associated with these faults. Thus, the simplified overall geometry of the thrust stack is that of a duplex structure with first-order thrust faults lying along the base of the large serpentinite sheets, and second-order thrust faults along the basement-cover contact and ramping into basalts and overlying sediments (cf. roof and floor thrusts in Fig. 19 in Boyer & Elliott 1982).
The amount of displacement accommodated by the first-order faults cannot be determined directly. A minimum value, however, can be estimated by measuring the distance in transport direction between the westernmost occurrence of a serpentinite sheet and the easternmost outcrop of sediments in the underlying sheet, which results in a minimum displacement of 9 km between the two serpentinite units. The displacement along the second-order thrust-faults is variable but of one magnitude less than that of the first-order faults, i.e. in the order of 500 m or less.

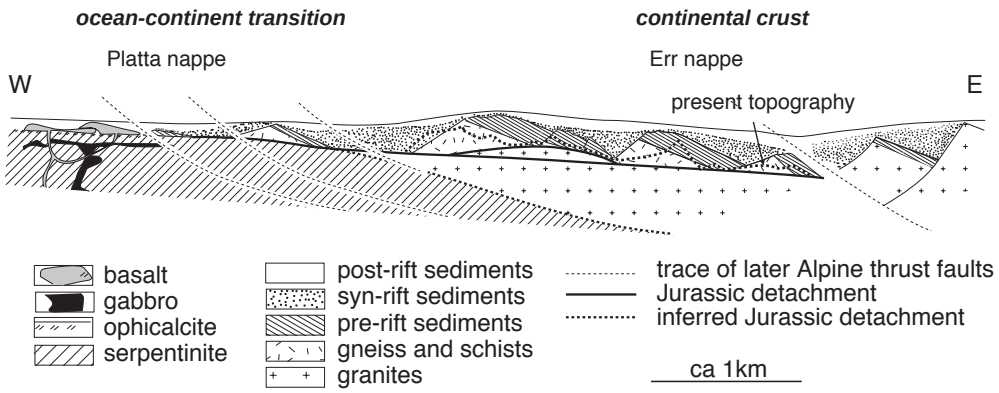

Figure 2-3: Palinspastic reconstruction of the Err-Platta ocean-continent transition, after Manatschal & Nievergelt (1997).

The most prominent post-stack structures are meter- to kilometer-scale folds which deform the thrust-stack including the thrust contact between the Err and the Platta nappe. This folding phase is associated with extensional faults (Manatschal & Nievergelt 1997), which, however, are not easily visible in the Platta nappe. The fold axes of the large-scale folds plunge slightly to the east and their axial planes are subhorizontal. Micas crystallising within the fold axial-plain cleavage of these folds yielded ages of 72.5±6.4 Ma (Handy et al. 1993). Structures post-dating this folding event become more pronounced towards the south (south of Bivio) and towards the base of the Platta nappe.
A qualitative kinematic inversion of the Platta nappe is only possible in the northern part of the Platta nappe, as for instance in the area of Falotta, where the architecture of the late Cretaceous thrust stack is still preserved (Fig. 2-4a). The kinematic inversion is achieved by aligning the stacked serpentinite sheets in a horizontal order in which the highest sheet is placed furthest to the east (opposite to the transport direction) (Fig. 2-4c). The imbricate structures between two serpentinite sheets can be reconstructed using the same approach, assuming that the imbricates lying between two serpentinite sheets were the cover of the underlying sheet. This qualitative kinematic inversion of the thrust stack leads to a palinspastic reconstruction for the Platta domain which allows to understand the relative position of individual outcrops

and the spatial distribution of specific rock associations relative to the ocean-continent transition (Fig. 2-3).

Pre-Alpine situation and stratigraphy

Kinematic inversion of the movements which assembled the imbricates of the Platta nappe resulted in a 20 to 30 km wide zone of transitional to incipient oceanic crust. The serpentinites of the individual imbricates of the Platta nappe are about 300 m thick and therefore document a crustal section about 300 m deep (Fig. 2-1). Deeper levels of the crust are not observed in the Platta nappe.

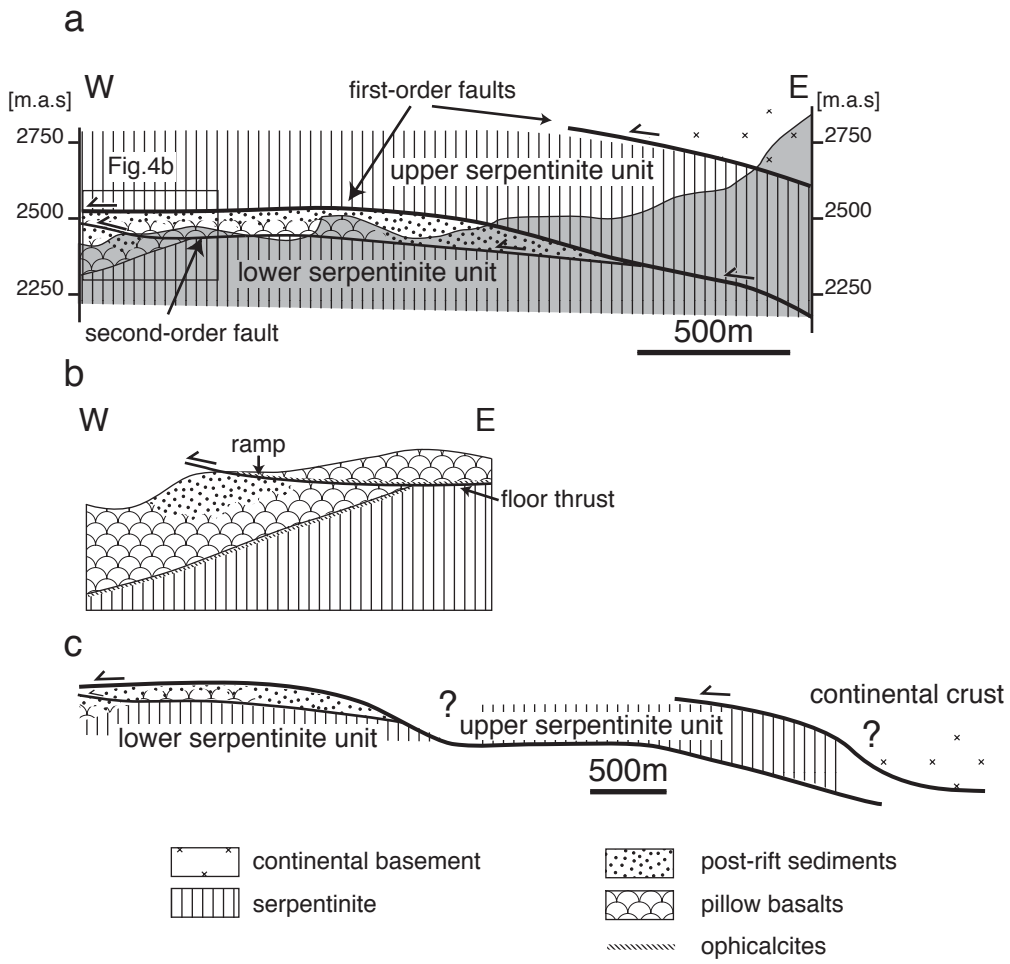

Figure 2-4: Qualitative palinspastic reconstruction of the Platta nappe in the Falotta area. (a) Alpine structure. The shaded lower part of the section is observed, the white upper part is a lateral projection of geometries mapped in the surroundings of the section. (b) Detail of (a) showing a second-order fault ramping across the basalts into the overlying sediments. (c) Kinematic inversion of section (a). The question marks indicate the uncertainties in the estimate of the amounts of displacement (pre-thrust distance between the different first-order tectonic units).

The base of the different imbricates of the Platta nappe is invariably formed by serpentinized peridotites derived from spinel lherzolites and harzburgites into which gabbros and basaltic dykes intruded. The top of the serpentinites is usually formed by ophicalcites, tectono-sedimentary breccias (Bernoulli & Weissert 1985; Lemoine *et al*. 1987) overlain by basalts toward the former ocean. Toward the former continent, the extensional allochthons mentioned above overlie the exhumed mantle rocks (Fig.

2-1; Froitzheim & Manatschal 1996; Manatschal & Nievergelt 1997). Clasts of continental basement rocks and pre-rift sediments occur within tectonic and sedimentary breccias associated with the extensional allochthons.
The gabbros occur as planar, sill-like bodies within the serpentinized peridotites. They are relatively rare, less than 10% of the total observed serpentinite volume. Massive basalts, pillow lava, pillow breccias and hyaloclastites occur in patches of variable thickness and size, and their abundance appears to increase oceanward. They stratigraphically overlie the serpentinites, ophicalcites, gabbros and associated breccias and their extrusion therefore postdates emplacement of the mantle rocks and gabbros at the sea floor. The original thickness of the basalts is in the order of 150 m, but was overestimated in the past: basalt bodies appearing to be several 100 meters thick are either folded or duplicated by thrust faults as indicated by relics of post-rift sediments or slices of serpentinite occurring between different basalt sequences.
Exhumed mantle rocks, ophicalcites, pillow lavas, extensional allochthons and syn-rift sediments are all overlain by post-rift deep-water sediments (Fig.2-1). Post-rift sediments also seal the faults associated with the emplacement of the extensional allochthons. These oldest sediments, found on both continental and oceanic basement rocks, define the base of the post-rift sedimentary sequence; they are thin-bedded cherts, siliceous shales, and turbidites of the upper Middle to Upper Jurassic Radiolarite Formation (Baumgartner 1987). This formation is often only a few meters thick. It is overlain by (1) well-bedded, light-coloured micritic limestones with shale intercalations (Calpionella Limestone or Aptychus Limestone) of Berriasian age; (2) dark siliceous shales and calcarenites alternating with dark gray micritic limestones (Argille a Palombini, approximately Valanginian to Barremian); (3) hemipelagic marls with interbedded sandstones turbidites, similar to the Scisti di Val Lavagna of the northern Apennines, and dated by planktonic foraminifera (Aptian-Albian-?Cenomanian, Dietrich 1970). In the radiolarites, the pelagic limestones of the Calpionella Limestone Formation, and the Argille a Palombini, intercalations of pebbly mudstones, clast-supported breccias and turbidites yield locally derived clasts of serpentinite and basalt and of crystalline basement rocks and pre-rift sediment derived from the distal continental margin and the extensional allochthons. These mass-flow deposits document a long-lived submarine topography.

Mantle exhumation

Serpentinized lherzolite is the major rock type all over the Platta nappe. The peridotites of the upper serpentinite unit (Fig. 2-4), which are derived from the originally continentward part of the transitional crust, preserve a spinel foliation and contain pyroxenite dykes parallel to the foliation indicating that they equilibrated in the spinel stability field. The peridotites of the lower serpentinite unit (Fig. 2-4), which originally were nearer to the ocean, are usually less deformed and generally free of pyroxenites. Since all these rocks are stratigraphically overlain by deep-marine sediments they must have been uplifted from mantle depth to the sea floor. Serpentinisation generally masks the earlier stages of retrograde evolution during exhumation, however, at places the relationships between deformation and retrograde evolution can be recognised.

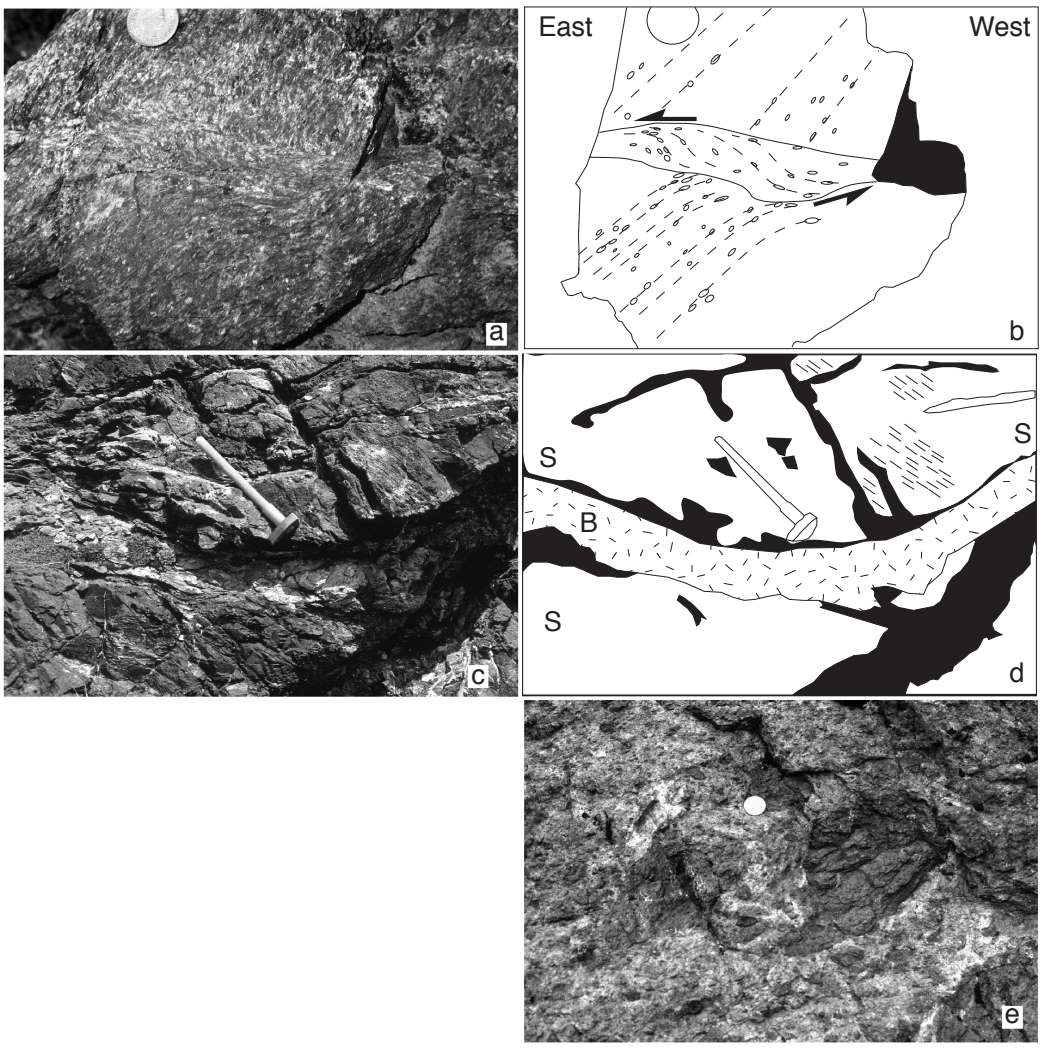

Figure 2-5: (a) and (b) High-tem perature top-to-the-east shear zone deforming the preexisting spinel foliation of the peridotite (diameter of coin: 2.3 cm). Val d'Err (Coordinates of Swiss Topographic Map: 772'750/159'750). (c) and (d) Serpentinite mylonite (S), deformed under low-temperature conditions and cut by undeformed basaltic dyke (B) indicating a pre-Alpine age of deformation (hammer is 50 cm long). Near Pt. 2594, east of Falotta (Coordinates of Swiss Topographic Map: 771'250/156'930). (e) Tectonic breccia with clasts of mylonitic serpentinite embedded in a serpentinite matrix (diameter of coin: 2 cm). Falotta (Coordinates of Swiss Topographic Map: 770'330/157'350).

Petrology and microstructures of the lower serpentinized peridotite

The serpentinized lherzolites of the lower serpentinite unit show a porphyroclastic structure with holly leaf spinel. They consist of large porphyroclastic Cr-diopside, orthopyroxene, Cr-Al spinel, and olivine which is always replaced by serpentine minerals. In a few samples, disseminated grains of phlogopite occur within the porphyroclastic assemblage. This assemblage partly re-equilibrated in the spinel stability field as shown by the recrystallisation of granoblastic diopside, Cr-Al spinel, and Ti-pargasite between the large porphyroclastic pyroxenes.
The evidence for retrograde high-temperature hydration in this unit is the appearance of Mg-hornblende in coronae around clinopyroxene and along its cleavage planes. This was followed by a more widespread hydration at lower temperature characterised by the crystallisation of tremolite at the expense of clinopyroxene and of Mg-hornblende. Olivine was transformed into a serpentinite mesh with magnetite,

whereas the spinel was altered to Cr-chlorite and magnetite. Finally the serpentine minerals were partially replaced by the assemblage calcite + talc.

Petrology and deformation of the upper-serpentinized peridotite

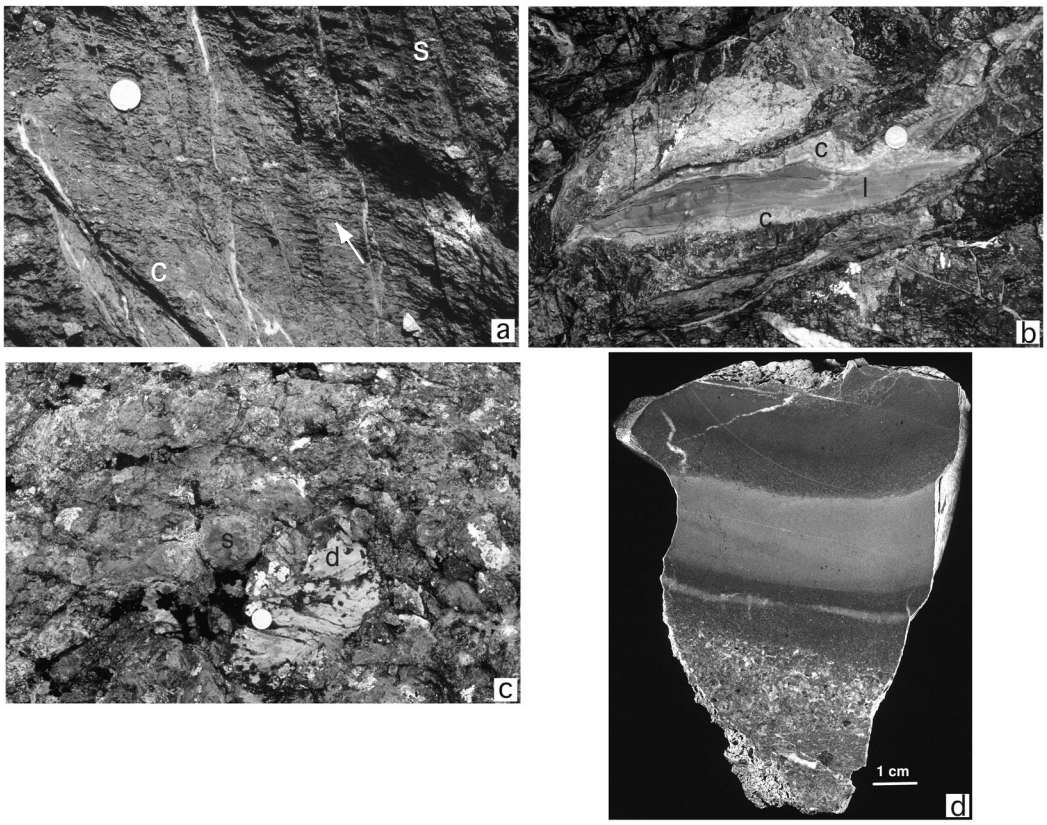

Figure 2-6: a) Calcite (c) partially replacing serpentinite (s). The replacement process is testified by the perfectly preserved high-temperature spinel foliation (indicated by the arrow) floating in the newly formed calcite matrix (diameter of coin: 2 cm). Falotta (Coordinates of Swiss Topographic Map: 769'550/157'350). (b) Geopetal structure in sediment-filled pocket in serpentinite (ophicalcite I). A first generation of cement (c) fringes the void and is overlain by grey lime mudstone (l) filling the lower part of the pocket. Clear sparry calcite (c) cements the remaining pore space above (diameter of coin: 2 cm). Near Pt. 2594, east of Falotta (Coordinates of Swiss Topographic Map: 771'250/156'930). (c) Sedimentary breccia with clasts of serpentinite (s) and of pre-rift Triassic dolomite (d) embedded in a serpentinite matrix. This breccia stratigraphically overlies the exposed mantle rocks; the dolomite clasts are derived from an extensional allochthon (diameter of coin: 2 cm). Plang Tguils (Coordinates of Swiss Topographic Map: 767'500/147'400). (d) Graded lithoclastic sandstone composed of serpentinite and ophicalcite clasts intercalated in the lowermost Radiolarite Formation. Polished surface, Arosa Zone, Obersasställi, Totalp (Coordinates of Swiss Topographic Map: 780'650/191'150).

In the upper serpentinite unit (Falotta and Val d'Err areas), several mylonitic shear zones occur within the peridotite which affected the previous high-temperature spinel foliation (Fig. 2-5a, b). The microstructures associated with these shear zones are still visible within small pyroxenite dykes (olivine websterite) present within the lherzolite host. They consist of rotated or kinked porphyroclastic ortho- and clinopyroxene showing undulous extinction and of neoblastic minerals growing in the plane of the new foliation or recrystallising in a mosaic fabric. The asymmetric clasts associated with this event of high-temperature shearing show a top-to-the-east, i.e. top-to-the-continent sense of shear. The neoblastic assemblage consists of secondary Al-diopside, orthopyroxene, olivine and spinel, which are altered to chlorite, serpentine

minerals and magnetite. We interpret this association as formed under spinel-peridotite facies conditions with a later low-grade overprint. As no pressure constraints are available for this deformation event, we cannot relate it with certainty to rifting. Only the late, hydrous serpentinite mylonites indicate deformation of the mantle rocks during their exhumation to the sea floor.

Deformation under greenschist-facies conditions produced a foliation defined by the assemblage chlorite, serpentine and rare talc. The associated shear zones show a top-to-the-west, i.e. oceanward sense of shear, and are cut by undeformed basaltic dykes demonstrating their pre-Alpine age (Fig. 2-5c, d).

Deformation under low-temperature conditions is recorded by tectonic breccias. In these, clasts from the greenschist-facies shear zones are embedded in a serpentinite matrix indicating that deformation extended into the brittle field during final exhumation of the mantle rocks (Fig. 2-5e). The clasts are rounded by frictional wear suggesting rotational deformation. Up-section the breccia is cut by chrysotile and calcite veins.

Replacement of serpentine minerals under static conditions by calcite occurred under still lower temperatures. This is illustrated by serpentinites which in a calcitised matrix preserve the relics of the high-temperature foliation (Fig. 2-6a). These calcitised serpentinites are transitional to tectono-sedimentary breccias (ophicalcite type I of Lemoine *et al*. 1987). Typically, the serpentinites grade rapidly through a narrow zone of host rock, cut by different generations of neptunic dikes, into complex breccias dominated by a carbonate matrix and occasionally preserving a jigsaw-puzzle structure documenting *in-situ* fragmentation of the host rock. Crevasses and dikes are filled by red or gray microsparitic limestone and/or white sparry calcite preserving typical cement fabrics (Fig. 2-6b). Geopetal infill of internal pelagic and/or diagenetic sediment into crevasses and pockets of the serpentinites (Fig. 2-6b) indicates proximity to the sea-floor (Bernoulli & Weissert 1985) that is also evidenced by their stratigraphic position underlying pillow-basalts or radiolarian cherts. Further evidence of the occurrence of the mantle rock on the sea-floor is the presence of mass-flow breccias (ophicalcite type II) with clasts of serpentinite and Triassic dolomites within a serpentine arenite or calcite matrix (Fig. 2-6c) and the occurrence of serpentinite arenites within the post-rift sediments (Fig. 2-6d).

Mineral chemistry

Clinopyroxene (Table 2-1 and Fig. 2-7): The porphyroclastic clinopyroxenes of the lower serpentinized lherzolite are always Cr-diopsides with Cr_2O_3 contents of up to 1.22 weight%. They are characterised by high Al_2O_3 (4.24-5.38 weight%) and TiO_2 (up to 1 weight%) contents. The granoblasts are depleted in Na and Al with respect to the porphyroclasts (Fig 2-7b).

The clinopyroxenes of the upper serpentinized lherzolite and of its pyroxenite dykes are both systematically enriched in Al_2O_3 (6.19-6.99 weight%) and Na_2O (1.23-1.46 weight%) in comparison with the clinopyroxenes of the pyroxenite-free lower serpentinite unit (Fig. 2-7a). The clinopyroxenes of the pyroxenites are depleted in Cr in comparison to those of the lherzolite (Fig. 2-7a). In the high-temperature shear zones, a difference in composition exists between the granoblasts underlining the mylonitic foliation and the porphyroclasts; the granoblasts show lower Al, Na and Cr contents (Fig. 2-7b), however, the granoblastic clinopyroxenes show still relatively high Al and Na values indicating that deformation occurred under spinel-peridotite metamorphic conditions (cf. Müntener *et al*. 2000).

Orthopyroxene: Orthopyroxene is rarely preserved and fresh minerals have only been found within the lower serpentinite unit. The orthopyroxene shows an enstatite-rich composition with a constant Mg# of 0.89. A zonation can be shown with Al, Cr, and Ca decreasing from core to rim.
Spinel: Fresh spinel compositions are present only in the lower serpentinite unit. The large porphyroclasts and the small granoblasts occurring along the interface between clino- and orthopyroxenes show the same composition. They are Cr-spinels with more than 30 weight% Cr_2O_3. The rim is systematically altered to magnetite.

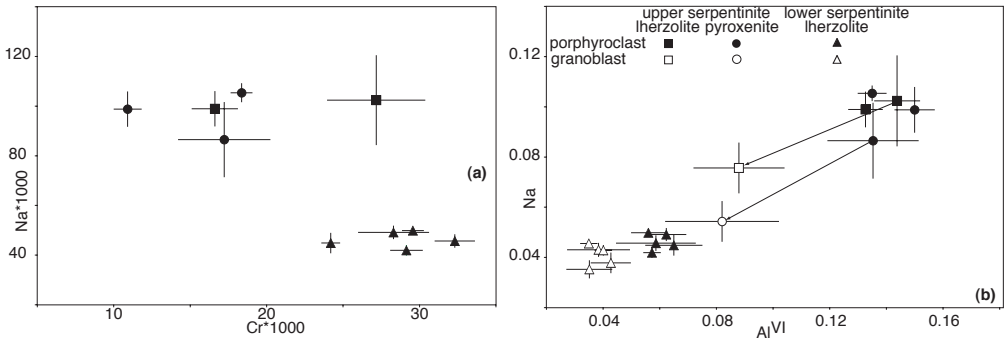

Figure 2-7: Chemical evolution of the clinopyroxenes of the peridotites. Each point represents the average composition of clinopyroxenes from one sample. The error bars represent the standart deviation. (a) Na vs. Cr diagram showing two different groups of clinopyroxenes: The pyroxenes from the lherzolites and the pyroxenites of the upper serpentinite unit show high Na and low Cr contents compared to the clinopyroxenes from the lherzolite of the lower serpentinite unit. (b) Na vs. Al^{VI} diagram showing the chemical evolution of the clinopyroxenes from porphyroclastic to neoblastic minerals. See text for discussion.

Amphibole: First-generation amphiboles are Ti-pargasites occuring as small granoblasts between the large porphyroclastic clino-and orthopyroxenes of the lower serpentinite unit. These amphiboles are rich in Al_2O_3 (12.1-12.9 weight%), TiO_2 (2.9-3.8 weight%) and Cr_2O_3 (1.7-1.9 weight%) but poor in K_2O (<0.07 weight %). As these high-temperature amphiboles are stable within a mantle assemblage, they do not necessarily record hydration of the mantle during rifting but rather indicate reequilibration under decreasing temperature (T<1100°C) and under lithospheric mantle conditions. In contrast, the amphiboles present in coronae statically overgrowing the clinopyroxenes record hydration of the mantle rocks during rifting. The first generation of these retrograde amphiboles is a Mg-hornblende with an Al_2O_3 content of up to 10 weight%. These hornblendes are further retrogressed to tremolitic hornblende characterised by lower Al_2O_3 and Na_2O contents.
Chlorite: Chlorites display different types of composition depending on their occurrence. The chlorites overgrowing the spinel in the mylonitic foliation of the deformed rocks are all chromian clinochlores with up to 13 weight% of Cr_3O_3. They are characterised by a low Si value, high Al and Cr contents and a highly variable Mg# between 0.69 and 0.86. The chlorites overgrowing the orthopyroxenes contain no Cr, have higher Si and lower Al contents and display higher Mg# values between 0.92 and 0.95.

Retrograde metamorphism of the mantle rocks

Thermobarometric calculations have been applied only to the porphyroclastic assemblages as they represent the only microstructures in which fresh orthopyroxene has been found. The single-orthopyroxene thermometers (Witt-Eickschen & Seck 1991) and the Al net-transfer thermometry (Webb & Wood 1986) yield temperatures

of 1000°± 50°C for pressures between 10 and 15 kb. The two-pyroxene thermometer (Brey & Köhler 1990) gives similar temperatures of 1010°±100°C for one of these samples and 810 ± 120°C for another one. The co-existence of spinel, Ti-pargasite and Al-clinopyroxene in the recrystallised assemblage indicates spinel-peridotite facies conditions (Evans 1977, 1982), suggesting that recrystallisation occurred in the upper mantle. We interpret these values as defining the P, T conditions present in the mantle before the onset of rifting.

The crystallisation of coronitic Mg- and tremolitic hornblende around the clinopyroxene documents high-temperature hydration of the mantle rocks during rifting. Such amphiboles are often found to be stable in the presence of orthopyroxene and spinel (e.g. Müntener *et al*. 2000) and therefore may have formed at high temperatures in the ultrabasic rocks (Evans 1982). We suggest that hydration of the mantle rocks started under upper amphibolite facies conditions, *i.e*. at temperatures between 600 and 700°C. Later, pervasive alteration of the mantle rocks below and near the sea floor is finally indicated by the crystallisation of chlorite, tremolite and serpentine minerals replacing the previous assemblages.

Table 2-1. *Representative chemical compositions of the minerals characterizing the metamorphic evolution of the lherzolites and the pyroxenites*

	Lherzolite of the lower serpentinite unit										
	porphyroclast							neoblast			
Sample	MSP		SUP2			NAP99-6		MSP		SUP2	
	cpx	opx	cpx	opx	spi	cpx	phl	spi	cpx	cpx	Ti-par
SiO_2	51.03	55.28	50.37	56.08	0.00	52.70	38.38	0.00	52.10	49.67	43.40
TiO_2	0.56	0.23	0.81	0.34	0.65	0.32	1.84	0.63	0.49	0.96	3.75
Cr_2O_3	1.04	0.79	1.04	0.64	29.16	0.86	0.88	33.03	0.94	1.04	1.84
Al_2O_3	5.74	3.43	4.83	3.06	33.39	4.96	17.48	29.81	3.30	4.26	12.26
Fe_2O_3	0.23	0.14	2.28	0.00	6.09	0.00	0.00	4.28	0.59	2.59	0.00
FeO	2.99	6.65	1.01	6.56	14.88	2.46	3.65	18.44	2.03	0.65	4.36
MnO	0.11	0.19	0.13	0.19	0.29	0.08	0.00	0.14	0.06	0.09	0.05
MgO	15.73	31.80	15.98	32.37	14.48	15.94	22.75	11.59	16.48	16.30	16.82
CaO	22.18	1.97	22.83	1.15	0.05	21.34	0.00	0.05	23.11	22.30	12.34
Na_2O	0.43	0.05	0.67	0.04	0.00	0.93	0.43	0.04	0.41	0.65	3.38
K_2O	0.00	0.00	0.00	0.00	0.00	0.00	8.74	0.00	0.00	0.00	0.05
H_2O	------	------	------	------	------	------	4.21	------	------	------	2.10
Total	100.11	100.61	99.97	100.53	99.19	99.61	98.55	98.20	99.54	98.56	100.53
Si	1.86	1.91	1.85	1.93	0.00	1.91	2.74	0.00	1.91	1.85	6.20
Ti	0.02	0.01	0.02	0.01	0.01	0.01	0.10	0.01	0.01	0.03	0.40
Cr	0.03	0.02	0.03	0.02	0.68	0.02	0.05	0.80	0.03	0.03	0.21
Al	0.25	0.14	0.21	0.12	1.16	0.21	1.47	1.08	0.14	0.19	2.06
Fe^{3+}	0.01	0.00	0.06	0.00	0.13	0.00	0.00	0.10	0.02	0.07	0.00
Fe^{2+}	0.09	0.19	0.03	0.19	0.37	0.07	0.22	0.47	0.06	0.02	0.52
Mn	0.00	0.01	0.00	0.01	0.01	0.00	0.00	0.00	0.00	0.00	0.01
Mg	0.85	1.64	0.88	1.66	0.64	0.86	2.42	0.53	0.90	0.91	3.58
Ca	0.87	0.07	0.90	0.04	0.00	0.83	0.00	0.00	0.91	0.89	1.89
Na	0.03	0.00	0.05	0.00	0.00	0.07	0.06	0.00	0.03	0.05	0.94
K	0.00	0.00	0.00	0.00	0.00	0.00	0.79	0.00	0.00	0.00	0.01
OH^-	------	------	------	------	------	------	2.00	------	------	------	2.00
Mg#	0.90	0.89	0.90	0.90	0.56	0.92	0.92	0.48	0.92	0.91	0.87

Ions calculated on the basis of six oxygens (pyroxenes), 3 cations (spinel, magnetite), 23 oxygens and ∑ (cat)-Ca-Na-K=13 (amphiboles), 18 oxygens (chlorite, serpentine minerals).

Table 2-1 *(continued)*

	Lherzolite of the lower				lherzolite of the upper			Pyroxenite of the upper			
	ocean				porphyroclast		neoblas	porphyroclast			neoblas
Sample	MSP		SUP2		FAP4	VEP8	VEP8	VEP3	FAP4	Cup1	Cup1
	serp	mt	chl	serp	cpx	cpx	cpx	cpx	cpx	cpx	cpx
SiO_2	44.43	0.49	27.97	36.94	51.17	51.87	52.51	51.87	51.74	52.12	51.84
TiO_2	0.03	0.17	0.01	0.03	0.80	0.53	0.44	0.47	0.81	0.60	0.48
Cr_2O_3	0.00	0.00	0.18	0.00	0.58	0.95	0.43	0.71	0.35	0.51	0.47
Al_2O_3	0.47	0.01	20.39	0.45	6.42	6.19	4.29	6.91	7.42	6.89	3.93
Fe_2O_3	0.00	67.88	0.00	0.00	1.75	1.30	1.70	1.51	0.00	0.42	1.54
FeO	1.56	31.09	12.15	9.55	1.60	1.32	0.74	1.20	3.20	2.84	1.28
MnO	0.09	0.09	0.19	0.02	0.09	0.11	0.09	0.04	0.10	0.10	0.12
MgO	39.09	0.20	25.92	35.28	15.15	15.18	16.30	14.43	13.67	15.96	16.57
CaO	1.25	0.04	0.15	0.09	21.41	21.21	22.67	21.34	21.27	19.28	22.11
Na_2O	0.02	0.05	0.00	0.02	1.41	1.46	1.07	1.86	1.58	1.47	0.82
K_2O	0.02	0.00	0.00	0.01	0.00	0.01	0.02	0.03	0.03	0.02	0.00
H_2O	12.92	------	12.11	11.61	------	------	------	------	------	------	------
Total	100.00	100.14	99.07	94.12	100.41	100.19	100.30	100.48	100.26	100.32	99.21
Si	2.06	0.02	2.77	3.82	1.86	1.88	1.90	1.88	1.87	1.88	1.90
Ti	0.00	0.00	0.00	0.00	0.02	0.01	0.01	0.01	0.02	0.02	0.01
Cr	0.00	0.00	0.01	0.00	0.02	0.03	0.01	0.02	0.01	0.01	0.01
Al	0.03	0.00	2.38	0.05	0.27	0.26	0.18	0.29	0.32	0.29	0.17
Fe^{3+}	0.00	1.96	0.00	0.00	0.05	0.04	0.05	0.04	0.00	0.01	0.04
Fe^{2+}	0.06	1.00	1.01	0.82	0.05	0.04	0.02	0.04	0.10	0.09	0.04
Mn	0.00	0.00	0.02	0.00	0.00	0.00	0.00	0.00	0.00	0.00	0.00
Mg	2.70	0.01	3.83	5.43	0.82	0.82	0.88	0.78	0.74	0.86	0.91
Ca	0.06	0.00	0.02	0.01	0.83	0.82	0.88	0.83	0.82	0.74	0.87
Na	0.00	0.00	0.00	0.00	0.10	0.10	0.08	0.13	0.11	0.10	0.06
K	0.00	0.00	0.00	0.00	0.00	0.00	0.00	0.00	0.00	0.00	0.00
OH^-	8.00	------	8.00	8.00	------	------	------	------	------	------	------
Mg#	0.98	0.00	0.79	0.87	0.90	0.92	0.93	0.91	0.88	0.90	0.92

Table 2-1 *(continued)*

	Pyroxenite of the upper serpentinite unit				
	oceanic alteration				
Sample	VEP3		CUP1		
	chl	Cr-chl	Cr-chl	serp	mt
SiO_2	34.38	22.39	24.39	42.00	0.42
TiO_2	0.04	0.10	0.10	0.03	0.59
Cr_2O_3	0.62	13.51	4.93	0.24	0.38
Al_2O_3	12.83	11.21	21.81	4.95	0.04
Fe_2O_3	0.00	0.00	0.00	0.00	65.28
FeO	3.70	17.56	7.38	5.16	30.95
MnO	0.03	0.82	0.27	0.19	0.15
MgO	34.36	23.55	27.46	34.46	0.21
CaO	0.03	0.10	0.26	0.71	0.14
Na_2O	0.00	0.18	0.01	0.01	0.00
K_2O	0.00	0.03	0.02	0.02	0.00
H_2O	12.56	11.29	12.09	12.83	------
Total	98.56	101.07	98.92	100.62	98.16
Si	3.28	2.38	2.42	3.93	0.02
Ti	0.00	0.01	0.01	0.00	0.02
Cr	0.05	1.13	0.39	0.02	0.01
Al	1.44	1.40	2.55	0.55	0.00
Fe^{3+}	0.00	0.00	0.00	0.00	1.92
Fe^{2+}	0.30	1.56	0.61	0.40	1.01
Mn	0.00	0.07	0.02	0.02	0.01
Mg	4.89	3.73	4.06	4.80	0.01
Ca	0.00	0.01	0.03	0.07	0.01
Na	0.00	0.04	0.00	0.00	0.00
K	0.00	0.00	0.00	0.00	0.00
OH^-	8.00	8.00	8.00	8.00	------
Mg#	0.94	0.70	0.87	0.92	0.00

Gabbroic intrusions

Field relationships

The mantle rocks of the lower serpentinite unit of the Platta nappe are intruded by gabbros and locally by rodingitised mafic dykes. Magmatic intrusions within the upper serpentinite unit are limited to few dolerite dykes and a single small gabbro sill. In Val da Natons, the exhumation history of a gabbro from shallow intrusion into serpentinised peridotite to exposure on the sea floor can be documented (Fig. 2-8). A cataclastic gabbro which is cut by small dykes of albitite (Fig. 2-9c) includes enclaves of serpentinite and fractures filled by ophicalcite. It is stratigraphically overlain by a sedimentary megabreccia including first metre-sized blocks of serpentinite, then of gabbro set in a matrix of serpentine arenite. A few gabbro blocks, several metres across, show localised bands of flaser gabbro fragmented and overprinted by cataclastic deformation (Fig. 2-9a, b). An overlying breccia contains clasts of these flaser gabbros together with serpentinite and abundant pillow-basalt fragments embedded in a matrix of serpentinite arenite. The breccias are overlain by pillow breccias covered in turn by red shales. The absence of a pre-Alpine foliation and the random arrangement of the unsorted polymictic blocks suggest that the gabbro breccias have a sedimentary origin. Together, these observations show that the gabbros were exhumed on the sea floor along discrete shear zones active under decreasing temperatures. Clasts of flaser gabbro and albitite occur also in pillow-breccias overlying the exposed mantle rocks in Val Savriez (Fig. 2-9d).

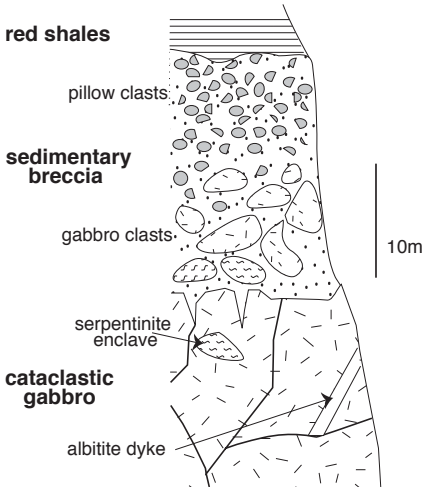

Figure 2-8: Stratigraphic succession from exhumed gabbro to overlying sediments. Val da Natons (Coordinates of Swiss Topographic Map: 770'690 to '850/152'200 to '300).

In the Fuorcla da Faller area, a gabbro body shows a great diversity in composition and mineralogy suggesting a complex intrusion history. The main part of this body (90%) consists of coarse-grained Mg-gabbro (clinopyroxene-plagioclase) with localised high-temperature shear zones. In places, the gabbro grades into a microgabbro of the same mineralogy (Fig. 2-10a), locally it is cut by the latter (Fig. 2-10b). The microgabbro crystallised simultaneously with a Fe-gabbro (clinopyroxene-hastingistic hornblende-Fe-oxide-plagioclase, 5% of the outcrop, Fig. 2-10a) and is cut by a Fe-Ti-P-gabbro (clinopyroxene-pargasitic hornblende-ilmenite-plagioclase-apatite-zircon). Pegmatitic diorite (pargasitic hornblende-plagioclase-clinopyroxene-

quartz, Fig. 2-10c) occurs as patches or dykes, which can form boudins or folds within the Mg-gabbro. The entire gabbro body is cut by basaltic dykes with chilled margins indicating that emplacement of the basalts took place after cooling of the gabbro.

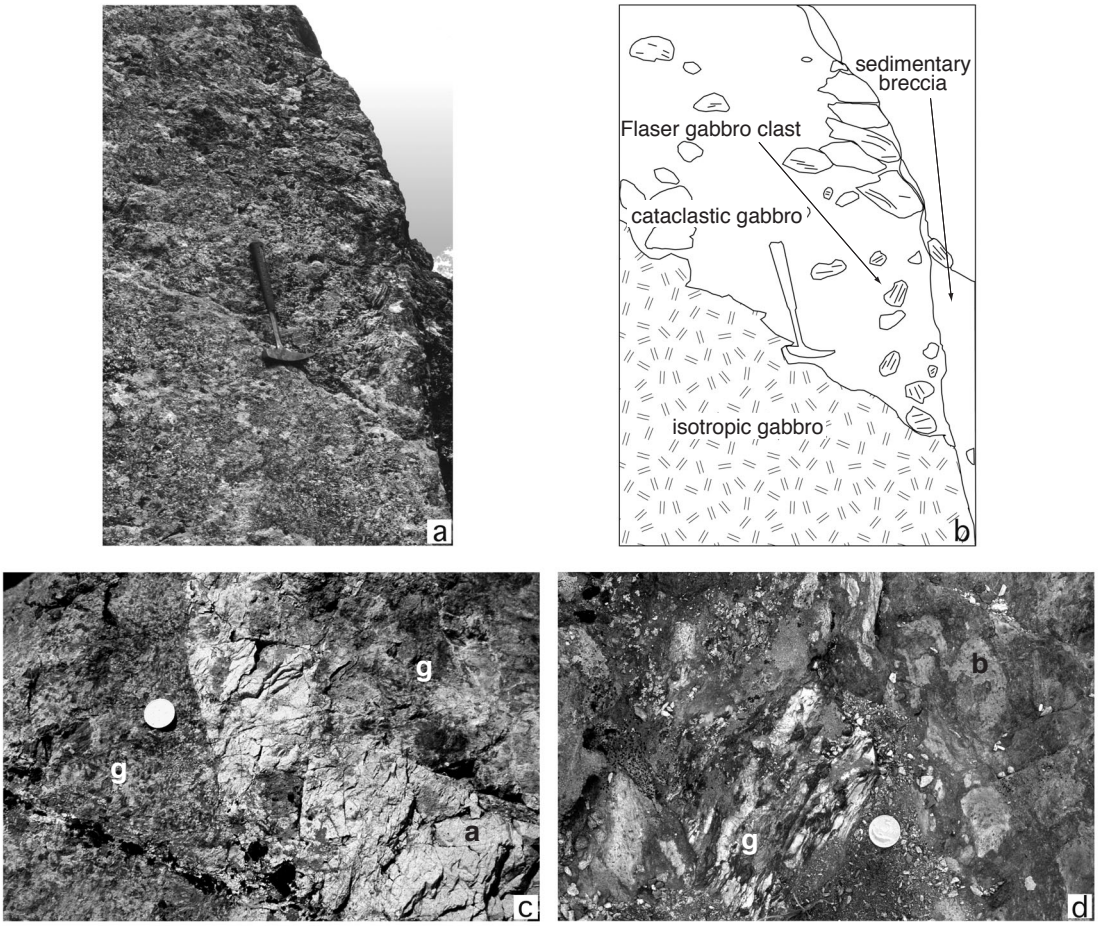

Figure 2-9: (a) and (b) Coarse-grained isotropic Mg-gabbro (below) with a zone of flaser gabbro overprinted and disrupted by cataclastic deformation (above). The unconformably overlying sedimentary breccia to the right contains clasts of both flaser and undeformed gabbro (hammer is 33 cm long). Val da Natons (Coordinates of Swiss Topographic Map: 770'690/152'200). (c) Albitite dyke (a) within a Mg-gabbro (g) (diameter of coin: 2.3 cm). Val da Natons (Coordinates of Swiss Topographic Map: 770'830/152'250). (d) Pillow (b) breccia with fragments of flaser gabbro (g) (diameter of coin: 2 cm). Val Savriez (Coordinates of Swiss Topographic Map: 771'725/153'660).

Contact with mantle rocks

Above Alp da Starschagns, the serpentinites show evidence of contact metamorphism along the contact with the gabbro sills intruding them. These intrusions are characterised by chilled margins and intense veining is observed within the serpentinite near the contact with the gabbros. Thin-sections show the veins to cut accross the pre-existing serpentine mesh; they consist of chlorite minerals growing parallel to the edges of the veins and of tremolite growing perpendicularly to them. Inside the veins, equigranular grains of diopside and antigorite? overgrow tremolite and serpentine minerals. This mineral assemblage occurs also in patches within the serpentinites suggesting that these were metamorphosed by hot fluids during the intrusion of the dyke. Where the contact was not overprinted by later deformation, it

appears that the intrusion of the gabbroic sills led to prograde metamorphism of the already serpentinized mantle rocks.

Age

One Fe-Ti-P-gabbro from the Fuorcla da Faller area, an associated diorite, a pegmatitic Mg-gabbro from Val da Natons and an albitite clast from a pillow breccia in Val Savriez were dated by U-Pb on zircon (Desmurs *et al*. 1999). These four rocks gave an identical intrusion age of 161±1 Ma (middle-late Callovian in the time scale of Gradstein *et al*. 1995) and belong to the same very short-lived magmatic event.

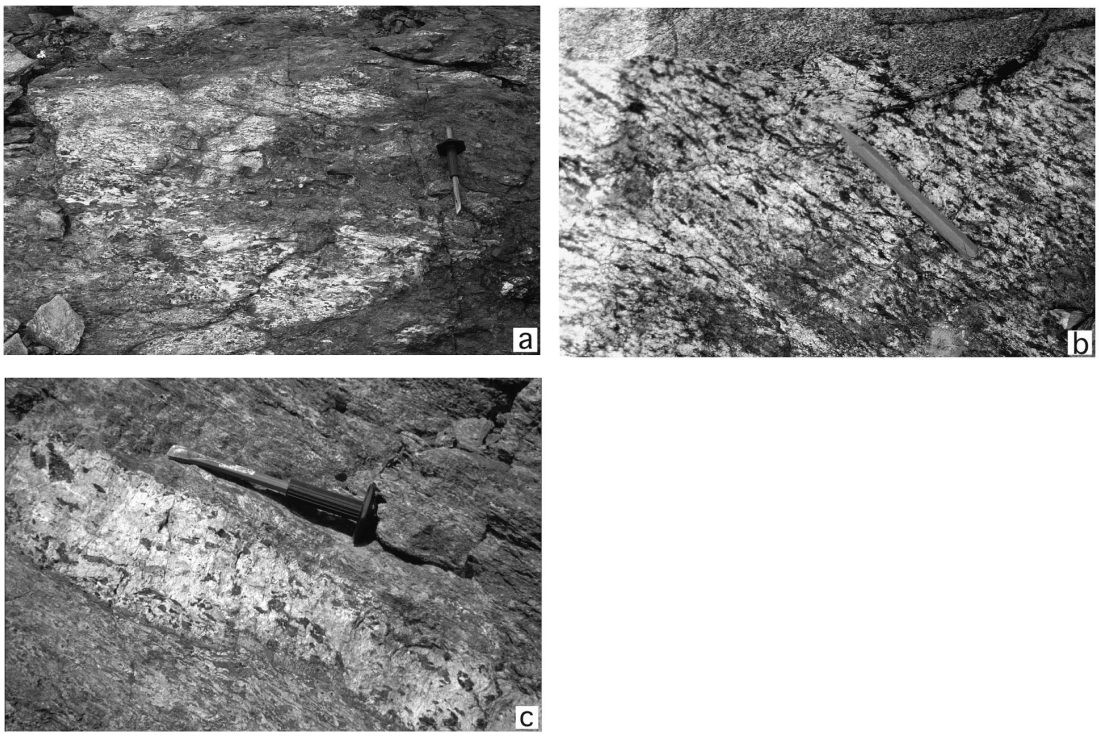

Figure 2-10: (a) Mg-gabbro grading into a darker Fe-gabbro (chisel is 28 cm long). Fuorcla da Faller (Coordinates of Swiss Topographic Map: 765'150/177'650). (b) Mg-flaser gabbro cut by Mg-microgabbro (pencil is 9.5 cm long). Fuorcla da Faller (Coordinates of Swiss Topographic Map: 765'150/177'650). (c) Pegmatitic diorite dyke cutting across a Mg-gabbro (chisel is 28 cm long). Fuorcla da Faller (Coordinates of Swiss Topographic Map: 765'150/177'650).

Magmatic and deformational textures

Most of the gabbros of the Platta nappe show a well preserved magmatic texture, whereas the magmatic mineral assemblage was partially hydrated. This is shown by the growth of amphibole at the expense of pyroxene. Hydration was followed by a more widespread low-temperature alteration recorded by the systematic break-down of plagioclase to albite, chlorite, and epidote.
At Fuorcla da Faller, the Mg-gabbros (coarse grained and microgabbro) show euhedral plagioclase, sub- to anhedral clinopyroxene and interstitial Ti-pargasite (Fig. 2-11a). In many places clinopyroxene and plagioclase show graphic intergrowth indicating cotectic crystallisation of the two phases. The plagioclase was altered to a fine-grained mixture of albite, chlorite and epidote and later to prehnite and pumpellyite; the pyroxenes show a rim of hornblende. The Fe-gabbros consist of

anhedral to subhedral clinopyroxene and plagioclase with interstitial iron oxide. Hastingitic hornblende developed between the iron oxide and the clinopyroxene. The Fe-Ti-P gabbro is made of euhedral plagioclase and apatite, subhedral clinopyroxene, and of interstitial pargasite and ilmenite (Fig. 2-11b); euhedral zircon occurs as an accessory mineral. As in the Fe-gabbro, pargasitic hornblende developed between ilmenite and clinopyroxene and the plagioclase shows the same alteration as in the other gabbro types. A younger rim of actinolite is present around the pyroxene and the pargasite. It is interpreted to result from Alpine overprint. The pegmatitic diorite is made of large euhedral plagioclase crystals, large sub-to anhedral magnesian hornblende, rare and strongly altered clinopyroxene showing symplectitic texture with an unidentified phase, quartz, and zircon. Clinopyroxenes with a similar texture occur also in the Mg-gabbro at the contact with the diorite suggesting that the clinopyroxenes within the diorite are xenocrysts from the Mg-gabbro.

In Val da Natons, all gabbros types (Mg- and Fe-Ti-P-gabbro) are cut by discrete mylonitic shear zones. Deformation occurred under decreasing temperatures. The highest temperature deformation event is recorded by a high-temperature foliation defined by small clinopyroxene, pargasite and apatite granoblasts showing typical triple-junction grain boundaries. Pargasite and all the ilmenite occur also as undeformed interstitial grains between the neoblasts indicating that they are of magmatic origin (Fig. 2-11c, d). These observations suggest that the earliest deformation was syn-magmatic because granoblastic and interstitial magmatic grains coexist within the foliation. As no evidence for the deformation of ilmenite was found, deformation probably ceased when the temperature fell below the solidus.

In other shear zones, still in Val da Natons, the clinopyroxene porphyroclasts were statically retrogressed to brown Mg-hornblende and later to actinolite, and the mylonitic foliation is defined by small neoblasts of actinolite and albite. In a few shear zones, albite, elongated chlorite and biotite crystallised between clasts of stretched pyroxene aligned parallel to the foliation (Fig. 2-11e). The recrystallisation of albite and actinolite and the deformation of chlorite and biotite suggest that these shear zones were active under lower amphibolite- to greenschist-facies conditions. These zones of deformation were later affected by cataclastic deformation and intense veining during which epidote, chlorite and albite crystallised.

Mineral chemistry

Clinopyroxene (Table 2-2): The augitic clinopyroxenes of the gabbros of the Platta nappe are characterized by their low Al_2O_3 (<3.4 weight %), Na_2O (0.6 weight %) and Cr_2O_3 (<0.07 weight %) contents which are similar for the different gabbro types. However, the Mg# of these minerals continuously decreases from the Mg- and microgabbro (0.74-0.80) to the Fe-gabbro (0.69-0.71) and the highly differentiated Fe-Ti-P-gabbro (0.61-0.69). This decrease in Mg# correlates with an increase of MnO and a decrease of TiO_2 and Al^{IV} (Fig. 2-12a, b, c). According to Ulmer (1986), this decrease could be related to a decrease of the temperature of crystallisation, however, the clinopyroxenes of the highly differentiated pegmatitic diorite show the highest Mg# (0.83-0.89) of the entire gabbro suite. These clinopyroxenes could therefore represent xenocrysts from the Mg-gabbro host-rock preserved within the diorite. This interpretation is favoured by their composition similar to that of the clinopyroxenes of the Mg-gabbro.

In the high-temperature mylonitic Fe-Ti-P-gabbro, the neoblasts are slightly different from the porphyroclasts. They show a decrease in Al_2O_3 from 1.1-1.8 weight% from the porphyroclasts to 0.7-1.1 weight% in the neoblasts and in Na_2O from 0.6-0.95 to 0.42-0.53 weight%, respectively.

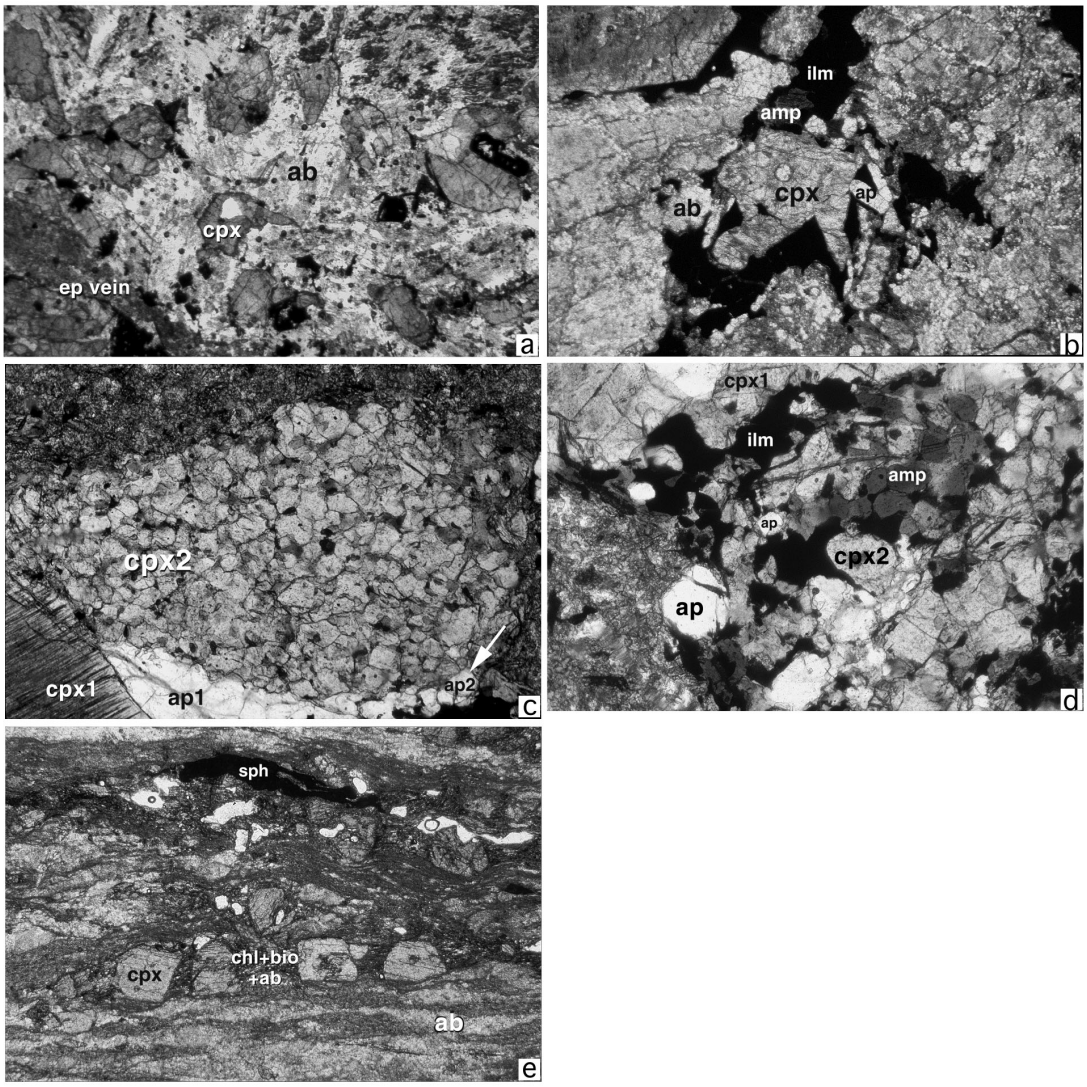

Figure 2-11: (a) Magmatic assemblage of Mg-gabbro with euhedral plagioclase (now albite, ab) and interstitial clinopyroxene (cpx). Note the late epidote (ep) vein cutting across the magmatic texture. Fuorcla da Faller. Length of picture 6.3 mm, plane light. (b) Magmatic assemblage of Fe-Ti-P-gabbro with numerous grains of apatite (ap), pargasite (amp) and interstitial ilmenite (ilm). Fuorcla da Faller. Length of picture 6.3 mm, plane light. (c) Neoblastic clinopyroxene (cpx2) within a high-temperature shear zone in a Fe-Ti-P-gabbro. Note the large porphyroclasts of clinopyroxene (cpx1) and apatite (ap1) and the interstitial brown magmatic amphiboles between the clinopyroxene neoblasts, Val da Natons. Length of picture 1.2 mm, plane light. (d) Neoblastic pargasite and apatite with interstitial magmatic ilmenite within the same shear zone. Val da Natons. Length of picture 1.2 mm, plane light. (e) Low-temperature shear zone within a Mg-gabbro. The clinopyroxenes are rotated or brittlely stretched whereas the albite and sphene (sph) were ductilely deformed; the space between the clinopyroxene clasts is filled by the assemblage chlorite (chl)+biotite (bio)+albite (ab). Val da Natons. Length of picture 6.3 mm, plane light.

Plagioclase: All plagioclases in the gabbros of the Platta nappe are now pure albite and no relics of a more anorthitic composition have been found.

Amphibole: Crystallisation of magmatic brown amphibole was observed in all gabbro types but is more frequent in the differentiated gabbros (Fe-, Fe-Ti-P-gabbro and diorite). These magmatic amphiboles are Ti-rich calcic amphiboles and plot in the Ti-pargasite to edenitic hornblende fields according to the classification of Leake (1978). Only the amphiboles of the Fe-gabbro show a hastingistic composition. They are characterised by rather high TiO_2 (4.3-3.1 weight%) and Al_2O_3 (up to 13 weight%) contents and a low Na^{M4} content (0.13-0.29 p.f.u.). The neoblastic amphiboles of the mylonitic shear zones show a composition similar to that of the magmatic amphiboles suggesting that deformation started at high temperature (syn-magmatic) compatible with the textural observations.

The retrograde coronitic amphiboles in the diorites and the Fe-Ti-P gabbros are magnesian hornblendes whereas those of the Mg-gabbros plot in the edenite field. They show lower Al_2O_3 (4.6-9.1 weight%) and TiO_2 (1.5-2.1 weight%) contents than the first generation of amphiboles. Again, their Na^{M4} (0.07-0.2 p.f.u) is rather low. They show systematically higher Mg# than the high-temperature amphiboles in the same rock type.

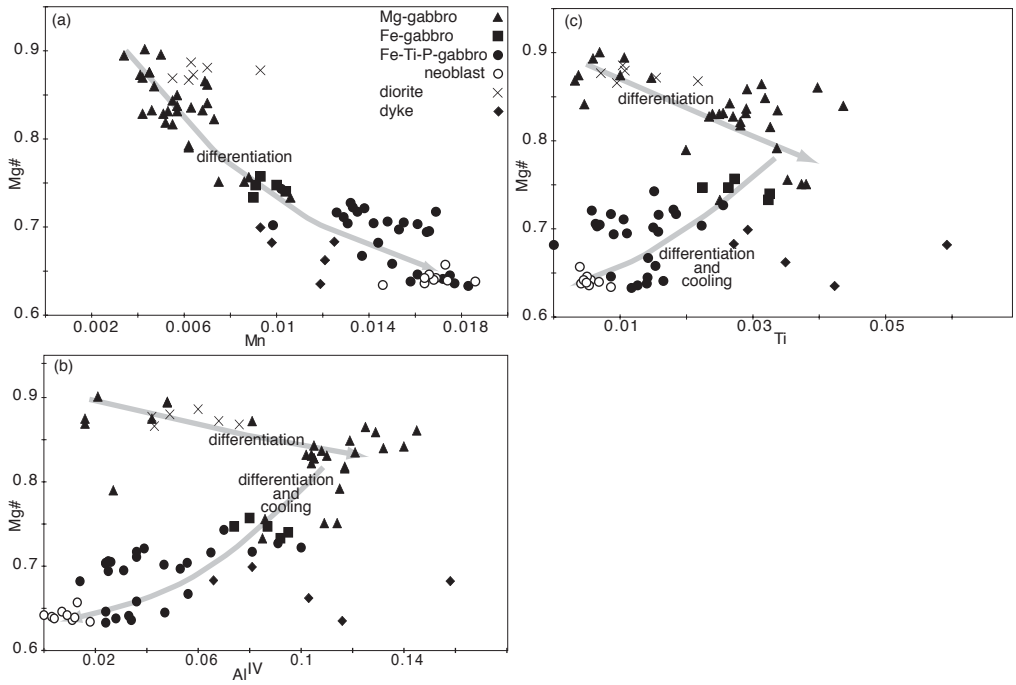

Figure 2-12: Chemical evolution of the clinopyroxenes of the different gabbros. (a) Mg# ($Mg/Mg+Fe^{2+}$) vs. Mn diagram showing an increase of Mn from Mg-gabbro to Fe-Ti-P-gabbro and decreasing Mg# reflecting the magmatic differentiation. (b) Mg# vs. Al^{IV} showing first an increase of Al^{IV} during magmatic differentiation and then a decrease of Al^{IV} during further differentiation due to lower crystallisation temperatures of the more differentiated gabbros. (c) Mg# vs. Ti diagram showing Ti first increasing with magmatic differentiation and then decreasing with ongoing differentiation due to lower crystallisation temperatures of the more differentiated gabbros.

Table 2-2. *Representative chemical compositions of the magmatic and retrograde minerals of the gabbros*

	Magmatic assemblage												
	Mg-gabbro					Fe-gabbro					Fe-Ti-P-gabbro		
Sample	MS8		MS9	NAG3	NAG9	MS3		NAG5			P2		
	cpx	Hbl	cpx	cpx	cpx	cpx	Hbl	cpx	Hbl	ilm	cpx	Hbl	ilm
SiO_2	50.40	42.52	50.87	50.88	51.93	50.96	42.05	52.30	42.50	0.45	51.51	42.50	0.04
TiO_2	1.43	4.31	1.21	0.85	0.53	0.93	4.37	0.39	3.13	49.86	0.56	3.11	47.98
Cr_2O_3	0.03	0.06	0.07	0.13	0.16	0.00	0.02	0.03	0.02	0.02	0.01	0.00	0.03
Al_2O_3	3.41	12.00	3.44	2.74	3.35	2.55	10.85	1.20	9.86	0.05	1.89	11.26	0.39
Fe_2O_3	3.69	2.11	2.16	0.00	1.57	1.82	2.40	1.00	3.06	3.17	2.35	1.03	6.35
FeO	4.30	8.49	5.18	5.70	4.19	8.63	11.93	10.26	13.73	41.86	9.32	13.30	39.91
MnO	0.22	0.12	0.20	0.18	0.13	0.31	0.13	0.52	0.32	2.20	0.40	0.24	2.97
MgO	14.99	14.60	14.73	15.71	15.94	14.28	12.46	13.12	11.26	0.31	13.19	11.86	0.07
CaO	21.66	11.21	21.78	22.61	20.77	19.87	10.79	20.63	10.34	0.15	19.93	11.11	0.01
Na_2O	0.54	3.17	0.51	0.41	0.83	0.58	2.95	0.59	3.14	0.10	0.71	3.33	0.03
K_2O	0.02	0.14	0.00	0.01	0.04	0.01	0.29	0.00	0.16	0.01	0.01	0.30	0.00
H_2O	---	2.08	---	---	---	---	2.03	---	2.00	---	---	2.03	---
Total	100.7	100.8	100.1	99.27	99.43	99.95	100.2	100.0	99.57	98.23	99.88	100.0	97.77
Si	1.85	6.14	1.88	1.90	1.92	1.91	6.21	1.97	6.37	0.01	1.94	6.30	0.00
Ti	0.04	0.47	0.03	0.02	0.01	0.03	0.49	0.01	0.35	0.96	0.02	0.35	0.93
Cr	0.00	0.01	0.00	0.00	0.00	0.00	0.00	0.00	0.00	0.00	0.00	0.00	0.00
Al	0.15	2.04	0.15	0.12	0.15	0.11	1.89	0.05	1.74	0.00	0.08	1.97	0.01
Fe^{3+}	0.10	0.23	0.06	0.00	0.04	0.05	0.27	0.03	0.34	0.06	0.07	0.12	0.12
Fe^{2+}	0.13	1.03	0.16	0.18	0.13	0.27	1.47	0.32	1.72	0.90	0.29	1.68	0.86
Mn	0.01	0.01	0.01	0.01	0.00	0.01	0.02	0.02	0.04	0.05	0.01	0.03	0.07
Mg	0.82	3.14	0.81	0.87	0.88	0.80	2.74	0.74	2.52	0.01	0.74	2.62	0.00
Ca	0.85	1.73	0.86	0.90	0.82	0.80	1.71	0.83	1.66	0.00	0.80	1.77	0.00
Na	0.04	0.89	0.04	0.03	0.06	0.04	0.84	0.04	0.91	0.00	0.05	0.96	0.00
K	0.00	0.03	0.00	0.00	0.00	0.00	0.05	0.00	0.03	0.00	0.00	0.06	0.00
OH	---	2.00	---	---	---	---	2.00	---	2.00	2.00	---	2.00	---
Mg#	0.78	0.71	0.79	0.83	0.84	0.71	0.61	0.68	0.55	0.01	0.67	0.59	0.00

Calculations as in Table 1; 2 cations (ilmenite), 12 oxygens (epidote) and 3 cations (sphene).

Table 2-2 *(Continued)*

	Magmatic assemblage				HT		Static HT hydration			LT deformation			
Sample	Fe-Ti-gabbro			diorite	Fe-Ti-gabbro		Mg-	Fe-	Fe-Ti-	Mg-gabbro			
	NAG7			MS10	NAG7		NAG9	NAG5	P2	NAG9	NAG3		
	cpx	Hbl	ilm	cpx	cpx	hbl	Hbl	Hbl	Hbl	Tr	biot	chl	ab
SiO_2	51.70	43.08	0.01	53.03	52.53	43.35	47.95	43.64	47.66	54.90	37.29	29.25	69.13
TiO_2	0.54	2.15	49.18	0.25	0.17	2.77	0.86	1.24	1.82	0.46	0.23	0.09	0.00
Cr_2O_3	0.00	0.00	0.01	0.05	0.00	0.03	0.21	0.00	0.00	0.09	0.02	0.04	0.00
Al_2O_3	1.38	8.99	0.00	1.37	0.82	8.94	8.11	9.89	6.53	2.51	15.94	16.73	20.39
Fe_2O_3	1.09	4.23	4.28	1.69	0.46	4.18	0.00	8.63	1.75	1.09	0.00	0.00	0.00
FeO	11.12	13.62	39.37	3.99	12.03	12.41	8.22	9.47	12.65	4.63	18.04	22.47	0.19
MnO	0.47	0.30	4.07	0.30	0.54	0.29	0.09	0.52	0.50	0.10	0.23	0.41	0.02
MgO	12.01	10.52	0.06	16.00	11.96	11.41	16.55	12.49	13.32	20.54	11.72	13.90	0.02
CaO	20.75	10.88	0.31	22.75	21.08	10.55	13.04	8.59	11.23	12.79	0.46	0.18	0.06
Na_2O	0.68	2.72	0.00	0.52	0.49	3.08	2.00	2.92	2.01	0.76	0.09	0.04	10.38
K_2O	0.02	0.28	0.00	0.01	0.00	0.26	0.09	0.10	0.33	0.06	8.08	1.96	0.05
H_2O	---	1.98	---	---	---	2.00	2.08	2.03	2.04	2.16	3.82	15.54	---
Total	99.75	98.82	97.53	99.97	100.0	99.28	99.26	99.52	99.86	100.0	96.00	100.6	100.2
Si	1.96	6.52	0.00	1.96	1.99	6.49	6.92	6.46	7.00	7.64	2.93	4.51	3.04
Ti	0.02	0.24	0.96	0.01	0.00	0.31	0.09	0.14	0.20	0.05	0.01	0.01	0.00
Cr	0.00	0.00	0.00	0.00	0.00	0.00	0.02	0.00	0.00	0.01	0.00	0.00	0.00
Al	0.06	1.60	0.00	0.06	0.04	1.58	1.38	1.72	1.13	0.41	1.48	3.04	1.06
Fe^{3+}	0.03	0.48	0.08	0.05	0.01	0.47	0.00	0.96	0.19	0.11	0.00	0.00	0.00
Fe^{2+}	0.35	1.73	0.85	0.12	0.38	1.55	0.99	1.17	1.55	0.54	1.19	2.90	0.01
Mn	0.02	0.04	0.09	0.01	0.02	0.04	0.01	0.07	0.06	0.01	0.02	0.05	0.00
Mg	0.68	2.37	0.00	0.88	0.67	2.55	3.56	2.75	2.92	4.26	1.37	3.20	0.00
Ca	0.84	1.76	0.01	0.90	0.85	1.69	2.02	1.36	1.77	1.91	0.04	0.03	0.00
Na	0.05	0.80	0.00	0.04	0.04	0.89	0.56	0.84	0.57	0.20	0.01	0.01	0.89
K	0.00	0.05	0.00	0.00	0.00	0.05	0.02	0.02	0.06	0.01	0.81	0.39	0.00
OH	---	2.00	---	---	---	2.00	2.00	2.00	2.00	2.00	2.00	16.00	---
Mg#	0.64	0.52	0.00	0.84	0.63	0.56	0.78	0.56	0.63	0.87	0.54	0.52	0.16

Table 2-2 *(Continued)*

Sample	Static oceanic alteration							
	Mg-gabbro			Fe-gabbro		Fe-Ti-P-gabbro		
	MSG			MS3		NAG7		
	chl	epi	ab	sph	act	sph	act	chl
SiO_2	26.78	37.01	67.23	30.53	56.55	31.17	54.05	27.03
TiO_2	0.16	0.00	0.00	39.67	0.05	34.89	0.05	0.00
Cr_2O_3	0.01	0.03	0.01	0.00	0.01	0.01	0.00	0.00
Al_2O_3	20.61	21.18	20.88	0.43	0.62	1.51	0.72	16.49
Fe_2O_3	0.00	15.88	0.00	0.79	0.31	1.59	0.86	0.00
FeO	24.60	0.00	0.12	0.00	7.18	0.00	15.86	26.80
MnO	0.45	0.08	0.03	0.00	0.19	0.00	0.25	0.31
MgO	13.48	0.05	0.10	0.01	19.77	0.14	13.18	13.81
CaO	0.05	23.16	0.99	28.77	12.80	29.10	11.76	0.23
Na_2O	0.02	0.06	9.71	0.00	0.55	0.01	0.81	0.01
K_2O	0.01	0.01	0.03	0.00	0.08	0.00	0.03	0.02
H_2O	15.76	1.85	---	0.17	2.15	0.45	2.05	15.20
Total	101.97	99.40	99.10	100.38	100.25	98.88	99.62	99.93
Si	4.08	2.99	3.00	0.99	7.90	1.02	7.92	4.26
Ti	0.02	0.00	0.00	0.97	0.01	0.86	0.01	0.00
Cr	0.00	0.00	0.00	0.00	0.00	0.00	0.00	0.00
Al	3.70	2.02	1.10	0.02	0.10	0.06	0.12	3.07
Fe^{3+}	0.00	0.97	0.00	0.02	0.03	0.04	0.09	0.00
Fe^{2+}	3.13	0.00	0.00	0.00	0.84	0.00	1.94	3.54
Mn	0.06	0.01	0.00	0.00	0.02	0.00	0.03	0.04
Mg	3.06	0.01	0.01	0.00	4.12	0.01	2.88	3.25
Ca	0.01	2.01	0.05	1.00	1.92	1.02	1.85	0.04
Na	0.01	0.01	0.84	0.00	0.15	0.00	0.23	0.00
K	0.00	0.00	0.00	0.00	0.01	0.00	0.01	0.00
OH	16.00	1.00	---	0.04	2.00	0.10	2.00	16.00
Mg#	0.49	0.01	0.60	0.03	0.83	0.15	0.59	0.48

A last generation of pre-Alpine amphiboles consists of actinolites forming rims around the pargasitic hornblende and the clinopyroxene or underlining, together with albite neoblasts, a mylonitic foliation. They are characterised by low Al_2O_3 (0.62-2.53 weight%) and TiO_2 (0.02-0.09 weight%) contents and differ from the Alpine actinolite by their low Na^{M4} (0.02-0.09 p.f.u. versus 0.49-1.02 p.f.u. for the Alpine actinolite).

The evolution of the composition of the amphiboles is shown in Fig. 2-13a, where two trends can be observed, one related to magmatic, the other to metamorphic processes. The first trend shows a decrease of the Mg# with Ti for the high-temperature amphiboles from the Mg- to the Fe-Ti-P gabbros. This suggests that the Ti-rich amphiboles record magmatic differentiation (reflected by the Mg#) under decreasing crystallisation temperatures (reflected by the Ti content; Heltz 1973; Otten 1984). The second trend shows increasing Mg# with decreasing Ti from the high-temperature to the retrograde amphiboles suggesting ongoing hydration of the gabbro under decreasing temperatures. Figures 2-13b, c, d show a general decrease of Al^{IV} and Na + K^A together with Na^{M4} and Al^{VI} + Fe^{3+} + Cr. The decrease in Al^{IV} and Na + K^A is thought to be temperature sensitive while Na^{M4} and Al^{VI} reflect the pressure at a given Al^{IV} and Na+K^A (Laird 1982 and references therein). Thus, these diagrams allow to qualitatively evaluate the P, T conditions of crystallisation of the different generations of amphiboles. The magmatic amphiboles are characterised by high Al^{IV} and Na + K^A values indicating high-temperature crystallisation and rather low Na^{M4} and Al^{VI} suggesting a low-pressure environment. Part of the coronitic amphiboles plot within the same field suggesting high temperature hydration of the gabbros. A second group of coronitic and neoblastic amphiboles is characterised by lower Al^{IV} and Na + K^A and very low Na^{M4} and Al^{VI} + Fe + Cr^{3+} indicating that they formed when the gabbro

was at relatively shallow depth. A third group can be distinguished by their low Al^{IV} and Na + K^A contents, and high Na^{M4} and Al^{VI} + Fe^{3+} + Cr. These low-temperature, high-pressure amphiboles most probably crystallised during Alpine metamorphism.

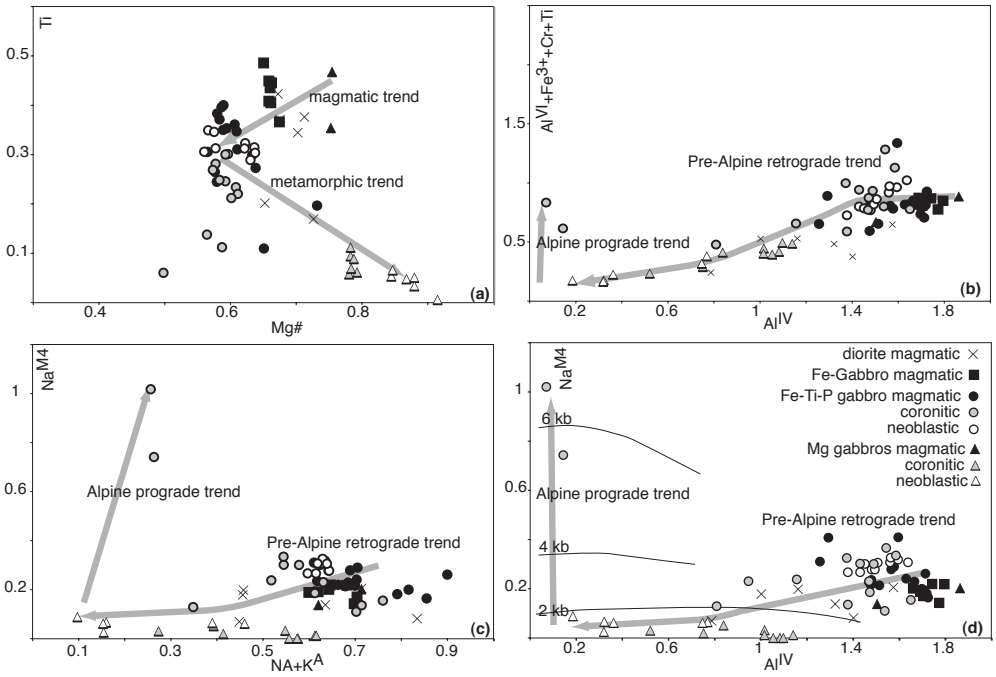

Figure 2-13: Chemical evolution of the amphiboles of the different gabbros. (a) Ti versus Mg# diagram showing two different trends. The first is a magmatic trend showing decreasing Ti contents and decreasing Mg# in the high-temperature amphiboles from the Mg- to the Fe-Ti-P-gabbros. The second, metamorphic trend shows increasing Mg# and decreasing Ti contents in all gabbro types indicating hydration under decreasing temperatures. (b) Al^{VI}+Fe^{3+}+Cr+Ti vs. Al^{IV} diagram . (c) Na^{M4} vs. Na+K^A diagram and (d) Na^{M4} vs. Al^{VI} from Brown (1977). The pressure estimates apply only to the low Al (IV), i.e. the actinolitic amphiboles. Discussion in the text.

Conditions of intrusion

The conditions of the intrusion of the gabbros are determined by the crystallisation sequence and by the chemical composition of the clinopyroxenes. All the gabbros except the Fe-Ti-P-gabbro show idiomorphic plagioclase and interstitial clinopyroxene suggesting that the plagioclase was the first phase to crystallise. This crystallisation sequence suggests an emplacement at a pressure less than 8 Kb (Green & Ringwood 1967; Bender *et al*. 1978, Elthon & Scarfe 1984). This is supported by the low Al_2O_3 and Na_2O contents of the augite in all the gabbro types. Fig. 2-14 shows that the clinopyroxenes have a composition close to that of clinopyroxenes from oceanic gabbros and show a composition different from that of the pyroxenes of high-pressure gabbros like the Permian Braccia Gabbro of Val Malenco (Hermann *et al*. in press). As magmatic amphiboles are observed in all gabbro types, the temperature of crystallisation of the gabbros can be constrained to less than 1100°C which is the upper thermal stability for amphibole in basaltic systems (Allen *et al*. 1975). The clinopyroxene geobarometer (Nimis & Ulmer 1998) gives pressures below 5 kb at temperatures between 1000°C and 1100°C for all gabbros. The thermometer of Otten (1984) based on the Ti content of hornblende gives temperatures between 950 and 1025 °C for the magmatic amphiboles of the diorite, the Fe- and the Fe-Ti-P-gabbros. The observation that the gabbros intruded already serpentinized peridotites

places the intrusion of the gabbros above the serpentinisation front, i.e around 6 to 8 km or around 2 kb according to the interpretation of the change of seismic velocities west of Iberia (Boillot *et al*. 1992).

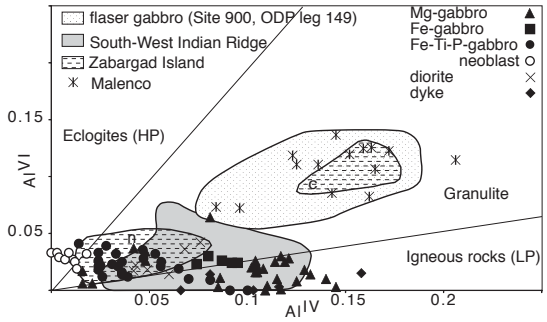

Figure 2-14: Al^{VI} vs. Al^{IV} diagram for the clinopyroxenes of the different gabbros. All clinopyroxenes plot in the low-pressure field in contrast to the clinopyroxenes of the high-pressure Permian Braccia Gabbro from Val Malenco. Areas for high, low and intermediate pressures from Aoki and Shiba (1973), clinopyroxenes from the South West Indian Ridge from Hébert *et al*. (1991) and Stakes *et al*. (1991), clinopyroxenes from Zabargad Island (c: porphyroclasts, n: neoblasts) from Bonatti *et al*. (1987) and Boudier *et al*. (1988), clinopyroxenes from ODP Site 900 from Cornen *et al*. (1993) and from the Braccia gabbro (Malenco crust-mantle boundary) from Hermann (1997).

High-temperature deformation and hydration

The microstructural data suggest syn-magmatic deformation of the gabbros. This is supported by the similar composition of the magmatic and neoblastic amphiboles and clinopyroxenes in the high-temperature shear zones. The Otten thermometer (1984) applied on the neoblastic amphiboles gives temperatures between 900 and 975°C similar to the temperature obtained on the magmatic amphiboles. This thermometer is less reliable for coronitic amphiboles as the Ti-content of the amphiboles depends on the bulk-rock chemistry and the temperatures obtained should be considered as minimum temperatures. However, the coronitic amphiboles yield temperatures between 900 and 600°C suggesting high-temperature static hydration of the gabbros during cooling. This high temperature of crystallisation is in accordance with the high Al^{IV} content of the amphiboles which increases with temperature in both metamorphic and magmatic amphiboles (Anderson & Smith 1995; Laird 1982; Heltz 1982), and with the experimental data of Spear (1981) indicating that the assemblage clinopyroxene + hornblende + ilmenite is stable at temperature above 750˚C.

Low-temperature deformation

The gabbros were deformed again under lower amphibolite to greenschist temperature conditions and finally in the brittle field before they were ultimately exposed on the sea floor. This is documented by the assemblage actinolite + albite or biotite + chlorite + albite underlining the foliation in low-temperature shear zones. The low Na^{M4} content of the actinolites suggests that they crystallised at low pressure less than 2 kb (Brown 1977). The shear zones are overprinted by cataclastic deformation implying that the gabbros were deformed also at very shallow depth or at the sea-floor during their exhumation. The P, T path of the gabbros is summarised in Fig. 2-15.

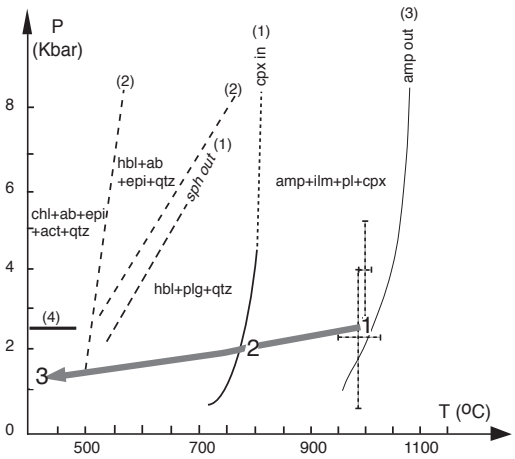

Figure 2-15: P, T paths for the gabbros and the diorite of the Platta nappe. 1: Magmatic crystallisation; 2: Oceanic hydration; 3: Greenschist deformation and alteration. Pressure conditions during intrusion were determined by the cpx-geobarometer (Nimis and Ulmer, 1998). Reactions (1) from Spear (1981); reactions (2) from Apted & Liou (1983); (3) Amph-in reaction under QFM redox condition from Heltz (1982); (4) depth of serpentinisation front from Boillot (1992).

Basalts and dolerites

Basaltic rocks cover a large area in the Platta nappe; they occur as massive basalts, pillow lavas, pillow breccias, hyaloclastites and dolerite dykes. The extrusive rocks stratigraphically overlie the serpentinites, gabbros, and the different types of breccias including ophicalcites. Sedimentary breccias underlying the submarine volcanics contain clasts of serpentinite, continental basement rocks and pre-rift sediments and clearly show that tectonic emplacement of the extensional allochthons and exhumation of the mantle rocks predated the extrusion of the basaltic rocks. Clasts of foliated gabbro, deformed under high-temperature conditions and occurring in weakly deformed pillow breccias (Fig. 9d) show that intrusion, deformation and exhumation of the gabbros also preceded the emplacement of the volcanic rocks at these specific locations. The volcanic rocks are overlain by post-rift sediments of the Radiolarite or the Calpionella Limestone Formations.

The dolerite dykes show a typical intersertal structure between plagioclase and augite, and chilled margins along the contact with serpentinites or gabbros expressed by a grain-size reduction along the edges of the dykes. Rodingitisation of these dykes is limited to the first centimetre at the contact with the serpentinite suggesting intrusion into an already cool and serpentinized mantle.

The dolerites and basalts show a major element composition typical for tholeiitic magmas (Frisch *et al*. 1994). These authors distinguished two groups of basalt; one including the dolerites and part of the pillow basalts shows a major and trace element composition typical for MORB, whereas the second group of pillow basalts shows an enrichment in incompatible elements. Frisch *et al*. (1994) interpreted this difference by a change from a subcontinental to a MOR magma source. However, all pillow basalts analysed so far have high eNd (+7.8 to 9.8) and low $^{87}Sr/^{86}Sr$ ratios (0.7028 to 0.7049) indicating a depleted mantle source compatible with a ridge environment (Stille *et al*. 1989; U. Schaltegger personal communication 1999).

Discussion

Steinmann (1905) thought that all the rocks of his trinity were intrusive; nevertheless he recognised that the serpentinites were the oldest rocks, followed by the gabbros and finally the basalts and "variolites" (Steinmann 1927). However, in contrast to Steinmann's interpretation that the ophiolites observed in the Alps and Apennines were parts of a consanguineous magmatic association (like the ophiolites of Troodos, Semail etc.), the mantle and the magmatic rocks of the transitional crust appear to be related to different geodynamic processes. The serpentinites and associated ophicalcites document exhumation of mantle rocks and their exposure at the sea floor; the gabbros and related dikes intruded into already serpentinized mantle rocks *during* exhumation of the mantle; the basaltic pillow breccias finally contain fragments of flaser gabbro and therefore are younger than the gabbros with which they occur together today (we do not see the plutonic equivalents of the basalts and dolerites). However, as we shall discuss later, this does not exclude that the deformed gabbros and the basalts belong to the same magmatic cycle and reflect the interplay between tectonic and magmatic processes.

Mantle exhumation

Exhumation of mantle rocks and their exposure at the sea floor are well documented in different present-day tectonic settings, e.g. along oceanic transform faults (Fox *et al*. 1976; Bonatti *et al*. 1980), slow-spreading ridges (Lagabrielle & Cannat, 1990), along the foot of "non-volcanic" passive continental margins (Boillot *et al*. 1988, Whitmarsh, Beslier *et al*. 1998) and along compressional ridges like the Gorringe Bank in the central Atlantic (Lagabrielle & Auzende 1982). In many of these settings, tectonic and/or sedimentary breccias resembling the different types of ophicalcites are associated with serpentinised peridotites (e.g. Bonatti *et al*. 1974; Whitmarsh *et al*. 1998). In the Alps, the exposure of serpentinized peridotites at the ocean floor has been interpreted (1) within the context of Mesozoic transform faults (Lemoine 1980; Weissert & Bernoulli 1985), (2) by exhumation along a slow spreading ridge (Lagabrielle & Lemoine 1997) and (3) by exhumation along a system of low-angle detachment faults along a lower-plate continental margin (Lemoine *et al*. 1987; Froitzheim & Manatschal 1997; Manatschal & Bernoulli 1999). In the case of the Platta nappe, final exhumation of mantle rocks along a system of low-angle detachments is suggested by the association of the mantle rocks with extensional continental allochthons which overlie them along gently inclined fault planes (Manatschal & Nievergelt 1997). In addition, the tectono-sedimentary breccias form a more or less continuous carapace along the surface of the serpentinites. Manatschal & Bernoulli (1999) have emphasised the numerous analogies between mantle exhumation along the south-Pennine-Austroalpine transition zone and the passive continental margin west of Iberia.

As the serpentinized lherzolites preserve a high-temperature spinel foliation and are stratigraphically overlain by sediments, they must have been exhumed from the deep lithosphere to the sea floor. Hermann *et al*. (1997) showed in Val Malenco that mantle rocks, ultimately derived from the asthenosphere, were in a shallow mantle position long before rifting initiated. Therefore the structures and mineralogical changes recorded in the mantle rocks are not necessarily related to the rifting process alone, and it is not possible without further age constraints to unambiguously relate the anhydrous high-temperature shear zones showing a top-to-the-continent sense of shear

to Jurassic rifting. However, we assume that most of the hydration processes within the mantle were associated with Jurassic rifting as documented for the Malenco complex by Müntener *et al.* (2000). In the Platta nappe, static high-temperature hydration is documented by the growth of Mg-hornblende at the expense of diopside which in turn was followed by further hydration at lower temperature as testified by the crystallisation of tremolite. We do not know the age of these transformations, however, Hermann *et al.* (1997) related the hydration of lower crustal and upper mantle rocks in the Malenco complex to early rifting during the early Jurassic (± 190 Ma), based on Ar-Ar age determinations on pargasitic hornblende (Villa *et al.* 2000). We therefore think, that the top-to-the-continent high-temperature shear zones predate the Jurassic rifting and may be related to an earlier phase of extension (cf. Manatschal & Bernoulli 1998).
Serpentinisation preceded or was contemporaneous with the following deformation under decreasing temperatures. Low-temperature deformation produced serpentinite mylonites and tectonic breccias overprinting them, and was followed by the replacement of serpentinite minerals by calcite and by final exhumation and the formation of the tectono-sedimentary breccias at the sea floor (ophicalcites I). The observations (1) that the sense of shear found in the serpentinite mylonites is top-to-the-ocean as along the low-angle detachments cutting across the distal continental margin (Manatschal and Nievergelt 1997) and (2) that the gabbros intruding the already serpentinized mantle show evidence of intrusion in a tectonically active setting suggest that serpentinisation and intrusion were contemporaneous with the exhumation of the mantle rocks to the sea floor.

Gabbro intrusion and exhumation

Gabbros associated with rifted continental margins represent either magmatic underplating of continental crust, passively exhumed during much later rifting or, alternatively, initiation of partial melting during late rifting and incipient sea-floor spreading. Both types of occurrences have been described along present-day ocean-continent transitions (Schärer *et al.* 1995, Cornen *et al.* 1999 and references therein). In many cases the unknown stratigraphic and structural relationships and the lack of age and thermobarometric data do not allow for an unambiguous interpretation. However, deep-sea drilling and submersible observations along the non-volcanic Galicia margin and in the Iberia abyssal plain off western Spain and Portugal have shown that only minor volumes of syn-rift basaltic melts were produced along this "non-volcanic" margin before initiation of sea-floor spreading (Manatschal *et al.* this volume). Likewise, the proportion of gabbro in the transitional crust of the Platta nappe is relatively small.

The gabbros of the Platta nappe intruded into already serpentinized mantle rocks in an active tectonic system at about 161 Ma (Desmurs *et al.* 1999). A shallow level of intrusion is supported by our mineral chemistry data, and the chilled margins along the intrusions. The gabbros were subsequently intruded by basaltic dykes, and finally exposed on the sea floor, as recorded by their occurrence as clasts in pillow and sedimentary breccias stratigraphically overlying the exhumed mantle rocks. The microstructures in the gabbros indicate syn-magmatic deformation, followed by deformation under greenschist and lower temperature conditions during final exhumation. On the basis of these observations and considering the short time gap between crystallisation and exposure on the sea floor, we favour the interpretation that

the gabbros were emplaced during or after continental break-up and cooled rapidly during their exhumation in the footwall of detachment structures active during extension.

Basalt extrusion and related dykes

Our field observations document that the massive basalts, pillow lavas and pillow breccias stratigraphically overlying the exhumed mantle rocks and the associated tectono-sedimentary breccias are younger than the gabbros which *today* are found in the Platta nappe: clasts of the previously deformed gabbros are found together with clasts of albitites in pillow breccias and sedimentary breccias associated with them. On the other hand, we found no basalt but only serpentinite and gabbro clasts in the tectono-sedimentary breccias overlying the exhumed mantle. Undeformed basaltic dikes show chilled margins along their contacts with the serpentinites and the gabbros. This clearly shows that the emplacement of the basalts and of the dykes related to them occurred after serpentinisation of the mantle rocks, and after the intrusion, deformation, cooling and exposure of the gabbros on the sea-floor. The latest basalts are thus clearly post-tectonic and are the youngest magmatic rocks emplaced at the foot of this passive margin.

Magmatic sources

The gabbros and the basalts yield the same high εNd values (Stille *et al*. 1989; U. Schaltegger personal communication 1999). This means that both were not contaminated by continental lithosphere and come from similar asthenospheric sources or from the same. This geochemical signature is similar to that of the magmatic rocks of the internal Liguride ophiolites (Borsi *et al*. 1996; Rampone *et al*. 1998). Only in the slightly older magmatic rocks of the Gets nappe (166±1 Ma, Bill *et al*. 1997), pillow basalts and dikes intruding continental crustal rocks yielded lower εNd values and REE-patterns indicating contamination of the magma by a continental component (Bill *et al*. in press). Together these data document an evolution similar to the evolution of the sources of the magmatic rocks recorded along the Galicia margin. There, the εNd of the syn- and post-rift gabbros and basalts suggests contamination of the liquids extracted from the asthenosphere by the overlying subcontinental mantle. However, the younger the magmatic rocks, the higher the εNd, suggesting a decrease in crustal contamination during rifting and thinning of the continental lithosphere (Charpentier *et al*. 1998). In the Platta nappe, the geochemical signatures of the magmatic rocks are compatible with the field and petrological observations that the magmatic rocks were emplaced when the continental lithosphere was extremely thinned, i.e. during or shortly after the break-up of the continental lithosphere.

Timing of emplacement of the different rock types

A relative chronology of the emplacement of the rocks of the Platta nappe at the deep-sea floor can be established that corresponds to the sequence of relative age proposed by Steinmann (1927) for his trinity. Our data show that exhumation of the mantle rocks to the sea-floor was accompanied by the intrusion of the gabbros into an already cooled, serpentinized mantle. These gabbroic rocks were exhumed to the sea floor before the extrusion of still younger basalts and deposition of the post-rift sediments.

Rates of processes, however, are more difficult to establish. The syn-rift sediments preserved in the extensional allochthons and locally onlapping onto exposed inactive segments of the low-angle detachment(s) are not directly dated but are younger than the Pliensbachian hardground along the top of the pre-rift sediments of the distal margin (± 190 Ma in the time scale of Gradstein *et al*. 1995). Ar-Ar determination of phlogopite in a pyroxenite of the Totalp peridotite of the Arosa zone to the north yielded an age of 160±8 Ma (Peters & Stettler 1987, the error including middle Bathonian to late Oxfordian in the time scale of Gradstein *et al*. 1995). This age is interpreted as the age of mantle exhumation to 10 km depth or less and fits well with the crystallisation age of the gabbros of the Platta nappe (161±1 Ma, Desmurs *et al*. 1999).

Dating of the oceanic basalts by the age of the overlying oceanic sediments proves to be difficult. Both, the transitional crust with its tectonically emplaced allochthons as well as the accumulations of pillow lavas present a pronounced submarine relief. The oldest sediments of slow spreading oceans are typically ponded between the submarine highs of the volcanic basement on which they rest with an onlap (see e.g. Lancelot *et al*. 1972, their Fig. 27); the same observation is made along distal "non-volcanic" margins (e.g. Whitmarsh, Beslier *et al*. 1998). The age of the sediments directly overlying transitional or oceanic crust may thus vary over a short distance, in the Alps and Apennines within the same tectonic unit (cf. Decandia & Elter 1972). In the Platta nappe, the oldest post-rift sediments unconformably overlying the exposed mantle rocks and the pillow-lavas are bedded cherts and siliceous shales of the Radiolarite Formation. This formation is not directly dated in our area. In less deformed areas in the Alps, its base is dated as late Bathonian to early Callovian (Bill *et al*. 1997; between 166.5 and 162 Ma in the time scale of Gradstein *et al*. 1995) or younger. This age would be slightly older than or the same as our intrusion age of the gabbros. The base of the Radiolarite Formation, however, is certainly diachronous and, in our area, most probably younger than the early Callovian. Nevertheless we suspect that only a few million years separated the intrusion of the gabbros and the (late Callovian?) onset of deposition of the radiolarites (Table 2-3). A short time span for this entire evolution is suggested in the Gets nappe of the French Alps where only a few million years lay between the intrusion of the gabbros (166±1 Ma) and deposition of the overlying radiolarites (166.5-162 Ma, Bill *et al*. 1997). Some uncertainty, however, remains because of the still considerable errors in the calibration of the biochronology of the middle Jurassic time interval (±4 Ma, Gradstein *et al*. 1995).

Table 2-3. *Summary of the geochronological data from the south-Pennine-Austroalpine*

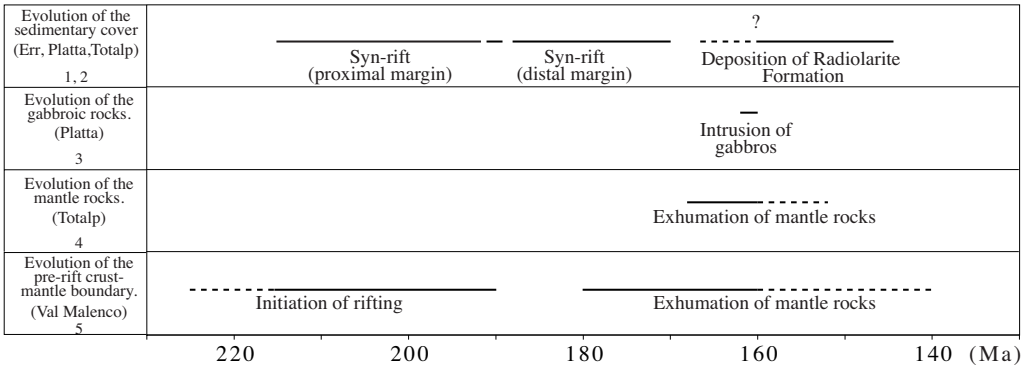

1: Froitzheim & Eberli 1990; 2: Weissert & Bernoulli 1985; 3: Desmurs et al. 1999; 4: Peters & Stettler 1987; 5: Villa et al. (2001).

Relationships between tectonic and magmatic processes

Along non-volcanic margins, the transition from continental to oceanic crusts occurs over a transition zone with an intermediate, transitional crust which consists of serpentinised peridotites. Along the Iberian margin (Manatschal *et al*. this volume) and along the Err-Platta margin (Froitzheim & Manatschal 1996; Manatschal & Nievergelt 1997), these exhumed mantle rocks are overlain by extensional allochthons, stranded klippen of continental basement, emplaced along low-angle detachment systems. Magmatic rocks are subordinate in this type of crust, but increase in volume towards the future ocean, and in the case of the Platta nappe, they carry a typical isotopic MORB signature without indications of continental crustal contamination (Stille et al. 1989). Towards the ocean, and with ongoing extension and mantle exhumation, we laterally pass from a regime in which extension was accommodated, by and large, by mechanical deformation to a regime in which it was more and more compensated by the emplacement of magmatic rocks. In the context of "non-volcanic" margins, the passage from tectonic extension to sea-floor spreading appears to be gradual and it becomes difficult to clearly separate continental and ocean lithosphere and to define continental break-up. Although it is evident that this transition records the processes finally leading to sea-floor spreading and the formation of oceanic lithosphere, we do not yet understand the precise temporal evolution.

Our chronological data do not allow to clearly separate extensional and magmatic events (Table 2-3). During late rifting, extension and magmatic processes overlap in time: gabbros intruding the exhumed mantle rocks were deformed under decreasing temperature conditions, and were finally exhumed to the sea floor and covered in turn by pillow lavas (Fig. 2-16). Cross-cutting relationships on an outcrop scale show that mantle exhumation started before the first mafic melts intruded during a late stage of rifting and into previously serpentinised mantle. These relationships also show that undeformed basaltic dykes and extrusives are, on a local scale, distinctly younger than the deformed gabbros we observe today at shallow depth and at the surface of the former transitional crust. As gabbros and basalts crystallised at different crustal levels - the basalts at the sea floor, the gabbros within the serpentinised mantle rocks - the gabbros could not have been be the magma chambers of the basalts with which they are spatially associated today (e.g. Val da Natons). Unfortunately we observe today only the uppermost few hundreds of meters of the former transitional crust. We can therefore not decide whether gabbros and basalts record two different phases of magmatism separated by a phase of extension (Fig. 2-16, right) or whether gabbros and basalts were more or less contemporaneous and the products of the same steady processes, i.e. of processes similar to those envisaged for slow spreading ridges. In this case, gabbros and basalts which formed together were subsequently separated by faulting, whereas basalts directly overlying exhumed gabbros are younger (Fig. 2-16, left), an interpretation which we favour for the time being. These overlapping extensional and magmatic processes might record the initiation of a slow spreading ridge.

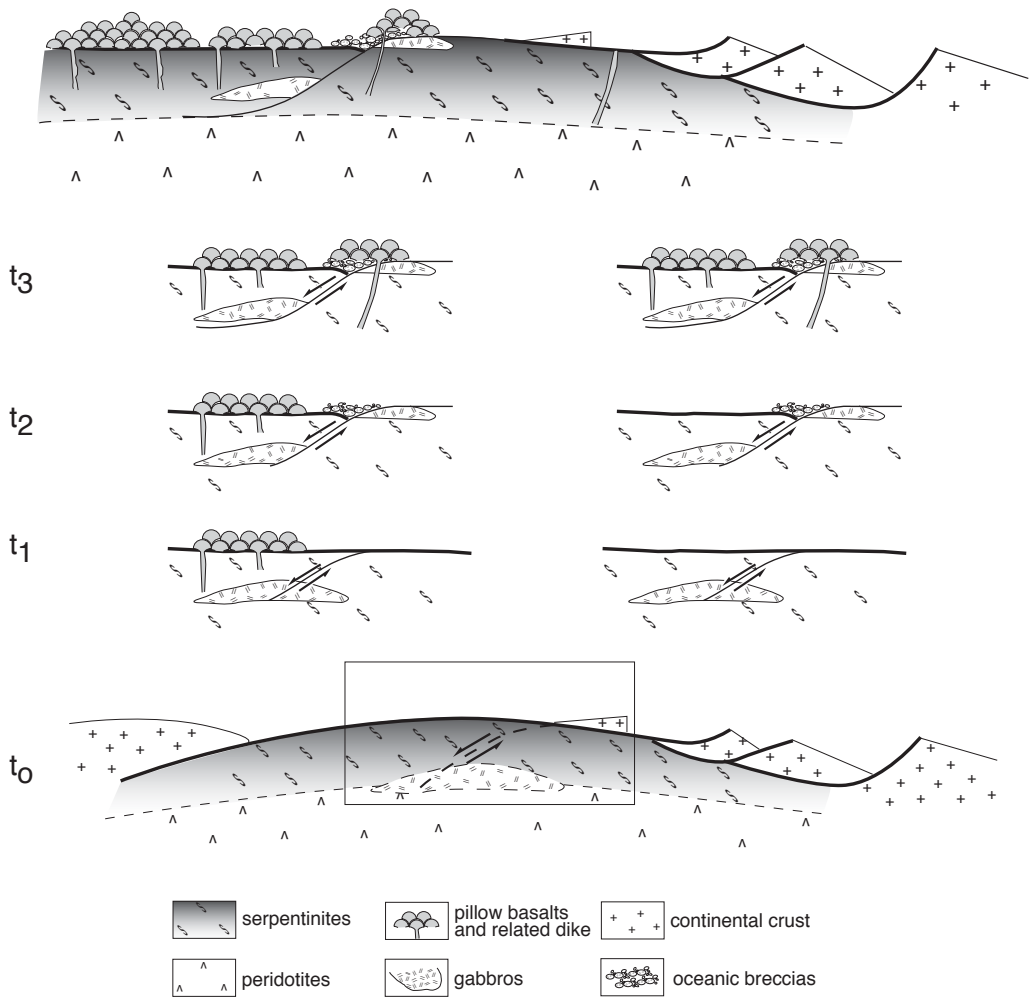

Figure 2-16: Sketch illustrating the evolution of emplacement of the different basement rocks. t_0: detachment faulting leading to the exhumation of mantle rocks and intrusion of the gabbros near the serpentinisation front. t_1 to t_3: Exhumation of the gabbros and emplacement of the pillow-basalts. Two hypothesis are shown: On the left, gabbros and basalts are part of the same magmatic cycle; on the right, all the extrusive rocks were emplaced after the exhumation of the gabbros. Both scenarios can lead to the geometries and stratigraphic relationships observed today.

Conclusions

In its type area, the south-Pennine Platta nappe, the Steinmann Trinity is dominated by serpentinites and includes significant amounts of pillow basalts and oceanic sediments. Careful mapping of the field relationships shows that the subcontinental mantle rocks were exhumed to the sea floor along a low-angle detachment system similar to what observed along the Iberian non-volcanic margin. Gabbros intruded at shallow depth into the already serpentinized mantle rocks but were continuously deformed under decreasing temperatures and exposed at the sea floor during ongoing extension. With the overlying locally younger basalts the gabbros share typical isotopic MORB signatures and we suspect that they are only the older intrusive members of a magmatic suite, which were deformed, brought to the surface and overlain by younger extrusives of the same suite in a steady process of extension, magma generation and emplacement leading to the evolution of a slow spreading ridge.

Our work is part of the research project "Comparative anatomy of passive continental margins: Iberia and Eastern Alps" supported by the Swiss National Science Foundation, projects 21-049117.96/1 and 20-55284.98. We thank U. Schaltegger, O. Müntener, G. Bernasconi-Green, N. Froitzheim, G. Boillot, Y. Lagabrielle, F. Chalot-Prat, V. Gardien, J. Hermann, V. Trommsdorff for stimulating discussions and helpful suggestions, and Y. Lagabrielle, F. Chalot-Prat, O. Müntener, and N. Froitzheim for critical review.

References

ALLEN, J.C, BOETTSCHER, A.L. & MARLAND, G. 1975. Amphibole in andesite and basalt: I. stability as a function of P-T-f_{O2}. *American Mineralogist,* **60**, 1069-1085.

ANDERSON, J.L & SMITH, D.R. 1995. The effect of the temperature and f_{O2} on the Al in hornblende barometer. *American Mineralogist,* **80**, 549-559.

ANONYMOUS, 1972. Penrose Field Conference Ophiolites. *Geotimes,* December **1972**, 24-25.

AOKI, K. & SHIBA, I. 1973. Pyroxenes from lherzolite inclusions of Itinome-gata, Japan. *Lithos,* **6**, 41-51.

APTED, M.J. & LIOU, J. G. 1983. Phase relations among greenschist, epidote-amphibolite and amphibolite in a basaltic system. *American Journal of Science,* **283**, 328-354.

AVIGAD, D., CHOPIN, C., GOFFÉ, B. & MICHARD, A. 1993. Tectonic model for the evolution of the western Alps. *Geology,* **21**, 659-662.

BAILEY, E.B. & MCCALLIEN, W.J. 1950. The Ankara Mélange and the Anatolian Thrust. *Nature,* **166**, 938-943.

BAUMGARTNER, P. O. 1987. Age and genesis of Tethyan radiolarites. *Eclogae Geologicae Helvetiae,* **80**, 831-879.

BENDER, J.F., HODGES, F.N. & BENCE, A.E. 1978. Petrogenesis of basalts from the project FAMOUS area: experimental study from 0 to 15 kbars. *Earth and Planetary Science Letters,* **41**, 277-302.

BERNOULLI, D. & WEISSERT, H.J. 1985. Sedimentary fabrics in Alpine ophicalcites, South Pennine Arosa zone. *Geology,* **13**, 755-758.

BILL, M., BUSSY, F., COSCA, M., MASSON, H. & HUNZIKER, J. 1997. High-precision U-Pb and $^{40}Ar/^{39}Ar$ dating of an Alpine ophiolite (Gets nappe, French Alps). *Eclogae Geologicae Helvetiae,* **90**, 43-54.

BILL, M., NÄGLER, T.F. & MASSON, H. (2000). Geochemistry, Sm-Nd and Sr isotopes of mafic rocks from the earliest oceanic crust of Alpine Tethys. *Schweizerische Mineralogische und Petrographische Mitteilungen,* **80**, 131-145.

BOILLOT, G., BESLIER, M.O. & COMAS, M. 1992. Seismic images of undercrusted serpentinite beneath a rifted margin. *Terra Nova*, **4**, 25-33.

BOILLOT, G., COMAS, M. C., GIRARDEAU, J., KORNPROBST, J., LOREAU, J.-P., MALOD, J., MOUGENOT, D. & MOULLADE, M. 1988. Preliminary results of the Galinaute cruise: dives of the submersible Nautile on the western Galicia margin, Spain. *In:* Boillot G., Winterer E. L. *et al*. (eds) *Proceedings of the Ocean Drilling Program, Scientific Results,* **103**, College Station, Texas (Ocean Drilling Program), 37-51.

BOILLOT, G., RECQ, M., WINTERER, E.L., MEYER, A.W., APPLEGATE. J., BALTUCK, M., BERGEN, J.A., COMAS, M.C., DAVIES, T.A., DUNHAM, K., EVANS, C.A., GIRARDEAU, J., GOLDBERG, G., HAGGERTY, J., JANSA, L.F., JOHNSON, J.A., KASAHARA, J., LOREAU, J.P., LUNA-SIERRA, E., MOULLADE M., OGG, J., SARTI, M., THUROW, J. & WILLIAMSON, M. 1987. Tectonic denudation of the upper mantle along passive margin: a model based on drilling results (ODP Leg 103, Western Galicia Margin, Spain). *Tectonophysics*, **132**, 334-342.

BONATTI, E., CHERMAK, A. & HONNOREZ, J. 1980. Tectonic and igneous emplacement of crust in oceanic transform zones. *In:* Talwani, M., Harrison, C.G. & Hayes, D. (eds) *Deep Drilling Results in the Atlantic Ocean: Ocean crust*. American Geophysical Union, Maurice Ewing Series, **2**, 239-248.

BONATTI, E., FERRARA, G., HONNOREZ, J. & RYDELL, H. 1974. Ultramafic carbonate breccias from the equatorial mid-Atlantic ridge. *Marine Geology*, **16**, 83-102.

BONNATTI, E. & SEYLER, M. 1987. Crustal underplating and evolution in the Red Sea Rift: uplifted gabbro/gneiss complexes on Zabargad and Brothers islands. *Journal of Geophysical Research,* **92**, 12803-12821.

BORSI, L., SCHÄRER, U., GAGGERO, L. & CRISPINI, L. 1996. Age, origin and geodynamic significance of plagiogranites in lherzolites and gabbros of the Piedmont-Ligurian ocean basin. *Earth and Planetary Science Letters*, **140**, 227-241.

BOUDIER, F., NICOLAS, A., JI, S., KIENAST, J. R. & MEVEL, C. 1988. The gneisses of Zabargad Island: deep crust of a rift. *Tectonophysics*, **150**, 209-227.

BOYER, S. & ELLIOTT, D. 1982. 'Thrust systems'. *Bulletin of the American Association of Petroleum Geologists,* **66**, 1196-1230.

BREY, G. P. & KOHLER, T. 1990. Geothermobarometry in four phases lherzolite II. New thermobarometers and practical assessment of existing thermobarometers. *Journal of Petrology*, **31**,1353-1378.

BROWN, E. H. 1977. The crossite content of Ca-amphibole as guide to pressure of metamorphism. *Journal of Petrology,* **18**, 53-72.

CHARPENTIER, S., KORNPROBST, J., CHAZOT, G., CORNEN, G. & BOILLOT, G. 1998, Interaction entre lithosphère et asthenosphère au cours de l'ouverture océanique: données isotopiques préliminaires sur la Marge passive de Galice (Atlantique-Nord). *Comptes-Rendus de l'Académie des Sciences, Sciences de la Terre et des Planètes*, *Paris,* **326**, 757-762.

CORNEN, G., BESLIER, M.-O. & GIRARDEAU, J. 1996. Petrology of mafic rocks cored in the Iberia Abyssal Plain. *In:* Whitmarsh, R. B., Sawyer, D. S., Klaus, A. & Masson, D. G. (eds) *Proceedings of the Ocean Drilling Program, Scientific Results,* **149**, College Station, Texas, (Ocean Drilling Program), 449-465.

CORNEN, G., GIRARDEAU, J. & MONNIER, C. 1999. Basalts, underplated gabbros and pyroxenites record the rifting process of the West Iberian margin. *Mineralogy and Petrology,* **67**, 111-142.

DECANDIA, F.A. & ELTER, P. 1972. La "zona" ofiolitifera del Bracco nel settore compreso tra Levanto e la Val Graveglia (Appennino ligure). *Memorie della Società Geologica Italiana*, **11**, 503-530.

DESMURS, L., SCHALTEGGER, U., MANATSCHAL, G. & BERNOULLI, D. 1999. Geodynamic significance of gabbros along ancient ocean-continent transitions: Tasna and Platta nappes, Eastern Alps. *Terra Abstracts*, **10**, 379.

DEWEY, J.F. & BIRD, J. 1970. Mountain belts and the new global tectonics. *Journal of Geophysical Research*, **75**, 2625-2647.

DIETRICH, V. 1970. Die Stratigraphie der Platta-Decke: Fazielle Zusammenhänge zwischen Oberpenninikum und Unterostalpin. *Eclogae Geologicae Helvetiae,* **63**, 631-671.

DÜRR, S.B. 1992. Structural history of the Arosa Zone between Platta and Err nappes east of Marmorera (Grisons): Multi-phase deformation at the Pennine-Austroalpine plate boundary. *Eclogae Geologicae Helvetiae,* **85**, 361-374.

ELTHON, D. & SCARFE, C. M. 1984. High pressure equilibria of a high-magnesian basalt and the genesis of primary oceanic basalt. *American Mineralogist,* **69**, 1-15.

EVANS, B.W. 1977 Metamorphism of alpine peridotite and serpentinite. *Annual Reviews in Earth and Planetary Sciences*, **5**, 397-447.

EVANS, B.W. 1982 Amphiboles in metamorphosed ultramafic rocks. *In:* Veblen, D.R. & Ribbe, P.H. (eds) *Amphiboles: Petrology and Experimental Phases Relations*. Reviews in Mineralogy, Mineralogical Society of America, **9B**, 98-112.

FERREIRO-MÄHLMANN, R. 1995. Das Diagenese-Metamorphose-Muster von Vitrinit-Reflexion und Illit-"Kristallinität" in Mittelbünden und im Oberhalbstein, Teil 1: Bezüge zur Stockwerktektonik. *Schweizerische Mineralogische und Petrographische Mitteilungen*, **75**, 85-122.

FOX, P.J., SCHREIBER, E., ROWLETT, H. & MCCAMY, K. 1976. The geology of the Oceanographer Fracture zone: A model for fracture zones. *Journal of Geophysical Research*, **81**, 4117-4128.

FRISCH, W., RING, U., DÜRR, S., BORCHERT, S. & BIEHLER, D. 1994. The Arosa zone and Platta nappe ophiolites (Eastern Swiss Alps): Geochemical characteristics and their meaning for the evolution of the Penninic Ocean. *Jahrbuch der Geologischen Bundes-Anstalt (Wien),* **137**, 19-33.

FROITZHEIM, N. & EBERLI, G.P. 1990. Extensional detachment faulting in the evolution of a Tethys passive continental margin (Eastern Alps, Switzerland). *Geological Society of America Bulletin*, **102**, 1297-1308.

FROITZHEIM, N. & MANATSCHAL, G. 1996. Kinematics of Jurassic rifting, mantle exhumation, and passive-margin formation in the Austroalpine and Penninic nappes (eastern Switzerland). *Geological Society of America Bulletin*, **108**, 1120-1133.

FROITZHEIM, N., SCHMID, S.M. & CONTI, P. 1994. Repeated change from crustal shortening to orogen-parallel extension in the Austroalpine units of Graubünden. *Eclogae Geologicae Helvetiae,* **87**, 559-612.

FROITZHEIM, N., SCHMID, S.M. & FREY, M. 1996. Mesozoic paleogeography and the timing of eclogite-facies metamorphism in the Alps: A working hypothesis. *Eclogae Geologicae Helvetiae,* **89**, 81-110.

GLENNIE, K.W., BOEUF, M.G.A., HUGHES CLARKE, M.W., MOODY.STUART, M., PILAAR, W.F. & REINHARDT, B.M. 1974. Geology of the Oman Mountains. *Verhandelingen van het Koninklijk Nederlands Geologisch Mijnbouwkundig Genootschap*, **31**, 1-423.

GRADSTEIN, F., AGTERBERG, F.P., OGG, J.G., HARDENBOL, J., VAN VEEN, V., THIERRY, J. & HUANG, Z. 1995. A Triassic, Jurassic and Cretaceous time scale. *In:* Berggren, W.A., Kent, D.V., Aubry, M.-P. & Hardenbol, J. (eds) *Geochronology, Time Scales and Global Stratigraphic Correlation*. Society of Economic Paleontologists and Mineralogists Special Publication, **54**, 94-126.

GREEN, D.H & RINGWOOD, A.E. 1967. The genesis of basaltic magma. *Contributions to Mineralagy and Petrology,* **15**, 103-190.

HANDY, M.R., HERWEGH, M. & REGLI, C. 1993. Tektonische Entwicklung der westlichen Zone von Samedan (Oberhalbstein, Graubünden, Schweiz). *Eclogae Geologicae Helvetiae,* **86**, 785-817.

HÉBERT, R., CONSTANTIN, M. & ROBINSON, P. T. 1991. Primary mineralogy of Leg 118 gabbroic rocks and their place in the spectrum of oceanic mafic igneous rocks. *In:* Von Herzen, R. P., Robinson, P. T. *et al. Proceedings of the Ocean Drilling Program, Scientific Results*, **118**, College Station, Texas (Ocean Drilling Program), 3-20.

HELTZ, R. T. 1973. Phase relations of basalts in their melting range at P_{H2O}=5 kb as a function of oxygene fugacity. Part I. Mafic phases. *Journal of Petrology,* **14**, 249-302.

HELTZ, R. T. 1982. Phase relations and compositions of amphiboles produced in studies of the melting behaviour of rocks. *In:* Veblen, D.R. & Ribbe, P.H. (eds) *Amphiboles: Petrology and experimental phases relations*. Reviews in Mineralogy, Mineralogical Society of America, **9B**, 279-346.

HERMANN, J. 1997. *The Braccia Gabbro (Malenco, Alps): Permian Intrusion at the Crust-Mantle Interface and Jurassic Exhumation during Rifting*. Ph.D. Thesis No 12102, ETH Zurich.

HERMANN, J. MÜNTENER, O. & GÜNTHER, D. in press. Differentiation of mafic magma in a continental crust-to-mantle transition zone. *Journal of Petrology*.

HERMANN, J., MÜNTENER, O., TROMMSDORFF, V. & HANSMANN, W. 1997. Fossil crust to mantle transition, Val Malenco (Italian Alps). *Journal of Geophysical Research*, **102**, B9, 20123-20132.

HESS, H.H. 1955. Serpentines, orogeny, and epeirogeny. *In:* Poldervaart, A. (ed.) *The Crust of the Earth*. Geological Society of America Special Paper, **62**, 391-408.

LAGABRIELLE, Y. & AUZENDE, J.M. 1982. Active in situ disaggregation of oceanic crust and mantle on Gorringe Bank: analogy with ophiolite massives. *Nature*, **297**, 490-493.

LAGABRIELLE, Y. & CANNAT, M. 1990. Alpine Jurassic ophiolite resemble the modern central Atlantic basement. *Geology,* **18**, 319-322.

LAGABRIELLE, Y. & LEMOINE, M. 1997. Alpine, Corsican and Apennine ophiolites: the slow-spreading ridge model. *Compte Rendus de l'Académie des Sciences. Sciences de la Terre et des Planètes*, **325**, 909-920.

LAGABRIELLE, Y. 1987. *Les ophiolites: marqueurs de l'histoire tectonique des domaines océaniques. Le cas des Alpes franco-italiennes (Queyras-Piémont), comparaison avec les ophiolites d'Antalya (Turquie) et du Coast Range de Californie*. Thèse d'Etat, Université de Brest, 350p.

LAGABRIELLE, Y., POLINO, R., AUZENDE, J.-M., BLANCHET, R., CABY, R., FUDRAL, S., LEMOINE, M., MEVEL, C., OHNENSTETTER, M., ROBERT, D. & TRICART, P. 1984. Les témoins d'une tectonique intra-océanique dans le domaine téthysien: Analyse des rapports entre les ophiolites et leur couverture métasédimentaire dans la zone piémontaise des Alpes franco-italiennes. *Ofioliti*, **9**, 67-88.

LAIRD, J. 1982. Amphiboles in metamorphosed basaltic rocks. *In:* Veblen, D.R. & Ribbe, P.H. (eds) *Amphiboles: Petrology and experimental phases relations*. Reviews in Mineralogy, Mineralogical Society of America, **9B**, 113-159.

LANCELOT, Y., HATHAWAY, J.C. & HOLLISTER, C.D. 1972, Lithology of sediments from the western North Atlantic, Leg 11, Deep Sea Drilling Project. *In:* Hollister, C.D., Ewing, J. *et al*. (eds) *Initial Reports of the Deep Sea Drilling Project,* **11**, Washington (U.S. Government Printing Office), 901-949.

LAUBSCHER, H. 1969. Mountain building. *Tectonophysics*, **7**, 551-563.

LEAKE, B. E. 1978. Nomenclature of amphiboles. *Mineralogical Magazine,* **42**, 533-563.

LEMOINE, M. 1980. Serpentinites, gabbros and ophicalcites in the Piemont-Ligurian domain of the Western Alps: Possible indicators of oceanic fracture zones and of associated serpentinite protrusions in the Jurassic-Cretaceous Tethys. *Archives des Sciences (Genève)*, **33**, 103-115.

LEMOINE, M., TRICART, P. & BOILLOT, G. 1987. Ultramafic and gabbroic ocean floor of the Ligurian Tethys (Alps, Corsica, Apennines): In search of a genetic model. *Geology* **15**, 622-625.

MANATSCHAL, G. & BERNOULLI, D. 1998. Rifting and early evolution of ancient ocean basins: the record of the Mesozoic Tethys and of the Galicia-Newfoundland margins. *Marine Geophysical Researches*, **20**, 371-381.

MANATSCHAL, G. & BERNOULLI, D. 1999. Architecture and tectonic evolution of non-volcanic margins: present-day Galicia and ancient Adria. *Tectonics,* **18**, 1099-1119.

MANATSCHAL, G. & NIEVERGELT, P. 1997. A continent-ocean transition recorded in the Err and Platta nappes (Eastern Switzerland). *Eclogae Geologicae Helvetiae,* **90**, 3-27.

MANATSCHAL, G., FROITZHEIM, N. & TURIN, B. (this volume) The role of detachment faulting in the formation of an ocean-continent transition: insights from the Iberia Abyssal Plain.

MOORES, E.M. & VINE, F.J. 1971. The Troodos Massif, Cyprus and other ophiolites as oceanic crust: evaluations and implications. *Philosophical Transactions of the Royal Society of London*, **A. 268**, 443-466.

MÜNTENER, O., HERMANN, J. & TROMMSDORFF, V. 2000. Cooling history and exhumation of lower-crustal granulite and upper mantle (Malenco, Central Alps). Journal of Petrology, **41**, 1-25.

NIMIS, P. & ULMER, P. 1998. Clinopyroxene geobarometry of magmatic rocks: Part I. An expanded structural geobarometer for anhydrous and hydrous, basic and ultrabasic systems. *Contributions to Mineralogy and Petrology,* **133**, 122-135.

OTTEN, M. T. 1984. The origin of brown hornblende in the Artfjället gabbro and dolerites. *Contributions to Mineralogy and Petrology,* **86**, 189-199.

PETERS, T. J. & STETTLER, A. (1987). Radiometric age, thermobarometry and mode of emplacement of the Totalp peridotite in the Eastern Swiss Alps. *Schweizerische Mineralogische und Petrographische Mitteilungen*, **67**, 285-294.

RAMPONE, E., HOFMANN, A.E. & RACZECK, I. 1998. Isotopic contrast within the Internal Liguride Ophiolite (N. Italy): the lack of a genetic mantle-crust link. *Earth and Planetary Science Letter*s, **163**, 175-189.

RING, U., RATSCHBACHER, L. & FRISCH, W. 1988. Plate-boundary kinematics in the Alps: Motion in the Arosa suture zone. *Geology,* **16**, 696-698.

RING, U., RATSCHBACHER, L., FRISCH, W., BIEHLER, D. & KRALIK, M. 1988. Kinematics of the Alpine plate-margin: structural styles, strain and motion along the Penninic-Austroalpine boundary in the Swiss Austrian Alps. *Journal of the Geological Society*, **146**, 835-849.

RUBATTO, D., GEBAUER, D. AND FANNING, M. 1998. Jurassic formation and Eocene subduction of the Zermatt-Saas Fee ophiolites: implications for the geodynamic evolution of the Central and Western Alps. *Contributions to Mineralogy and Petrology*, **132**, 269-287.

SCHÄRER, U., KORNPROBST, J., BESLIER, M.-O., BOILLOT, G. & GIRARDEAU, J. 1995. Gabbro and related rock emplacement beneath rifting continental crust: U-Pb geochronological and geochemical constraints for the Galicia passive margin (Spain). *Earth and Planetary Science Letters*, **130**, 187-200.

SPEAR, F. S. (1981). An experimental study of hornblende stability and compositional variability in amphibolite. *American Journal of Science*, **281**, 697-734.

STAKES, D., MÉVEL, C., CANNAT, M. & CHAPUT, T. (1991). Metamorphic stratigraphy of Hole 735B. *In:* Von Herzen R. P., Robinson P. T. *et al.* (eds) *Proceedings of the Ocean Drilling Program, Scientific Results*, **118**, College Station, Texas, (Ocean Drilling Program), 153-180.

STEINMANN, G. 1905. Geologische Beobachtungen in den Alpen. II. Die SCHARDTsche Ueberfaltungstheorie und die geologische Bedeutung der Tiefseeabsätze und der ophiolitischen Massengesteine. *Berichte der Naturfoschenden Gesellschaft zu Freiburg i.B.*, **16**, 18-67.

STEINMANN, G. 1925, Gibt es fossile Tiefseeablagerungen von erdgeschichtlicher Bedeutung? *Geologische Rundschau*, **14**, 435-468.

STEINMANN, G. 1927, Die ophiolitischen Zonen in den mediterranen Kettengebirgen. *Compte-Rendu, XIVe Congrès Géologique International, 1926,* Madrid, Gráficas Reunidas, **2**, 637-667.

STILLE, P., CLAUER, N. & ABRECHT, J. 1989. Nd isotopic composition of Jurassic seawater and the genesis of Alpine Mn deposits: evidence from Sr-Nd isotope data. *Geochimica et Cosmochimica Acta*, **53**, 1095-1099.

TROMMSDORFF, V. & EVANS, B. 1974. Alpine metamorphism of peridotitic rocks. *Schweizerische Mineralogische und Petrographische Mitteilungen,* **54**, 333-352.

TROMMSDORFF, V. 1983. Metamorphose magnesiumreicher Gesteine: Kritischer Vergleich von Natur, Experiment und thermodynamischer Datenbasis. *Fortschritte der Mineralogie*, **61**, 283-308.

ULMER, P. 1986. *Basische und ultrabasische Gesteine des Adamello*. Ph.D. Thesis, No.8105, ETH Zurich.

VILLA, I., HERMANN, J., MÜNTENER, O. & TROMMSDORFF, V. 2001. ^{39}Ar-^{40}Ar dating of multiply zoned amphibole generations (Malenco, Italian Alps). *Contributions to Mineralogy and Petrology*, **140**,363-381.

WEISSERT, H.J. & BERNOULLI, D. 1985. A transform margin in the Mesozoic Tethys: Evidence from the Swiss Alps. *Geologische Rundschau*, **74**, 665-679.

WHITMARSH, R., BESLIER, M.-O & WALLACE, P.J. (eds) 1998. *Proceedings of the Ocean Drilling Program, Initial Reports,* **173**, College Station, Texas (Ocean Drilling Program).

WITT-EICKSCHEN, G. & SECK, H. A. 1991. Solubility of Ca and Al in orthopyroxene from spinel peridotite: an improved version of an empirical geothermometer. *Contribution to Mineralogy and Petrography*, **106**,431-439.

Chapter 3-Tectono-metamorphic and geochemical evolution of the mantle rocks of the Platta nappe.

1. Introduction

The ophiolites of the Platta nappe bear several common features with the ocean-continent transition of the Iberian margin (Manatschal & Bernoulli 1999, Desmurs *et al*. 2001). With other ophiolites of the Liguria-Piedmont ocean they share the predominance of a serpentinite basement intruded by only small volumes of mafic rocks, and pillow-basalts and pelagic sediments stratigraphically overlie the serpentinized mantle rocks. Locally, these ophiolites are associated with lower continental crust (e.g. Val Malenco; Trommsdorff *et al*. 1993; Müntener & Hermann 1996), upper crustal derived extensional allochthones (e.g. Platta nappe; Froitzheim and Manatschal 1996; Manatschal and Nievergelt 1997; Desmurs *et al*. 2001), and continent-derived breccias (e.g. external Ligurides; Marroni *et al*. 1998, Gets nappe; Bill *et al*. 2000).
From field and geochemical evidence, it results that in several areas of the Alps the serpentinite basement represents former subcontinental mantle (e.g. Piccardo *et al*. 1990, Trommsdorff *et al*. 1993, Rampone *et al*. 1995, 1998), exhumed during the opening of the Alpine Tethys. However the compositions and conditions of equilibration of the mantle rocks are very different from place to place; they range however between two different "end members". One "end-member" consists of fertile peridotite commonly associated with pyroxenites, which equilibrated at the base of a 30 km thick continental crust (e.g. Malenco complex; Müntener *et al*. 2000). The second "end-member" is a more depleted, commonly plagioclase-bearing peridotite that recorded high temperatures of equilibration (> 1000°C) (e.g. internal Ligurides; Rampone *et al*. 1998; Lanzo; Boudier 1978).
Serpentinized lherzolite is the major rock type all over the Platta nappe. Two large serpentinite bodies, an upper and a lower serpentinite unit, can be recognized within the Platta nappe (Fig. 3-1). A palinspastic reconstruction of the Platta nappe shows that the peridotites of the upper serpentinite unit are derived from the originally continentward part of the transitional crust whereas those of the lower serpentinite unit were originally nearer to the ocean. Both units are stratigraphically overlain by deep-sea sediments indicating that they must have been uplifted from mantle depth to the sea floor. The palinspastic reconstruction allows also to track changes within the former Platta ocean-continent transition in composition and structure of the mantle rocks from the continent towards the ocean. In the following, I shall document the tectono-metamorphic and geochemical evolution of the upper and lower serpentinites and compare them with each other, and discuss the structure associated with their exhumation during Mesozoic rifting.

2. Tectono-metamorphic evolution of the Platta mantle rocks

2.1. Field Relationships

2.1.1 The upper serpentinite unit

The upper serpentinite unit crops out in the northeastern part of the Platta nappe (Val d'Err, east of Falotta; see location on Fig. 3-1) and is sandwiched between the overlying continental Err nappe above and the lower serpentinite unit, below (Fig. 3-

1). In this unit, the serpentinite basement is overlain by tectono-sedimentary breccias of continental origin (Parsettens, Fig. 3-2a, see location on Fig. 3-1) or by post-rift sediments and is almost free of magmatic rocks except for one basaltic flow and few dolerite dykes. The two main rock types consist of former spinel-lherzolite showing a weak spinel foliation intruded by numerous pyroxenite dykes that never exceed 15 cm in thickness (Fig 3-2b).

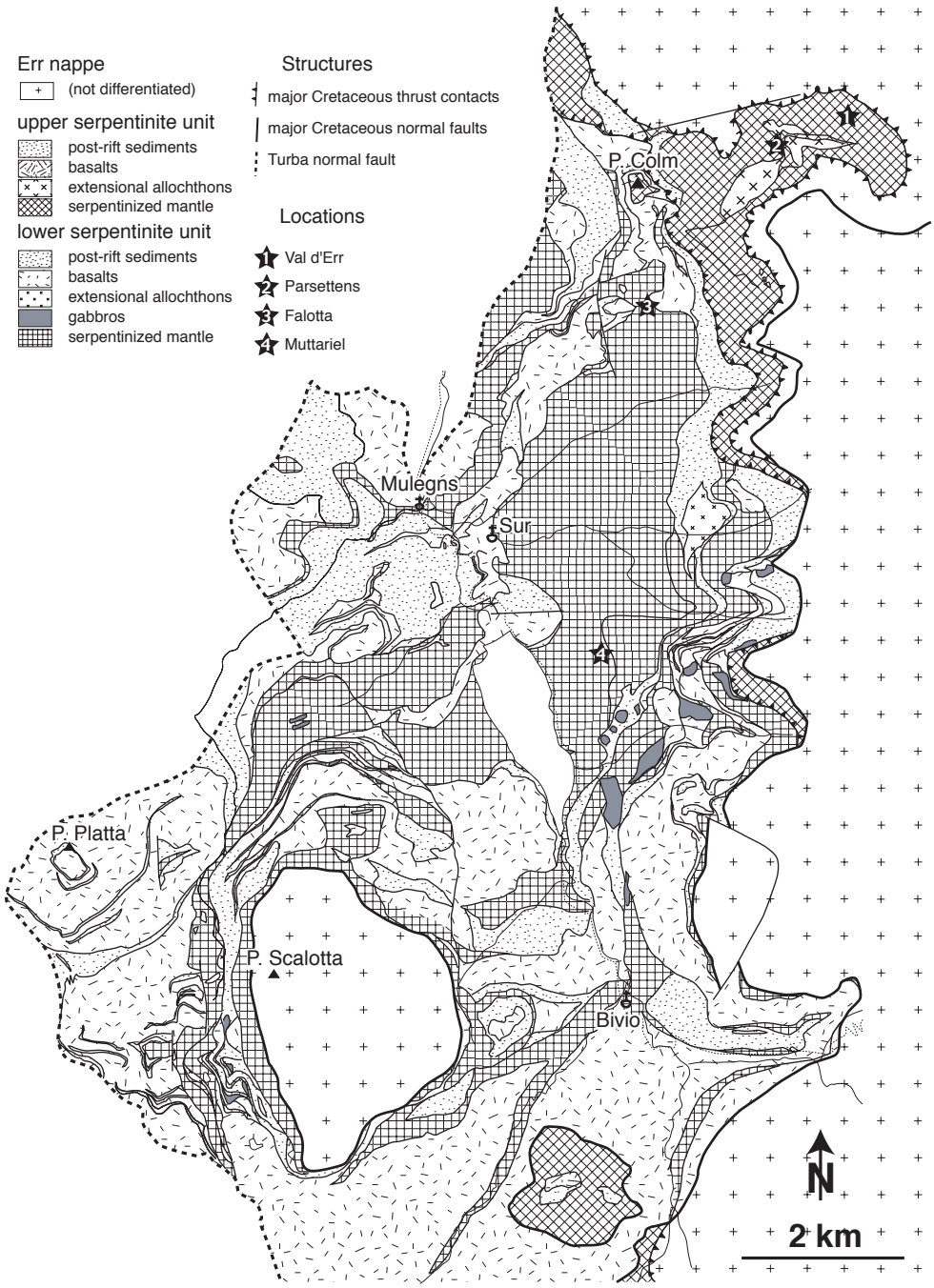

Figure 3-1: Tectonic map of the Platta nappe (after Cornelius (1932), Dietrich (1969) and own mapping).

The original fabric is, however, only rarely observed as both rock types are affected by an almost pervasive high-temperature deformation leading to a secondary tectonite fabric, which is the major structure observed in the field. The new foliation is locally discordant to the previous spinel foliation of the lherzolite and the pyroxenite banding

(Fig 3-2c). Increasing strain led to a composition banding of the rocks as indicated by serpentinite-rich bands alternating with clinopyroxene-rich layers on a millimeter scale (Fig. 3-2d). These tectonites show a strong foliation plunging steeply towards the east and the associated lineations are east-west. In the field, asymmetric clinopyroxene clasts indicate a top-to-the-east sense of shear.
Low-temperature deformation is expressed by a foliation underlined by serpentine minerals and is crosscut by undeformed basaltic dykes testifying its pre-alpine origin (Desmurs et al. 2001, fig. 2-5c and 2-5d). The lineation associated with this foliation is again east-west but the shear-sense indicators show a top-to-the-west movement.

2.1.2. The lower serpentinite unit

The ultramafic rocks of the lower serpentinite unit are spinel lherzolites showing a well-defined spinel foliation (Fig. 3-2e), which constitutes the main fabric throughout this unit. The serpentinites are directly overlain either by post-rift sediments, basaltic flows and pillow lavas or by tectono-sedimentary breccias including ophicalcites (Desmurs et al. 2001). Pyroxenite dykes are nearly absent but the mantle rocks are intruded by gabbroic bodies and numerous, small dolerite dykes. In a few places, extensional allochthones occur on top of the mantle rocks (Manatschal and Nievergelt 1997).

Locally, mylonitic shear-zones overprint the general tectonite fabric. In one place (Muttariel, see location on figure 3-1), a 20 meters thick peridotite mylonite is overprinted by cataclastic deformation. At the top of the section, ophicalcites fill the interstices and fractures, indicating proximity to the sea floor and an upright position of the section. The foliation within the mylonite dips towards the east, and the mineral lineation is east-west. Rotated clasts indicate a top-to-the east sense of shear.
In one outcrop (Sur al Cant), the mylonitic fabric is cut by a gouge zone, which also cuts across a dolerite dyke (Fig. 3-2f). Within the gouge, rotated clasts, shear bands, and s-c fabrics indicate a top-to-the west to southwest sense of shear. At Falotta (see location on figure 3-1), low-temperature deformation is also recorded by tectonic breccias. In these breccias, mylonitized as well as undeformed peridotite clasts are embedded in a cataclastic serpentinite matrix. The clasts are rounded by frictional wear suggesting rotational deformation. Up-section the breccia is cut by chrysotile and calcite veins.

In summary, the field relationships show that the rock types and the structure are different in the upper and lower serpentinite unit. The upper serpentinites unit is characterized by the occurrence of numerous pyroxenite dykes, which are absent within the lower one. In terms of structure, where east-dipping shear-zones are observed the associated deformation is pervasive in the upper serpentinite unit and very localized in the lower one. Only the low-grade deformation seems to be similar in both units as evidenced by the presence of serpentinite mylonites, gouges and tectono-sedimentary breccias.

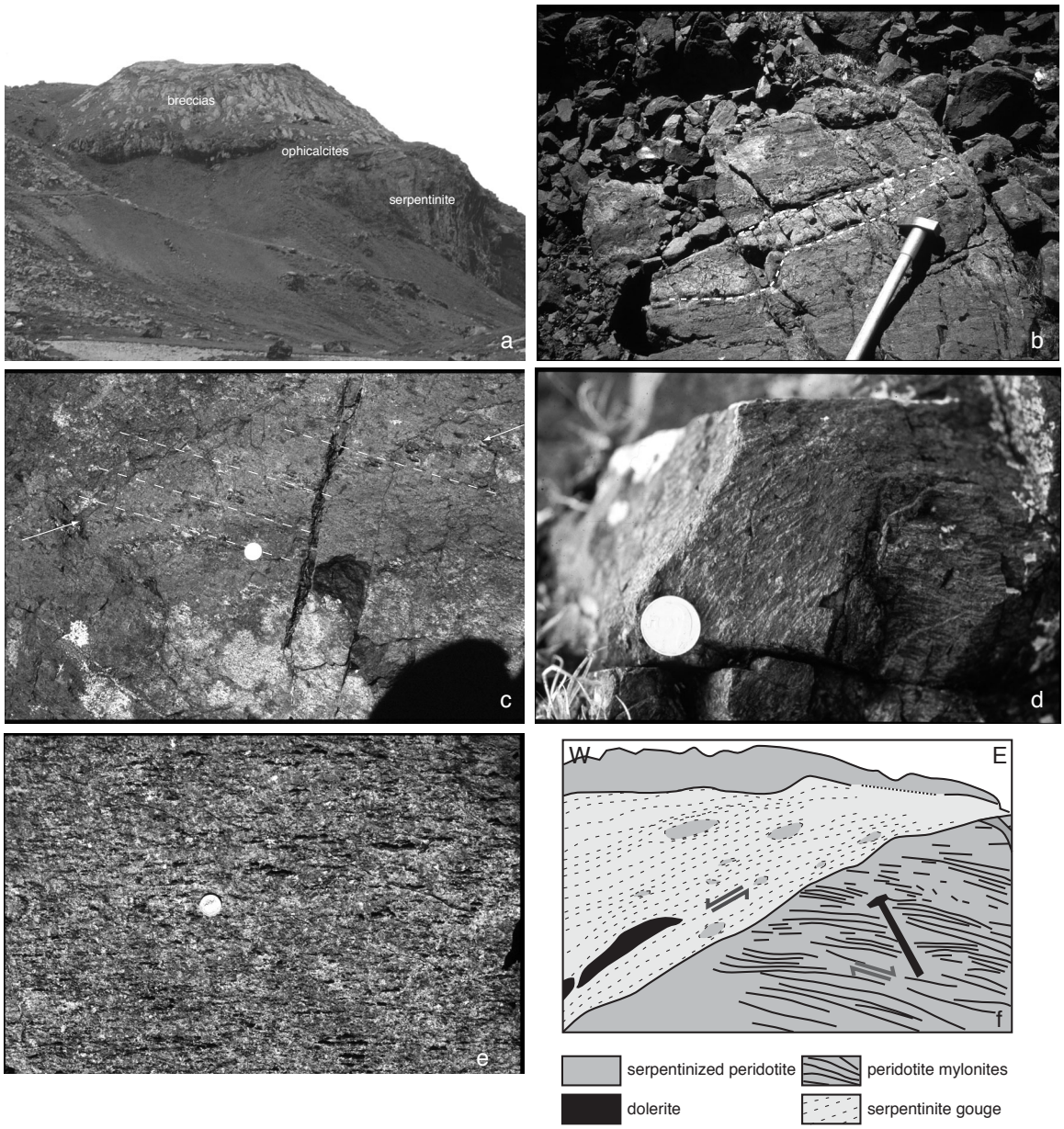

Figure 3-2: Field relationships in the Platta mantle rocks. a) Continental-derived breccias stratigraphically overlying serpentinite, upper serpentinite unit, Parsettens (Swiss coordinates: 772'000/169'625), view from Val d'Err. b) Pyroxenite dyke intruding spinel-lherzolite, upper serpentinite unit, Bovas Blavas (Swiss coordinates: 771'005/157'600). c) High-temperature foliation (dashed line) discordant to a pyroxenite dyke (indicated by the arrow), upper serpentinite unit, Bovas Blavas (Swiss coordinates: 771'005/157'600). d) Penetrative high-temperature foliation affecting the upper serpentinite, upper serpentinite unit, Parsettens (Swiss coordinates765'625/169'625). e) Spinel-lherzolite tectonite, lower serpentinite unit, Fuorcla da Faller (Swiss coordinates 771'500/147'625). f) Intra-mantle gouge cutting across a previous granulite facies mylonitic foliation and deforming a rodingitized dolerite dykes, lower serpentinite unit, Sur al Cant (Swiss coordinates 768'470/144'650)

2.2. Petrography and microtexture

2.2.1. Upper serpentinite unit

The two rock-types recognized within the upper serpentinite unit are spinel-lherzolite intruded by pyroxenite dykes. This type of fabric is rare as most of the

mantle rocks of the upper serpentinite unit show a strong foliation consisting of thin bands of serpentinite (former lherzolite) alternating with clinopyroxene-rich zone (former pyroxenite). In the followings, the micro-texture will be referred as a porphyroclastic 1 fabric in the less deformed rocks and as a porphyroclastic 2 fabric in strongly deformed samples. This notation is arbitrary and used for the commodity of the description. It does not refer to a different timing of the formation of the two types of fabric.

Stage I: Spinel foliation in the lherzolite and pyroxenite intrusion

In the less deformed rocks, the lherzolite and the pyroxenite show a porphyroclastic fabric (porphyroclastic 1), which is characterized by the lack of a well-defined foliation.

The pyroxenite includes large strained clino- and orthopyroxenes in a fine-grained matrix of neoblastic clinopyroxenes and of pseudomorphs of neoblastic orthopyroxene and spinel now altered to serpentine, chlorite and magnetite, respectively. The coarse and elongated orthopyroxenes (up to 1 cm long) is systematically altered to serpentine and chlorite. The porphyroclastic clinopyroxenes (2-3 mm) show orthopyroxene exsolution lamellae (now altered to chlorite) and are generally kinked. A peculiar feature of this assemblage is the occurrence of round, concentrically zoned clusters of worm-like intergrowths of spinel and pyroxenes, which appear to be undeformed (Fig. 3-3a). The center of the clusters consists of orthopyroxene, clinopyroxene, spinel and plagioclase. The clinopyroxene may be replaced by kaersutite (Fig. 3-3b, c, d). In one kaersutite-bearing sample, phlogopite occurs in a small vein cutting across the porphyroclastic assemblage. The rim of the clusters consists of much smaller grains of orthopyroxene, spinel, plagioclase, and kaersutite showing a symplectitic texture (Fig. 3-3a, c, d. e).
The neoblastic pyroxenes (150-250 μm) show a equigranular mosaic texture with some interstitial spinel (100 μm) occurring at grain boundaries. Within this assemblage the spinel and the orthopyroxene are now altered to chlorite, serpentine and magnetite.

In the spinel lherzolite, the porphyroclastic assemblage is characterized by large holly-leaf spinel (up to 2.5 mm) underlying a weak foliation, strain-free large clinopyroxene (2-3 mm) and pseudomorphs of elongated orthopyroxene (up to 5 mm), now altered to serpentine and chlorite.

Stage II: Anhydrous deformation (main structure-granulite facies)

Most of the mantle rocks in the upper serpentinite unit show a pervasive high-temperature foliation producing a compositional banding. In thin section, this deformation stage is also characterized by a porphyroclastic fabric (porphyroclastic 2), which differs from the porphyroclastic fabric 2 by the presence of a strong foliation. The spinel-pyroxene clusters of the pyroxenites are elongated along the foliation planes with rotated or kinked porphyroclastic pyroxene and neoblastic minerals growing in the plane of the new foliation (Fig. 3-4a). The asymmetric clasts associated with this event of high-temperature shearing show a top-to-the-east sense of shear. The neoblastic assemblage consists of small clinopyroxene (50-200 μm), orthopyroxene, olivine and spinel, which are generally altered to chlorite, serpentine minerals and magnetite. We interpret this assemblage as formed under spinel-peridotite facies conditions with a later low-grade overprint.

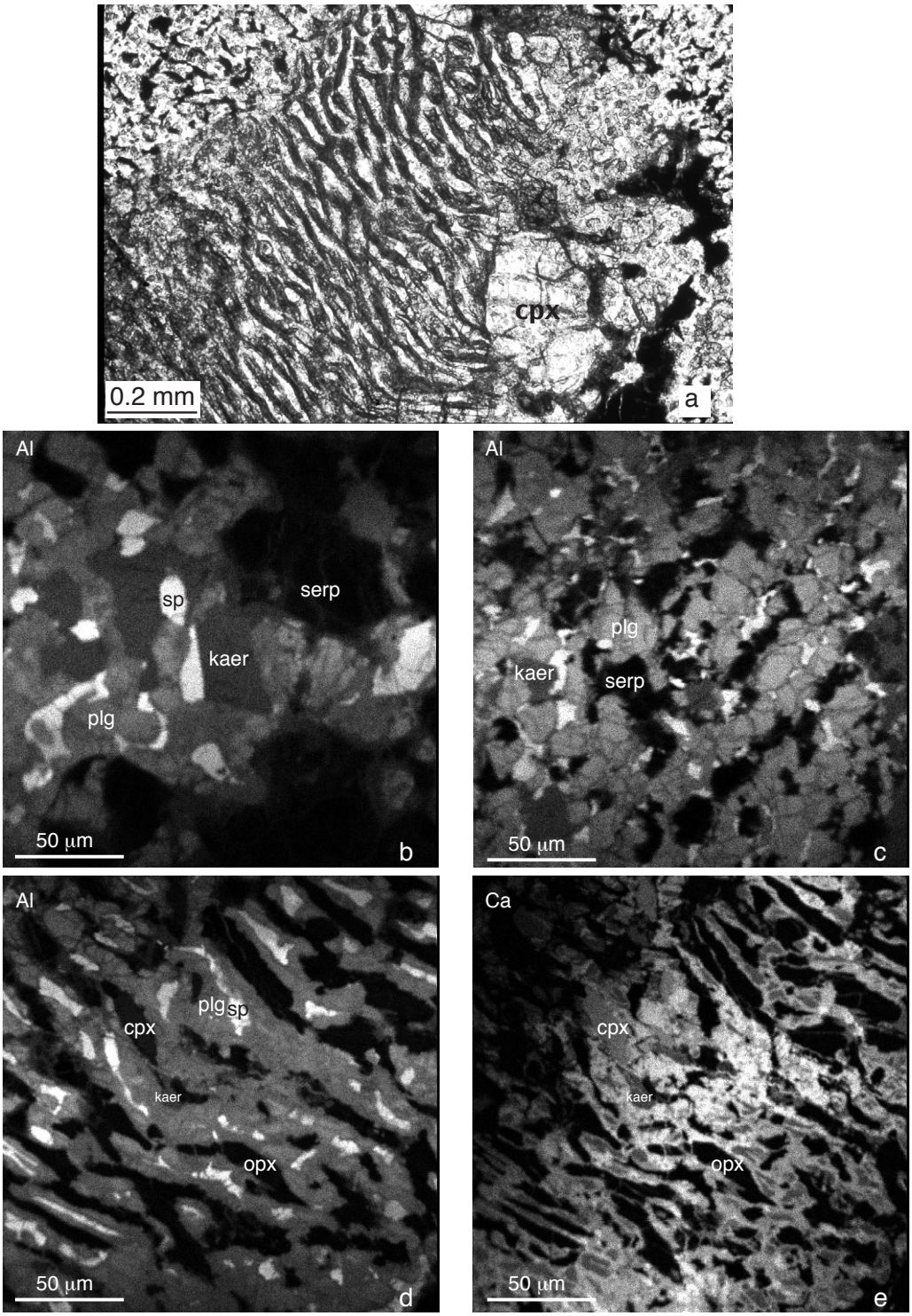

Figure 3-3: Texture and mineralogy of the undeformed spinel-pyroxene clusters (Sample FAP6, upper serpentinite unit). a) Texture of spinel-pyroxene cluster at contact with a clinopyroxene. Note the smaller grain-size in the upper-left corner, plane light. b). Al distribution x-ray maps of the center of a cluster consisting of kaersutite (kaer), spinel (sp), plagioclase (plg) and serpentine (serp), which represent former orthopyroxene. c) Al distribution x-ray map of the rim of the same cluster. Note the smaller grain-size and the lower amount of kaersutite. d) and e) Al and Ca distribution x- ray maps of a spinel-pyroxene cluster showing a symplectite texture. Note the spinel inclusion rimmed by plagioclase.

Stage III: Static hydration (amphibolite and greenschist facies)

The evidence for retrograde high-temperature hydration in the upper serpentinite unit is rare and restricted to the appearance of Mg-hornblende in coronae around clinopyroxene and along its cleavage planes. This was followed by a more widespread hydration at lower temperature characterized by the crystallization of tremolite at the expense of clinopyroxene and of Mg-hornblende. Olivine was transformed into a serpentine mesh with magnetite, whereas the spinel was altered to Cr-rich chlorite and magnetite. Finally, the serpentine minerals were partially replaced by the assemblage calcite + talc.

Stage IV: Hydrous deformation (greenschist facies and lower grade)

The last deformation event is characterized by the presence of shear bands reorienting the previous high-temperature foliation (Fig. 3-4b). The shear-bands are localized at the edges of the large clinopyroxene porphyroclasts and contain magnetite, serpentine and chlorite indicating greenschist facies condition of deformation. This low-temperature deformation event shows a top-west sense-of-shear opposite to the high-temperature deformation event.

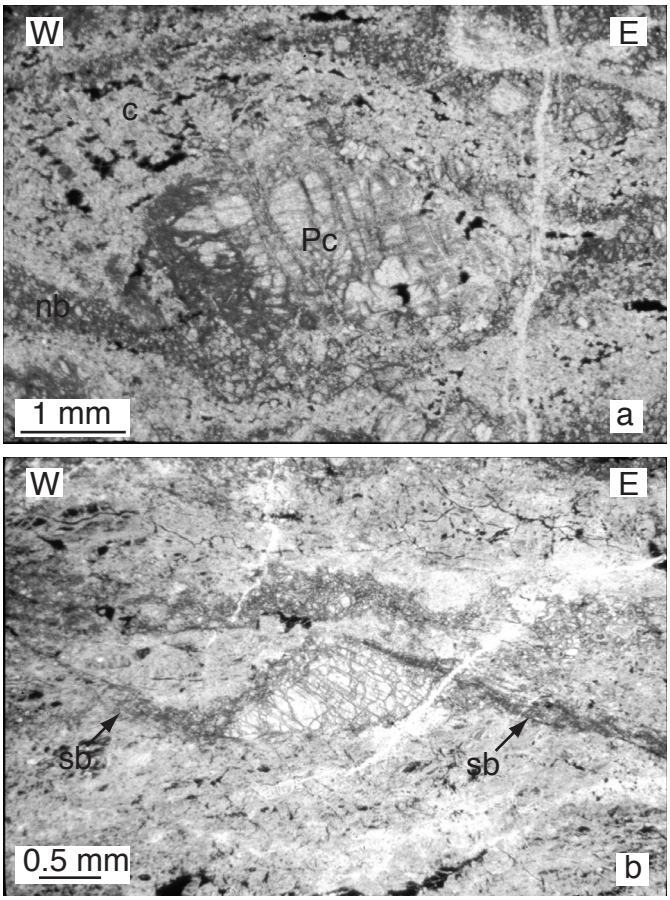

Figure 3-4: a) Thin-section showing the texture associated with the high-temperature deformation deforming the spinel-pyroxene cluster. Pc: large orthopyroxene porphyroclast, nb: neoblastic assemblage crystallizing along the foliation plane and c: elongated cluster along the foliation plane (plane light, sample CUP2, upper serpentinite unit). b). Greenschist facies shear-bands (sb) overprinting the older high-temperature foliation (plane light, sample VEP7, upper serpentinite unit).

2.2.2 Lower serpentinite unit

Stage I: Spinel foliation (main fabric)

The serpentinized lherzolites of the lower serpentinite unit show a porphyroclastic texture with large holly leaf spinel (up to 1 cm) defining a weak foliation. The mineral assemblage consists of large porphyroclastic Cr-diopside, orthopyroxene, Cr-Al spinel, and olivine, which is always replaced by serpentine minerals. Two types of pyroxene porphyroclasts can be distinguished: large clinopyroxenes (2.5-3 mm) and orthopyroxenes (up to 5 mm) with exsolution lamellae, and exsolution-free pyroxene (1-2 mm) porphyroclasts. The exsolution lamellae are systematically altered to chlorite or secondary diopside and tremolite. In one samples, disseminated grains of phlogopite occur within the porphyroclastic assemblage. Except for the spinel, none of the porphyroclastic minerals do show a preferred orientation or optical evidence for internal strain. This assemblage partially re-equilibrated in the spinel stability field as shown by the static recrystallization of neoblastic exsolution-free clinopyroxene, Cr-Al spinel, and Ti-pargasite showing a mosaic texture.

Stage II: Anhydrous deformation (localized)

At places, localized mylonitic shear zones overprint the porphyroclastic assemblage. Due to the strong alteration, only fresh holly-leaf spinels are preserved, which, together with former pyroxenes, form porphyroclasts. The mylonitic foliation is underlined by prismatic magnetite associated with serpentine minerals, which may have replaced former olivine. Radial tremolite is present within the foliation plane indicating static low-temperature alteration.

Stage III: Static hydration (Amphibolite and greenschist facies)

Retrograde metamorphism and hydration of the mantle rocks is expressed by the development of Mg-hornblende at the expense of clinopyroxene and of chlorite coronae around the spinel. Low-grade alteration is characterized by the association of diopside, serpentine minerals and tremolite indicating widespread hydration of the mantle rocks under greenschist-facies conditions.

2.3. Mineral chemistry

The composition of the high-temperature mineral characteristic for the evolution under upper mantle condition is always different in the upper and lower serpentinite units. Only, the composition of retrograde amphiboles indicating hydration of mantle rocks under retrograde conditions is similar in the two units.

2.3.1. Clinopyroxene

Upper serpentinite unit (table 3-1)

The clinopyroxenes of the serpentinized lherzolites and pyroxenites of the upper serpentinite unit are rich in Al_2O_3 (6.19-6.99 weight %) and Na_2O (1.23-1.46 weight %). The porphyroclastic clinopyroxenes of the pyroxenites show lower Mg#, Cr_2O_3, Na_2O and slightly higher TiO_2 contents than that of the host lherzolite (Fig. 3-5). The metamorphic clinopyroxenes of the cluster show generally higher Mg# and

TiO_2 contents and lower Al_2O3, Na_2O and Cr_2O_3 contents than those of pyroxenites and lherzolites. However, in the most deformed sample (Sample FAP4 and VEP8), the clinopyroxenes of the clusters show composition similar to those of the porphyroclastic clinopyroxenes except for the Cr_2O_3 content suggesting a reequilibration of their composition during the granulite-facies deformation event. The neoblasts in the lherzolites and the pyroxenites underlining the foliation show lower Al_2O_3, Na_2O, TiO_2 and Cr_2O_3 contents and higher Mg# than the porphyroclasts (see arrows in Fig. 3-5), which is characteristic for a retrograde evolution. However, the neoblastic clinopyroxenes show still relatively high Al and Na values indicating that deformation occurred under granulite-facies metamorphic conditions (cf. Müntener *et al*. 2000). It should be noted that the porphyroclasts and the neoblasts of the porphyroclastic fabric 1 do not show a chemical composition different from that of the porphyroclastic fabric 2.

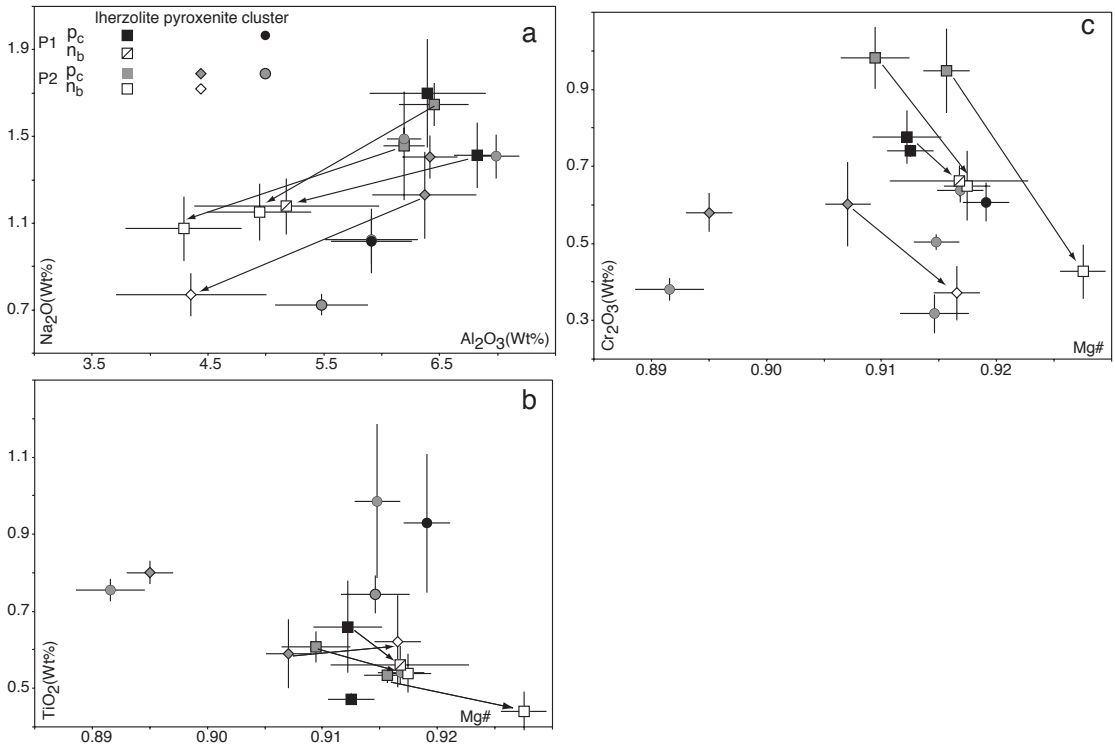

Figure 3-5: Chemical composition of the clinopyroxenes of the ultramafic rocks of the upper serpentinite unit. a) Na_2O vs Al_2O_3 diagram. The neoblasts show lower Na_2O and Al_2O_3 contents than the porphyroclasts indicating that they equilibrated at a lower P-T conditions than the porphyroclasts. The clinopyroxenes of the clusters show lower Na_2O than those of the lherzolites. b) TiO_2 vs Mg# diagram. The clinopyroxenes of the clusters are enriched in TiO_2 in comparison to those of the lherzolites and pyroxenites. The neoblasts show higher Mg# than the associated porphyroclasts. c) Cr_2O_3 vs Mg# diagram. The clinopyroxenes of the clusters and of the pyroxenite are depleted in Cr_2O_3 compared to those of the lherzolites. P1 refers to minerals of the porphyroclastic texture 1, P2 to those of the porphyroclastic texture 2; p_c: porphyroclast, n_b: neoblast; arrows indicate porphyroclast and neoblasts from the same sample; each point is an average of the composition of the clinopyroxenes for each sample and the error bars represent the standard deviation (2s) (see text for discussion).

Table 3-1. *Chemical composition of the minerals characteristic of the anhydrous evolution of the mantle rocks of the upper serpentinite unit*

	porphyroclasts											
Sample	VEP3		VEP8		VEP11		FAP4		FAP6		FAP4	
	cpx *		cpx *		cpx *		cpx *		cpx *		cpx **	
SiO_2	51.51	0.65	51.87	0.41	51.72	0.41	51.17	0.21	50.78	0.97	51.18	0.59
TiO_2	0.47	0.03	0.53	0.04	0.61	0.09	0.80	0.07	0.66	0.25	0.76	0.06
Cr_2O_3	0.74	0.03	0.95	0.22	0.98	0.16	0.58	0.11	0.78	0.15	0.38	0.06
Al_2O_3	6.40	0.98	6.19	0.36	6.45	0.58	6.42	0.48	6.83	0.40	6.99	0.42
Fe_2O_3	1.63	0.58	1.30	0.68	0.85	0.32	1.75	0.17	1.43	0.58	1.72	0.80
FeO	1.02	0.49	1.32	0.60	1.97	0.44	1.60	0.29	1.33	0.54	1.79	0.87
MnO	0.08	0.04	0.11	0.03	0.07	0.02	0.09	0.01	0.06	0.03	0.10	0.02
MgO	14.60	0.29	15.18	0.72	15.32	0.84	15.15	0.51	15.22	0.63	15.36	1.36
NiO	0.06	0.03	0.04	0.02	0.04	0.04	0.05	0.03	0.05	0.03	0.05	0.03
CaO	21.56	0.90	21.21	0.89	20.10	1.02	21.41	0.63	20.94	1.10	20.82	1.56
Na_2O	1.70	0.48	1.46	0.51	1.65	0.22	1.41	0.21	1.41	0.37	1.41	0.21
K_2O	0.03	0.01	0.01	0.01	0.00	0.00	0.00	0.01	0.00	0.00	0.04	0.06
Total	99.79		100.19		99.75		100.41		99.50		100.60	
Si	1.877	0.011	1.879	0.009	1.878	0.011	1.858	0.009	1.854	0.024	1.852	0.013
Ti	0.013	0.001	0.015	0.001	0.017	0.002	0.022	0.002	0.018	0.007	0.021	0.002
Cr	0.021	0.001	0.027	0.006	0.028	0.005	0.017	0.003	0.022	0.004	0.011	0.002
Al	0.275	0.040	0.265	0.015	0.276	0.024	0.275	0.021	0.294	0.017	0.298	0.018
Fe^{3+}	0.045	0.016	0.036	0.019	0.023	0.009	0.048	0.005	0.039	0.016	0.047	0.022
Fe^{2+}	0.031	0.015	0.040	0.018	0.060	0.013	0.049	0.009	0.041	0.016	0.054	0.026
Mn	0.003	0.001	0.003	0.001	0.002	0.000	0.003	0.000	0.002	0.001	0.003	0.001
Mg	0.793	0.021	0.820	0.035	0.829	0.041	0.820	0.026	0.829	0.033	0.828	0.070
Ni	0.002	0.001	0.001	0.001	0.001	0.001	0.001	0.001	0.001	0.001	0.001	0.001
Ca	0.842	0.038	0.823	0.037	0.782	0.042	0.833	0.025	0.819	0.045	0.807	0.064
Na	0.120	0.034	0.102	0.036	0.116	0.016	0.099	0.015	0.100	0.026	0.099	0.014
K	0.001	0.001	0.001	0.001	0.000	0.000	0.000	0.000	0.000	0.000	0.002	0.003
Mg#	0.913	0.004	0.916	0.004	0.909	0.006	0.895	0.005	0.912	0.006	0.892	0.006

Ions calculated on the basis of six oxygens (pyroxenes), 3 cations (spinel, magnetite), 23 oxygens and ∑(cat)-Ca-Na-K=13 (amphiboles), 11 oxygens and ∑(cat)-Na-K=7-Ti (phlogopite). * lherzolite, ** pyroxenite, *** clusters and V alkaline veins. For each sample, the average composition and the standard deviation (2σ) are presented.

Table 3-1. *(continued)*

	Porphyroclasts													
Sample	CUP1		VEP8		VEP11				FAP6					
	cpx **		cpx ***		cpx ***		cpx***		opx***		sp***		plg***	
SiO_2	51.50	0.77	51.17	0.65	51.32	0.72	51.00	0.65	55.83	1.11	0.00	0.00	53.55	0.89
TiO_2	0.59	0.18	0.54	0.03	0.99	0.39	0.93	0.36	0.20	0.08	0.08	0.02	0.05	0.02
Cr_2O_3	0.60	0.22	0.64	0.06	0.50	0.05	0.61	0.11	0.22	0.05	10.36	2.26	0.05	0.03
Al_2O_3	6.37	0.89	6.19	0.32	5.91	0.78	5.91	0.71	3.18	0.95	56.91	2.55	28.66	0.74
Fe_2O_3	1.30	0.95	1.93	0.57	0.96	0.28	1.22	0.39	0.55	0.64	1.35	0.55	0.29	0.19
FeO	1.82	0.91	0.74	0.41	1.75	0.28	1.34	0.30	5.58	0.51	10.33	0.68	0.05	0.11
MnO	0.10	0.02	0.11	0.03	0.08	0.04	0.06	0.03	0.15	0.03	0.00	0.00	0.03	0.03
MgO	16.40	3.20	15.34	0.27	15.70	0.33	15.54	0.45	33.97	0.58	19.60	0.75	0.05	0.05
NiO	0.04	0.04	0.04	0.03	0.04	0.04	0.03	0.03	0.08	0.05	0.36	0.05	0.01	0.01
CaO	20.24	2.80	21.42	0.55	21.91	0.58	22.26	0.79	0.55	0.10	0.06	0.04	11.56	1.12
Na_2O	1.23	0.42	1.49	0.10	1.02	0.22	1.02	0.30	0.02	0.02	0.01	0.01	5.09	0.53
Total	100.18		99.64		100.19		99.92		100.29		99.07		99.39	
Si	1.864	0.018	1.868	0.010	1.863	0.023	1.858	0.017	1.921	0.025	0.000	0.000	2.433	0.037
Ti	0.016	0.005	0.015	0.001	0.027	0.011	0.025	0.010	0.005	0.002	0.002	0.000	0.002	0.001
Cr	0.017	0.006	0.018	0.001	0.014	0.001	0.017	0.003	0.006	0.001	0.215	0.050	0.002	0.001
Al	0.272	0.039	0.267	0.014	0.253	0.033	0.254	0.031	0.129	0.039	1.756	0.054	1.534	0.033
Fe^{3+}	0.035	0.026	0.053	0.016	0.026	0.008	0.034	0.011	0.014	0.017	0.027	0.011	0.010	0.006
Fe^{2+}	0.055	0.027	0.023	0.013	0.053	0.008	0.041	0.009	0.160	0.014	0.226	0.018	0.002	0.004
Mn	0.003	0.001	0.003	0.001	0.002	0.001	0.002	0.001	0.004	0.001	0.000	0.000	0.001	0.001
Mg	0.884	0.169	0.835	0.018	0.849	0.018	0.844	0.023	1.742	0.024	0.765	0.018	0.003	0.004
Ni	0.001	0.001	0.001	0.001	0.001	0.001	0.001	0.001	0.002	0.001	0.008	0.001	0.000	0.000
Ca	0.785	0.112	0.838	0.016	0.852	0.023	0.869	0.028	0.020	0.004	0.002	0.001	0.563	0.056
Na	0.086	0.030	0.105	0.007	0.072	0.016	0.072	0.022	0.001	0.001	0.001	0.000	0.449	0.047
Mg#	0.907	0.008	0.917	0.005	0.915	0.004	0.919	0.005	0.909	0.004	0.763	0.018		
Cr#											10.916	2.573		
Xan													0.555	0.050

Table 3-1 *(continued)*

	porphyroclast		neoblasts										V
	FAP6		VEP8		VEP11		FAP6		CUP1				FAP6
	amp***		cpx*		cpx*		cpx*		cpx**		cpx***		phlog
SiO_2	41.30	0.34	52.51	0.71	52.37	0.74	51.77	1.43	52.10	0.81	51.27	0.31	37.35
TiO_2	5.60	0.65	0.44	0.10	0.54	0.10	0.56	0.10	0.62	0.25	0.74	0.11	6.84
Cr_2O_3	0.99	0.10	0.43	0.14	0.65	0.19	0.66	0.08	0.37	0.14	0.32	0.10	0.61
Al_2O_3	13.23	0.19	4.29	0.99	4.94	0.87	5.18	1.66	4.35	1.34	5.48	0.86	15.10
Fe_2O_3	0.14	0.37	1.70	0.43	1.02	0.46	0.87	0.38	1.17	0.30	1.09	0.43	5.16
FeO	3.99	0.40	0.74	0.44	1.66	0.42	1.76	0.51	1.62	0.28	1.71	0.47	0.00
MnO	0.04	0.04	0.09	0.03	0.08	0.02	0.06	0.02	0.11	0.02	0.09	0.01	0.04
MgO	15.97	0.41	16.30	0.60	16.09	0.50	15.74	0.92	16.48	0.95	16.20	0.31	19.93
NiO	0.10	0.05	0.05	0.04	0.04	0.03	0.06	0.02	0.05	0.05	0.05	0.03	0.00
CaO	11.83	0.24	22.67	0.93	21.68	0.66	21.38	1.45	22.38	0.32	22.13	0.66	0.01
Na_2O	3.48	0.10	1.07	0.30	1.15	0.26	1.18	0.27	0.77	0.23	0.72	0.17	0.67
K_2O	0.20	0.09	0.02	0.01	0.00	0.01	0.01	0.02	0.00	0.01	0.01	0.01	9.04
H2O	2.06	0.01	---	---	---	---	---	---	---	---	---	---	4.26
Total	98.91		100.30		100.22		99.22		100.02		99.82		99.01
Si	6.017	0.069	1.904	0.019	1.897	0.019	1.893	0.032	1.896	0.027	1.868	0.013	2.627
Ti	0.614	0.072	0.012	0.003	0.015	0.003	0.015	0.003	0.017	0.007	0.020	0.003	0.362
Cr	0.113	0.011	0.012	0.004	0.019	0.005	0.019	0.002	0.011	0.004	0.009	0.003	0.034
Al	2.271	0.024	0.183	0.043	0.211	0.037	0.224	0.074	0.187	0.057	0.235	0.036	1.252
Fe^{3+}	0.015	0.040	0.046	0.012	0.028	0.013	0.024	0.011	0.032	0.008	0.030	0.012	0.273
Fe^{2+}	0.486	0.049	0.023	0.013	0.050	0.012	0.054	0.016	0.049	0.008	0.052	0.014	0.000
Mn	0.005	0.004	0.003	0.001	0.002	0.001	0.002	0.001	0.003	0.001	0.003	0.000	0.002
Mg	3.467	0.072	0.881	0.031	0.868	0.027	0.858	0.043	0.894	0.052	0.880	0.021	2.089
Ni	0.011	0.006	0.001	0.001	0.001	0.001	0.002	0.001	0.001	0.001	0.001	0.001	0.000
Ca	1.846	0.045	0.881	0.037	0.841	0.027	0.837	0.050	0.872	0.011	0.864	0.028	0.001
Na	0.982	0.033	0.076	0.021	0.081	0.018	0.084	0.020	0.054	0.016	0.051	0.012	0.092
K	0.037	0.016	0.001	0.001	0.000	0.000	0.000	0.001	0.000	0.000	0.000	0.000	0.811
OH^-	2.000	0.000	---	---	---	---	---	---	---	---	---	---	2.000
Mg#	0.874	0.004	0.928	0.005	0.917	0.005	0.917	0.013	0.917	0.004	0.915	0.006	0.884

Table 3-2. *Chemical composition of the minerals characterizing the high-temperature evolution of the lherzolites of the lower serpentinite unit.*

	porphyroclast													
	MSP1						SUP2				CRP3			
Sample	cpx		opx		sp		cpx		opx		cpx*		cpx	
SiO_2	50.48	0.61	54.69	0.75	0.15	0.27	50.10	1.00	54.52	1.12	49.53	0.22	51.24	0.60
TiO_2	0.66	0.13	0.25	0.02	0.43	0.18	0.94	0.02	0.25	0.06	0.75	0.01	0.72	0.05
Cr_2O_3	1.14	0.07	0.70	0.12	30.25	2.81	1.01	0.05	0.61	0.03	0.94	0.01	1.12	0.07
Al_2O_3	5.00	0.52	3.27	0.21	27.83	6.78	4.70	0.17	3.35	0.44	6.63	0.37	4.43	0.74
Fe_2O_3	0.97	0.62	0.47	0.49	9.04	8.56	2.21	0.67	1.30	1.11	1.62	0.74	1.73	0.65
FeO	2.11	0.66	6.39	0.54	16.83	1.52	1.12	0.53	5.51	0.98	1.79	0.76	1.47	0.53
MnO	0.10	0.02	0.18	0.01	1.28	1.92	0.10	0.03	0.15	0.03	0.14	0.01	0.10	0.02
MgO	15.78	0.23	31.83	0.35	11.39	2.12	15.99	0.77	32.87	0.45	15.04	0.73	16.07	0.54
NiO	0.06	0.05	0.08	0.04	0.23	0.06	0.07	0.03	0.09	0.03	0.03	0.04	0.05	0.03
CaO	22.65	0.32	1.67	0.38	0.13	0.09	22.42	0.77	1.01	0.58	22.38	0.30	22.99	0.43
Na_2O	0.43	0.06	0.06	0.03	0.05	0.01	0.70	0.02	0.03	0.03	0.69	0.02	0.63	0.06
Total	99.39		99.60		97.62		99.36		99.70		99.50		100.56	
Si	1.858	0.007	1.913	0.007	0.005	0.009	1.851	0.010	1.902	0.020	1.824	0.003	1.868	0.015
Ti	0.018	0.004	0.007	0.001	0.010	0.004	0.026	0.000	0.007	0.002	0.021	0.000	0.020	0.001
Cr	0.033	0.002	0.019	0.003	0.743	0.049	0.030	0.001	0.017	0.001	0.027	0.000	0.032	0.002
Al	0.217	0.021	0.135	0.009	1.013	0.206	0.205	0.009	0.138	0.018	0.288	0.015	0.190	0.032
Fe^{3+}	0.027	0.017	0.012	0.013	0.218	0.215	0.062	0.019	0.034	0.029	0.045	0.021	0.047	0.018
Fe^{2+}	0.065	0.020	0.187	0.014	0.438	0.045	0.035	0.016	0.161	0.027	0.055	0.023	0.045	0.016
Mn	0.003	0.001	0.005	0.000	0.035	0.053	0.003	0.001	0.004	0.001	0.004	0.000	0.003	0.001
Mg	0.866	0.013	1.659	0.021	0.525	0.076	0.880	0.040	1.710	0.034	0.825	0.042	0.873	0.031
Ni	0.002	0.002	0.002	0.001	0.006	0.002	0.002	0.001	0.003	0.001	0.001	0.001	0.001	0.001
Ca	0.894	0.019	0.063	0.014	0.004	0.003	0.888	0.031	0.038	0.022	0.883	0.010	0.898	0.013
Na	0.031	0.004	0.004	0.002	0.003	0.001	0.050	0.002	0.002	0.002	0.049	0.001	0.044	0.004
Mg#	0.904	0.004	0.893	0.002	0.445	0.225	0.902	0.002	0.898	0.001	0.892	0.008	0.904	0.004
Cr#					42.68	4.85								

Calculation as in table 3-1. * porphyroclast with exsolution lamellae.

Table 3-2 *(continued)*

	porphyroclast													
	CRP3		NAP6				SUP3				NAP5			
Sample	sp		cpx		phlog		cpx		sp		cpx		sp	
SiO_2	0.00	0.00	53.18	0.61	38.14	0.50	51.16	0.66	0.38	0.54	50.84	0.58	0.00	0.00
TiO_2	0.70	0.36	0.23	0.11	1.80	0.64	0.76	0.02	0.53	0.01	0.86	0.12	0.37	0.16
Cr_2O_3	33.60	1.76	0.64	0.20	0.98	0.30	1.02	0.01	27.38	0.21	1.00	0.12	32.16	0.84
Al_2O_3	28.10	2.63	4.49	0.86	16.50	1.37	4.54	0.56	35.85	0.86	4.24	0.66	31.00	1.31
Fe_2O_3	6.90	1.58	0.03	0.08	2.90	2.10	0.69	0.70	5.07	0.27	0.00	0.00	6.71	0.56
FeO	17.20	1.78	2.43	0.14	1.25	1.55	2.38	0.60	13.39	0.05	2.95	0.17	15.84	0.68
MnO	0.55	0.23	0.09	0.02	0.07	0.07	0.10	0.02	0.29	0.00	0.10	0.03	0.40	0.02
MgO	12.12	1.77	16.21	0.30	24.34	1.52	16.11	0.74	15.60	0.16	15.98	0.48	13.57	0.51
NiO	0.19	0.05	0.05	0.04	0.19	0.04	0.07	0.03	0.20	0.01	0.04	0.03	0.18	0.03
CaO	0.03	0.03	22.09	0.61	0.01	0.02	22.02	0.72	0.37	0.52	22.86	0.56	0.00	0.00
Na_2O	0.08	0.16	0.76	0.14	0.42	0.11	0.58	0.08	0.03	0.01	0.66	0.06	0.02	0.01
K_2O	0.01	0.01	0.00	0.00	6.96	1.76	0.00	0.01	0.01	0.01	0.01	0.01	0.00	0.01
H_2O	---	---	---	---	4.26	0.05	---	---	---	---	---	---	---	---
Total	99.47		100.18		97.81		99.41		99.07		99.55		100.27	
Si	0.000	0.000	1.921	0.020	2.686	0.066	1.877	0.012	0.011	0.016	1.869	0.019	0.000	0.000
Ti	0.016	0.008	0.006	0.003	0.095	0.033	0.021	0.001	0.011	0.000	0.024	0.003	0.008	0.004
Cr	0.809	0.056	0.018	0.006	0.054	0.016	0.030	0.001	0.626	0.002	0.029	0.004	0.753	0.027
Al	1.006	0.071	0.191	0.036	1.371	0.127	0.196	0.024	1.221	0.024	0.184	0.028	1.082	0.034
Fe^{3+}	0.159	0.040	0.001	0.002	0.153	0.110	0.019	0.020	0.110	0.005	0.000	0.000	0.149	0.013
Fe^{2+}	0.439	0.056	0.073	0.004	0.075	0.092	0.073	0.018	0.324	0.003	0.091	0.005	0.393	0.020
Mn	0.014	0.006	0.003	0.000	0.004	0.004	0.003	0.001	0.007	0.000	0.003	0.001	0.010	0.001
Mg	0.548	0.067	0.873	0.018	2.553	0.128	0.881	0.042	0.672	0.004	0.001	0.001	0.599	0.017
Ni	0.005	0.001	0.001	0.001	0.011	0.002	0.002	0.001	0.005	0.000	0.876	0.025	0.004	0.001
Ca	0.001	0.001	0.855	0.020	0.001	0.001	0.866	0.029	0.012	0.016	0.901	0.023	0.000	0.000
Na	0.004	0.010	0.053	0.009	0.057	0.015	0.041	0.006	0.002	0.001	0.047	0.004	0.001	0.001
K	0.000	0.000	0.000	0.000	0.627	0.165	0.000	0.000	0.000	0.000	0.000	0.000	0.000	0.000
OH^-	---	---	---	---	2.000	0.000	---	---	---	---	---	---	---	---
Mg#	0.478	0.413	0.922	0.006	0.919	0.007	0.906	0.003	0.608	0.337	0.906	0.005	0.525	0.334
Cr#	44.60	3.42							33.88	0.37			37.97	1.42

Table 3-2. *(continued)*

	porphyroclast													
	STP4				STP5-20000				NAP2		STP2		LAP1	
	cpx		sp		cpx		sp		cpx		cpx		cpx	
SiO_2	51.05	0.46	0.04	0.06	51.01	0.49	0.00	0.00	49.43	1.32	52.16	0.41	51.37	0.44
TiO_2	0.93	0.07	0.68	0.01	0.89	0.06	0.58	0.08	0.84	0.06	0.24	0.04	0.83	0.06
Cr_2O_3	1.01	0.07	35.82	0.44	0.94	0.04	28.52	0.88	0.83	0.04	0.81	0.07	0.99	0.09
Al_2O_3	4.43	0.32	27.95	0.14	4.51	0.35	34.74	1.02	5.38	0.38	4.90	0.31	4.21	0.35
Fe_2O_3	1.38	0.34	6.32	0.02	1.42	0.50	6.00	0.73	2.71	1.20	0.70	0.36	1.16	0.55
FeO	1.69	0.31	17.11	0.73	1.91	0.37	15.75	1.05	0.92	1.02	1.85	0.30	1.96	0.54
MnO	0.10	0.03	0.34	0.05	0.07	0.03	0.00	0.00	0.11	0.02	0.10	0.02	0.10	0.01
MgO	16.02	0.56	12.96	0.45	16.34	0.37	14.41	0.86	16.42	1.99	16.35	0.43	16.31	0.46
NiO	0.04	0.03	0.18	0.01	0.04	0.03	0.20	0.03	0.04	0.01	0.04	0.03	0.04	0.03
CaO	22.92	1.05	0.03	0.02	22.28	0.37	0.00	0.00	21.86	2.41	22.29	0.47	22.30	0.53
Na_2O	0.59	0.06	0.01	0.01	0.59	0.04	0.01	0.01	0.62	0.11	0.69	0.04	0.63	0.05
Total	100.4		101.42		99.98		100.21		99.16		100.15		99.92	
Si	1.866	0.009	0.001	0.002	1.866	0.011	0.000	0.000	1.830	0.023	1.892	0.009	1.879	0.010
Ti	0.026	0.002	0.015	0.000	0.024	0.002	0.013	0.002	0.023	0.002	0.007	0.001	0.023	0.002
Cr	0.029	0.002	0.844	0.010	0.027	0.001	0.655	0.022	0.024	0.001	0.023	0.002	0.029	0.003
Al	0.191	0.014	0.982	0.006	0.194	0.016	1.189	0.025	0.235	0.018	0.210	0.014	0.182	0.015
Fe^{3+}	0.038	0.009	0.142	0.001	0.039	0.014	0.131	0.017	0.076	0.034	0.019	0.010	0.032	0.015
Fe^{2+}	0.052	0.010	0.426	0.018	0.058	0.011	0.383	0.030	0.028	0.031	0.056	0.009	0.060	0.016
Mn	0.003	0.001	0.008	0.001	0.002	0.001	0.000	0.000	0.003	0.001	0.003	0.001	0.003	0.000
Mg	0.873	0.034	0.576	0.020	0.891	0.019	0.624	0.031	0.906	0.106	0.884	0.024	0.889	0.026
Ni	0.001	0.001	0.004	0.000	0.001	0.001	0.005	0.001	0.001	0.000	0.001	0.001	0.001	0.001
Ca	0.898	0.038	0.001	0.001	0.873	0.014	0.000	0.000	0.868	0.100	0.866	0.017	0.874	0.021
Na	0.042	0.004	0.000	0.000	0.042	0.003	0.000	0.001	0.045	0.008	0.048	0.003	0.045	0.004
Mg#	0.907	0.006	0.503	0.507	0.901	0.004	0.548	0.399	0.898	0.005	0.922	0.003	0.906	0.004
Cr#			46.23	0.43			35.52	1.18						

Table 3-2. *(continued)*

Sample	Porphyroclast										neoblast			
	SUP6		NAP1		NAP7		STP1		stp11		CRP3		SUP2	
	Cpx		cpx		cpx		cpx		cpx		cpx		cpx	
SiO_2	50.27	0.55	50.17	0.55	50.36	0.44	51.67	0.99	50.80	0.39	51.63	0.85	49.50	0.24
TiO_2	0.84	0.08	0.86	0.13	0.92	0.06	0.79	0.14	0.76	0.12	0.73	0.14	0.94	0.03
Cr_2O_3	0.87	0.03	0.97	0.16	0.98	0.07	0.89	0.11	1.01	0.13	1.02	0.24	1.11	0.10
Al_2O_3	5.96	0.87	4.82	0.71	4.60	0.63	4.43	0.75	5.58	0.63	3.66	0.77	4.22	0.06
Fe_2O_3	1.33	0.56	2.12	0.37	2.11	0.39	1.34	1.15	1.49	0.24	1.30	0.58	2.73	0.19
FeO	1.82	0.34	1.12	0.34	1.06	0.33	1.96	0.75	1.74	0.36	1.70	0.53	0.52	0.19
MnO	0.10	0.03	0.08	0.03	0.11	0.03	0.11	0.03	0.06	0.04	0.10	0.03	0.11	0.02
MgO	15.55	0.71	15.89	0.50	15.82	0.32	16.43	1.08	15.96	0.71	16.41	0.56	16.07	0.33
NiO	0.05	0.03	0.04	0.03	0.04	0.02	0.05	0.03	0.06	0.04	0.06	0.03	0.03	0.04
CaO	22.08	1.26	22.60	0.52	23.17	0.29	22.79	1.12	22.28	0.94	22.82	0.83	22.66	0.51
Na_2O	0.74	0.15	0.69	0.08	0.63	0.07	0.54	0.11	0.70	0.11	0.56	0.11	0.63	0.03
Total	99.63		99.35		99.79		101.00		100.43		99.99		98.51	
Si	1.844	0.020	1.852	0.018	1.854	0.017	1.872	0.025	1.849	0.014	1.889	0.022	1.849	0.003
Ti	0.023	0.002	0.024	0.004	0.026	0.002	0.022	0.004	0.021	0.003	0.020	0.004	0.026	0.001
Cr	0.025	0.001	0.028	0.005	0.029	0.002	0.026	0.003	0.029	0.004	0.029	0.007	0.033	0.003
Al	0.257	0.038	0.210	0.031	0.199	0.027	0.189	0.032	0.239	0.027	0.158	0.033	0.186	0.002
Fe^{3+}	0.037	0.016	0.059	0.010	0.058	0.011	0.037	0.032	0.041	0.007	0.036	0.016	0.077	0.006
Fe^{2+}	0.056	0.010	0.034	0.010	0.033	0.010	0.059	0.022	0.053	0.011	0.052	0.016	0.016	0.006
Mn	0.003	0.001	0.002	0.001	0.003	0.001	0.003	0.001	0.002	0.001	0.003	0.001	0.003	0.001
Mg	0.850	0.039	0.875	0.029	0.868	0.018	0.887	0.063	0.866	0.038	0.895	0.033	0.895	0.015
Ni	0.002	0.001	0.001	0.001	0.001	0.001	0.002	0.001	0.002	0.001	0.002	0.001	0.001	0.001
Ca	0.868	0.049	0.894	0.019	0.914	0.012	0.884	0.040	0.869	0.037	0.894	0.029	0.907	0.023
Na	0.053	0.011	0.049	0.005	0.045	0.005	0.038	0.008	0.050	0.008	0.040	0.008	0.046	0.002
Mg#	0.902	0.005	0.904	0.006	0.905	0.006	0.903	0.006	0.902	0.004	0.911	0.009	0.906	0.001

Table 3-2. *(continued)*

	neoblast													
	SUP2				NAP2		NAP1		STP4				STP11	
	sp		amp		cpx		cpx		cpx		amp		cpx	
SiO_2	0.00	0.00	42.32	1.44	49.62	0.57	51.55	0.49	52.17	0.79	42.86	0.76	51.90	1.08
TiO_2	0.57	0.13	3.52	0.38	0.88	0.06	0.66	0.06	0.71	0.16	3.33	0.36	0.60	0.16
Cr_2O_3	30.65	2.10	1.74	0.08	0.92	0.08	0.85	0.09	0.78	0.17	1.46	0.28	0.73	0.25
Al_2O_3	31.68	2.41	12.39	0.31	4.40	0.72	3.46	0.35	3.15	0.70	11.83	0.72	4.10	0.97
Fe_2O_3	6.20	0.71	0.71	1.20	2.77	0.47	1.84	0.26	1.42	0.30	0.42	0.59	1.29	0.42
FeO	15.51	1.55	3.63	0.98	0.42	0.50	1.29	0.26	1.59	0.17	4.15	0.49	1.58	0.27
MnO	0.31	0.02	0.06	0.01	0.09	0.02	0.08	0.03	0.10	0.04	0.04	0.01	0.07	0.03
MgO	13.72	1.23	16.92	0.34	16.15	0.89	16.87	0.60	16.58	0.50	16.94	0.71	16.49	0.55
NiO	0.22	0.05	0.13	0.03	0.05	0.03	0.05	0.03	0.04	0.02	0.11	0.01	0.04	0.04
CaO	0.01	0.02	12.13	0.49	23.04	0.79	22.46	0.87	23.46	0.54	12.55	0.22	22.95	0.56
Na_2O	0.02	0.02	3.40	0.06	0.60	0.08	0.60	0.06	0.50	0.10	2.96	0.17	0.58	0.07
K_2O	0.00	0.00	0.07	0.02	0.00	0.00	0.00	0.00	0.00	0.00	0.02	0.01	0.00	0.01
H_2O	---	---	2.07	0.04	---	---	---	---	---	---	2.07	0.01	---	---
Total	98.89		99.09		98.94		99.72		100.4		98.72		100.32	
Si	0.000	0.000	6.119	0.111	1.845	0.016	1.891	0.011	1.900	0.017	6.217	0.072	1.888	0.031
Ti	0.013	0.003	0.383	0.045	0.025	0.002	0.018	0.002	0.019	0.004	0.363	0.041	0.016	0.004
Cr	0.724	0.059	0.199	0.010	0.027	0.002	0.025	0.003	0.022	0.005	0.168	0.034	0.021	0.007
Al	1.113	0.066	2.113	0.067	0.193	0.031	0.149	0.015	0.135	0.031	2.023	0.134	0.176	0.042
Fe^{3+}	0.139	0.017	0.078	0.131	0.078	0.013	0.051	0.007	0.039	0.008	0.046	0.065	0.035	0.012
Fe^{2+}	0.388	0.045	0.439	0.116	0.013	0.015	0.040	0.008	0.048	0.006	0.504	0.063	0.048	0.008
Mn	0.008	0.001	0.007	0.001	0.003	0.001	0.003	0.001	0.003	0.001	0.005	0.002	0.002	0.001
Mg	0.609	0.045	3.647	0.061	0.895	0.048	0.922	0.029	0.900	0.021	3.662	0.131	0.894	0.028
Ni	0.005	0.001	0.015	0.003	0.002	0.001	0.001	0.001	0.001	0.001	0.013	0.002	0.001	0.001
Ca	0.000	0.001	1.879	0.055	0.918	0.035	0.883	0.035	0.916	0.022	1.951	0.046	0.895	0.021
Na	0.001	0.001	0.954	0.028	0.043	0.005	0.043	0.004	0.035	0.007	0.832	0.051	0.041	0.005
K	0.000	0.000	0.013	0.004	0.000	0.000	0.000	0.000	0.000	0.000	0.003	0.001	0.000	0.000
OH^-	---	---	2.000	0.000	---	---	---	---	---	---	2.000	0.000	---	---
Mg#	0.536	0.418	0.876	0.004	0.908	0.007	0.911	0.005	0.911	0.008	0.870	0.004	0.915	0.009
Cr#	39.42	3.33												

Lower serpentinite unit (table 3-2)

The porphyroclastic clinopyroxenes of the serpentinized lherzolite of the lower serpentinite unit are Cr-diopsides with Cr_2O_3 contents of up to 1.22 weight %. They are characterized by high Al_2O_3 (4.24-6.63 weight %) and TiO_2 (0.66-0.94 weight %) contents. The Na_2O content of the porphyroclasts is positively correlated

with their Al_2O_3 content (Fig. 6a) and negatively correlated with their Cr_2O_3 content (Fig. 3-6b). The porphyroclasts with exsolution lamellae show higher Al_2O_3 and Na_2O content and lower Mg# and Cr_2O_3 content than the exsolution-free porphyroclasts of the same sample. The neoblasts are depleted in Na_2O, and Al_2O_3 and show higher Mg# with respect to the porphyroclasts (Fig. 3-6c). They also are depleted in Cr_2O_3 compared to the porphyroclasts except for two samples (SUP2 and NAP99-2) where the neoblasts show significantly higher Cr_2O_3 contents than the coexisting porphyroclast.

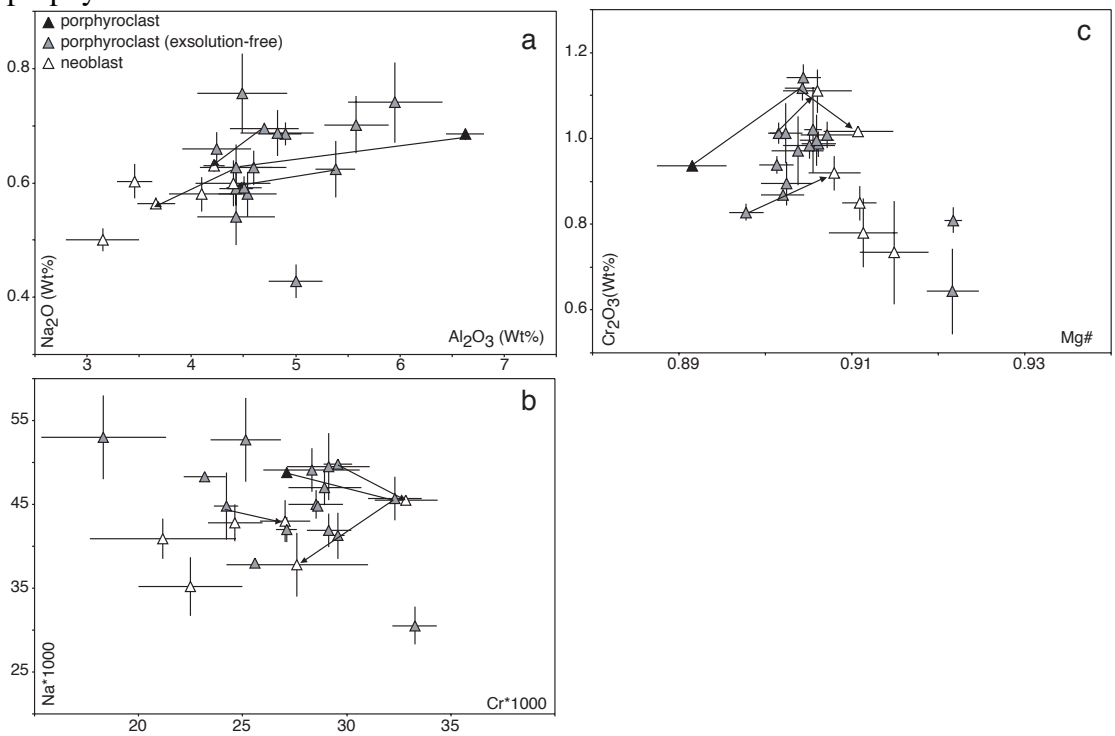

Figure 3-6: Chemical composition of the clinopyroxenes of the lherzolites from the lower serpentinite unit. a) Na_2O_3 vs. Al_2O_3 diagram. The porphyroclasts with exsolution have the highest Al_2O_3 contents whereas the neoblasts are depleted in Na_2O and Al_2O_3 in comparison to the porphyroclast. Arrows indicate porphyroclasts and neoblasts from the same sample. b) Na*1000 vs. Cr*1000 diagram. The porphyroclasts show a weak negative correlation. The porphyroclasts with exsolution show higher Na but lower Cr contents than the coexisting exsolution-free porphyroclasts; the neoblasts are generally depleted in these two elements if compared to the porphyroclasts except for two samples indicated by arrows. c) Cr_2O_3 vs Mg# diagram. Arrows indicate porphyroclasts and neoblasts from the same sample; each point represent the average composition of the clinopyroxenes for each sample and the error bars represent the standard deviation (2σ) (see text for discussion).

Comparison of the chemical composition of the clinopyroxenes of the lherzolite of the upper and lower serpentinite units

In figure 3-7, the chemical composition of the clinopyroxene porphyroclasts of the spinel-lherzolite from the upper and lower serpentinite units are presented and compared to those of other ultramafic massifs from the Alps and the Apennine.
The clinopyroxenes from the lherzolite of the upper serpentinite unit are rather fertile and have a composition similar to that of the lherzolite of the Malenco complex and of the less depleted lherzolites from the external Ligurides. They are enriched in Na, Al with respect to those from the lower serpentinite unit (Fig. 3-7a) but show similar Cr (Fig. 3-7b) and slightly lower Ti content except for two samples (Fig. 3-7c).

The chemical composition of the clinopyroxenes from the lower serpentinite is rather homogeneous and is similar to that of the plagioclase-bearing lherzolite from the external Ligurides. Only two samples (STP2 and NAP6) show a different composition with a strong depletion in Ti and a high Mg#. It should be noted that the sample NAP6 contains disseminated grains of phlogopite within the porphyroclastic assemblage. The observation that the clinopyroxenes of the lherzolite of the lower serpentinite unit are depleted in Al and Na but enriched in Ti compared to those of the upper serpentinite unit can not be explained by different degree of partial melting alone as these three elements are incompatible and should have a common behavior during melting processes. This is supported by the trace element composition of the clinopyroxene porphyroclasts and neoblasts from the lower serpentinite. Müntener et al. (2001) show that most of them are depleted in Sr and Eu which together with their rather low Al and Na and high Ti content suggest that they equilibrated with plagioclase (Rampone *et al*. 1993). The two samples (STP2 and NAP6), which show a strong depletion in Ti do not show these negative anomalies in Sr and Eu. The clinopyroxenes from sample STP2 show trace elements compositions similar to those of abyssal peridotites. The clinopyroxenes of sample NAP6 show composition similar to that of sample STP2 except that they show enrichment in LREE and highly incompatible trace element such as U, Nb and Th. It indicates that this particular sample suffered alkaline metasomatism superposed on an earlier depletion event (Müntener *et al*. 2001).

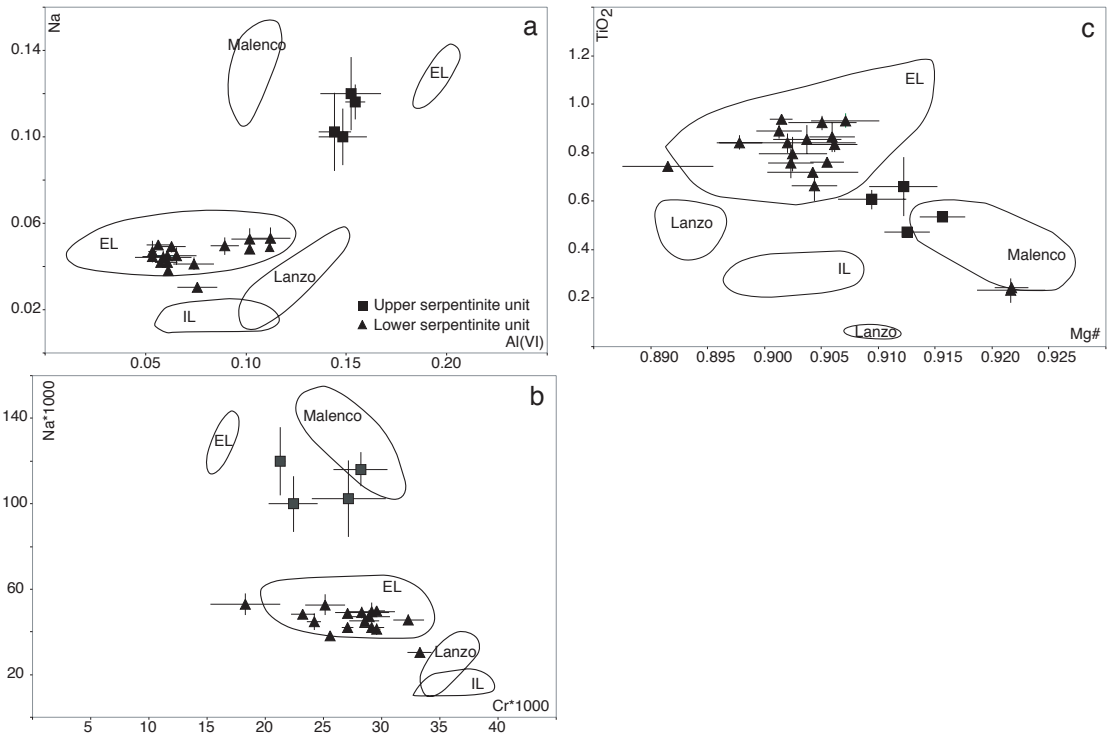

Figure 3-7: Comparison of the clinopyroxene cores composition of the spinel-lherzolite from the upper and lower serpentinite unit with those of other ultramafic massifs in the Alps (Malenco from Müntener 1997; external Liguride (EL) from Rampone et al. 1993; internal Liguride (IL) from Rampone et al. 1996 and Lanzo from Boudier 1978).

2.3.2 Orthopyroxene

Fresh orthopyroxene compositions are rare and only found within the cluster assemblages of the pyroxenite of the upper serpentinite unit (table 3-1) and within the

porphyroclastic assemblages of lherzolite of the lower serpentinite unit (table 3-2). Both types of orthopyroxene are enstatite rich but the metamorphic orthopyroxenes of the upper serpentinite are characterized by higher Mg# than those of the lower serpentinite (0.903-0.916, 0.890-0.900, respectively) and lower Cr_2O_3 (0.11-0.79, 0.53-0.79 weight %, respectively) and CaO content (0.38-0.68, 0.61-2.09 weight %, respectively).

2.3.3 Spinel

Similar to the orthopyroxene, fresh spinel compositions are preserved only within the cluster assemblages of the pyroxenites of the upper serpentinite unit (Table 3-1). Within the lower serpentinite, fresh compositions have been found in both the porphyroclastic and the neoblastic assemblages (table 3-2). The spinels of the upper serpentinite are Al-rich spinels with low Cr# (0.07-0.13) and TiO_2 contents and a high Mg# (0.76-0.78).
The porphyroclastic and neoblastic spinels of the lherzolite of the lower serpentinite unit show a similar composition and are Cr-spinels with higher Cr# (0.33-0.50) and TiO_2 and lower Mg# (0.43-0.66) than those of the upper serpentinite unit. They have Cr# and TiO_2 contents similar to those of abyssal plagioclase peridotite (Dick and Bullen 1984).

2.3.4. Amphibole

In both serpentinite units, two generations of amphiboles were found. The first generation is a Ti-amphibole, which occurs within the cluster assemblage of the pyroxenites of the upper serpentinite unit (Fig. 3-3) and within the neoblastic assemblages of the lherzolites of the lower serpentinite unit. According to the classification of Leake (1978), the Ti-amphiboles of the upper serpentinite (table 3-1) is a kaersutite (Ti>0.5 p.f.u), which is rich in Al_2O_3 (13.19-13.43 weight %), Cr_2O_3 (0.88-1.11 weight %) and contain significant amounts of K_2O (0.21-0.26 weight %). The Ti-amphibole of the lower serpentinite (table 3-2) is a Ti-pargasite (Ti<0.5 p.f.u) and shows lower TiO_2 (2.89-3.75 weight %), Al_2O_3 (12.12-12.43 weight %) and K_2O (< 0.07 weight %) contents than the kaersutite of the upper serpentinite but a higher Cr_2O_3 (1.65-1.84 weight %) content.
In contrast to the Ti-amphiboles, the second generation of amphibole shows very similar composition in the upper and the lower serpentinite unit (table 3-3). In both units, these coronitic amphiboles overgrow clinopyroxenes. These retrograde amphiboles are Mg-hornblende with an Al_2O_3 content of up to 10 weight %. They show lower TiO_2, Na_2O and Cr_2O_3 contents and higher Mg# than the Ti-amphiboles. These hornblendes are further retrogressed to tremolitic hornblende characterized by lower Al_2O_3 and Na_2O contents and higher Mg#.
In both units, the high-temperature Ti-amphibole is stable within a mantle assemblage (clinopyroxene+orthopyroxene+spinel±plagioclase) and does not necessarily record hydration of the mantle during rifting. In the upper serpentinite unit, the kaersutites contain significant amount of K_2O and occur in one sample together with phlogopite veins. This suggests that these amphiboles document localized alkaline metasomatism of the mantle rocks of the upper serpentinite unit under lithospheric mantle conditions. The Ti-pargasites present in the neoblastic assemblages of the lherzolite of the lower serpentinite unit only contain traces of K_2O and are not associated with any other K-bearing phase. This suggests that they simply record reequilibration under

decreasing temperature (T<1100°C) and under lithospheric mantle conditions of the lherzolites.

In contrast, the coronitic amphiboles overgrowing the clinopyroxenes record hydration of the mantle rocks under decreasing P-T conditions and are most probably related to the rifting event.

2.3.5. Phlogopite

Phlogopite occurs along small veins cutting across the porphyroclastic assemblage 1 of the lherzolite of the upper serpentinite unit and as disseminated grains within the porphyroclastic assemblage of the lherzolite of the lower serpentinite unit. The phlogopites of the upper serpentinite (table 3-1) are Ti-rich (more than 6 weight % TiO_2), show a Cr_2O_3 content of 0.6 weight % and have Mg# of 0.89. The ones of the lower serpentinite (table 3-2) contain less TiO_2 (1.73-1.84 weight %) and show higher Cr_2O_3 (0.89-1.36) contents and Mg# values (0.917-0.926). These phlogopites also contain significant amounts of NiO (0.20-0.23 weight %)

Table 3-3. *Chemical composition of the retrograde amphiboles of the Platta mantle rocks*

Sample	Lower serpentinite unit				Upper serpentinite unit			
	SUP6				VEP3			
	Mg-hornblende		tremolite		Mg-hornblende		tremolite	
SiO_2	47.92	1.55	52.99	0.59	48.95	0.71	53.39	0.90
TiO_2	0.13	0.13	0.68	0.28	0.21	0.10	0.31	0.06
Cr_2O_3	0.12	0.16	0.88	0.31	0.40	0.07	0.70	0.16
Al_2O_3	10.97	2.34	4.77	0.98	10.29	0.73	4.84	0.94
Fe_2O_3	3.92	0.33	1.13	1.10	3.88	0.35	2.42	0.55
FeO	0.01	0.02	1.70	1.02	0.10	0.13	0.30	0.46
MnO	0.07	0.03	0.06	0.02	0.08	0.04	0.07	0.01
MgO	20.00	1.49	21.11	0.48	20.02	0.13	22.06	0.47
NiO	0.09	0.01	0.07	0.05	0.06	0.05	0.07	0.02
CaO	12.14	0.48	13.04	0.36	12.60	0.35	12.81	0.43
Na_2O	1.96	0.42	0.84	0.15	2.12	0.12	1.08	0.23
K_2O	0.04	0.01	0.03	0.03	0.01	0.01	0.02	0.01
H_2O	2.17	0.03	2.16	0.02	2.18	0.00	2.19	0.01
Total	99.52	1.11	99.48	0.54	100.86	0.28	100.25	0.57
Si	6.631	0.143	7.355	0.105	6.735	0.096	7.311	0.113
Ti	0.013	0.014	0.071	0.029	0.021	0.010	0.032	0.007
Cr	0.013	0.018	0.097	0.034	0.043	0.008	0.075	0.017
Al	1.791	0.393	0.780	0.156	1.668	0.119	0.781	0.152
Fe^{3+}	0.408	0.036	0.117	0.113	0.401	0.036	0.249	0.055
Fe^{2+}	0.001	0.003	0.198	0.119	0.011	0.015	0.034	0.053
Mn	0.008	0.004	0.007	0.002	0.010	0.005	0.008	0.002
Mg	4.124	0.272	4.367	0.093	4.106	0.025	4.502	0.080
Ni	0.010	0.002	0.008	0.006	0.006	0.006	0.007	0.002
Ca	1.800	0.083	1.939	0.065	1.858	0.052	1.880	0.073
Na	0.526	0.115	0.227	0.040	0.564	0.033	0.286	0.061
K	0.008	0.003	0.006	0.005	0.001	0.002	0.003	0.002
OH^-	2.000	0.000	2.000	0.000	2.000	0.000	2.000	0.000
Mg#	0.909	0.013	0.933	0.009	0.909	0.004	0.941	0.002

Calculation as in table 1.

2.3.5. Plagioclase

Fresh plagioclases was only found in coronae around the spinels of the spinel-pyroxene clusters of the pyroxenite of the upper serpentinite unit and show an anorthite content of 0.55±0.05 (table 3-1).

Although, the chemical composition of the clinopyroxene of the lherzolite of the lower serpentinite unit suggests the presence of plagioclase (Müntener et al. 2001), no relicts of such phase have been found in thin section.

2.4. Thermobarometry and mineral equilibria

2.4.1 Upper serpentinite unit

The oldest structure preserved within the upper serpentinite unit, is the intrusion of pyroxenite dykes within a spinel-lherzolite host. The associated texture observed in thin-section is the porphyroclastic assemblage 1 of the spinel-lherzolite and of the pyroxenite. This stage is characterized by the occurrence of undeformed spinel clusters, which may represent the breakdown products of former garnet (e.g. Smith 1977). Similar symplectite rim consisting of spinel+plagioclase+orthopyroxene has been described around garnet from garnet-pyroxenite (Obata 1994) owing to the reaction clinopyroxene + garnet → orthopyroxene + spinel + anorthite. Two-pyroxene (Brey & Köhler 1990) and single-orthopyroxene thermometry (Witt-Eickschen & Seck 1991) yield temperatures of 850±50°C for the center of the clusters. The orthopyroxenes from the rim of the clusters yield similar temperatures. Experimental work in simple systems showed that the assemblage clinopyroxene+orthopyroxene+anorthite+spinel is stable between 8 and 10 kb at 1000°C for a basaltic composition (Kushiro & Yoder 1966). It is limited by the stability of garnet above 10 kb and by the stability of forsterite+anorthite below 8 kb (Kushiro & Yoder 1966). However, this stability field is dependent on bulk composition and the assemblage olivine + orthopyroxene + clinopyroxene + plagioclase + Al-spinel can be stable up to 14 kb when one uses a pyrolite composition (Green & Hibberson 1970). Similarly, petrogenetic grids calculated for a low-CaO pyroxenitic rock composition (Schmädicke 2000) indicates that at 850°C, the assemblage clinopyroxene + orthopyroxene + spinel + plagioclase is stable between 12 and 7 kb. At lower temperature and similar pressure, amphibole is stable and clinopyroxene disappears suggesting that the upper serpentinite cooled to temperature of 800°C. Such conditions are consistent with the observation that spinel is still stable in the host lherzolite. These observations indicate that the upper serpentinite underwent decompression after the intrusion of garnet pyroxenite and that they equilibrated in shallow upper mantle position before the onset of rifting.

2.4.2 Lower serpentinite unit

Thermobarometric calculations have been applied only to the porphyroclastic assemblage as it represents the only microstructure in which fresh orthopyroxene has been found. The single-orthopyroxene thermometers (Witt-Eickschen & Seck 1991) and the Al net-transfer thermometry (Carrol-Webb & Wood 1986) yield temperatures of 1000°± 50°C for pressures between 10 and 15 kb. The two-pyroxene thermometer (Brey & Köhler 1990) gives similar temperatures of 1010°±100°C for one of these samples and 810 ± 120°C for another one. The co-existence of spinel, Ti-pargasite, clinopyroxene, and probably plagioclase in the recrystallized assemblage indicates plagioclase-peridotite facies conditions, suggesting reequilibration at relatively low-pressure.

2.5. Discussion

Field, petrography and mineral chemistry show that the mantle rocks of the upper and lower serpentinite unit record different tectono-metamorphic evolutions. In this section, the evolution of the mantle rock of both units will be compared and the structures associated with their exhumation on the sea floor will be discussed.

2.5.1 Anhydrous evolution of the Platta mantle rocks

The oldest fabric present in the mantle rocks of the Platta nappe is a spinel tectonite in the upper and lower serpentinite units. However, this fabric is only locally preserved in the upper serpentinite and is associated with the intrusion of pyroxenitic dykes. In contrast, it is the main structure observed in the lower serpentinite but pyroxenite dykes are very rare. In both units, the micro-texture associated to this stage is porphyroclastic in the spinel-lherzolite but the clinopyroxene porphyroclasts and neoblasts do not show any preferred orientation. In the pyroxenites of the upper serpentinite unit, this stage is characterized by the presence of undeformed spinel-pyroxene clusters representing the breakdown products of former garnets.
The chemistry of the clinopyroxenes of the spinel-lherzolites of the upper serpentinite unit indicates that they are fertile lherzolites similar to those of the Malenco complex whereas the clinopyroxenes of the lower serpentinite are more refractory and show composition similar to those from plagioclase lherzolite of the external Ligurides (Fig. 3-7). Trace element composition of the clinopyroxene (Müntener *et al.* 2001) and the high Cr# and TiO_2 content of the spinel also suggest that they equilibrated with plagioclase.
Mineral equilibria and thermobarometric calculations indicate that the upper serpentinite equilibrated in a shallow upper mantle position (850°C±50°C-7-12kb) whereas the lower serpentinite equilibrated at higher temperatures (≈1000°C), presumably in the plagioclase field.

Anhydrous deformation of the mantle rocks occurred within both upper and lower serpentinite units. Although the deformation is nearly pervasive in the upper serpentinite unit and localized and mylonitic within the lower one, both are characterized by a foliation dipping towards the east and by east-west mineral lineations. In both units, shear-sense indicators suggest a top-to-the-east sense of shear. The conditions associated with this deformation are poorly constrained. In the upper serpentinite, this stage is characterized by the deformation of the spinel clusters, which equilibrated at a temperature of 850±50°C and at a pressure of 7-12 kbars. But the undeformed and deformed clusters have a similar mineralogy and their clinopyroxene show similar compositions when not reequilibrated with the host peridotite. This suggests that the "anhydrous" shear zones in the upper serpentinite are not related to the exhumation of the mantle rocks on the sea-floor but to an earlier extensional event, which brought the upper serpentinite in a shallow upper mantle position.
In the lower serpentinite, the anhydrous shear zones are localized and mylonitic. They overprint the porphyroclastic assemblage and the foliation was most likely underlined by olivine, now altered to serpentinite minerals. As no P-T conditions can be determined for this assemblage, it is difficult to relate this deformation to a specific tectonic event.

2.5.2. Hydrous evolution of the mantle rocks

Whereas the anhydrous evolution of the mantle rocks of the two serpentinite units is different, their retrograde evolution under hydrous conditions shows striking similarities.

Crystallization of coronitic Mg- and tremolitic hornblende around clinopyroxene is observed in both units and documents hydration of the mantle rocks. The amphiboles have similar chemical compositions in both units; the first to form are Mg-hornblendes. Such amphiboles with high Al_2O_3 content are often found to be stable in the presence of orthopyroxene and spinel (e.g. Müntener *et al*. 2000) suggesting that hydration of the mantle rocks started under upper amphibolite facies conditions, *i.e*. at temperatures between 600 and 700°C. The tremolitic hornblende overgrowing the Mg-hornblende are characterized by lower Al_2O_3 and Na_2O contents and higher Mg# which is characteristic for a retrograde evolution. It suggests that they are related to the ongoing hydration of the mantle rocks under decreasing temperatures, which may be related to Jurassic rifting.

Low-grade deformation is also visible in both units. It is characterized by the presence of localized shear-bands (Fig. 4b), serpentinite mylonites, gouges and tectonic breccias. The sense of shear associated to these structures is always top-to-the west, i.e. top-to-the ocean and could be related to the activity of the Jurassic low-angle detachment system documented in the overlying Err nappe (Froitzheim & Eberli 1990, Froitzheim & Manatschal 1996). This detachment system can be traced to the Platta nappe, as shown by the occurrence of extensional allochthones (Manatschal & Nivergelt 1997) on top of the mantle rocks. The low-grade condition (greenschist facies and lower grade conditions) associated with these structures appears to be only responsible for the final exhumation of the mantle rocks to the sea floor. As these structures are cut by or cut across basaltic dykes (Fig. 1f), their activity overlaps in time with the Jurassic magmatism.

2.5.3. Structures associated with the mantle exhumation

Correlation of deformational structures with Mesozoic rifting events is hampered by the lack of time markers, inherited structures and late, post-kinematic serpentinization commonly obliterating the pre-existing fabrics and mineralogy. However, two types of possible rift-related structures can be identified in the mantle rocks, which were active under different metamorphic conditions.

The first are the anhydrous (granulite facies) shear zones, which occur mostly in the upper serpentinite unit and show a top-to-the-continent sense of shear. Such shear zones are related to decompression and cooling event to pressures between 7 and 12 kbars. The uncertainty in the determination of the pressure and the lack of time constraints do not permit to relate it unambiguously to Jurassic rifting. Indeed, such pressures could represent the one prevailing before onset of rifting as determined in the Malenco complex (Müntener *et al*. 2000). However, the upper serpentinite could represent a deeper part of the subcontinental mantle than the ultramafic rocks of the Malenco complex. In this area, a Jurassic continentward-dipping normal fault separates lower crustal rocks from upper crustal rocks of Adriatic units (Margna normal fault; Müntener & Hermann. 2001). Based on P-T-t data, Müntener & Hermann (2001) showed that the Margna normal fault thinned the crust to about 10 km. Thus the anhydrous shear-zones in the upper serpentinite unit could represent a deeper, anhydrous, part of the same or an analogous fault system and be related to

uplift of the subcontinental mantle to shallow levels during rifting. On the other hand, we can not exclude that it is related to an earlier, pre-rift deformation event.
The second type of structures is the hydrous shear-zones active under greenschist facies and lower grade condition that shows a top-to-the-ocean sense of shear. Such faults can be related to the Middle-Jurassic low-angle detachment system documented in the overlying Err nappe (Froitzheim & Eberli 1990, Froitzheim & Manatschal 1996, Manatschal & Nievergelt 1997), which show a similar sense of shear. In the Err nappe, the detachments affected post-Variscan granites (Manatschal & Nievergelt 1997), but lower crustal rocks were not found along these faults. In both the continental and ophiolitic unit, these faults are characterized by the presence of cataclasites and gouges indicating low-grade metamorphic conditions during their activity. In the Platta nappe, such structures are contemporaneous with Jurassic magmatism. This suggests that the low-angle detachments affecting the upper crust of the distal margin (Err nappe) and the mantle rocks of the ocean-continent transition (Platta nappe) are late, shallow crustal structures responsible for the final exhumation of the subcontinental mantle on the sea floor. This assumption is in line with kinematic inversion of detachment structures imaged in the Iberian Abyssal plain, where Manatschal et al. (2001) demonstrated that the continental crust was thinned to less than 12 km before the onset of detachment faulting.

3. Chemical evolution of the Platta mantle rocks

The previous section showed that the upper and lower serpentinite underwent a different anhydrous evolution under granulite facies conditions before they get juxtaposed during Jurassic rifting. The upper and originally continentward serpentinite consist of subcontinental mantle that equilibrated in a shallow upper-mantle position before rifting similarly to the neighboring ultramafics of the Malenco complex. In contrast, the lower and originally oceanward serpentinites record high temperatures (1000°C) of equilibration under plagioclase-peridotite facies conditions. In this section, the geochemistry of the upper and lower serpentinite will be documented in order to: 1) determine if the two serpentinite unit also record a different geochemical evolution; 2) clarify the origin of the plagioclase that equilibrated with the pyroxenes of the lherzolite of the lower serpentinites unit (melt impregnation versus subsolidus reaction) and 3) determine the origin of the mantle rocks of the lower serpentinite unit (subcontinental vs. oceanic mantle).

3.1. Whole rock chemistry (Table3-4).

The mantle rocks of the Platta nappe are all strongly serpentinized with high loss on ignition varying from 8.56 to 13.06 weight percent, therefore the modal composition of the mantle rocks has been calculated on the basis of anhydrous bulk rock analyses of major element with MANNOR (written by P. Ulmer 1992), a FORTRAN program, which converts anorthite and corundum to pyroxene and spinel. In all calculations, a Tschermak component of 0.1 has been adopted assuming Fe^{3+}=0. Calculations performed with a lower Tschermak component led to a decrease in calculated olivine and an increase in spinel. The calculated modal composition of the mantle rocks of the upper serpentinite unit shows that they are clinopyroxene-rich lherzolites, with one sample (VEP7) plotting in the olivine websterite field. Their clinopyroxene content varies from 8.6 to 25 % and their orthopyroxene from 28.1 to 33.9 %. Such

high pyroxene contents indicate that these mantle rocks are mixtures of variable proportion of spinel lherzolite and pyroxenite, consistent with field observations (Fig. 2c). Excluding samples with obvious Ca-loss during serpentinization, the mantle rocks of the lower serpentinite unit show rather fertile modal compositions with 27 to 34 % orthopyroxene, 6 to 20 % clinopyroxene and 1.4 to 3.2 % spinel. Their olivine content is particularly low (48-62 %).

3.1.1 Major elements and transition metals

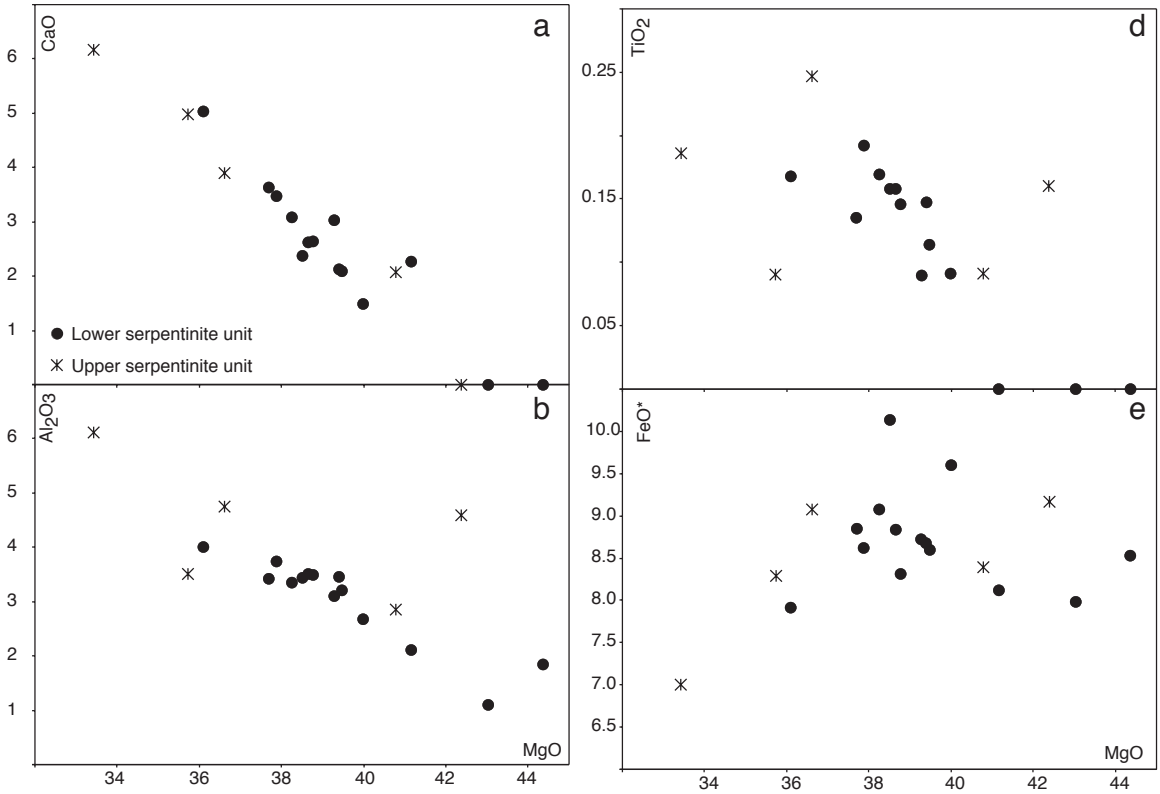

Figure 3-8: Variation diagrams of major elements versus MgO. a) CaO, b) Al_2O_3, c) TiO_2, and d) FeO*

Although the ultramafic rocks of the Platta nappe are all highly serpentinized, their major and transition element composition shows a large variation and several systematic trends are observed (Fig. 3-8, 3-9). CaO, Al_2O_3, TiO_2 and V are negatively correlated with MgO and correspond to the trend defined in various other peridotite massifs (e.g. Ronda, Frey *et al.* 1985; Lanzo, Bodinier 1988; Malenco, Müntener 1997). The most serpentinized sample (100% serpentinization) show the highest MgO content and a CaO content below the detection limit (Fig. 3-8). This suggests that the trend between CaO and MgO may not be entirely due to melting processes but could also reflect Ca-Mg exchange during low-temperature hydration of the mantle rocks. The rocks from the upper serpentinite unit show the highest Al_2O_3, TiO_2, CaO and V contents, the lowest MgO and Ni contents and a larger scatter of compositions than those from the lower serpentinite unit. This is in accordance with the previous observations that the mantle rocks of the upper unit are mixture of lherzolite and pyroxenite, whereas those of the lower unit are free of pyroxenite. Indeed, samples with a high concentration of spinel clusters show higher concentrations in Al_2O_3, TiO_2 and V independently of their MgO content. Except for one clinopyroxene-rich sample, the mantle rocks of the upper serpentinite unit display a rather constant Ni

concentration and Cr# values (Fig. 3-9). In contrast, the Ni content of the lherzolite of the lower serpentinite unit is positively correlated with MgO indicating that these elements are mainly controlled by olivine (Fig. 3-9). In contrast to Ni, FeO_{tot} does not show any clear correlation with MgO (Fig. 3-8). Cr is more randomly distributed among the analyzed samples (Fig. 3-9), which may be caused by a heterogeneous distribution of Cr-spinel within the samples. However, the Cr# of the peridotite is positively correlated with MgO, reflecting the increasing depletion of Al_2O_3 with increasing MgO.

Table 3-4. *Major and trace element composition of the Platta serpentinites*

	Upper serpentinite unit					Lower serpentinite unit							
Sample	VEP2	VEP7	VEP8	FAP3-I	FAP4	NAP7	NAP3	LAP1	NAP2	SUP2	SUP3	SUP4	SUP5
Major (Wt%)													
SiO_2	40.72	41.87	39.17	37.05	39.24	39.26	38.16	38.53	39.62	40.13	39.31	39.3	39.43
Al_2O_3	3.11	5.57	2.51	4.01	4.23	3.74	1.84	3.44	3.42	3.5	3.2	3.45	3.51
Fe_2O_3	8.14	7.1	8.19	8.9	8.99	8.47	8.25	9.97	8.74	8.23	8.37	8.51	8.7
MnO	0.14	0.13	0.11	0.12	0.12	0.12	0.08	0.16	0.14	0.12	0.13	0.11	0.11
MgO	31.59	30.49	35.84	37.03	32.63	33.5	38.6	34.1	33.51	34.56	34.6	34.75	34.27
CaO	4.4	5.62	1.82	< d.l.	3.48	3.08	< d.l.	2.11	3.23	2.35	1.83	1.88	2.32
Na_2O	0.1	0.15	0.07	< d.l.	0.1	< d.l.	< d.l.	< d.l.	< d.l.	< d.l.	< d.l.	< d.l.	0.06
K_2O	< d.l.	< d.l.	< d.l.	< d.l.	< d.l.	< d.l.	< d.l.	< d.l.	< d.l.	< d.l.	< d.l.	< d.l.	< d.l.
TiO_2	0.08	0.17	0.08	0.14	0.22	0.17	< d.l.	0.14	0.12	0.13	0.1	0.13	0.14
P_2O_5	0.13	0.11	0.08	0.11	0.1	0.12	0.08	0.09	0.1	0.1	0.11	0.09	0.11
L.O.I	11.68	8.56	12.35	12.82	10.98	11.37	13.06	11.73	11.21	11.37	12.41	11.85	11.32
Total	100.11	99.77	100.22	100.27	100.09	99.85	100.11	100.28	100.09	100.5	100.08	100.09	99.97
Trace element (ppm)													
Cr	2904	3104	2663	2773	2697	2764	2734	2773	2537	2491	2650	2660	2866
Ni	1996	1572	1904	1859	1877	1896	2044	1961	1910	1797	1878	2009	1940
Co	105	76	100	103	102	101	109	102	101	97	99	104	104
Cu	20	75	21	22	40	15	16	28	25	21	26	24	15
Zn	59	46	66	37	73	54	30	50	53	49	94	54	49
V	68	143	65	92	121	88	52	79	74	74	72	75	77
Zr	2.83	5.55	2.24	6.04	7.52	8.57	< d.l.	7.36	5.96	6.69	4.84	5.99	6.56
Y	2.63	3.20	1.58	4.52	7.55	4.09	0.74	3.63	3.21	3.31	2.97	3.13	3.31
Hf	0.0676	0.1408	0.0818	0.1918	0.2609	0.2115	< d.l.	0.2046	0.1744	0.2015	0.1518	0.1684	0.1994
Th	<d.l.	0.0079	0.0012	0.0066	0.0045	0.0016	0.0021	0.0043	0.0028	0.0031	0.0153	0.0012	0.0050
U	0.1159	0.0046	0.0036	0.0043	0.0083	<d.l.	<d.l.	0.0054	<d.l.	0.0028	0.0105	0.0011	<d.l.
Ba	5.17	3.35	< d.l.	< d.l.	< d.l.	< d.l.	< d.l.	< d.l.	< d.l.	< d.l.	< d.l.	< d.l.	< d.l.
Rb	1.02	< d.l.	< d.l.	< d.l.	< d.l.	< d.l.	< d.l.	< d.l.	< d.l.	1.12	1.10	< d.l.	< d.l.
Sr	24.97	11.41	9.29	< d.l.	8.33	< d.l.	< d.l.	< d.l.	4.55	9.44	5.98	4.85	5.89
Nb	0.022	0.082	0.022	0.083	0.048	0.027	0.060	0.054	0.028	0.038	0.049	0.014	0.053
Ta	0.001	0.008	0.002	0.009	0.007	0.004	0.004	0.006	0.004	0.006	0.010	0.002	0.007
REE (ppm)													
La	0.033	0.264	0.058	0.191	0.131	0.197	0.078	0.188	0.144	0.151	0.234	0.128	0.179
Ce	0.191	0.860	0.303	0.713	0.653	0.675	0.176	0.736	0.545	0.523	0.507	0.550	0.809
Pr	0.049	0.164	0.072	0.151	0.168	0.158	0.024	0.132	0.125	0.108	0.103	0.102	0.134
Nd	0.344	0.963	0.305	0.979	0.935	0.951	0.094	0.830	0.545	0.625	0.587	0.618	0.778
Sm	0.172	0.365	0.152	0.382	0.460	0.281	0.025	0.252	0.298	0.263	0.234	0.234	0.232
Eu	0.078	0.195	0.062	0.061	0.200	0.199	0.054	0.108	0.115	0.131	0.113	0.133	0.124
Gd	0.211	0.411	0.194	0.570	0.800	0.587	0.040	0.381	0.462	0.407	0.361	0.387	0.424
Tb	0.047	0.079	0.029	0.106	0.148	0.090	0.010	0.079	0.064	0.068	0.064	0.068	0.078
Dy	0.371	0.586	0.266	0.677	1.120	0.718	0.092	0.528	0.490	0.475	0.458	0.499	0.505
Ho	0.089	0.119	0.055	0.158	0.245	0.138	0.026	0.125	0.112	0.105	0.106	0.115	0.115
Er	0.237	0.296	0.145	0.436	0.698	0.388	0.076	0.340	0.311	0.314	0.268	0.342	0.308
Tm	0.037	0.057	0.026	0.062	0.137	0.058	0.014	0.060	0.051	0.054	0.049	0.058	0.054
Yb	0.266	0.385	0.150	0.442	0.903	0.432	0.111	0.349	0.309	0.325	0.300	0.356	0.369
Lu	0.043	0.061	0.025	0.071	0.110	0.070	0.019	0.061	0.051	0.063	0.057	0.067	0.051

Major element by emission-ICP. Trace elements and REE by ICP-MS. U and Th measured by ICP-MS after chromatographic separation.

Table 3-4. *(continued)*

	Lower serpentinite unit					
Sample	STP1	STP2	STP3	MSP1	CRP1	CRP3
Major elements (Wt%)						
SiO_2	39.24	39.56	39.14	39.57	41.01	40.26
Al_2O_3	3.35	2.11	2.67	3.11	1.1	4
Fe_2O_3	8.93	7.95	9.39	8.67	7.79	7.84
MnO	0.17	0.14	0.15	0.11	0.07	0.12
MgO	33.89	36.27	35.21	35.16	37.8	32.21
CaO	2.73	2	1.31	2.71	< d.l.	4.49
Na_2O	< d.l.	< d.l.	< d.l.	< d.l.	< d.l.	0.05
K_2O	< d.l.	< d.l.	< d.l.	< d.l.	< d.l.	< d.l.
TiO_2	0.15	< d.l.	0.08	0.08	< d.l.	0.15
P_2O_5	0.12	0.1	0.08	0.1	0.08	0.1
L.O.I	11.67	12.25	12.1	10.94	12.31	10.43
Total	100.28	100.43	100.13	100.45	100.18	99.65
Trace element (ppm)						
Cr	2970	2985	2890	2288	3317	2849
Ni	1995	2154	2056	1708	2295	1713
Co	105	111	91	96	114	93
Cu	18	6	15	8	< d.l.	37
Zn	107	48	70	31	59	39
V	84	71	66	76	36	90
Zr	7.16	< d.l.	3.73	2.00	< d.l.	6.97
Y	3.79	1.39	2.42	1.73	0.13	4.16
Hf	0.2280	< d.l.	0.1182	0.0505	< d.l.	0.2148
Th	0.0077	0.0069	0.0111	0.0066	<d.l.	0.0011
U	0.0083	0.0056	0.0082	0.0071	0.0524	<d.l.
Ba	< d.l.	< d.l.	< d.l.	< d.l.	< d.l.	< d.l.
Rb	< d.l.	< d.l.	1.04	< d.l.	< d.l.	2.70
Sr	< d.l.	< d.l.	8.22	< d.l.	< d.l.	7.81
Nb	0.055	0.033	0.040	0.012	0.007	0.011
Ta	0.004	0.002	0.005	0.003	0.001	0.003
REE (ppm)						
La	0.164	0.050	0.093	0.060	0.020	0.151
Ce	0.659	0.102	0.376	0.266	0.023	0.634
Pr	0.123	0.013	0.071	0.046	0.004	0.136
Nd	0.802	0.063	0.401	0.246	0.025	0.831
Sm	0.359	0.040	0.167	0.123	0.008	0.291
Eu	0.109	0.018	0.093	0.055	0.003	0.144
Gd	0.480	0.075	0.255	0.209	0.071	0.456
Tb	0.072	0.020	0.047	0.032	0.002	0.084
Dy	0.636	0.186	0.352	0.280	0.014	0.574
Ho	0.125	0.050	0.089	0.061	0.004	0.144
Er	0.393	0.136	0.253	0.188	0.015	0.396
Tm	0.068	0.023	0.041	0.028	0.003	0.069
Yb	0.422	0.176	0.283	0.160	0.025	0.433
Lu	0.062	0.029	0.043	0.028	0.005	0.063

3.1.2. Rare Earth Elements

The chondrite–normalized REE abundance of the mantle rocks is shown in Fig. 3-10. The REE concentrations of the ultramafic rocks of the upper serpentinite unit is characterized by a LREE depletion and shows rather fertile compositions with Ybn>1 (Fig. 3-10a). One sample is particularly enriched with Ybn of 5.55, which is probably due to a high concentration of former garnet pyroxenite in this particular sample. The La content shows a weak positive correlation with the Al_2O_3 content (Fig. 3-11a). The Yb content shows a similar correlation (Fig. 3-11b) although it is controlled by the distribution of cluster. The Tb/Yb ratio is below the chondritic value and is not correlated to the Yb content of the sample (Fig. 3-11c). These results confirm our interpretation that the clusters represent former garnet and that their concentration strongly controls the bulk chemistry of the upper serpentinites. Less clear is the presence of positive and negative Eu anomalies (Fig. 3-10a), which may be due either to low-temperature alteration or reflect primary signature of the garnet pyroxenite as

most garnet pyroxenites show such an anomaly without containing plagioclase as a magmatic phase (e.g. Pearson *et al*. 1993, Kornprobst *et al*. 1990, Müntener 1997).

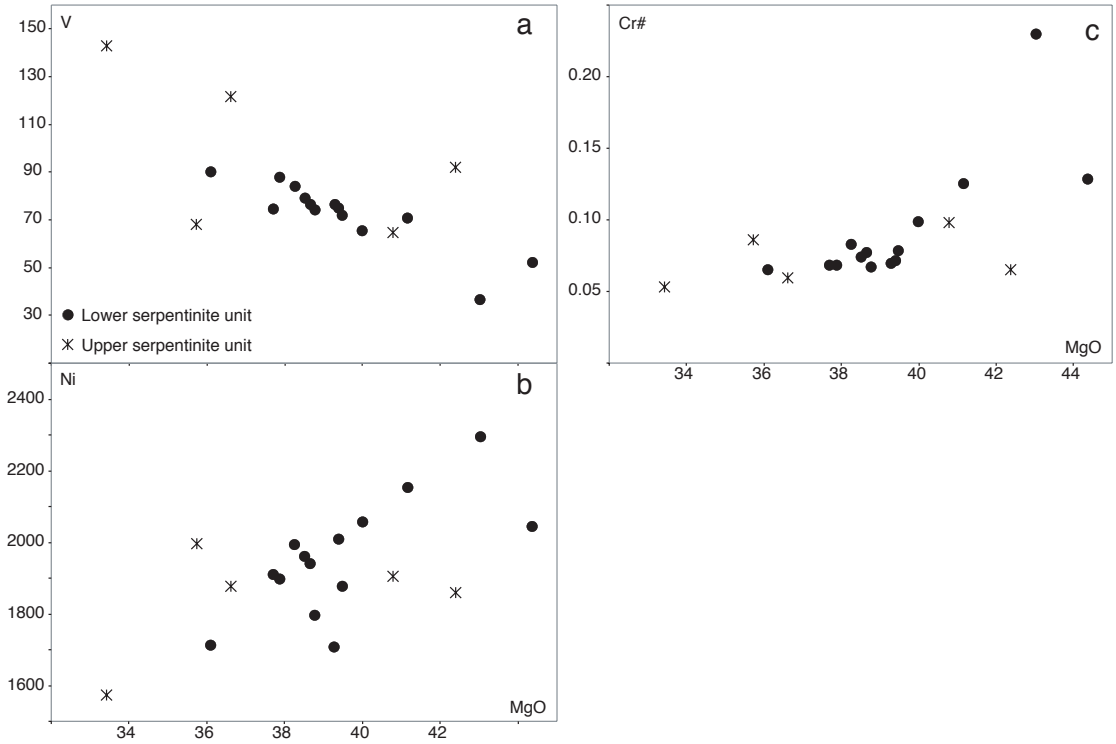

Figure 3-9: Variation diagrams of transition elements and Cr# versus MgO. a) V, b) Ni, and c) Cr.

The REE concentrations of the serpentinized lherzolite of the lower serpentinite unit can be characterized as follows: (1) two groups can be recognized: fertile peridotites with Ybn>1, a strong LREE depletion and rather flat spectra from MREE to HREE (Fig 3-10c); (2) the more refractory peridotites show a strong fractionation between HREE and MREE and are slightly enriched in LREE (Fig. 3-10e). It is not clear whether this enrichment reflects primary magmatic processes or if it results from secondary alteration. Experimental determination of peridotite-sea water interaction (Menzies *et al*. 1993) showed that serpentinization could produce a slight LREE enrichment in clinopyroxene-free rocks (harzburgite and dunite). However, this enrichment is very small and is visible only in the most depleted samples with LREE below 0.4 times chondrite. (3) Most of the fertile lherzolites and one refractory lherzolite present a positive Eu anomaly (Fig. 3-10). (4) The rocks from the lower serpentinite unit show Tb/Yb values below the chondritic ratio (Fig. 3-11c) indicating that the HREE are fractionated to some degree from the MREE. This ratio is roughly positively correlated with Yb indicating that the most refractory samples show the highest fractionation. According to Bodinier *et al*. (1988) and McDonough & Frey (1989), this feature may be interpreted as evidence for some melting in the garnet stability field as garnet strongly fractionates between HREE and MREE. This will be further discussed below.

3.1.3. Incompatible trace elements

Primitive-mantle normalized diagrams for incompatible element concentrations of the mantle rocks are presented in Fig. 3-10. The most remarkable features in the trace elements diagram are: (1) The occurrence of strong positive anomalies in U and Rb

and of an anomaly in Sr which can be positive or negative (Fig. 3-10b, d, f). However, in both units, samples with positive Sr anomalies, show also an anomaly in Eu indicating a "plagioclase signature". (2) Negative Zr anomalies in all samples from the upper serpentinite unit with respect to the surrounding REE Nd and Sm.

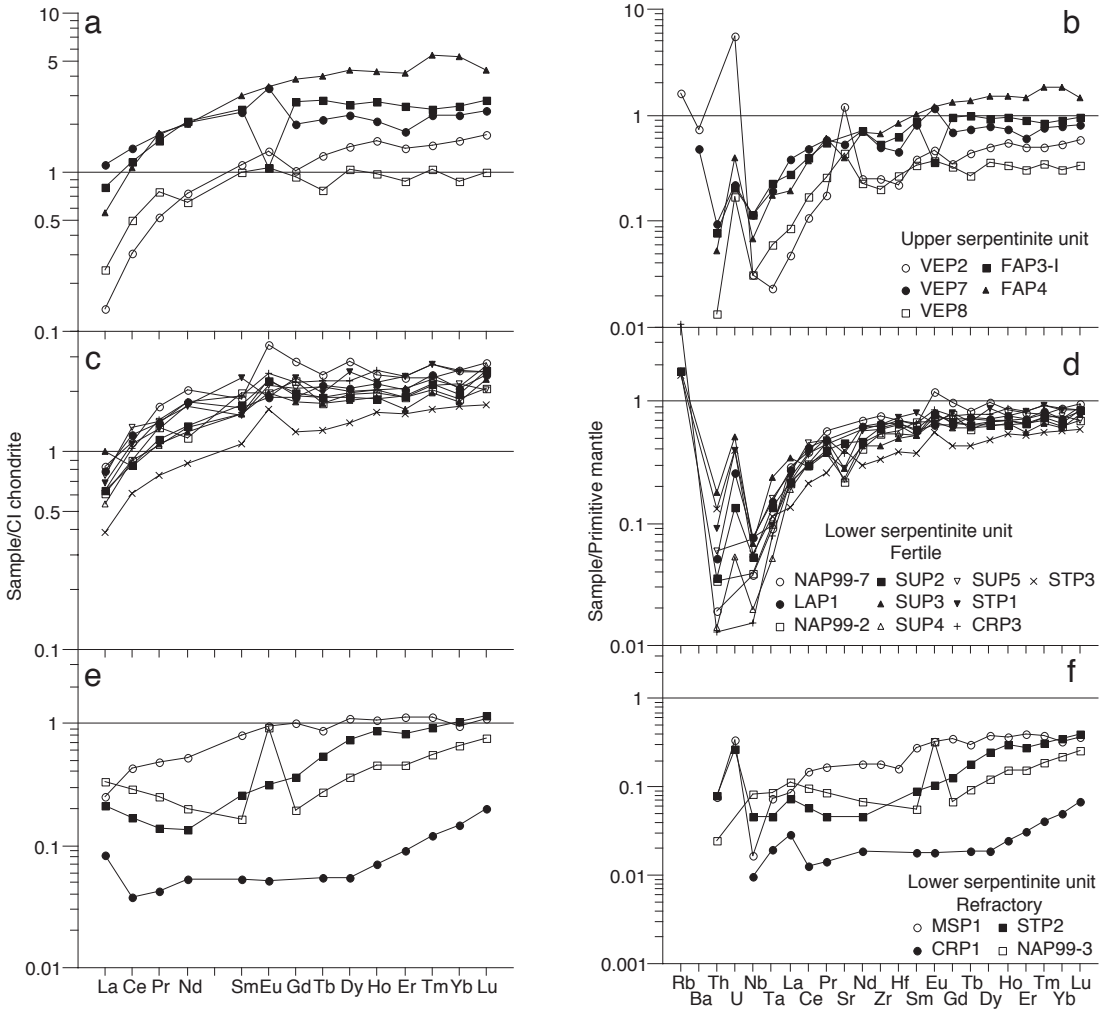

Figure 3-10: Chondrite normalized rare earth elements diagrams of a) sample from the upper serpentinite unit, c) fertile lherzolite form the lower serpentinite unit and e) refractory lherzolite from the lower serpentinite unit. C1 chondrite from Sun and McDonough (1989). b), d) and f) are the primitive mantle normalized diagrams for incompatible elements and REE of the same samples. The elements are arranged according to increasing peridotite-basaltic magma partition coefficient (Sun and McDonough 1989).

3.2. Discussion

3.2.1. Chemical effect of serpentinization

Although the peridotites of the Platta nappe are strongly serpentinized, they display compositional variations similar to those of other non-serpentinized ultramafic massifs. The elements most strongly affected by serpentinization are Na (always below XRF detection limit), Ca (and in minor proportion Mg), and Sr. The LREE are also affected but in minor proportion as the changes are noticeable for highly depleted samples with LREE concentration below 0.4 times chondrite.

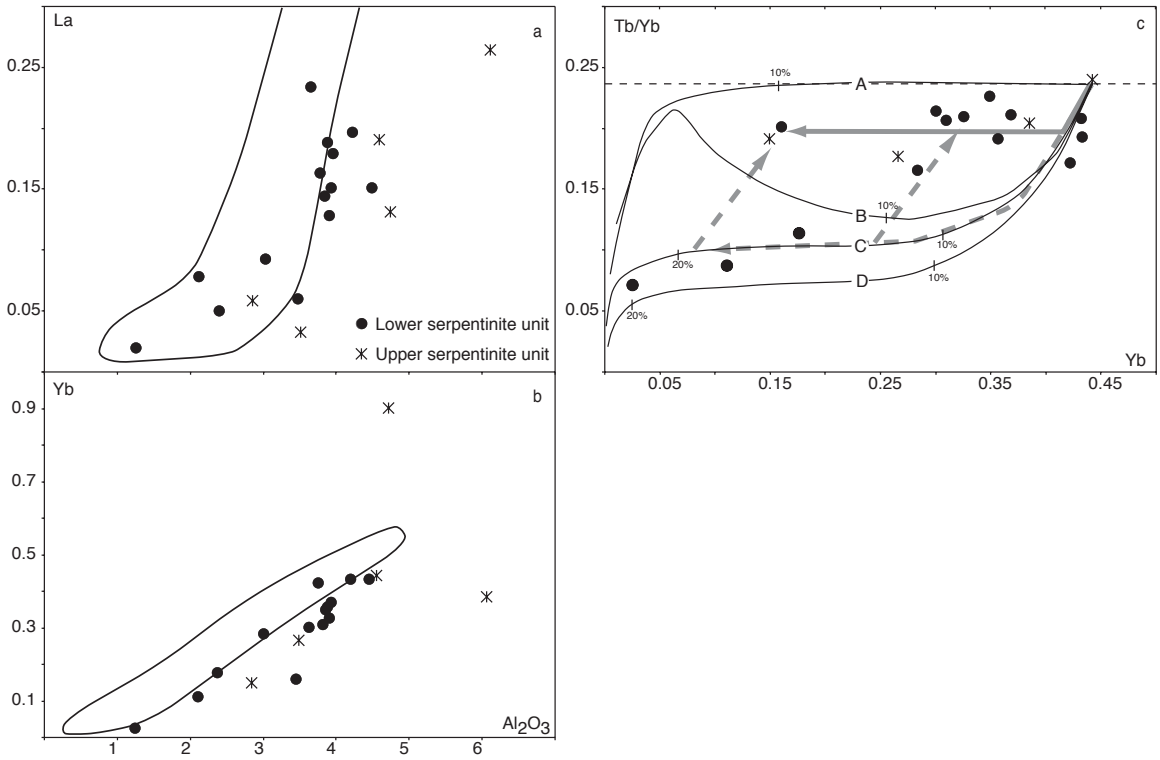

Figure 3-11: a) La versus Al_2O_3 diagram. The trend defined by the Ronda (Frey et al. 1985), Lanzo (Bodinier 1988) and Lherz peridotite (Bodinier et al. 1988) is added for comparison. b) Yb versus Al_2O_3 diagram. The trend defined by the Ronda (Frey et al. 1985), Lanzo (Bodinier 1988) and Lherz peridotite (Bodinier et al. 1988) is added for comparison. c) Tb/Yb versus Yb diagram. The horizontal straight line indicates Tb/Yb ratio in C1 chondrite (Sun and McDonough 1989). Solid lines: calculated variation of the Tb/Yb vs. Yb ratios in the residues after batch melting in the spinel stability field (A), batch melting in the garnet stability field (B), continuous melting in the garnet stability field (C) and fractional melting in the garnet stability field (after Bodinier et al. 1988b). The gray arrow indicates that the Tb/Yb vs. Yb ratios of the fertile lherzolite of the lower serpentinite unit might be produced by a few percents of melting in the garnet stability field followed by additional melting in the spinel stability field. The dashed gray arrow shows an alternative hypothesis, which implies a melt impregnation of the lherzolite leading to an increase of the Tb/Yb ratio after earlier melting in the garnet stability field (see text for discussion).

3.2.2. Evidence for partial melting of rocks of the lower serpentinite unit

Major and trace elements of the lherzolites of the lower serpentinite nit display several systematic trends similar to those of other peridotite occurrences (e.g. Ronda, Frey *et al*. 1985; Lanzo, Bodinier 1988; Malenco, Müntener 1997). In particular, the positive correlation of Yb with Al_2O_3 (Fig. 3-11a, b) is consistent with the view that they represent residues of variable degrees of partial melting. The very low Tb/Yb ratios displayed by the most depleted samples (Fig. 3-11c) suggests that this melting event started in the garnet stability field (Bodinier *et al*. 1988). According to the calculation of Bodinier *et al*. (1988), the refractory lherzolites could be produced by 15% to 20% of continuous melting (Langmuir *et al*. 1977) of a source with 10% garnet (Fig. 3-11c). However, the Tb/Yb ratios and the Yb concentrations of the more fertile peridotites do not follow the calculated trends for different melting processes in the stability field of spinel or garnet (Fig. 3-11c). According to these calculations, two processes could explain their concentrations in Tb and Yb. Either a few % of melting occurred in the garnet stability field, lowering their Tb/Yb ratio followed by melting

in the spinel stability field leading to a decrease in Yb without affecting the Tb/Yb ratio. A second possible mechanism to explain the observed signatures could be that the lherzolite suffered significant melting (5%-15%) in the garnet stability field followed by a later enrichment leading to an increase of the Tb/Yb ratios (Fig. 3-11d). Several arguments are against the first hypothesis: First, depleted samples with low Tb/Yb ratios coexist with fertile one with higher Tb/Yb ratios in the same outcrop at a distance of only a meter (e.g. CRP1 and CRP3, STP2 and STP3, NAP3 and NAP2). It seems unlikely that at such scale, the lherzolite did not melt to the same extend under the same pressure conditions. Furthermore, the rather fertile whole rock composition of most of the lherzolites, in particular with respect to their LREE concentration, and their high clinopyroxene content does not support the idea that they suffered more than a few percent of melting. Thus the hypothesis of a later enrichment of the lherzolite is better supported by the available data.

3.2.3. Significance of Eu anomaly

It has been shown that Eu can be concentrated in high-temperature, acidic, chloride-rich hydrothermal solutions (Michard 1989) when Eu^{3+} is reduced to Eu^{2+} because of the high temperature conditions (Michard & Albarède 1986). Such a process could be responsible for the negative Eu anomaly observed in few samples of the Platta nappe. However, most of the samples show a positive Eu anomaly, which is often associated with a positive Sr anomaly (upper serpentinite unit: samples VEP2 and VEP8 (Fig. 3-10b); lower serpentinite unit: samples SUP2 and STP3 (Fig. 3-10d) or with enrichment in LREE indicating a "plagioclase signature" (lower serpentinite: sample NAP3). The REE concentrations of the clinopyroxenes (Müntener *et al.* 2001) and the spinel composition of the samples from the lower serpentinites unit suggest that they reequilibrated in presence of plagioclase. These observations support the idea that the Eu anomalies are primary and are not related to serpentinization processes.
Within the upper serpentinite unit, a positive Eu anomaly could be explained by the presence of garnet-pyroxenite dykes as many garnet pyroxenites do present such an anomaly without containing plagioclase as a magmatic phase (e.g. Pearson *et al.* 1993, Kornprobst *et al.* 1990, Müntener, 1997).
For the lower serpentinites unit, the "plagioclase signatures" (Eu and Sr anomalies) are present in one depleted lherzolite (sample NAP3) and in most of the fertile lherzolite. Refractory samples without Eu anomaly and more fertile samples with a "plagioclase signature" can coexist in a same outcrop (e.g. samples CRP1 and CRP3, samples STP2 and STP3). This strong heterogeneity and the fact that the "plagioclase signature" is superposed on a pattern typical for fractional melting (sample NAP3, Fig. 3-10e) in the refractory sample suggest that Eu anomalies may be explained, at least partially, by melt impregnation and crystallization of plagioclase after the partial-melting event.

3.2.4. Chemical evolution of the mantle rocks of the upper serpentinite unit

As shown in chapter 2-2 and by the bulk rock chemistry, the mantle rocks of the upper serpentinite unit represent mixture of spinel-lherzolite and garnet pyroxenite. Mixing of these two rock types took place during anhydrous deformation under granulite-facies conditions. This process led to a refertilization of the host lherzolite. As no sample analyzed so far correspond to an end-member composition (spinel-

lherzolite or garnet-pyroxenite), processes related to an event preceding the deformation event could not be deciphered.

3.2.5. Chemical evolution of the lherzolite of the lower serpentinite unit.

In contrast to the upper serpentinite unit, the element correlations defined by the mantle rocks of the lower serpentinite unit are consistent with the view that they represent residues of variable degrees of partial melting. The very low Tb/Yb ratios displayed by the most depleted samples suggests that this melting event started in the garnet stability field by a process of continuous melting (Langmuir *et al.* 1977). However, the Yb concentrations and the Tb/Yb ratios of the more fertile lherzolite can not be explained by such a process alone. A later enrichment process, after the depletion event could explain the high Tb/Yb ratio of the fertile lherzolites, the outcrop-scale (meter scale) geochemical heterogeneity and the positive Eu anomalies observed in the lherzolites of the lower serpentinite unit. The positive Eu anomalies as well as the REE compositions of the clinopyroxenes (Müntener *et al.* 2001) suggest that the lower serpentinites equilibrated with plagioclase, which probably crystallized from the impregnating melts after the depletion event. This melt should have broadly a tholeiitic composition as the mantle rocks do not show a particular enrichment in incompatible elements as one might expect during alkaline metasomatism (Fig. 3-10d, f). However, we infer that these melts had a MORB signatures in order to produce an increase of the Yb concentration and Tb/Yb ratio of the lherzolite.

3.2.6. Origin of the Platta Mantle rocks

The ultramafic rocks of the Platta nappe consist mainly of fertile spinel-lherzolites. In both units (lower and upper serpentinite unit), disseminated grains of phlogopite has locally been found suggesting that both suffered alkaline metasomatism at some time. The mantle rocks of the upper serpentinite unit have been intruded by numerous pyroxenite dykes, which are not found within the lower unit. Petrographic and chemical evidence suggest that these pyroxenites were former garnet pyroxenite. Such an association of fertile spinel lherzolite and garnet pyroxenite was already described in the adjacent Malenco complex, which have been shown to be of shallow sub-continental origin (e.g. Müntener *et al.* 2000). This is in accordance with the rather cold and shallow conditions of equilibration determined in this unit (800°C, 12-7 kbars), although the temperature of reequilibration appears to be slightly higher than that determined within the Malenco complex (Müntener *et al.* 2000).
The lower serpentinite unit is characterized by a strong heterogeneity as fertile peridotites coexist with depleted ones in the same outcrop. These mantle rocks record a polyphase magmatic history. Trace-element mineral chemistry (Müntener *et al.* 2001) indicates that localized alkaline metasomatism occurred after an earlier partial-melting event, which started probably in the garnet stability field. These events are then followed by a infiltration of tholeiitic melts in the lower serpentinite. The compositional heterogeneity of the lower serpentinite and their rather complex magmatic evolution also suggest a subcontinental origin for this unit.

4. Discussion

Our study showed that the mantle rocks exposed in the two units of the Platta nappe are of subcontinental origin. Although they underwent similar processes from upper-

amphibolite-facies conditions to exposure on the sea floor, their high-temperature evolution is clearly different.
The upper serpentinites are characterized by a subsolidus temperature of equilibration and show many similarities with the Malenco ultramafics indicating that they were close to the Moho before rifting started (Hermann *et al*. 1997, Müntener *et al*. 2000).
The chemical evolution of the lherzolites of the lower serpentinite unit documents a polyphase magmatic evolution. During an early phase, the mantle rocks underwent partial melting that probably started within the garnet stability field. This melting event was followed first by localized "alkaline" metasomatism and then by a pervasive impregnation of the mantle rocks by tholeiitic melts. Subsequently the mantle rocks equilibrated at high temperature (>1000°C) in presence of plagioclase.
This shows that the mantle rocks exhumed along the Platta ocean-continent transition record increasing temperatures of equilibration and interaction with melts in an oceanward direction. It remains unclear, however, whether these differences are related to the pre-rift evolution of the mantle rocks implying that different parts of the subcontinental mantle were exhumed and juxtaposed during rifting, or whether they reflect processes associated with rifting.

4.1. Pre-rift location within the subcontinental mantle of the upper and lower serpentinite unit

In order to discuss whether the differences between the mantle rocks of the upper and lower serpentinite units reflect a different pre-rift evolution or the rifting history, one must consider the pre-rift structure and evolution of the Adriatic lithosphere.
Late Triassic-early Jurassic rifting leading to the opening of the Tethyan ocean affected an area that suffered crustal extension and cooling during Permian and Middle Triassic times (Müntener et al. 2000). This so-called post-Variscan extension is recorded by the intrusion of gabbros along the mantle-crust transition in the Ivrea zone (Rivalenti *et al*. 1981) and in the Malenco complex (Hermann *et al*. 1997). The intrusions were accompanied by granulite metamorphism and partial melting in the lower crust and by granite emplacement in the middle and upper crust, both contemporaneous with basin formation and volcanic activity at the surface (e.g. Handy *et al*. 1999).
The limited subsidence and the subaerial to shallow water conditions recorded from the late Permian to the late Triassic by the pre-rift sediments (e.g. Manatschal & Bernoulli 1999) indicate that this part of the Adriatic crust equilibrated to 30 km and was not overprinted by a strong tectonic activity before rifting started. This is in accordance with P-T-t data from the Permian mantle-crust boundary in the Malenco area (Müntener *et al*. 2000, Villa et al. 2000) indicating that after the Permian gabbroic intrusion isobaric cooling took place and lasted for about 50 Ma. Thus we infer that the Permian position of the mantle rocks were the one prevailing before onset of rifting.
In the Alps, Nd model ages have been determined for several peridotite massifs, which were exhumed to the sea floor of the Tethyan ocean. The Sm-Nd model ages range from Proterozoic ages (external Ligurides, Rampone *et al*. 1995), late Proterozoic-early Phanerozoic (Lanzo North, Bodinier e*t al*. 1991) to Permian (internal Ligurides, Rampone *et al*. 1998). These ages are interpreted as the time of accretion of the mantle rocks to the lithospheric mantle. Two ages of equilibration in the plagioclase stability field have also been determined based on clinopyroxenes-plagioclase isochrones although the equilibration is interpreted as subsolidus. The

ages obtained are Permian in the Erro-Tobbio massif (Piccardo *et al*. 2001) and Jurassic in the external Ligurides (Rampone *et al*. 1995). Field studies and P-T-t data showed that, in the Malenco area, mantle rocks (spinel lherzolite) were close to the mantle-crust transition during Permian times (e.g. Müntener *et al*. 2000). These data imply that during Permian times mantle rocks later exhumed to the sea floor were at different depth (Fig. 3-12a). Indeed, in Permian times, mantle rocks of the Erro-Tobbio and Malenco area were near the top of the continental mantle lithosphere whereas the mantle rocks of the internal Ligurides were accreted at the base of the mantle lithosphere.
The similarities between the mantle rocks of the upper serpentinite unit and the mantle rocks of the Malenco area as well as their low pressure of equilibration (7-12 kbars) suggest that the upper serpentinite unit was also close to the mantle crust transition before rifting started (Fig. 3-12a). Sm-Nd model ages determined on the clinopyroxenes of the lherzolites of the lower serpentinite unit yield Permian ages (Schaltegger, pers. comm.). These ages show that during Permian times, the mantle rocks of the lower serpentinite unit were accreted to the base of the continental lithosphere like the mantle rocks of the internal Ligurides whereas the mantle rocks of the upper serpentinite unit were at the base of the continental crust (fig. 12a). This suggests that a shallow part of the subcontinental mantle was exhumed close to the distal margin (upper serpentinite) and deeper level is exhumed oceanward (lower serpentinite) (Fig. 3-12b).

4.2. Rifting evolution of the upper and lower serpentinite units

Whereas the age of the accretion of the mantle rocks of the lower serpentinite unit to the subcontinental mantle lithosphere is Permian (Shaltegger, pers. Comm.), the age of melt impregnation and equilibration in the plagioclase stability field remains unknown. This low-pressure equilibration most probably happened after the accretion of the mantle rocks to the subcontinental mantle lithosphere; it must have occurred prior to the intrusion of the gabbros (161±1 Ma; Schaltegger *et al*. subm) as these intruded already serpentinized mantle rocks (Desmurs *et al*. 2001). As no major tectonic events are recorded in the Austroalpine domain during Triassic times (e.g. Manatschal and Bernoulli 1999), equilibration with plagioclase occurred either during Permian times as in the Erro-Tobbio mantle rocks (Piccardo *et al*. 2001) or during Jurassic rifting as it was documented in the external Ligurides (Rampone *et al*. 1995). The idea that during the Permian the mantle rocks of lower serpentinite unit were accreted to the base of the lithosphere and uplifted into the plagioclase stability field during this time is not supported by the sedimentological record and the tectonic evolution of the Adriatic crust for this period. Indeed, the recorded extension and basin formation during this time do not justify the assumption of vertical movement displacing material from the base of the lithosphere to its top during this time. Thus, we infer that the melt impregnation and equilibration in the plagioclase stability field of the mantle rocks of the lower serpentinite unit occurred during Mesozoic rifting.

Such processes are not recorded in the upper serpentinite unit, which is characterized by a colder Jurassic evolution. It suggests that the strong apparent lateral thermal gradients prevailed during Jurassic rifting with temperature increasing from the continent toward the future ocean (Fig. 3-12b).

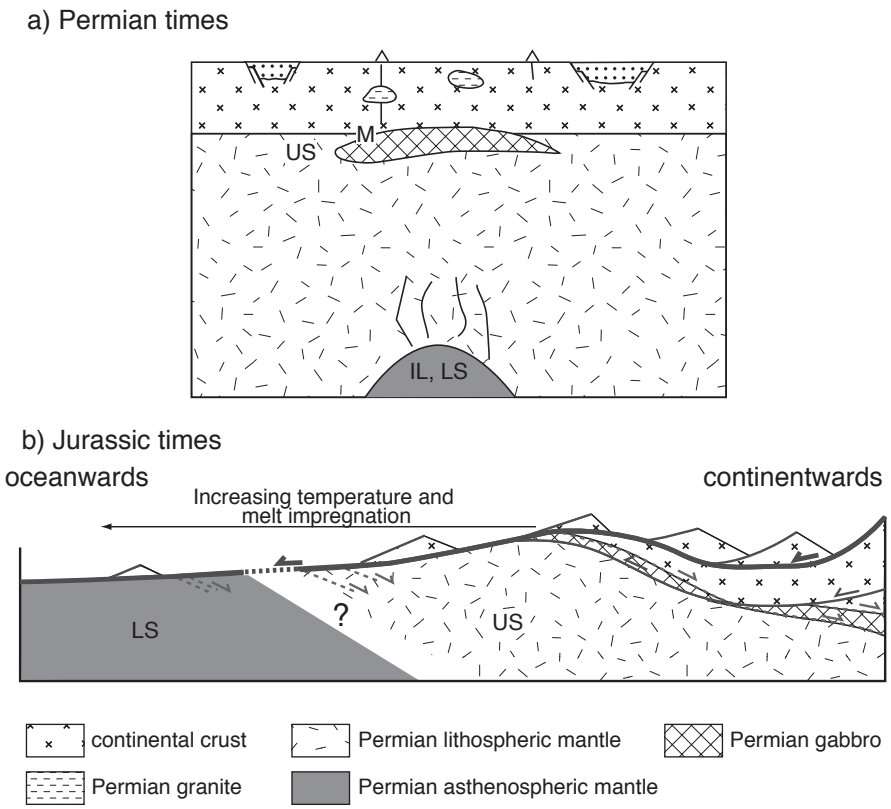

Figure 3-12: a) Schematic representation of the Adria lithosphere during Permian times. The relative positions of the different ultramafic bodies remain probably the same until the onset of rifting. M: Malenco peridotites, US: upper serpentinite unit, IL: internal Ligurides and LS: lower serpentinite unit (see text for discussion). b) Relative position of the upper and lower serpentinite unit after Jurassic exhumation and detachment faulting. The Jurassic structures separating the two units are not observed today (see text for discussion).

5. Summary and Conclusions

The serpentinized peridotite exhumed along the ocean-continent transition of the Platta nappe represent fertile subcontinental mantle. Although, they record similar processes during their exhumation from upper-amphibolite to low-grade alteration, their high-temperature evolution is different. The upper serpentinites, which were originally closer to the continent, record a lower temperature of equilibration than the lower serpentinites, which were originally in a more oceanward position.

The mantle rocks of the upper serpentinite unit were probably close to the mantle-crust transition before onset of rifting. The lherzolite of the lower serpentinite unit are residues of low amounts of melting and were later impregnated by basaltic melts. They represent deeper parts of the pre-rift subcontinental mantle that was impregnated by tholeiitic melts and equilibrated in the plagioclase stability field during its Mesozoic exhumation to the sea floor. Consequently, shallow parts of the subcontinental mantle were exhumed close to the distal margin and deeper levels oceanward. The originally deeper levels were impregnated by tholeiitic melts and equilibrated at high temperatures in presence of plagioclase during rifting. This reflects strong lateral thermal gradients during the formation of the ocean-continent transition. Thus, the differences between the mantle rocks exhumed along the Platta ocean-continent transition depends first on their pre-rift location before onset of rifting (Fig. 3-12a) and second on their pathways during their exhumation to the sea floor (Fig. 3-12b). More information on both, the original location of the mantle rocks

within the mantle lithosphere and the timing of their exhumation, is needed to better constrain tectonic models explaining exhumation of mantle rocks during rifting. Such a model will be proposed in the conclusion chapter.

References

BILL M., NÄGLER T.F. & MASSON H. 2000. Major, minor, trace element, Sm-Nd and Sr isotope compositions of mafic rocks from the earliest oceanic crust of the Alpine Tethys, Schweiz. Mineral. Petrogr. Mitt., **80**, 131-145.

BODINIER J. L. 1988. Geochemistry and petrogenesis of the Lanzo peridotite body, Western Alps, Tectonophysics, **149**, 67-88.

BODINIER J. L., DUPUY C. & DOSTAL J. 1988. Geochemistry and petrogenesis of eastern Pyrenean peridotites, Geochim. Cosmochim. Acta, **52**, 2893-2907.

BODINIER J. L., MENZIES M. A. & THIRLWALL M. F. 1991. Continental to oceanic mantle transition-REE and Sr-Nd isotopic geochemistry of the Lanzo lherzolite Massif, J. Petrol., **Special Lherzolite Issue**, 191-210.

BOUDIER F. 1978. Structure and petrology of the Lanzo peridotite Massif (Piedmont Alps), Geol. Soc. Amer. Bull., **89**, 1574-1591.

BREY G. P. & KÖHLER T. 1990. Geothermobarometry in four phases lherzolite II. New thermobarometers and practical assessment of existing thermobarometers, J. Petrol., **31**,1353-1378.

CARROL-WEBB S. A. & WOOD B. J. 1986. Spinel-pyroxene-garnet relationships and their dependance on Cr/Al ratio, Contrib. Mineral. Petrol., **92**, 471-480.

CORNELIUS H. P. 1932 Geologische Karte der Err-Julier Gruppe 1:25'000. Schweizerische Geologische Kommission Spezialkarte Nr. 115A.

DESMURS L., MANATSCHAL G. & BERNOULLI D. 2001. The Steinmann trinity revisited: mantle exhumation and magmatism along an ocean-continent transition: the Platta nappe, eastern Switzerland, in: R.C.L. Wilson, R.B. Whitmarsh, B. Taylor & N. Froitzheim (Eds): Non-volcanic Rifting of Continental Margins: a Comparison of Evidence from Land and Sea, Geol. Soc. London. Spec. Publ. (in press).

DICK H.J.B. & BULLEN T. 1984. Chromian spinel as petrogenetic indicator in abyssal and alpine-type peridotites and associated lavas, Contrib. Mineral. Petrol., **86**, 54-76.

DIETRICH V. 1969. Die Ophiolithe des Oberhalbsteins (Graubünden) und das Ophiolithmaterial der ostschweizerischen Molasseablagerungen, ein petrographischer Vergleich, Verlag Herbert Lang & Cie, Bern, 179 pp.

FREY F. A., SUEN C. J & STOCKMAN H. W. 1985. The Ronda high temperature peridotite: geochemistry and petrogenesis, Geochim. Cosmochim. Acta, **49**, 2469-2491.

FROITZHEIM N. & EBERLI G.P. 1990. Extensional detachment faulting in the evolution of a Tethys passive continental margin (Eastern Alps, Switzerland), Geol. Soc. Amer. Bull., **102**, 1297-1308.

FROITZHEIM N. & MANATSCHAL G. 1996. Kinematics of Jurassic rifting, mantle exhumation, and passive-margin formation in the Austroalpine and Penninic nappes (eastern Switzerland), Geol. Soc. Amer. Bull., **108**, 1120-1133.

GREEN D. H. & HIBBERSON W. 1970. The instability of plagioclase in peridotite at high pressure, Lithos, **3**, 209-221.

HANDY M. R., FRANZ L., HELLER F., JANOTT B. & ZURBRIGGEN R. 1999. Multistage accretion and exhumation of the continental crust (Ivrea crust section, Italy and Switzerland), Tectonics, **18**, 1154-1177

HERMANN J., MÜNTENER O., TROMMSDORFF V., HANSMANN W. & PICCARDO G. B. 1997. Fossil crust-to-mantle transition, Val Malenco (Italian Alps), J. Geophys. Res., **102**, B9, 20123-20132.

KORNPROBST J., PIBOULE M., RODEN M. & TABIT A. 1990. Corundum-bearing garnet pyroxenite at Beni Bousera (Morocco): Original plagioclase-rich gabbro recrystallized within the mantle?, J. Petrol., **32**, 717-745.

KUSHIRO I. & YODER H. S. 1966. Anorthite-forsterite and anorthite-enstatite reactions and their bearing on the basalt-eclogite transformation, J. Petrol., **7**, 337-362.

LANGMUIR C. H., BENDER J. F., BENCE A. E. HANSON G. N. & TAYLOR S. R. 1977. Petrogenesis of basalts from the FAMOUS area: Mid-Atlantic ridge, Earth Planet. Sci. Lett., **36**, 133-156.

LEAKE B. E. 1978. Nomenclature of amphiboles, Mineral. Mag., **42**, 533-563.

MANATSCHAL G. & BERNOULLI D. 1999. Architecture and tectonic evolution of non-volcanic margins: present-day Galicia and ancient Adria, Tectonics, **18**, 1099-1119.

MANATSCHAL G. & NIEVERGELT P. 1997. A continent-ocean transition recorded in the Err and Platta nappes (Eastern Switzerland), Eclogae Geol. Helv., **90**, 3-27.

Manatschal G., Froitzheim N., Rubenach M. J. & Turrin B. 2001. The role of detachment faulting in the formation of an ocean-continent transition: insights from the Iberia Abyssal Plain, in: R.C.L. Wilson, R.B. Whitmarsh, B. Taylor & N. Froitzheim (Eds): Non-volcanic Rifting of Continental Margins: a Comparison of Evidence from Land and Sea, Geol. Soc. London. Spec. Publ. (in press).

MARRONI G., MOLLI G., MONTANINI A. & TRIBUZIO R. 1998. The association of continental crust rocks with ophiolites in the Northern Appenines (Italy): implication for the continent-ocean transition in the western Tethys, Tectonophysics, **292**,43-66.

MCDONOUGH W. F. & FREY F. A. 1989. Rare earth elements in upper mantle rocks. In: Geochemistry and Mineralogy of Rare Earth Elements. Reviews in Mineralogy, **21**, 99-145.

MENZIES M. A., LONG A., INGRAM G., TATNELL M. & JANECKY D. 1993. MORB peridotite-sea water interaction: Experimental constraints on the behavior of trace elements, 87Sr/86Sr and 143Nd/144Nd. In Prichard H. M. et al. (eds) : Magmatic Processes and Plate Tectonics, Geol. Soc. London Spec. Publ., **76**, 309-322.

MICHARD A. & ALBARÈDE F. 1986. The REE content of some hydrothermal fluids, Chem. Geol., **55**, 51-60.

MICHARD A. 1989. Rare earth element sytematics in hydrothermal fluids, Geochim. Cosmochim. Acta, **53**, 745-750.

MÜNTENER O. & HERMANN J. 1996. The Val Malenco lower crust-upper mantle complex and its field relations (Italian Alps), Schweiz. Mineral. Petrogr. Mitt., **76**, 475-500.

MÜNTENER O. & HERMANN J. 2001. The role of lower crust and continental upper mantle during formation of nonvolcanic passive continental margins: evidence from the Alps, in: R.C.L. Wilson, R.B. Whitmarsh, B. Taylor & N. Froitzheim (Eds): Non-volcanic Rifting of Continental Margins: a Comparison of Evidence from Land and Sea, Geol. Soc. London Spec. Publ. (in press).

MÜNTENER O. 1997. The Malenco peridotites (Alps): Petrology and geochemistry of subcontinental mantle and Jurassic exhumation during rifting, Phd thesis n° 12103, ETH Zurich.

MÜNTENER O., DESMURS L., PETTKÈT., SCHALTEGGER U., MANATSCHAL G. & BERNOULLI D. 2001. Plagioclase peridotite along continental margins:

controlled by subsolidus equilibration or melt/rock reaction?, Terra Abstr., **11**, 731.

MÜNTENER O., HERMANN J. & TROMMSDORFF V. (2000). Cooling history and exhumation of lower-crustal granulite and upper mantle (Malenco, Central Alps), J. Petrol., **41**, 1-25.

OBATA M. 1994. Material transfert and local equilibria in a zoned kelyphite from garnet pyroxenite, Ronda, Spain, J. Petrol., **35**, 271-287.

PEARSON D. G., DAVIS G. R. & NIXON P. H. 1993. Geochemical constraints on the petrogenesis of diamond facies pyroxenite from the Beni Bousera peridotite massif, North Morocco, J. Petrol., **34**, 125-172.

PICCARDO G. B., RAMPONE E. & ROMAIRONE A. 2001. The oceanic lithosphere of the Jurassic Ligurian Tethys: inference from petrology and geochemistry of the Ligurian ophiolites, Terra Abstr., **11**, 310.

PICCARDO G.B., RAMPONE E., VANNUCCI R. 1990. Upper mantle evolution during continental rifting and ocean formation; evidences from peridotite bodies of the Western Alpine-Northern Apennine system. In: Roure, F., Heitzmann, P. & Polino, R. (Eds). Deep Structure of the Alps, Mém. Soc. Géol. Fr., **156**, 323-333.

RAMPONE E., HOFFMAN A. W., PICCARDO G. B., VANNUCCI R., BOTTAZZI P. & OTTOLINI L. 1996. Trace element and isotope geochemistry of depleted peridotites from a N-MORB type ophiolite (Internal Liguride, N-Italy), Contrib. Mineral. Petrol., **123**, 61-76.

RAMPONE E., HOFMANN A. W. & RACZEK I. 1998. Isotopic contrast within the Internal Liguride Ophiolite (N. Italy): the lack of a genetic mantle-crust link, Earth Planet. Sci. Lett., **163**, 175-189.

RAMPONE E., HOFMANN A. W., PICCARDO G. B., VANNUCCI R., BOTTAZZI P. & OTTOLINI L. 1995. Petrology, mineral and isotope geochemistry of the external Ligurides peridotites (Northern Apennines, Italy), J. Petrol., **36**, 81-105

RAMPONE E., PICCARDO G. B., VANNUCCI R., BOTTAZZI P. & OTTOLINI L. 1993. Subsolidus reactions monitored by trace element partitioning: the spinel to plagioclase transition in mantle peridotites, Contrib. Mineral. Petrol., **115**, 1-17.

RIVALENTI G., GARUTI G., ROSSI A., SIENA F. & SINIGOI S. 1981. Existence of different peridotite types and of a layered igneous complex in the Ivrea Zone of the Western Alps, J. Petrol., **22**, 127-153.

SCHALTEGGER U., DESMURS L., MANATSCHAL G., MÜNTENER O., MEIER M. & BERNOULLI D. (submitted). The transition from rifting to seafloor spreading within a magma-poor rifted margin: field and isotopic constraints, Terra Nova.

SCHMÄDICKE E. 2000. Phase relations in peridotitic and clinopyroxenitic rocks in the model systems CMASH and NCMASH, J. Petrol., **41**, 69-86.

SMITH D. 1977. The origin and interpretation of spinel-pyroxene clusters in peridotite, J. Geol., **85**, 476-482.

SUN S.S. & MCDONOUGH W.F. 1989. Chemical and isotopic systematics of oceanic basalts: implication for mantle composition and processes. In Saunders, A.D., & Norry, M. J. (Eds), Magmatism in the Ocean Basins, Geol. Soc. London. Spec. Publ., **42**, 313-345.

TROMMSDORFF V., PICCARDO G.B. & MONTRASIO A. 1993. From magmatism through metamorphism to sea floor emplacement of subcontinental Adria during pre-Alpine rifting (Malenco, Italy), Schweiz. Mineral. Petrogr. Mitt., **73**, 191-203.

VILLA I. M., HERMANN J., MÜNTENER O. & TROMMSDORFF V. 2000. ^{39}Ar-^{40}Ar dating of multiple zoned amphibole generations (Malenco, Italian Alps), Contrib. Mineral. Petrol., **140**, 363-381.

WITT-EICKSCHEN G. & SECK H. A. 1991. Solubility of Ca and Al in orthopyroxene from spinel peridotite: an improved version of an empirical geothermometer, Contrib. Mineral. Petrol., **106**, 431-439.

Chapter 4-The transition from rifting to seafloor spreading within a magma-poor rifted margin: field and isotopic constraints

Urs Schaltegger[1,2], Laurent Desmurs[1], Gianreto Manatschal[1,3], Othmar Müntener[1,4], Martin Meier[1], Daniel Bernoulli[1,5]

[1] Department of Earth Sciences, Federal Institute of Technology, ETH Zentrum, CH-8092 Zürich, Switzerland, [2] Present address: Département de Minéralogie, Université de Genève, 13, rue des Maraîchers, CH-1205 Genève, Switzerland, [3] Present address: EOST-UMR 7517 CNRS - ULP 1, rue Blessig, F – 67084 Strasbourg, France, [4] Present address: Institute of Geology, University of Neuchâtel, 11, rue Emile-Argand, CH-2007 Neuchâtel, Switzerland, [5] Present address: Department of Earth Sciences, University of Basel, Bernoullistrasse 32, CH-4056 Basel, Switzerland

(Submitted to Terra Nova)

Abstract

This study provides new geological and isotope geochemical constraints on the evolution from continental rifting to sea-floor spreading along a segment of the southeastern, Jurassic Tethyan rifted margin exposed today in the Platta and Err nappes in the eastern Central Alps (Eastern Switzerland). Field observations show that the Platta-Err ocean continent transition zone is characterized by oceanwards dipping detachment faults leading to the exhumation of subcontinental mantle rocks which are intruded by small gabbro bodies and dolerite dikes, and are partially covered by pillow basalts and/or radiolarites. Zircons extracted from gabbros and albitites yield concordant U-Pb ages of 161±1 Ma, and their initial Hf isotopic composition (+14.4 to +14.9) points to a MORB-type depleted mantle source, consistent with initial bulk rock eNd values of +7.3 to +9.5 from gabbros and basalts. Our data allow to demonstrate that the onset of magmatic activity coincides with the latest phase of mantle exhumation along low-angle detachment faults and may be controlled by localized and "fast" upwelling of the asthenosphere beneath a zone of exhumed continental mantle (ZECM).

Keywords: *Ocean-continent transition zone (OCTZ), zone of exhumed continental mantle (ZECM), MORB magmatism, magma-poor margins, slow spreading system, U-Pb dating, radiogenic isotopes, eastern Central Alps, ophiolites*

Introduction

Studies of present-day rifted margins allowed to distinguish between two "end-member" types of margins: volcanic margins at which magmatic activity is related to rifting of continental crust and non-volcanic margins where no or only limited magmatic activity is recorded prior to sea-floor spreading. Because passive margins laterally grade into oceanic crust, at a given time a transition from an non-magmatic to a magmatic system must occur; the processes involved are, however, not well understood. Despite the precise dating of some gabbro intrusions, which provide important time markers for specific magmatic events during the evolution of non-volcanic margins (e.g. Schärer et al., 2000), the spatial distribution of magmatic rocks within the margin and their relation to deformation is essentially unknown. This also explains the controversy about timing and duration of rifting along some passive margins (e.g. Wilson et al. 2001).

More recently, in the Err and Platta nappes in the eastern Central Alps (eastern Switzerland), Froitzheim and Manatschal (1996), Manatschal and Nievergelt (1997), and Desmurs et al. (2001) provided new constraints on the geometry of a fossil passive margin bordering the Liguria-Piemonte Ocean, a subbasin of the Alpine Tethys, to the southeast (Fig. 4-1). Palinspastic reconstruction of these nappes resulted in a restoration of an ocean-continent transition zone (OCTZ) which is characterized by a thinned continental crust (Err unit in Fig. 4-1a) bounded oceanwards by a zone of exhumed continental mantle (ZECM; upper serpentinite unit) which grades into oceanic crust and underlying mantle (lower serpentinite unit). Thus, the Platta-Err OCTZ shows the same architecture as that found along present-day magma-poor rifted margins (e.g. Iberia margin, Manatschal and Bernoulli 1999), and represents the only so far known example where the spatial relationships of exhumed subcontinental mantle rocks and associated magmatic and sedimentary rocks belonging to an atypical "ophiolite" sequence can be restored with some confidence. "Ophiolite" is put in brackets because the magmatic suite occurs within and on top of genetically unrelated continental mantle.

In this paper, we present new U-Pb age determinations and initial Hf isotopic compositions of zircons from oceanic gabbros, and whole-rock Sr and Nd isotopic compositions of gabbros and basalts from the Platta nappe (Fig. 4-1a). We will demonstrate that magmatism initiated during ongoing mantle exhumation and was contemporaneous with detachment faulting. As we shall show, in "non-volcanic" margins onset of magmatism postdates rifting (in classical terminology the process which involves extension of continental crust) but predates lithospheric breakup and sea-floor spreading (accretion of oceanic crust and loss of lithospheric mantle strength). In this paper we therefore prefer to use the term "magma-poor" instead of "non-volcanic" margin. The goal of our paper is to place time and isotopic constraints on the magmatism in the OCTZ within a well known geological framework.

The geological framework

The so-called Liguria-Piemonte domain of the Tethys ocean was located between Europe and Adria and its relics extend from eastern Corsica across the Ligurian Apennines and Western Alps to the Central and Eastern Alps, as outlined in Fig. 4-1 (map inset). The "ophiolites" are characterized along the whole length of the oceanic domain by very small volumes of mafic rocks, by the absence of sheeted dike

complexes and by pillow basalts and/or pelagic sediments of middle to late Jurassic age stratigraphically overlying presumably subcontinental mantle rocks.
All these features are elegantly explained by a detachment model that was first applied to the Liguria-Piemonte ocean by Lemoine et al. (1987). Detailed field work in recent years permitted to map rift-related detachment faults in a segment of the Liguria-Piemonte ocean (Err-Platta domain, eastern Swiss Alps; Froitzheim and Eberli 1990; Manatschal and Nievergelt 1997; Fig. 4-1b) and led to an improved model for the OCT (Fig. 4-1c) comprising the most distal part of the continental crust and a zone of exhumed continental mantle (ZECM) which laterally grades into oceanic crust. The distal continental margin (Err domain) is characterized by oceanward-dipping low-angle detachment faults that cut into the mantle and emplaced continent-derived extensional allochthons on top of exhumed subcontinental mantle. The ZECM (Platta domain) includes serpentinized peridotites, minor occurrences of gabbroic intrusions, tholeiitic pillow lavas and flows, and a succession of oceanic sediments (Desmurs et al., 2001). The mantle rocks exhibit systematic compositional differences with respect to their location within the OCT. Ultramafic rocks close to the continent are serpentinized spinel peridotites with abundant pyroxenite layers that are both parallel and discordant to a high-T spinel foliation (upper serpentinite unit), while the ultramafic rocks at some distance from the continent are pyroxenite-free peridotites that equilibrated in the plagioclase stability field (Müntener et al., 2001; lower serpentinite unit; see Fig. 4-1c).
Figure 4-1 also shows that the volume of mafic rocks intruding and overlying the serpentinized peridotites increases with distance from the continent. Gabbroic intrusions range from Mg-rich to Fe-oxide-rich and were emplaced at depths of less than 8 km below sea-floor (Desmurs et al., 2001). They contain pockets and veins of highly differentiated Fe-Ti gabbros, which are extremely enriched in accessory minerals like zircon and apatite, beside dikes and veins of diorite and albitite, respectively. The gabbros were partly deformed under decreasing temperatures and cut by dolerite dikes that were probable feeder dikes for overlying pillow basalts. Sedimentary breccias contain fragments of gabbroic and mantle rocks, suggesting submarine erosion and re-sedimentation processes during the development of the OCTZ.

U-Pb, Hf, Sr and Nd isotopic data

Zircons out of four lithologies were dated (Tab. 4-1; analytical details in the Appendix): a ferrogabbro (Platta-1) at 160.5 ± 0.5 Ma (all errors 95% c.l.); a dioritic dyke (Platta-2) at 161.3 ± 1.7 Ma; a coarse-grained Mg-gabbro intrusion (Platta-6) at 160.7 ± 0.9 Ma; and an albitite clast in a pillow breccia (MP56) at 160.9 ± 0.4 Ma (see Fig. 4-3). Since all our age determinations converge at a statistical mean of 160.9 ± 0.4 Ma (at 95% confidence level), we suggest an age of 161 ± 1 Ma to be representative for the entire gabbro suite in this area. Hf isotopic ratios were determined from some of the dated zircon fractions (Tab. 4-2) and yielded initial e_{Hf} values for three lithologies: +14.7 for a Fe-gabbro (N=1), +14.5 for a Mg-gabbro (N=3), and +14.7 (N=2) for the albitite. Nd isotopic values of bulk rock samples plot between eNd=7.3 and 9.6 without significant difference between gabbros and basalts (Tab. 4-3). In a $^{143}Nd/^{144}Nd$ vs. $^{87}Sr/^{86}Sr$ diagram (Fig. 4-3), the age-corrected data form a trend with strongly increasing Sr isotopic ratios at near constant Nd isotopic composition, which may be interpreted by seawater alteration. The four highest εNd values between +8.9 and +9.6 (i.e. from samples Platta-5, 6, 8 and 9, the latter is

identical to Platta-2) as well as their initial eHf values of 14.4 to 14.7 agree with an N-MORB reservoir at 160 Ma.

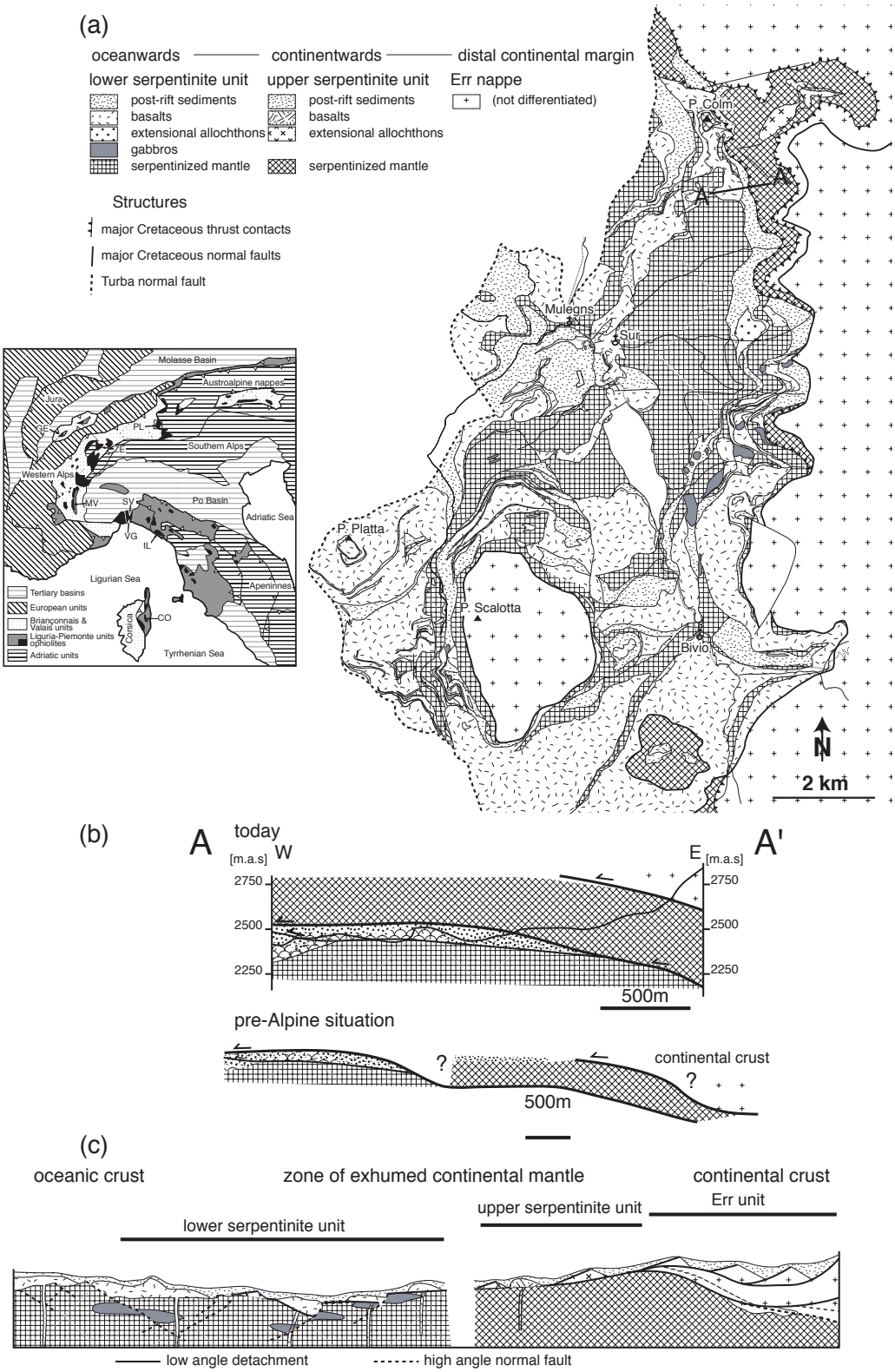

Figure 4-1: Map and palinspastic reconstruction of the Platta nappe. (a) Geological map of the Platta nappe (after Cornelius, 1932, Dietrich, 1969, and own observations). Inset shows the extension of the ophiolites derived from the Liguria-Piemonte oceanic domain within the Alps from Corsica to the Eastern Alps and the location of the Platta nappe (red box). (b) Palinspastic reconstruction of the Platta nappe (modified after Desmurs et al. 2001). Upper section shows the present observed Alpine structure, the shaded lower

part of the section is observed, the white upper part is a lateral projection of geometries mapped in the surroundings of the section. Lower section shows the kinematic inversion of the above section. Question marks indicate the uncertainities in the estimate of the amounts of displacement, i.e. the pre-thrust distance between the first-order tectonic units. (c)Tentative palinspastic section across the Platta-Err ocean-continent-transition (OCT) which is based on the kinematic inversion of the thrust sheets mapped in the Platta nappe (see b). Section shows the position of the upper serpentinite and lower serpentinite units within the former OCT and summarises the observed field relationships between fault structures, continental rocks, exhumed mantle rocks, and intrusive and extrusive mafic rocks and their position within the OCT.

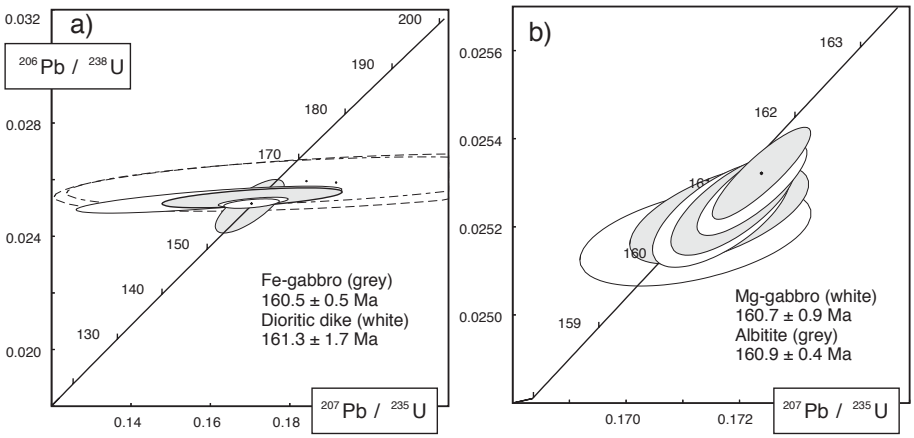

Figure 4-2: Concordia diagrams showing the results of U-Pb age determinations of four lithologies (a) a ferrogabbro (Platta-1) and a diorite dike (Platta-2) from Fuorcla da Faller; the $^{206}Pb/^{238}U$ ages of stippled ellipses (analyses 1 and 6) are biased by common lead compositions and were therefore excluded form mean age calculations; (b) a pegmatoid gabbro stock from Alp Natons (Platta-6) and a albitite clast in a pillow breccia from Val Savriez (MP56).

Discussion

Gabbroic rocks in the Liguria-Piemonte ocean have been previously dated in several places using high-precision U-Pb zircon techniques (see Fig. 4-1): 161 ± 3 Ma in northern Corsica (Ohnenstetter et al., 1981); 166 ± 1 Ma in blocks within the Penninic flysch of the Gets nappe (Bill et al., 1997); 164 ± 1 Ma in the Zermatt area (Rubatto et al., 1998) and at 163 ± 2 Ma in Monviso ophiolites (Rubatto, pers. comm.). Plagiogranites from the Ligurian Alps, the internal Apennines, and the Chenaillet and Monviso units were found to be significantly younger (150-153 Ma; Borsi et al., 1996; 148±2, Costa and Caby 2001; 152±2 Ma, Lombardo et al. 2001). The published zircon age values of gabbroic rocks from the Liguria-Piemonte oceanic domain are in line with our new U-Pb ages. The dated albitite MP56 is contemporaneous and cogenetic with the gabbros; albitite veins are indeed ubiquitous within the gabbros and are interpreted as residual melt fractions. The mafic igneous crust of the Platta area was covered by post-rift radiolarian cherts, which therefore must be younger than 161 Ma and which elsewhere are dated as middle to late Jurassic. The onset of radiolarite deposition appears to be diachronous, but not earlier than late Bathonian-early Callovian (De Wever and Baumgartner, 1995; Bill et al., 2001) except for the most distal margin in the Gets nappe (middle Bathonian, Bill et al. 2000, 2001). The age of the gabbros is therefore compatible with the new Jurassic time-scale of Palfy et al. (2000) placing the Bathonian-Callovian boundary at 160.4+1.1/-0.5 Ma.

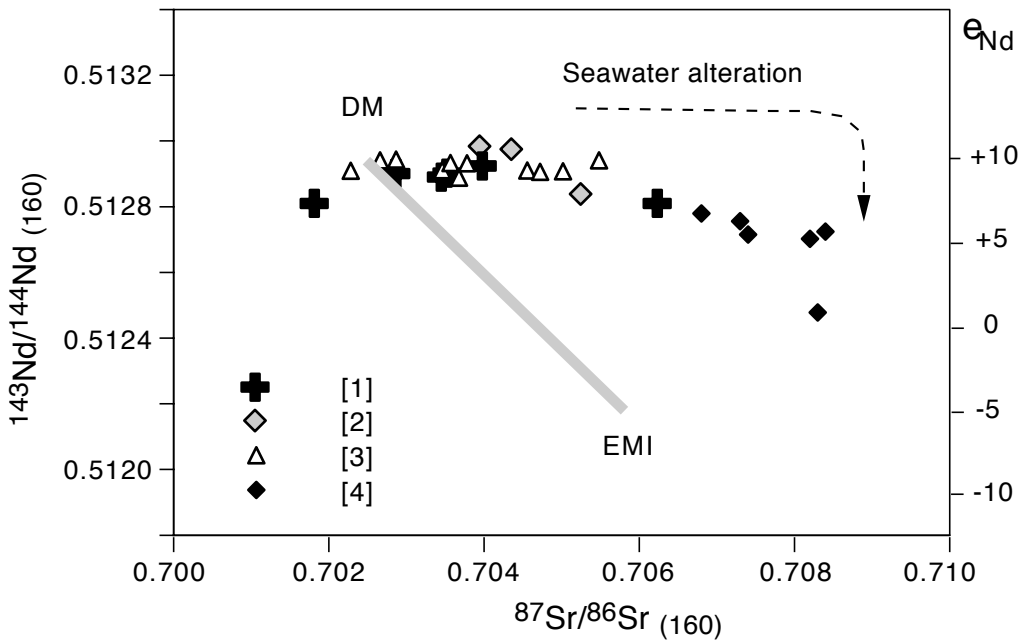

Figure 4-3: Nd-Sr diagram with mafic rocks from different localities of the Liguria-Piemonte ocean; own data from the Platta nappe [1] are compared to data of [2] Basalts from Platta nappe, Stille et al. (1989); [3] Gabbros and basalts from Internal Ligurides, Rampone et al. (1998); [4] Basalts from nappe des Gets, Bill et al. (2000), see Tab. 4-2. DM and EMI mantle reservoirs from Hart (1984).

There is no clear sequence of gabbro emplacement ages with respect to the paleotectonic position of the investigated localities within the Liguria-Piemonte ocean (Fig. 4-1). They, however, exhibit a surprisingly narrow window of crystallization ages within 5 million years, suggesting regional upwelling and partial melting of a MORB-type asthenospheric mantle. Sr and Nd isotopic data of basalts and gabbros from the Platta nappe (own data and data from Stille et al., 1989) agree with values from the Internal Ligurian ophiolites (Borsi et al. 1995, Rampone et al., 1998; Fig. 4-3). This demonstrates that gabbros and basalts were derived from the same depleted asthenospheric mantle source. The data points of the Gets nappe gabbro, on the other hand, form a distinct cluster at the lower limit of MORB-type ε_{Nd} values, which may be interpreted by strong oceanic alteration (Bill et al., 2000). The Hf data presented in this paper are the first initial Hf isotopic ratios for Tethyan ophiolites; the ε_{Hf} values of 14.4 to 14.9 for the gabbroic zircons are consistent with an origin from N-MORB type asthenospheric mantle (Nowell et al., 1998).

The asthenospheric source of mafic rocks is in contrast to the above described lithospheric nature of the mantle rocks in the ocean-continent transition zone, which they intruded (Desmurs et al., 2001). The narrow age range and the MORB-type character of the liquids support the interpretation that the gabbros intruded into the lithosphere close to or at the onset of active sea-floor spreading. We propose that lithospheric heating and/or intrusion of mafic melts may have drastically lowered the integrated strength of the lithosphere leading to a change in the mode of extension from solid-state controlled detachment faulting to igneous accretion dominated extension. Thus further extension may be accommodated by intruding magmas and minor normal faulting that allow for the emplacement of dolerite dikes and voluminous basalt flows on top of the exhumed mantle rocks.

Conclusions

The Err-Platta ocean-continent transition (OCT) is characterized by the typical association of relatively small bodies of mafic rocks derived from an asthenospheric source, which intruded a lithospheric mantle that was previously exhumed by means of passive rifting and detachment faulting, and overlain by discontinuous bodies of pillow basalts. This assemblage is regarded as typical for the OCTZ of magma-poor margins. The intrusion of MORB- type mafic liquids changes low-angle detachment from concave upward to concave downward in the continental mantle lithosphere and marks the onset of (slow?) sea-floor spreading. We therefore suggest that the Platta OCTZ is transitional to a slow-spreading system (cf. Lagabrielle and Lemoine, 1997). The timing of emplacement and the source of the mafic melts do not greatly differ along a ~600 km segment of the Liguria-Piemonte ocean, indicating that sea-floor spreading between Adria and Europe began 165 to 160 Ma ago. On a global scale, the association of exhumed subcontinental mantle intruded by small volumes of mafic liquids derived from a N-MORB-type depleted mantle source suggests that there is no genetic link between peridotite and mafic rocks along OCT's of magma-poor rifted margins.

Acknowledgements:

I. Ivanov, T. Bär and A. von Quadt are thanked for technical help at ETH. Financial support through Swiss National Science Foundation (project Nr. 20-55284.98) is kindly acknowledged. We thank V. Trommsdorff for a presubmission review.

References

BILL, M., BUSSY, F., COSCA, M., MASSON, H. AND HUNZIKER, J.C., 1997. High-precision U-Pb and $^{40}Ar/^{39}Ar$ dating of an Alpine ophiolite (Gets nappe, French Alps). *Eclogae Geol. Helv.*, **90**, 43-54.

BILL, M., NÄGLER, T. AND MASSON, H., 2000. Major, minor, and trace element, Sm-Nd and Sr isotope composition of mafic rocks from the earliest oceanic crust of the Alpine Tethys. *Schweiz. Mineral. Petrogr. Mitt.*, **80**, 131-146.

BILL, M., O'DOGHERTY, L., GUEX, J., BAUMGARTNER, P.O. AND MASSON, H., 2001. Radiolarite ages in Alpine-Mediterranean ophiolites: Constraints on the oeanic spreading and the Tethys-Atlantic connection. *Geol. Soc. Amer. Bull.*, **113**, 129-143

BLICHERT-TOFT, J. AND ALBARÈDE, F., 1997. The Lu-Hf isotope geochemistry of chondrites and the evolution of the mantle-crust system. *Earth Planet. Sci. Lett.* **148**, 243-258.

BORSI, L., SCHÄRER, U., GAGGERO, L. AND CRISPINI, L., 1996. Age, origin and geodynamic significance of plagiogranites in lherzolites and gabbros of the Piedmont-Ligurian ocean basin. *Earth Planet. Sci. Lett.*, **140**, 227-241.

CORNELIUS, H.P., 1932. Geologische Karte der Err-Julier-Gruppe 1:25000, Ost- und Westblatt: Spezialkarte 115A+B (Geological map) - Schweiz. Geol. Kommission.

COSTA, S. AND CABY, R., 2001. Evolution of the Ligurian Tethys in the Western Alps: Sm/Nd and U/Pb geochronology and rare-earth element geochemistry of the Montgenèvre ophiolite (France). *Chem. Geol.,* **175**, 449-466.

DESMURS, L., MANATSCHAL, G. AND BERNOULLI, D., 2001. The Steinmann trinity revisited: mantle exhumation and magmatism along an ocean-continent transition: the Platta nappe, eastern Switzerland. *In: Non-volcanic rifting of continental margins: evidence from land and sea.* (WILSON, R. C. L., WHITMARSH, R. B., FROITZHEIM, N. AND TAYLOR, B., eds.) *Geol. Soc. London, Spec. Publ.*, **187**, 000-000.

DE WEVER, P. AND BAUMGARTNER, P.O., 1995. Radiolarians from the base of the supra-ophiolitic Schistes Lustrés Formation in the Alps (Saint-Véran, France and Traversiera Massif, Italy), *in Middle Jurassic to Lower Cretaceous Radiolaria of Tethys: Occurrences, Systematics, Biochronology* (BAUMGARTNER, P.O., O'DOGHERTY, L., GORICAN, S., URQUHART, E., PILLEVUIT, A. AND DE WEVER, P., eds.) *Mém. Géol.* (Lausanne), **23**, 725-730.

DIETRICH, V., 1969. Die Ophiolithe des Oberhalbsteins (Graubünden) und das Ophiolithmaterial der ostschweizerischen Molasseablagerungen, ein petrographischer Vergleich. Verlag Herbert Lang & Cie AG, Bern, pp. 179.

FROITZHEIM, N. AND EBERLI, G., 1990. Extensional detachment faulting in the evolution of a Tethys passive continental margin, Eastern Alps, Switzerland: *Geol. Soc. Amer. Bull.*, **102**, 1197-1308.

FROITZHEIM, N. AND MANATSCHAL, G., 1996. Kinematics of Jurassic rifting, mantle exhumation, and passive-margin formation in the Austroalpine and Penninic nappes (eastern Switzerland). *Geol. Soc. Amer. Bull.*, **108**, 1120-1133.

HART, S.R., 1984. A large-scale isotope anomaly in the Southern Hemisphere. *Nature*, **309**, 753-757.

LAGABRIELLE, Y. AND LEMOINE, M., 1997. Alpine, Corsican and Apennine ophiolites: the slow-spreading ridge model. *C. R. Acad. Sci. Paris, Sci. Terre Planètes*, **325**, 909-920.

LEMOINE, M., TRICART, P. AND BOILLOT, G., 1987. Ultramafic and gabbroic ocean floor of the Ligurian Tethys (Alps, Corsica, Apennines): In search of a genetic model. *Geology*, **15**, 622-625

LOMBARDO, B., RUBATTO, D. AND CASTELLI, D. 2001. Ion microprobe U-Pb dating of zircon from a Monviso metaplagiogranite. Meeting in memory of G. Elter, Cogne, Abstract volume, 63.

MANATSCHAL, G. AND NIEVERGELT, P., 1997. A continent-ocean transition recorded in the Err and Platta nappes (Eastern Switzernland). *Eclogae Geol. Helv.*, **90**, 3-27.

MANATSCHAL, G. AND BERNOULLI, D. 1999. Architecture and tectonic evolution of non-volcanic margins: Present day Galicia and ancient Adria. *Tectonics,* **18**, 1099-1119.

MÜNTENER O., DESMURS, L., PETTKE T., U SCHALTEGGER, U., MANATSCHAL, G. AND BERNOULLI, D. 2001. Plagioclase peridotite along continental margins: Controlled by subsolidus equilibration or melt/rock reaction? *J. Conf. Abstracts*, **6/1**, 731.

NOWELL, G.M., KEMPTON, P.D., NOBLE, S.R., FITTON, J.G., SAUNDERS, A.D., MAHONEY, J.J. AND TAYLOR, R.N., 1998. High precision Hf isotopic measurements of MORB and OIB by thermal ionisation mass spectrometry: insights into the depleted mantle. *Chem. Geol.*, **149**, 211-233.

OHNENSTETTER, M., OHNENSTETTER, D., VIDAL, PH., CORNICHET, J., HERMITTE, D. AND MACE, J., 1981. Crystallization and age of zircon from Corsican ophiolitic albitites: consequences for oceanic expansion in Jurassic times. *Earth Planet. Sci. Lett.*, **54**, 397-408.

PÁLFY, J., SMITH, P.L. AND MORTENSEN, J.K., 2000. A U-Pb and $^{40}Ar/^{39}Ar$ time scale for the Jurassic. *Canad. J. Earth Sci.*, **37**, 923-944.

RAMPONE, E., HOFMANN, A.W. AND RACZEK, I., 1998. Isotopic contrasts within the Internal Liguride ophiolite (N. Italy): the lack of a genetic mantle-crust link. *Earth Planet. Sci. Lett.*, **163**, 175-189.

RUBATTO, D., GEBAUER, D. AND FANNING, M., 1998. Jurassic formation and Eocene subduction of the Zermatt - Saas-Fee ophiolites: implications for the geodynamic evolution of the Central and Western Alps. *Contr. Mineral. Petrol.*, **132**, 269-287.

SCHÄRER, U., GIRARDEAU, J., CORNEN, G. AND BOILLOT, G., 2000. 138-121 Ma asthenospheric magmatism prior to continental break-up in the North Atlantic and geodynamic implications. *Earth Planet. Sci. Lett.*, **181**, 555-572.

STACEY, J.S. AND KRAMERS, J.D. 1975. Approximation of terrestrial lead isotope evolution by a two-stage model. *Earth Planet Sci Lett.*, **26**, 207-221

STILLE, P., CLAUER, N. AND ABRECHT, J., 1989. Nd isotopic composition of Jurassic Tethys seawater and the genesis of Alpine Mn-deposits: Evidence from Sr-Nd isotope data. *Geochim. Cosmochim. Acta*, **53**, 1095-1099.

WILSON, R.C.L., MANATSCHAL, G., WISE, S., AND URQHUART, E., 2001. The location, timing and duration of rifting along non-volcanic passive margins : evidence from the Mesozoic of the Alps and Western Iberia. *In: Non-volcanic rifting of continental margins: evidence from land and sea.* (WILSON, R. C. L., WHITMARSH, R. B., FROITZHEIM, N. AND TAYLOR, B. Eds.) *Geol. Soc. London, Spec. Publ.*, **187**, 000-000.

APPENDIX 1. ANALYTICAL TECHNIQUES

U-Pb age determinations: Zircons were dated by conventional U-Pb techniques: Dissolution in HF-HNO_3 and chemical separation on anion exchange resin and mass spectrometry followed standard techniques. The zircons showed extremely low concentrations of uranium and radiogenic lead (see Tab. 4-1), which could only be analyzed involving low-blank micro-techniques with total procedural blanks of 1.5 * 10^{-12}g Pb. Isotopic ratios were measured on a MAT 262 mass spectrometer equipped with an ion counting system, which was calibrated using a NBS 982 standard solution. Common lead concentration in excess of the blank lead were corrected using depleted mantle lead isotopic ratios.

Hf isotopes: The Hf fraction was isolated using Eichrom Ln-spec resin, and measured in static mode on a NuPlasma multi-collector ICP-MS using a MCN-6000 nebulizer for sample introduction. Zircons are commonly characterized by extremely low $^{176}Lu/^{177}Hf$ of less than 0.005. Hf isotopic values were therefore not corrected for in-situ radiogenic ingrowth from ^{176}Lu, because corrections for 160 Ma old zircons are within the analytical uncertainty of the measured $^{176}Hf/^{177}Hf$ ratios. The Hf isotopic ratios were corrected for mass fractionation using a $^{179}Hf/^{177}Hf$ value of 0.7325 and normalized to $^{176}Hf/^{177}Hf$ = of 0.28216 of the JMC-475 standard (Blichert-Toft and Albarède, 1997).

Sr and Nd isotopes: Isotopic compositions were determined on whole-rock aliquots of 3 basalts and 3 gabbros; analytical procedures followed standard techniques. The samples were measured on a MAT 262 multicollector thermal ionisation mass spectrometer in static mode. The performance of the spectrometer was controlled using La Jolla and NBS 987 standard solutions, which were measured at $^{143}Nd/^{144}Nd$ = 0.511858 ± 1 (n=7) and $^{87}Sr/^{86}Sr$ = 0.710307 ± 19 (n=3), respectively. Measured $^{87}Sr/^{86}Sr$ ratios of samples were corrected by -0.000066 to account for the bias of the NBS 987 results.

Table 1: *U-Pb isotopic data of zircons from gabbros and an albitite of the Err-Platta domain*

Nr.	Description	Weight	nr.	Concentrations				Atomic ratios							Apparent ages			Error
	a)	[mg]	of grains	U	Pb rad.	Pb nonrad.	Th/U	206/204	206/238	Error 2s [%]	207/235	Error 2s [%]	207/206	Error 2s [%]	206/238	207/235	207/206	corr.
				[ppm]		[pg]	b)	c)	d)		d)		d)					
Metasomatized, amphibole-bearing diorite dyke, Fuorcla da Faller (Platta-1), 765'150/177'150 e)																		
13	anh frags clrls	0.0125	2	5.4	0.15	7.6	0.49	32	0.02596	2.70	0.1842	26.80	0.05146	25.40	165.2	--	--	0.56
14	round clrls	0.0126	2	6.9	0.18	3.4	0.51	59	0.02531	1.35	0.1597	17.00	0.04576	16.00	161.1	--	--	0.76
15	frags abr	0.0703	15	7.3	0.19	4.7	0.47	192	0.02517	0.54	0.1704	3.36	0.04910	3.12	160.3	159.8	152.5	0.51
16	frags abr small	0.0408	12	5.6	0.15	2.1	0.49	193	0.02522	0.55	0.1708	4.21	0.04911	3.90	160.6	160.1	153.0	0.61
Ferrogabbro, Fuorcla da Faller (Platta-2), 765'150/177'150 e)																		
17	tips and frags of pr	0.0059	1	10.6	0.30	1.4	0.96	90	0.02537	1.12	0.1705	10.85	0.04875	10.24	161.5	--	--	0.58
18	frags	0.0061	2	8.4	0.25	7.0	0.38	30	0.02591	3.20	0.1917	30.20	0.05365	28.80	164.9	--	--	0.48
19	frags unabr	0.0267	14	12.9	0.36	1.9	0.75	304	0.02507	3.08	0.1699	4.17	0.04915	2.74	159.7	159.4	155.2	0.75
Coarse-grained gabbro, Alp Natons (Platta-6), 769'175/151'270 e)																		
20	frags	0.1203	10	15.1	0.40	1.4	0.49	2141	0.02524	0.39	0.1717	0.58	0.04933	0.43	160.7	160.9	163.3	0.67
21	frags	0.1132	5	13.2	0.35	4.8	0.49	520	0.02519	0.36	0.1712	0.97	0.04929	0.86	160.4	160.5	161.9	0.47
22	small frags	0.1161	19	23.3	0.62	1.4	0.53	3237	0.02530	0.33	0.1722	0.46	0.04937	0.27	161.1	161.3	165.5	0.82
Plagiogranite interpillow component, Val Savriez (MP56), 771'725/153'660 e)																		
23	lge spr euh	0.0506	11	55.8	1.41	0.9	0.35	5031	0.02534	0.33	0.1724	0.41	0.04935	0.20	161.3	161.5	164.3	0.88
24	euh spr clrls incl	0.1237	5	55.6	1.42	9.9	0.39	1129	0.02526	0.37	0.1719	0.52	0.04934	0.35	160.8	161.1	164.2	0.74
25	lge incl	0.1111	6	23.3	0.58	5.5	0.30	778	0.02524	0.36	0.1716	0.75	0.04931	0.60	160.7	160.8	162.8	0.62

a) abr = abraded, anh = anhedral, clrls = colourless, euh = euhedral, frags = fragments, incl = inclusions, pr = prisms, unabr = unabraded
b) Calculated on the basis of radiogenic $^{208}Pb/^{206}Pb$ ratios, assuming concordancy
c) Corrected for fractionation and spike
d) Corrected for fractionation, spike, blank and common lead (Stacey & Kramers, 1975)
e) Swiss grid coordinates

Table 2: *Hf isotopic results from dated zircons*

Nr.	Sample nr.	$^{176}Hf/^{177}Hf$ measured	± 2s	$^{176}Hf/^{177}Hf$ (T)	εHf (0)	εHf (T)	± 2s
Fe-gabbro, Fuorcla da Faller (Platta-2)							
6	Platta-2/3	0.283084	0.000003	0.283082	11.0	14.7	0.1
Mg-gabbro, Alp Natons (Platta-6)							
8	Platta-6/1	0.283075	0.000002	0.283073	10.7	14.4	0.1
9	Platta -6/2	0.283076	0.000003	0.283074	10.8	14.4	0.1
9	Platta -6/2 duplicate	0.283083	0.000002	0.283081	11.0	14.7	0.1
9	Platta -6/2 triplicate	0.283085	0.000003	0.283083	11.1	14.7	0.1
10	Platta -6/3	0.283084	0.000003	0.283082	11.0	14.7	0.1
Albitite, Val Savriez (MP56)							
12	MP56/3	0.283079	0.000003	0.283077	10.9	14.5	0.1
13	MP56/4	0.283090	0.000003	0.283088	11.2	14.9	0.1

Table 3: *Sr and Nd isotopic data of gabbros and basalts from the Err-Platta domain*

sample No.	ppm Rb	ppm Sr	$^{87}Rb/^{86}Sr$	$^{87}Sr/^{86}Sr$ sample (0)	±2s	$^{87}Sr/^{86}Sr$ sample (T)	ppm Sm	ppm Nd	$^{147}Sm/^{144}Nd$ sample (0)	$^{143}Nd/^{144}Nd$ sample (0)	±2s	$^{143}Nd/^{144}Nd$ sample (T)	εNd (0)	εNd (T)	T DM (Ga)
Platta - 3	3.85	152.04	0.0734	0.706398	7	0.706231	2.024	6.887	0.1777	0.512996	3	0.512810	6.94	7.34	0.65
Platta - 4	44.54	78.26	1.6481	0.705560	5	0.701811	0.288	0.903	0.1931	0.513012	69	0.512810	7.26	7.34	1.02
Platta - 5	0.43	89.14	0.0141	0.703480	5	0.703448	4.604	15.062	0.1848	0.513083	3	0.512890	8.65	8.89	0.35
Platta - 6	1.69	85.90	0.0569	0.702991	7	0.702862	3.535	10.038	0.2129	0.513124	5	0.512901	9.45	9.12	5.56
Platta - 8	17.95	81.51	0.6377	0.704973	8	0.703522	4.769	15.401	0.1872	0.513098	4	0.512902	8.93	9.13	0.30
Platta - 9	0.63	108.89	0.0168	0.704014	7	0.703976	22.599	73.454	0.1860	0.513119	3	0.512924	9.34	9.57	0.17

Chapter 5-Onset of magmatic accretion within a magma-poor rifted margin: A case study from the Platta ocean-continent transition, Eastern Switzerland.

L. Desmurs[1], O. Müntener[1,3], G. Manatschal [2]
[1]Department of Earth Sciences, Federal Institute of Technology, ETH-Zentrum, 8092 Zürich, Switzerland; Tel.: +41 1 6323690; Fax: +41 1 632 10 80; E-mail: desmurs @erdw.ethz.ch [2] CGS-EOST - UMR 7517 CNRS-ULP, 1 rue Blessig, F-67064 Strasbourg, France [3] present address: Institute de géologie, Université de Neuchâtel, Rue Emile Argand 11, 2007 Neuchâtel, Switzerland;

(Submitted to Contributions to Mineralogy and Petrology)

Abstract

Exhumation of subcontinental mantle rocks and its exposure at the sea floor is known from different magma-poor passive continental margins; however, the transition from largely amagmatic passive rifting to sea-floor spreading is still poorly documented.
In this contribution we use MOR-type gabbroic and basaltic rocks to characterize the magmatism associated with the formation of an ancient ocean-continent transition preserved in the Platta nappe, eastern Switzerland. Gabbros form individual small intrusions into exhumed serpentinized subcontinental mantle rocks. Mineral and bulk rock chemistry and simple modeling indicate that each gabbro body records different magmatic processes ranging from predominantly fractional crystallization to solidification without fractionation. Mg numbers and Ni contents of equilibrium olivine calculated from basalts and gabbros indicate that few mafic rocks are primary melts but most represent fractionated compositions ranging from T- to N-MORB. Whereas most mafic rocks may be explained by low to moderate degrees of melting of an N-MORB type mantle, the source of some basalt is enriched in incompatible elements. This compositional variation seems to correlate with the spatial distribution of the mafic rocks within the ocean-continent transition whereby mafic rocks with T-MORB signatures occur close to the continental margin whereas N-MORB signatures are more frequently found oceanwards. As in an opening system time and space are closely linked, the chemical evolution of the mafic rocks along the passive margin suggests continuous thinning of the subcontinental mantle and associated uplift of the underlying asthenosphere during the time between the crustal and the lithospheric break-up of the Liguria-Piedmont ocean.

Introduction

In the Alps, ophiolites derived from the Mesozoic Liguria-Piedmont ocean consist predominantly of a serpentinized peridotite basement covered by deep-sea sediments, magmatic rocks being only subordinate. This stratigraphy, related to the exposure of mantle rocks on the sea floor, has been interpreted as formed either along a slow-spreading ridge (Lagabrielle and Lemoine 1997) or by tectonic exhumation of subcontinental mantle during earlier Jurassic rifting (Lemoine et al. 1987; Piccardo et al. 1990; Froitzheim and Manatschal 1996).

Recently, Dick et al. (2000) questioned that postulated on-land analogues of slow spreading crust can directly be compared to the at least 1500 meters of continuous igneous crust drilled at the Southwest Indian Ridge (ODP Leg 176). In any case, the formation of a slow spreading ridge is necessarily preceded by a period of rifting and at some point there must be a transition from (largely) amagmatic passive rifting to the formation of igneous crust and finally the establishment of a slow spreading system.

Geological studies on land and geophysical studies at sea show that, along so-called non-volcanic margins, an ocean-continent transition zone several tens-of-km wide separates thinned continental crust from oceanic crust (e.g. Manatschal and Nievergelt 1997; Müntener and Hermann 2001; Whitmarsh et al. 2001). This zone consists predominantly of exhumed mantle rocks locally intruded and overlain by MOR-type mafic rocks. It is the purpose of this paper to provide constraints on the igneous accretion within this transition zone.

Based on field and geochemical evidence, it has been demonstrated that in the Alps, the serpentinite basement of the ocean-continent transition represents former subcontinental mantle (e.g. Piccardo et al. 1990, Trommsdorff et al. 1993, Rampone et al. 1995) exhumed during rifting leading to the opening of the Alpine Tethys (e.g. Müntener et al. 2000). This subcontinental mantle was intruded by gabbroic rocks with MORB affinity and locally covered by basaltic volcanics with a similar chemical composition. By analogy with results obtained from the Galicia bank and the Iberian margin (Boillot et al. 1987; Charpentier at al. 1998; Cornen et al. 1999; Schärer et al. 1995, 2000), the gabbros are classically interpreted as pre-dating break-up of the continental crust (syn-rift gabbros) (Rampone et al. 1998) whereas, according to this terminology, the basalts overlying exhumed mantle rocks necessarily belong to the post-rift sequence. However, as they overly tectonically exhumed subcontinental mantle, their extrusion pre-dates the break-up of the continental lithosphere, which corresponds to the emplacement of an oceanic spreading system.

The Platta-Malenco ultramafic and mafic rocks, in eastern Switzerland and northern Italy, are, together with the overlying Austro-alpine Err and Margna nappes, the relicts of a fossil magma-poor rifted margin which can be reconstructed with some confidence (Manatschal and Nievergelt 1997; Müntener and Hermann 2001; Desmurs et al. 2001). In this contribution, we provide new mineralogical and chemical data on mafic rocks from the Platta nappe, which demonstrate that these isolated bodies of MORB-type magmatic rocks record the initiation of magmatic accretion within the ocean-continent transition zone during a transitional stage between the crustal and lithospheric break-up of the continental lithosphere.

Regional geology

The Err and Platta nappes are part of a late Cretaceous west-directed thrust wedge, which was probably associated with subduction along the eastern border of Adria (Froitzheim et al. 1996). In a later stage, this nappe stack was thrust 'en bloc' towards the north over the European units during the Tertiary (Froitzheim et al. 1996; Rubatto et al. 1998). The south-Pennine ophiolites of the Arosa zone, the Platta nappe and the Malenco complex lack a high-pressure metamorphic overprint associated elsewhere with the Tertiary subduction, and show only a general increase of Alpine metamorphism from deep burial diagenesis in the north (Arosa zone) (Trommsdorff 1983) to epidote-amphibolite facies conditions in the south (Malenco complex) (Trommsdorff and Evans 1974; Ferreiro-Mählmann 1995).

Together with the lower Austroalpine Err nappe, the Platta nappe preserves the remnants of a segment of the southeastern margin of the Liguria-Piedmont Ocean (Fig. 5-1). The Err nappe includes the relicts of the distal Adriatic margin and was thrust onto the Platta nappe during late Cretaceous time. It consists of a thinned continental crust, overlain by a number of extensional allochthons, slivers of continental crust and pre-rift sediments which were tectonically emplaced during the late-Middle Jurassic along an oceanward-dipping low-angle detachment system (Froitzheim and Eberli 1990; Froitzheim and Manatschal 1996; Manatschal and Nievergelt 1997). The Platta nappe, originally situated oceanward of the Err nappe, represents the ocean-continent transition s.str. and exposes serpentinized peridotites, minor gabbroic rocks, basaltic volcanics and oceanic sediments. Far-travelled extensional allochthons, derived from the distal continental margin, were emplaced on the exhumed mantle rocks prior to the deposition of the basalts (Manatschal and Nievergelt 1997).

Palinspastic reconstructions (Manatschal and Nievergelt 1997, Desmurs et al. 2001) have shown that the Platta nappe consists of two large sheets of ultramafic rocks, an upper and originally continentalward one and a lower originally oceanward one (Fig. 5-1b, c). The latter is covered by pillow lavas and basaltic flows and was locally intruded by Jurassic gabbros 161±1 Ma ago (Schaltegger et al. Subm), which crystallized at shallow depth within an already serpentinized mantle (Desmurs et al. 2001). The upper serpentinite unit is almost free of magmatic rocks except for a few dolerite dykes, one gabbro sill and a single basaltic flow. All these magmatic rocks (gabbro and basalt) are presumably derived from the same mantle source as demonstrated by their εNd values up to +9 determined on whole rocks and by the εHf up to +15 of the zircons of the gabbros (Schaltegger et al. Subm).

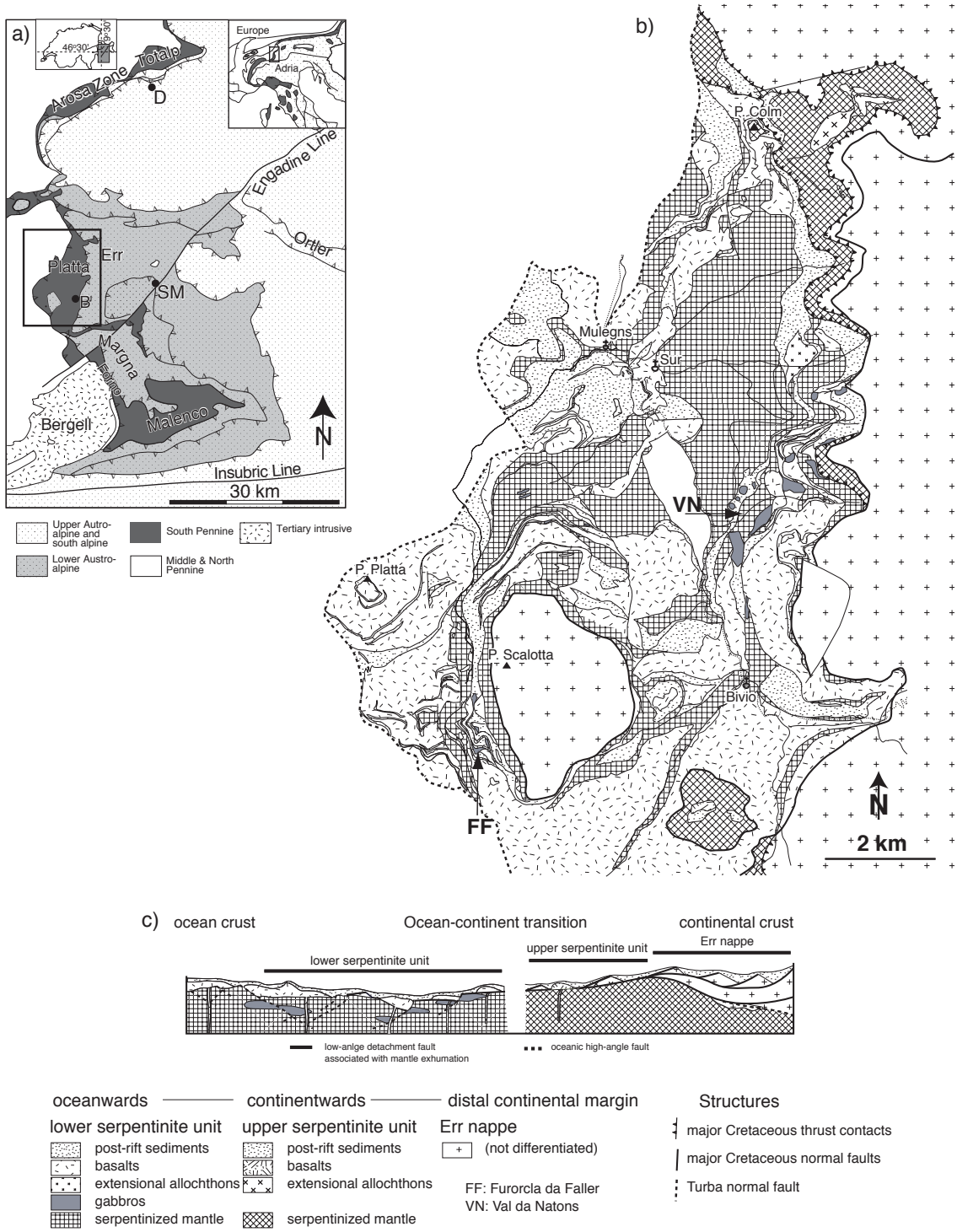

Figure 5-1: a) Simplified tectonic map and location of the study area. B: Bivio; D: Davos; SM: St. Moritz; modified after Froitzheim et al. (1994). b) Tectonic map and c) palinspastic profile of the Platta nappe (after Cornelius (1932), Dietrich (1969) and own mapping).

Gabbros

Field relationships

Within the Platta nappe, gabbros occur in two main areas in the lower serpentinite unit, near Fuorcla da Faller and in Val da Natons (Fig. 5-1b). In the

Fuorcla da Faller area, an individual gabbro body, about one hundred meter across, largely preserved its internal magmatic relationships. This body shows a great diversity in composition from primitive olivine-gabbro to highly differentiated Fe-Ti-P- gabbros and diorite and is characterized by a lack of layering and of systematic vertical changes (Fig. 5-2). The main part of the body (~90%) consists of Mg-gabbro (samples P4, MS13, MS15, MS9) with plagioclase and clinopyroxene as the main constituents. Locally, the gabbros are cut by or grade into high-temperature shear zones showing a drastic decrease in grain size. The Mg-gabbro shows a diffuse contact with a Fe-gabbro (sample MS3, clinopyroxene-hastingsitic hornblende-Fe-Ti oxide-plagioclase, 5% of the outcrop). The Mg-gabbros may also contain small pockets of Fe-gabbros but the opposite relationship is also observed. Both gabbro types are cut by a Fe-Ti-P-gabbro (sample P9, clinopyroxene-pargasitic hornblende-ilmenite-plagioclase-apatite-zircon). Pegmatitic diorite (sample MS10, pargasitic hornblende-plagioclase-clinopyroxene-quartz) occurs as patches or dykes, which form boudins or folds within the Mg-gabbro indicating syn-magmatic deformation. In some of these patches, Fe-Ti-P-gabbro and diorite occur together (Fig 5-2). The gabbro body is locally cut by basaltic dykes with chilled margins indicating that emplacement of the dykes took place after cooling of the gabbro. The primary contact to the host rock, most likely serpentinite, is strongly overprinted by Alpine deformation; however, we assume that the association of sediments, serpentinite and gabbro observed in the field largely represent the primary context.
In Val da Natons, several gabbro outcrops (Fig. 5-1b) consist mainly of Mg-gabbro bodies, some tens of meters across, except for a much larger one (half a km long and fifty meters thick) that shows the same diversity of rock types as at Fuorcla da Faller. One of the small Mg-gabbros (sample NAG3) shows an increase in grain size from the rim to the core of the body; the other one is cut by few, small dykes of diorite (sample NAG9). Both show evidence for localized internal deformation under retrograde metamorphic conditions from amphibolite to greenschist facies. Locally, they are stratigraphically overlain by sedimentary breccias containing gabbro clasts demonstrating their exhumation and exposure at the sea floor (Desmurs et al. 2001).

Petrography

The Mg-gabbros show euhedral plagioclase, sub- to anhedral clinopyroxene and in a few samples interstitial Ti-pargasite. In many places clinopyroxene and plagioclase show graphic intergrowth indicating cotectic crystallization of the two phases. Plagioclase is always altered to a fine-grained mixture of albite, chlorite, epidote, prehnite and pumpellyite. In the Mg-gabbros, Ti-pargasite occurs as interstitial grains between plagioclase and/or clinopyroxene or may form rims around or patches within clinopyroxene grains. Fe-gabbros consist of anhedral to subhedral clinopyroxene and plagioclase with interstitial ilmenite. Ti-rich hornblende occurs mainly as rims around ilmenite or as interstitial grains between Fe-Ti-oxide and clinopyroxene. The Fe-Ti-P-gabbro is made of euhedral plagioclase and apatite, subhedral clinopyroxene, and of interstitial pargasite and ilmenite; euhedral zircon also occurs in few samples. The pegmatitic diorite contains large euhedral plagioclase crystals, large sub- to anhedral magnesian hornblende, quartz, large anhedral zircon and rare and strongly altered clinopyroxene showing a symplectitic texture with Ti-pargasite. Clinopyroxenes with a similar texture and mineralogy occur in the Mg-gabbro at the contact with the diorite suggesting that the clinopyroxenes in the diorite are xenocrysts from the Mg-gabbro.

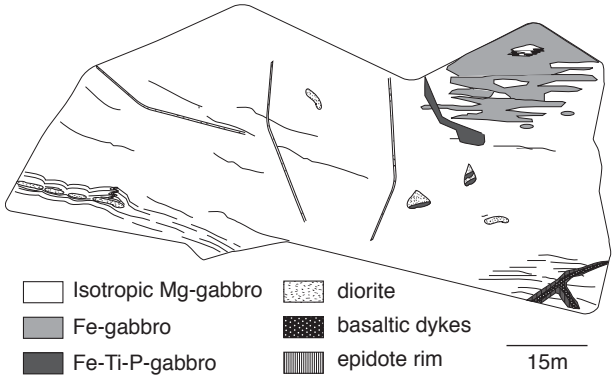

Figure 5-2: Schematic sketch of the magmatic relationships observed in the Fuorcla da Faller gabbro. Mg-gabbros make up the main part of the body. They show large grain-size variations and are cut by discrete high-temperature shear zones. A more differentiated Fe-gabbro crystallized at the edge of the body and is interfingering with the Mg-gabbro. Both rock types are cut by a Fe-Ti-P-gabbro, which was also found in pockets at the center of the body together with diorite. The diorite is also present as dykes throughout the whole body, but never exceeds 20 cm in thickness. Basaltic dykes cut across the gabbros and are characterized by a wide epidote-rich rim and by chilled margins.

Internal deformation is observed in all gabbro bodies mostly as discrete, high-temperature shear zones related to the magmatic emplacement. However, in Val da Natons, retrograde mylonitic shear zones are also observed. The highest temperature deformation is recorded by a syn-magmatic foliation defined by small clinopyroxene, pargasite and apatite granoblasts showing typical triple-junction grain boundaries and no crystal-plastic deformation. Pargasite and ilmenite occur also as undeformed interstitial grains between the neoblasts, which has been interpreted as evidence for a late-magmatic stage of deformation (Desmurs et al. 2001).
In retrograde shear zones, the mylonitic foliation is defined by small neoblasts of actinolite and albite, or by albite, elongated chlorite and biotite that crystallized between clasts of stretched clinopyroxene. The recrystallization of albite and actinolite and the deformation of chlorite and biotite suggest that these shear zones were active under lower amphibolite- to greenschist-facies conditions. These shear zones were later affected by cataclastic deformation and intense veining during which epidote, chlorite and albite crystallized.

Mineral chemistry

Clinopyroxene (Table 5-1): The augitic clinopyroxenes of the gabbros of the Platta nappe are characterized by low Al_2O_3 (<4.5 weight %) and Na_2O (<0.71 weight %) contents which are similar for the different gabbro types and are also similar to those of gabbros from the Ligurian Appennines (Tribuzio et al. 1999). However, the Mg# of these minerals continuously decreases from the Mg-gabbro (0.74-0.90) to the Fe-gabbro (0.68-0.71) and the highly differentiated Fe-Ti-P-gabbro (0.63-0.66). This decrease in Mg# correlates with an increase of MnO and a decrease of TiO_2, Al_2O_3 and Cr_2O_3 (Fig. 5-3). The composition of the clinopyroxene is generally homogeneous within single samples. In two samples, however, clinopyroxene rims and/or neoblasts are enriched in MnO and in TiO_2 and show lower Mg# and Cr_2O_3 than the composition of the core (NAG3, SC5) indicating post-cumulus crystallization (e.g. Tribuzio et al. 1999).

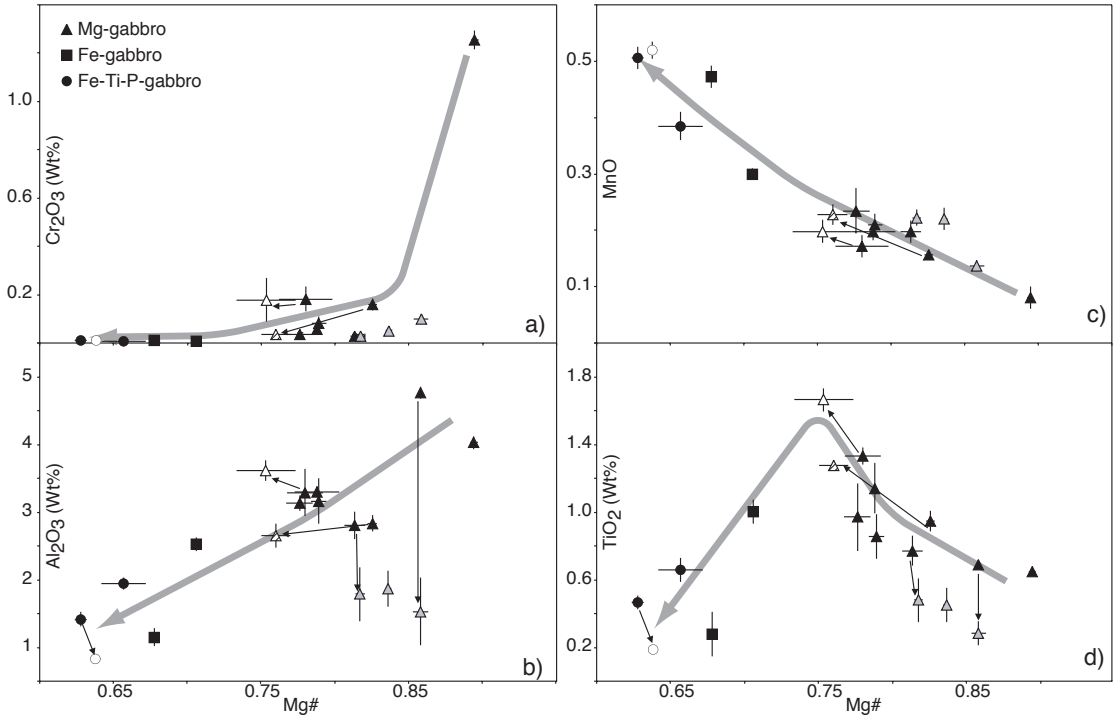

Figure 5-3: Chemical composition of the clinopyroxene of the different gabbro types. Gray symbols represent clinopyroxene that record post-cumulus re-equilibration with amphiboles, dashed symbol represents clinopyroxene rims and white symbols represent neoblastic grains. Black arrows indicate the shift in composition within a single sample; gray arrows indicate the differentiation trend. a), Cr_2O_3 vs. Mg#; b). Al_2O_3 vs. Mg#. The compatible elements continuously decrease together with Mg# from Mg- to Fe-Ti-P gabbro. The decrease of Mg# and Cr_2O_3 from core to rim and from porphyroblast to neoblast indicates the presence of differentiated interstitial melts. Sub-solidus re-equilibration of the clinopyroxene with high-temperature amphiboles leads to a decrease of Al_2O_3 but does not change the Mg# of the clinopyroxene. c). MnO vs. Mg#; MnO continuously increases with decreasing Mg# from Mg- to Fe-Ti-P-gabbro. d). TiO_2 vs. Mg#; TiO_2 first increases and then decreases with decreasing Mg#. This is due to the lower temperature of crystallization of the Fe- and Fe-Ti-P-gabbros. Late reequilibration of the clinopyroxene with high-temperature amphiboles leads to a decrease of TiO_2 of the clinopyroxene (Mg#= molecular $Mg/(Mg+Fe_{tot})$).

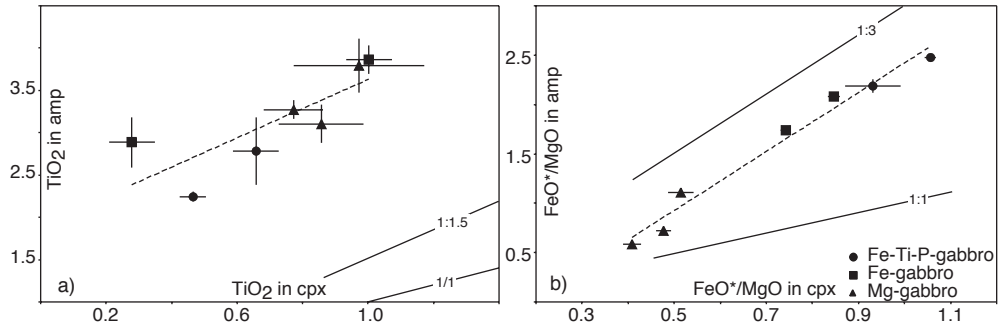

Figure 5-4: FeO*/MgO and TiO_2 partitioning between clinopyroxene and amphibole. Contours of K_d^{Ti} (amp-cpx) indicate equilibration between clinopyroxene and amphibole.

Amphibole (Table 5-2)*:* Crystallization of interstitial Ti-pargasite is observed in all gabbro types except for the Mg-rich sample P4, but is more frequent in the differentiated gabbros (Fe-, Fe-Ti-P-gabbro and diorite). These high temperature amphiboles are Ti-rich calcic amphiboles characterized by high Al_2O_3 (up to 13 weight %) contents and a low Na^{M4} content (0.13-0.29 p.f.u.). They show a decrease in Mg# from Mg- to Fe-Ti-P-gabbros that correlate with a decrease in TiO_2 and CaO

and with an increase in MnO. The FeO*/MgO ratio and the TiO_2 content of pargasite is positively correlated with that of clinopyroxene but are higher than that of the coexisting clinopyroxene. FeO*/MgO and Ti partitioning among amphibole and clinopyroxene indicates conditions close to equilibrium (Fig. 5-4a, b).

Table 5-1: *Chemical composition of the clinopyroxenes of the Platta gabbros.*

	Mg-gabbro													
Sample	P4		MS9		SC5				MS8		NAG9		MS13	
	core		core		core		neoblast		core		core*		core	
SiO_2	51.12	0.44	51.33	0.86	50.31	0.89	49.45	0.96	51.03	0.77	53.50	0.78	51.16	0.94
TiO_2	0.65	0.05	1.14	0.31	1.33	0.28	1.66	0.15	0.97	0.39	0.28	0.15	0.86	0.26
Cr_2O_3	1.26	0.09	0.06	0.02	0.18	0.08	0.18	0.19	0.03	0.02	0.10	0.04	0.08	0.06
Al_2O_3	4.03	0.18	3.30	0.16	3.29	0.58	3.62	0.79	3.13	0.23	1.53	1.00	3.16	0.68
Fe_2O_3	1.85	0.39	2.24	1.33	2.36	0.55	2.58	0.30	3.02	1.09	1.03	0.52	1.48	0.84
FeO	1.79	0.39	5.11	0.90	5.39	0.70	6.09	1.31	5.16	0.48	3.78	0.45	5.97	1.07
MnO	0.08	0.04	0.20	0.03	0.17	0.05	0.20	0.05	0.23	0.09	0.14	0.02	0.21	0.05
MgO	16.41	0.25	14.84	0.60	14.95	0.63	14.41	0.78	15.30	0.60	15.98	0.47	15.31	0.50
CaO	21.99	0.41	21.46	0.48	21.65	0.50	21.47	0.18	20.85	1.06	23.41	1.69	20.60	1.52
Na_2O	0.69	0.09	0.56	0.07	0.54	0.10	0.60	0.11	0.54	0.09	0.48	0.20	0.56	0.16
K_2O	0.01	0.01	0.03	0.05	0.00	0.01	0.01	0.01	0.01	0.01	0.03	0.01	0.01	0.01
Total	99.89	0.59	100.26	0.80	100.20	0.61	100.30	0.92	100.28	0.62	100.27	0.54	99.41	0.65
Si	1.876	0.007	1.893	0.045	1.874	0.022	1.851	0.019	1.882	0.018	1.961	0.024	1.906	0.030
Ti	0.018	0.001	0.032	0.009	0.037	0.008	0.047	0.005	0.027	0.011	0.008	0.004	0.024	0.007
Cr	0.036	0.003	0.002	0.001	0.005	0.002	0.005	0.006	0.001	0.001	0.003	0.001	0.002	0.002
Al	0.174	0.008	0.144	0.007	0.144	0.025	0.159	0.033	0.136	0.011	0.066	0.043	0.139	0.030
Fe^{3+}	0.051	0.011	0.062	0.037	0.066	0.016	0.073	0.009	0.084	0.031	0.028	0.014	0.042	0.024
Fe^{2+}	0.055	0.012	0.158	0.029	0.168	0.023	0.191	0.044	0.159	0.015	0.116	0.014	0.186	0.033
Mn	0.002	0.001	0.006	0.001	0.005	0.002	0.006	0.002	0.007	0.003	0.004	0.000	0.007	0.001
Mg	0.897	0.013	0.815	0.027	0.830	0.030	0.804	0.032	0.841	0.033	0.873	0.025	0.850	0.027
Ca	0.865	0.015	0.848	0.014	0.864	0.018	0.861	0.015	0.824	0.040	0.919	0.065	0.822	0.060
Na	0.049	0.007	0.040	0.005	0.039	0.007	0.043	0.008	0.038	0.006	0.034	0.014	0.040	0.011
K	0.000	0.000	0.001	0.002	0.000	0.000	0.000	0.000	0.001	0.000	0.001	0.001	0.000	0.001
Mg#	0.895	0.005	0.788	0.003	0.780	0.024	0.753	0.040	0.776	0.018	0.858	0.011	0.789	0.011

For each sample, the average composition is shown in the first column and the second one indicates the standard deviation (2σ). * indicates analyses of clinopyroxenes that suffered sub-solidus reequilibration with high-temperature amphiboles. Ions calculated on the basis of 6 oxygens. $Mg\#=Mg/(Fe^{3+}+Fe^{2+}+Mg)$

Table 5-1 *(continued)*

	Mg-gabbro										Fe-gabbro			
Sample	NAG3				MSG2-2				MS10		MS3		NAG5	
	core		rim		core		core*		core*		core		core	
SiO_2	50.33	0.35	49.74	0.56	51.25	0.71	52.51	1.21	52.76	0.66	51.18	0.33	52.02	0.50
TiO_2	0.94	0.11	1.27	0.07	0.77	0.18	0.48	0.27	0.45	0.19	1.00	0.15	0.28	0.14
Cr_2O_3	0.17	0.05	0.03	0.02	0.03	0.02	0.03	0.02	0.05	0.01	0.01	0.02	0.01	0.01
Al_2O_3	2.79	0.25	2.65	0.36	2.81	0.42	1.79	0.80	1.87	0.54	2.52	0.19	1.15	0.27
Fe_2O_3	2.45	0.56	2.35	0.56	2.68	0.55	1.90	0.73	1.70	0.30	1.99	0.21	1.36	0.42
FeO	3.60	0.48	5.79	1.03	3.90	0.63	4.76	0.98	4.14	0.29	8.40	0.36	9.75	0.43
MnO	0.16	0.02	0.23	0.04	0.20	0.04	0.22	0.03	0.22	0.04	0.30	0.02	0.47	0.04
MgO	15.49	0.17	14.07	0.47	15.45	0.55	16.25	0.96	16.25	0.18	13.74	0.32	12.97	0.27
CaO	22.32	0.24	21.84	0.19	21.88	0.69	21.20	2.16	22.02	0.88	20.66	0.45	20.92	0.57
Na_2O	0.46	0.05	0.60	0.02	0.75	0.12	0.55	0.26	0.59	0.11	0.71	0.12	0.62	0.10
K_2O	0.01	0.01	0.01	0.01	0.01	0.01	0.00	0.01	0.01	0.01	0.02	0.01	0.01	0.02
Total	98.73	0.48	98.61	0.42	99.73	0.68	99.70	1.02	100.04	0.69	100.53	0.38	99.59	0.73
Si	1.891	0.006	1.890	0.015	1.906	0.015	1.945	0.036	1.944	0.014	1.914	0.008	1.970	0.010
Ti	0.026	0.003	0.036	0.002	0.022	0.005	0.013	0.007	0.012	0.005	0.028	0.004	0.008	0.004
Cr	0.005	0.002	0.001	0.001	0.001	0.001	0.001	0.001	0.001	0.000	0.000	0.000	0.000	0.000
Al	0.124	0.011	0.119	0.016	0.123	0.019	0.078	0.035	0.081	0.024	0.111	0.009	0.051	0.012
Fe^{3+}	0.069	0.016	0.067	0.016	0.075	0.016	0.053	0.020	0.047	0.009	0.056	0.006	0.039	0.012
Fe^{2+}	0.113	0.015	0.184	0.033	0.121	0.020	0.147	0.030	0.128	0.009	0.263	0.012	0.309	0.013
Mn	0.005	0.001	0.007	0.001	0.006	0.001	0.007	0.001	0.007	0.001	0.010	0.001	0.015	0.001
Mg	0.868	0.011	0.797	0.026	0.856	0.026	0.897	0.047	0.892	0.009	0.766	0.019	0.732	0.012
Ca	0.899	0.010	0.889	0.012	0.872	0.028	0.841	0.088	0.869	0.032	0.828	0.016	0.849	0.023
Na	0.033	0.003	0.044	0.002	0.054	0.009	0.040	0.018	0.042	0.008	0.051	0.009	0.045	0.008
K	0.000	0.000	0.001	0.000	0.001	0.001	0.000	0.000	0.000	0.000	0.001	0.001	0.001	0.001
Mg#	0.826	0.007	0.760	0.021	0.813	0.014	0.817	0.006	0.836	0.004	0.706	0.007	0.678	0.007

Table 5-1 *(continued)*

Sample	Fe-Ti-P-gabbro					
	P9		NAG7			
	core		porphyroclast		neoblast	
SiO_2	51.20	0.53	51.39	0.55	52.18	0.31
TiO_2	0.66	0.14	0.47	0.08	0.19	0.05
Cr_2O_3	0.01	0.01	0.01	0.01	0.01	0.01
Al_2O_3	1.94	0.18	1.42	0.22	0.83	0.13
Fe_2O_3	3.30	1.41	0.99	0.79	0.22	0.30
FeO	8.85	0.51	11.52	0.64	11.77	0.26
MnO	0.38	0.05	0.51	0.05	0.52	0.03
MgO	12.69	0.63	11.75	0.21	11.82	0.22
CaO	19.92	0.94	20.49	0.36	21.01	0.25
Na_2O	0.94	0.54	0.64	0.13	0.48	0.05
K_2O	0.02	0.01	0.03	0.04	0.00	0.01
Total	99.92	0.59	99.23	0.84	99.03	0.66
Si	1.926	0.020	1.965	0.011	1.992	0.007
Ti	0.019	0.004	0.013	0.002	0.005	0.001
Cr	0.000	0.000	0.000	0.000	0.000	0.000
Al	0.086	0.008	0.064	0.010	0.037	0.006
Fe^{3+}	0.093	0.040	0.029	0.023	0.006	0.008
Fe^{2+}	0.279	0.017	0.368	0.020	0.376	0.009
Mn	0.012	0.002	0.016	0.002	0.017	0.001
Mg	0.712	0.036	0.670	0.009	0.673	0.010
Ca	0.803	0.039	0.839	0.013	0.859	0.009
Na	0.069	0.039	0.048	0.010	0.035	0.003
K	0.001	0.000	0.001	0.002	0.000	0.000
Mg#	0.657	0.030	0.628	0.008	0.638	0.006

Table 5-2: *Chemical composition of the high-temperature amphiboles of the Platta gabbro*

Sample	Mg-gabbro								Fe-gabbro					
	MS8		MS13		MSG2-1				NAG5		MS3		MSG2-3	
Texture	interstitial		interstitial		interstitial		exsolution		interstitial		interstitial		interstitial	
SiO_2	43.75	1.73	43.22	1.38	42.58	0.29	44.03	1.75	42.87	0.72	42.59	2.35	46.44	2.01
TiO_2	3.79	0.74	3.10	0.46	3.26	0.23	2.52	0.33	2.87	0.63	3.86	0.92	2.13	0.65
Cr_2O_3	0.06	0.01	0.07	0.03	0.04	0.02	0.05	0.04	0.02	0.02	0.02	0.01	0.03	0.02
Al_2O_3	10.98	1.45	10.52	1.02	10.72	0.24	9.79	1.66	8.96	0.99	10.67	1.53	6.48	1.51
Fe_2O_3	1.60	0.73	5.78	1.59	4.20	1.15	3.83	4.92	3.88	2.45	2.44	0.67	1.89	1.13
FeO	8.72	0.33	5.62	0.95	4.93	0.45	6.73	4.50	12.67	2.28	11.63	0.93	13.05	0.27
MnO	0.12	0.01	0.12	0.02	0.15	0.02	0.19	0.03	0.34	0.04	0.19	0.10	0.49	0.01
MgO	14.90	0.42	14.76	0.51	15.92	0.19	15.11	1.75	11.57	0.56	12.69	1.15	13.31	1.26
CaO	11.51	0.42	11.35	0.23	11.49	0.17	11.61	0.76	10.02	0.31	10.98	0.42	10.46	0.41
Na_2O	2.88	0.41	2.44	0.35	3.13	0.07	2.66	0.32	2.94	0.10	2.81	0.55	2.59	0.53
K_2O	0.16	0.03	0.19	0.04	0.11	0.05	0.11	0.10	0.21	0.03	0.22	0.06	0.26	0.10
H_2O	2.08	0.00	2.06	0.03	2.05	0.01	2.05	0.03	1.98	0.02	2.03	0.02	2.02	0.03
Total	100.5	0.43	99.25	1.00	98.62	0.66	98.70	0.74	98.33	0.89	100.1	0.75	99.16	1.08
Si	6.317	0.254	6.300	0.153	6.228	0.016	6.450	0.158	6.481	0.126	6.277	0.292	6.901	0.249
Ti	0.411	0.080	0.340	0.051	0.359	0.026	0.279	0.038	0.327	0.073	0.428	0.103	0.238	0.071
Cr	0.007	0.001	0.008	0.003	0.005	0.002	0.005	0.005	0.002	0.003	0.002	0.001	0.003	0.003
Al	1.868	0.245	1.809	0.187	1.849	0.050	1.694	0.317	1.595	0.166	1.853	0.276	1.136	0.271
Fe^{3+}	0.174	0.079	0.634	0.174	0.462	0.124	0.420	0.537	0.440	0.276	0.271	0.075	0.212	0.128
Fe^{2+}	1.053	0.039	0.685	0.117	0.603	0.057	0.830	0.563	1.603	0.296	1.434	0.117	1.622	0.025
Mn	0.014	0.001	0.015	0.002	0.018	0.002	0.024	0.004	0.043	0.004	0.024	0.013	0.062	0.001
Mg	3.206	0.092	3.206	0.089	3.472	0.052	3.296	0.330	2.606	0.111	2.789	0.229	2.947	0.264
Ca	1.781	0.067	1.772	0.028	1.801	0.036	1.823	0.128	1.623	0.057	1.734	0.052	1.665	0.056
Na	0.807	0.115	0.690	0.102	0.887	0.018	0.756	0.100	0.861	0.028	0.803	0.160	0.746	0.156
K	0.029	0.004	0.036	0.007	0.020	0.010	0.021	0.020	0.040	0.007	0.042	0.012	0.048	0.020
OH	2.000	0.000	2.000	0.000	2.000	0.000	2.000	0.000	2.000	0.000	2.000	0.000	2.000	0.000
Mg#	0.724	0.012	0.709	0.017	0.765	0.021	0.724	0.046	0.560	0.015	0.621	0.034	0.616	0.039

Presentation as in table 5-1. Ions calculated on the basis of 23 oxygens and $\sum$ (cat)-Ca-Na-K=13. Mg#=Mg/(Fe^{3+}+Fe^{2+})

Table 5-2(continued)

	Fe-gabbro		Fe-Ti-P-gabbro						diorite					
Sample	MSG2-3		P9		NAG7				MS10		MSG-2		MSG2-3	
Texture	exsolution		interstitial		neoblastic		interstitial		euhedral		euhedral		euhedral	
SiO_2	45.45	0.97	43.14	1.24	42.96	0.36	43.03	0.08	46.20	0.44	43.03	0.08	45.60	1.91
TiO_2	2.25	0.09	2.77	0.84	2.78	0.15	2.24	0.12	2.84	0.35	2.24	0.12	2.66	0.58
Cr_2O_3	0.03	0.01	0.01	0.02	0.01	0.01	0.00	0.00	0.01	0.01	0.00	0.00	0.02	0.02
Al_2O_3	7.41	0.33	10.94	1.52	9.16	0.63	8.92	0.10	7.18	0.20	8.92	0.10	6.96	1.28
Fe_2O_3	2.02	0.53	1.40	0.67	3.74	1.07	3.87	0.51	1.01	0.38	3.87	0.51	1.51	0.86
FeO	11.31	1.30	13.45	1.33	12.91	1.17	13.79	0.23	11.66	0.20	13.79	0.23	14.45	1.34
MnO	0.38	0.02	0.21	0.04	0.31	0.02	0.32	0.03	0.42	0.04	0.32	0.03	0.52	0.08
MgO	14.02	0.64	11.68	0.48	10.94	0.42	10.59	0.09	14.58	0.19	10.59	0.09	12.20	0.93
CaO	11.12	0.51	10.79	0.33	10.53	0.12	10.92	0.05	10.94	0.19	10.92	0.05	10.10	0.65
Na_2O	2.73	0.21	3.26	0.19	2.95	0.14	2.74	0.02	2.42	0.12	2.74	0.02	2.71	0.50
K_2O	0.12	0.03	0.36	0.10	0.30	0.04	0.33	0.06	0.24	0.08	0.33	0.06	0.31	0.12
H_2O	2.02	0.03	2.05	0.02	1.98	0.03	1.98	0.00	2.04	0.01	1.98	0.00	2.00	0.02
Total	98.93	0.86	100.0	0.45	98.57	1.12	98.75	0.10	99.54	0.63	98.75	0.10	99.05	0.59
Si	6.741	0.061	6.394	0.169	6.492	0.079	6.522	0.000	6.785	0.048	6.522	0.000	6.827	0.232
Ti	0.251	0.010	0.309	0.093	0.316	0.019	0.255	0.014	0.314	0.038	0.255	0.014	0.300	0.066
Cr	0.003	0.001	0.002	0.002	0.001	0.001	0.000	0.000	0.001	0.001	0.000	0.000	0.002	0.002
Al	1.295	0.062	1.912	0.268	1.630	0.096	1.593	0.015	1.246	0.035	1.593	0.015	1.229	0.231
Fe^{3+}	0.225	0.057	0.156	0.074	0.424	0.117	0.441	0.057	0.111	0.040	0.441	0.057	0.171	0.097
Fe^{2+}	1.405	0.182	1.714	0.153	1.633	0.163	1.748	0.033	1.433	0.024	1.748	0.033	1.811	0.185
Mn	0.048	0.002	0.026	0.004	0.039	0.002	0.041	0.004	0.053	0.005	0.041	0.004	0.066	0.011
Mg	3.099	0.097	2.579	0.106	2.463	0.072	2.392	0.025	3.191	0.045	2.392	0.025	2.722	0.185
Ca	1.766	0.072	1.713	0.055	1.705	0.021	1.772	0.011	1.722	0.034	1.772	0.011	1.620	0.085
Na	0.788	0.072	0.938	0.059	0.863	0.034	0.804	0.009	0.691	0.039	0.804	0.009	0.789	0.150
K	0.023	0.007	0.068	0.019	0.058	0.008	0.063	0.012	0.044	0.014	0.063	0.012	0.058	0.023
OH	2.000	0.000	2.000	0.000	2.000	0.000	2.000	0.000	2.000	0.000	2.000	0.000	2.000	0.000
Mg#	0.656	0.026	0.580	0.026	0.545	0.014	0.522	0.006	0.673	0.008	0.522	0.006	0.579	0.037

Whole rock composition

The compositions of the different gabbro types are given in Table 5-3. The evolution from Mg- to Fe- and highly differentiated Fe-Ti-P-gabbro and diorite is well reflected in the change of the bulk rock Mg# (Fig. 5-5). SiO_2 is roughly constant for the Mg-gabbro but decreases dramatically in the Fe- and Fe-Ti-P-gabbros and slightly increases in the diorite. The pervasive low-temperature alteration and the systematic breakdown of plagioclase in all samples make it difficult to use major elements and especially the alkalies to decipher the magmatic evolution of the gabbros. Therefore, the differentiation of the gabbros will be discussed mainly on the base of their trace element concentrations. Compatible elements as Ni and Cr continuously decrease with decreasing Mg# whereas incompatible elements such as Ti, P, Zr, Th, and U increase. Two samples (NAG9, a Mg-gabbro and MS3, a Fe-gabbro) are out of the general trend. NAG9 is strongly enriched in U and Th and MS3 is enriched in Ti. These features suggest open-system post-cumulus crystallization of differentiated liquids within both samples.

The highly differentiated Fe-Ti-P-gabbros and the diorite display low Mg# and show complementary trace element compositions. The Fe-Ti-P gabbros show higher concentrations in Ti, P, V, and Mn that are mainly incorporated in ilmenite and apatite. SiO_2, Al_2O_3, Zr, U, and Th are preferentially concentrated within the diorite and are incorporated in plagioclase and zircon, respectively.

Gabbros from Fuorcla da Faller and Val da Natons display strongly different REE patterns (Fig. 5-6). The gabbros from Fuorcla da Faller show parallel REE patterns with a strong increase of REE concentrations with decreasing Mg#. The Mg-gabbros display a positive Eu anomaly which decreases with Mg# and becomes negative for the highly differentiated diorite and Fe-Ti-P-gabbros (Fig. 5-6a).

Table 5-3: *Major and trace element composition of the Platta gabbros*

	Mg-gabbro							Fe-gabbro		Fe-Ti-P-gabbro		diorite	
Sample	P6	NAG3	NAG9	P4	MS15	MS9	MS13	NAG5	MS3	NAG7	P9	MS10	P7
SiO_2	49.55	51.87	52.75	46.95	48.59	49.79	49.92	43.30	44.13	39.76	34.50	52.23	55.12
Al_2O_3	13.97	17.04	13.96	23.19	16.75	16.28	15.77	12.81	10.55	12.38	9.98	17.56	18.82
Fe_2O_3	7.68	6.93	4.18	2.61	5.70	6.21	5.48	15.47	11.47	17.18	22.44	6.33	4.77
MnO	0.13	0.14	0.07	0.05	0.10	0.10	0.10	0.19	0.20	0.29	0.32	0.07	0.07
MgO	9.51	5.17	9.55	7.42	8.34	8.43	7.96	5.97	13.58	6.54	8.29	3.03	3.28
CaO	11.78	7.96	10.17	8.59	12.28	10.91	13.36	10.10	9.26	11.95	10.20	11.71	9.72
Na_2O	3.43	5.51	4.74	2.91	3.24	3.81	3.40	3.26	2.25	2.44	1.97	5.57	5.99
K_2O	0.15	0.91	0.29	2.60	0.69	0.46	0.29	0.13	0.00	0.00	0.00	0.00	0.11
TiO_2	0.71	1.49	0.23	0.11	0.47	0.60	0.37	6.40	3.88	3.86	5.27	1.01	0.38
P_2O_5	0.16	0.32	0.09	0.08	0.09	0.09	0.08	0.14	0.12	1.90	2.58	0.28	0.10
L.O.I	2.75	2.51	3.82	5.38	3.61	3.14	3.08	2.22	4.39	3.20	3.45	2.09	1.50
Total	99.82	99.85	99.85	99.89	99.86	99.82	99.81	99.99	99.83	99.51	99.04	99.90	99.86
Mg#	0.71	0.60	0.82	0.85	0.74	0.73	0.74	0.43	0.70	0.43	0.42	0.49	0.58
Trace element (ppm)													
V	265	202	87.6	38.5	198	179	169	869	532	290	398	77.5	117
Cr	163	1456	365	1031	50.83	84.5	135	44.8	79.7	24.4	7.21	0.00	132
Ni	138	40.5	216	352	81.7	101	83.5	76.6	87.6	23.62	39.2	15.3	42.0
Co	54.5	24	29.8	25.1	35.0	33.7	33.3	53.1	39.6	16.98	48.2	13.2	17.9
Cu	106	81.4	47.6	21.7	47.7	27.2	46.0	70.6	38.5	30.25	31.1	22	8.30
Zn	71.6	58.8	20.7	15.4	30.1	38.5	25.5	111	76.6	156	125	32.2	34.1
Zr	73.3	145	26.6	3.66	32.5	86.9	11.7	72.6	59.9	91.06	70.1	621	238
Y	32.3	28.7	13.9	2.33	14.1	18.6	9.27	17.6	19.3	115	124	120	81.2
Hf	1.89	2.98	1.64	0.12	0.85	1.92	0.44	1.79	1.50	2.44	1.74	14.2	7.39
Th	0.05	0.636	0.604	0.015	0.078	0.033	0.102	0.027	0.018	0.112	0.089	1.010	1.570
U	0.022	0.227	0.264	0.005	0.034	0.016	0.016	0.035	0.012	0.071	0.058	0.457	0.893
Ba	3.33	249	25.5	191	38.8	7.01	15.8	41.8	5.11	9.88	3.56	8.29	3.38
Rb	2.27	23.17	5.13	45.21	11.04	4.51	5.34	5.39	-	-	-	-	1.56
Sr	92.8	272	526	82.0	844	326	363	1271	218	794	116	829	780
Nb	1.11	8.05	7.45	-.	0.74	0.75	0.14	2.55	1.86	4.31	4.40	10.1	14.47
Ta	0.08	0.60	0.86	-	0.05	0.05	0.01	0.23	0.17	0.40	0.41	0.95	1.55
REE (ppm)													
La	3.17	8.56	1.72	0.36	1.01	1.45	0.58	0.94	1.04	19.23	18.65	17.95	22.95
Ce	10.81	22.06	5.31	1.05	3.33	5.01	1.91	3.40	3.71	66.84	68.00	55.73	58.86
Pr	1.88	3.21	0.71	0.18	0.62	0.90	0.37	0.68	0.82	11.31	12.42	9.33	6.92
Nd	9.93	14.71	3.46	0.80	3.71	5.37	2.22	4.07	4.64	65.26	72.04	47.59	28.76
Sm	3.50	4.07	1.02	0.26	1.31	1.79	1.02	1.91	2.11	20.72	21.96	14.86	7.26
Eu	1.44	1.46	0.45	0.39	0.83	0.94	0.64	0.83	1.10	5.65	5.88	4.81	1.95
Gd	4.92	4.70	1.39	0.31	2.02	2.52	1.42	2.68	2.86	24.43	26.67	17.94	7.55
Tb	0.80	0.80	0.30	0.06	0.33	0.39	0.24	0.42	0.47	3.57	3.77	2.96	1.41
Dy	5.07	4.73	1.97	0.41	1.99	2.53	1.52	2.74	3.07	19.64	21.26	19.25	9.77
Ho	1.06	0.99	0.43	0.08	0.46	0.59	0.35	0.58	0.64	4.15	4.18	4.61	2.31
Er	2.82	2.84	1.37	0.23	1.41	1.70	0.91	1.61	1.73	10.47	10.44	13.04	7.08
Tm	0.44	0.43	0.27	0.04	0.18	0.24	0.13	0.25	0.25	1.39	1.32	1.85	1.32
Yb	2.76	3.01	2.18	0.22	1.32	1.79	0.83	1.66	1.79	7.92	7.71	13.25	9.95
Lu	0.45	0.41	0.37	0.03	0.21	0.27	0.13	0.24	0.26	1.17	1.14	1.98	1.53

Major element by emission-ICP. Trace elements and REE by ICP-MS. U and Th measured by ICP-MS after chromatographic separation.

The gabbros from Val da Natons display more variable and complicated REE patterns (Fig. 5-6b). Two Mg-gabbros (P6 and NAG3) display rather flat patterns with no Eu anomaly and represent liquid compositions. Another Mg-gabbro (NAG9) shows a fairly high REE concentration compared to its Mg#. It is particularly enriched in HREE and shows a small positive Eu anomaly. The enrichment in HREE, U, Th and Hf suggests a possible late reaction with and/or infiltration by dioritic liquids. Despite the evidence for late intrusion and reaction with dioritic melts, the sample NAG9 contains primitive clinopyroxene cores with Mg# of 0.86. Only the diorite and the Fe-Ti-P-gabbros show REE concentrations and patterns similar to the Fuorcla da Faller samples. At both localities, the diorite and the Fe-Ti-P-gabbro show complementary REE concentrations. Diorites are enriched in HREE and depleted in MREE and LREE relative to the Fe-Ti-gabbros.

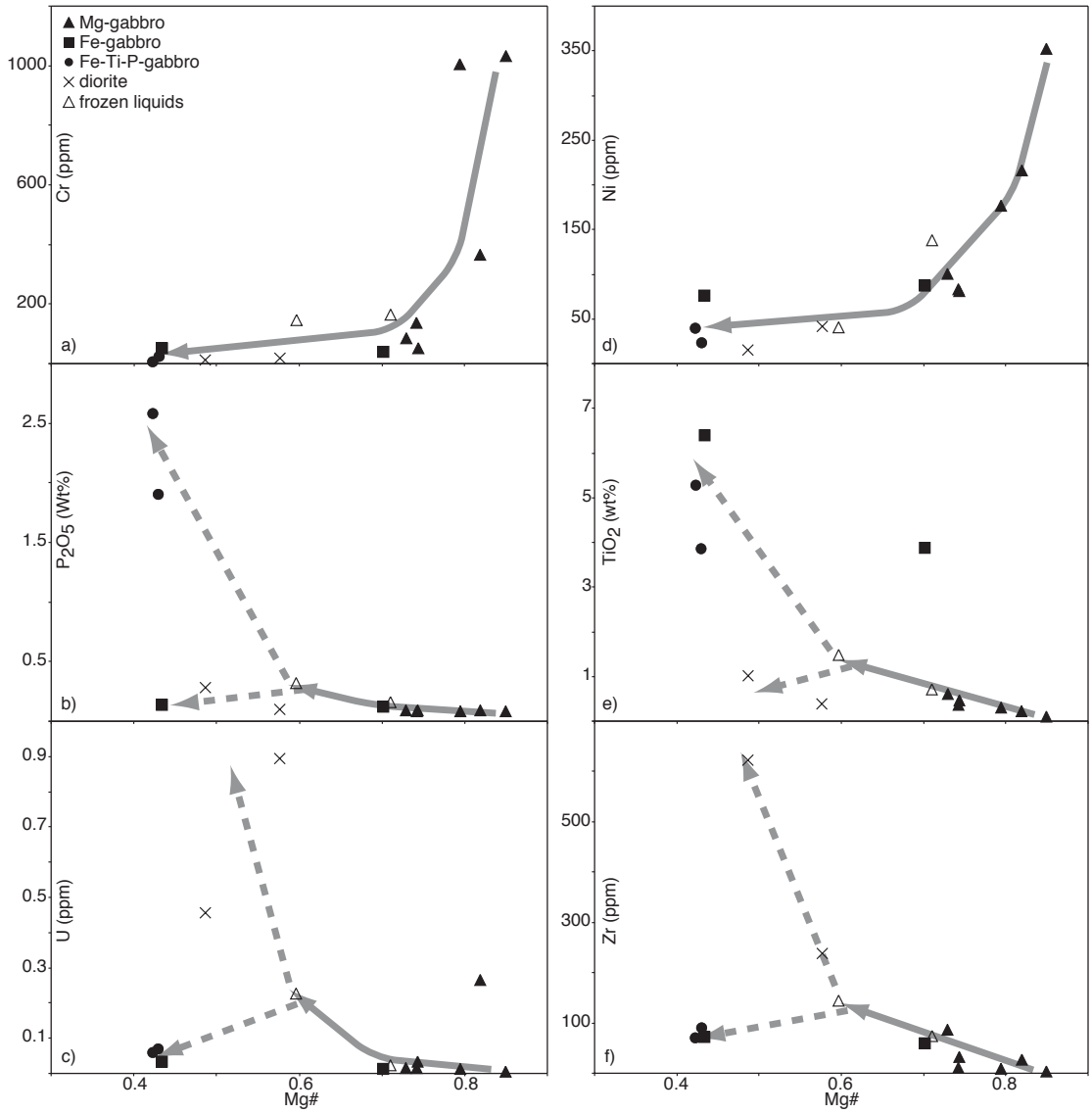

Figure 5-5: Variation diagrams for bulk major and trace elements in the Platta gabbros. Arrows indicate the differentiation trend. a). Cr vs. Mg#; b). P_2O_5 vs. Mg#; c). U vs. Mg#; d). Ni vs..Mg#; e). TiO_2 vs. Mg# and f). Zr vs. Mg#. The compatible elements such as Ni and Cr continuously decrease with decreasing Mg# whereas the incompatible elements increase during differentiation. Note the "split" of the differentiation trend for P_2O_5, TiO_2, U and Zr between the Fe-T-P-gabbro and the diorite (see text for discussion). The black symbols represent 'cumulates', the open symbol represents liquid compositions (see text).

Basalts and dolerite

Field relationships

Basaltic rocks cover a large area in the Platta nappe (Fig. 5-1b); they occur as massive basaltic flows, pillow lavas, pillow breccias, hyaloclastites and individual dolerite dykes cutting across serpentinized peridotites and locally gabbroic rocks and showing chilled margins against the country rocks (Dietrich 1969; Desmurs et al. 2001). Most of the basalts occur in the lower serpentinite unit, but they are limited to one basaltic flow and a few dolerite dykes within the upper serpentinite unit. They seem to be the youngest magmatic rocks emplaced in the Platta nappe as they overlie serpentinites and gabbro breccias. However, the relative timing of emplacement of basalt and

gabbros can not be unambiguously deciphered from field relationships alone (Desmurs et al. 2001).

Petrography

The massive basaltic flows and the dolerites show an intersertal to intergranular texture with interstitial clinopyroxene and round patches of chlorite that may represent former olivine. Low-grade alteration is widespread in all samples; olivine and plagioclase are completely altered. In a few samples, interstitial brown hornblende and oxide occur as well as few acicular grains of apatite. The pillow-basalts can be coarsely plagioclase phyric or aphyric. The aphyric pillow lavas are variolitic and exhibit the classical variation from intersertal to divergent and arborescent texture from core to rim (Dietrich 1969). The phyric pillow basalts contain albite phenocrysts (pseudomorphs after primary plagioclase) within a recrystallized groundmass of fine-grained albite, chlorite, pumpellyite, epidote, actinolite and calcite (Dietrich 1969).

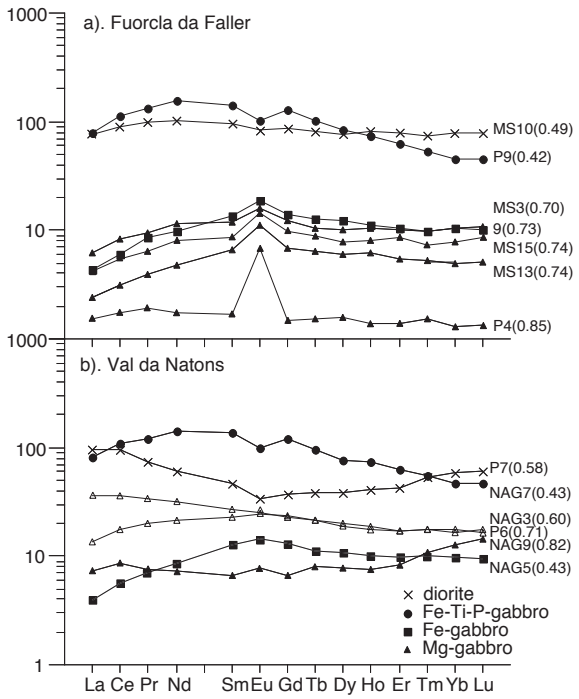

Figure 5-6: REE patterns of different gabbro types. a). Fuorcla da Faller. b). Val da Natons. Normalization to C1 chondrite (Sun and McDonough 1989). The black symbol represent cumulates, the open symbol represents frozen melts (see text). Numbers in parenthese indicate Mg# (Mg#= $Mg/Mg+Fe^{tot}$)

Whole rock chemistry

The whole rock major and trace element composition of basaltic rocks are given in Table 5-4. Additional analysis may be found in Frisch et al. (1994). The major element abundances indicate an olivine-tholeiite composition, similar to ophiolite basalts from other occurrences in the Alps and northern Apennines (Venturelli et al. 1981; Vannucci et al. 1993; Puschnig 2000; Bill et al. 2000). The basalts from the Platta ocean-continent transition show positive correlations of Mg# with Ni and Cr and negative correlations with P_2O_5 and TiO_2 (Fig. 5-7). The large range of MgO (4.52-10.32 weight %) indicates that most basalts record differentiation processes and

only a few samples provide evidence of being near-primary liquids. The Platta basalts are characterized by two groups of different REE chondrite-normalized patterns, one with Ce_n/Sm_n and $Ce_n/Yb_n > 1$, and a second one with Ce_n/Sm_n and $Ce_n/Yb_n <1$, respectively. Similarly, the Nb_n/Zr_n and Th/Hf ratios are higher in the first group (0.89-1.39; 0.17-0.26, respectively) than in the second one (0.24-0.28; 0.03-0.05). These features are common to other basalts from the ocean continent transition and suggest T- to N-MORB affinity (Frisch et al. 1994; Puschnig 2000).

Table 5-4 : *Major and trace element composition of the Platta basalts.*

	Lower unit								Upper unit	
sample	P8	P5	C14	OE73**	OE74	201	SGO4	SGO5	PCD1	FAB1
SiO_2	47,19	48,17	47.77	50.54	46.83	48.32	47.61	48.01	49,49	47,35
TiO_2	1,69	1,82	0.96	1.92	2.29	2.18	1.33	1.26	1,72	1,46
Al_2O_3	14,99	15,88	16.98	16.46	14.53	15.58	19.78	16.61	17,01	15,67
Fe_2O_3	9,11	9,91	7.94	8.48	12.04	10.12	10.37	7.83	8	8,83
MnO	0,15	0,16	0.12	0.11	0.21	0.12	0.17	0.13	0,11	0,13
MgO	5,54	6,58	9.33	4.33	5.20	7.36	8.56	7.47	6,23	9,76
CaO	10,5	9,78	11.41	8.12	9.05	5.92	2.82	10.12	8,58	8,11
Na_2O	4,36	4,3	2.22	5.47	3.09	4.01	5.42	3.50	5,02	2,86
K_2O	0,76	0	0.06	0.47	0	1.32	0.55	0.87	0,06	0,12
P_2O_5	0,27	0,25	0.10	0.34	0.36	0.31	0.15	0.12	0,32	0,28
L.O.I	5,27	2,98	1.56	3.50	6.35	3.32	4.61	3.42	3,28	5,27
Total	99,83	99,83	98.54	99.75	99.95	98.56	101.37	99.34	99,82	99,84
Mg#	0,55	0,57	0.70	0.50	0.46	0.59	0.62	0.65	0,61	0,69
Trace elements (ppm)										
V	245	259	166	204	283	260	131	187	202	170
Cr	242	188	430	114	118	141	265	249	151	277
Ni	82	95	191	91	58	67	213	110	81	209
Co	34	31	30						30	45
Cu	60	39	42						50	52
Zn	84	78	51						73	74
Zr	169	158	53	227	216	271	85	106	184	132
Y	38	36	10	33	43	40	24		29	23
Hf	4,14	3,78							4,11	2,72
Th	0,19	0,18							0,72	0,70
U	0,12	0,07							0,27	0,23
Ba	28	7,54		107	81	83	50	68	44	38
Rb	18	-		15			16	17	-	4,10
Sr	82	94	142	301	177	285	78	230	212	175
Nb	2,66	2,80							10,94	11,53
Ta	0,23	0,24							0,77	0,75
REE (ppm)										
La	5,84	5,73	2.74	11	10	8	2	3	10,18	8,95
Ce	19,25	18,52	7.31	27	26	22	5	10	25,14	21,47
Pr	3,20	3,03	1.35						3,49	2,77
Nd	15,74	14,46	7.43	19	24	21			15,67	12,38
Sm	4,86	4,39	2.77	5.3	7.2	6.2	2.2	2.9	4,29	3,35
Eu	1,70	1,66	1.18	1.6	2.1	1.8	0.9	1.1	1,44	1,26
Gd	5,89	5,16	3.71						4,52	3,77
Tb	0,94	0,84	0.50						0,76	0,62
Dy	6,11	5,64	3.66						4,85	3,62
Ho	1,37	1,27	0.79						1,04	0,76
Er	3,52	3,28	2.21						2,77	2,05
Tm	0,54	0,52	0.32						0,45	0,33
Yb	3,57	3,29	2.04	4	5	5	3	2	2,94	2,00
Lu	0,60	0,53	0.28	0.5	0.7	0.6	0.4	0.3	0,49	0,28

* sample from the Forno unit (Puschnig, 2000);** Sample from Frisch et al. (1994)

Discussion

Primitive liquids in ocean-continent transitions

Most MORB that erupted on the sea floor had been modified from their primary composition by fractional crystallization during ascent (e.g. Grove et al. 1992). This greatly complicates the determination of primary liquids that were in equilibrium with the mantle source. In order to test whether any of the analyzed basalts and/or gabbroic

rocks from the continent-ocean transition could represent near primary liquids, we calculated olivine compositions for primitive basalts with MgO > 8 weight % by using the K_d Fe-Mg olivine-liquid which is near 0.3 at low pressure for a wide variety of liquid compositions (Roeder and Emslie 1970; Ulmer 1989). All data are normalized on an anhydrous basis and $Fe^{3+}/\Sigma Fe = 0.05$ (36) was used. Because of the altered nature of the basalts we applied a second criterion to check for a possible primary nature of the basalt. Ni is highly compatible in olivine and is therefore a sensitive criterion to account for olivine fractionation. We used the Ni content of the basalts and the equation of Kinzler et al. (1990) to calculate the Ni content of the equilibrium olivine. As can be seen from figure 5-8 there are just a few compositions that satisfy a 'mantle criterion' (Ni: 2500-3500ppm, Mg# of olivine: 0.88 to 0.91) of being liquids in equilibrium with mantle olivine. Gabbro sample P6 is close to a primary liquid. Correction for crystal fractionation shows that about 4% of equilibrium olivine have to be added to P6 in order to obtain a composition which falls within the field of mantle olivine (Fig. 5-8). These primitive liquids have been considered further in the discussion about the origin of the mafic rocks in the Platta nappe.

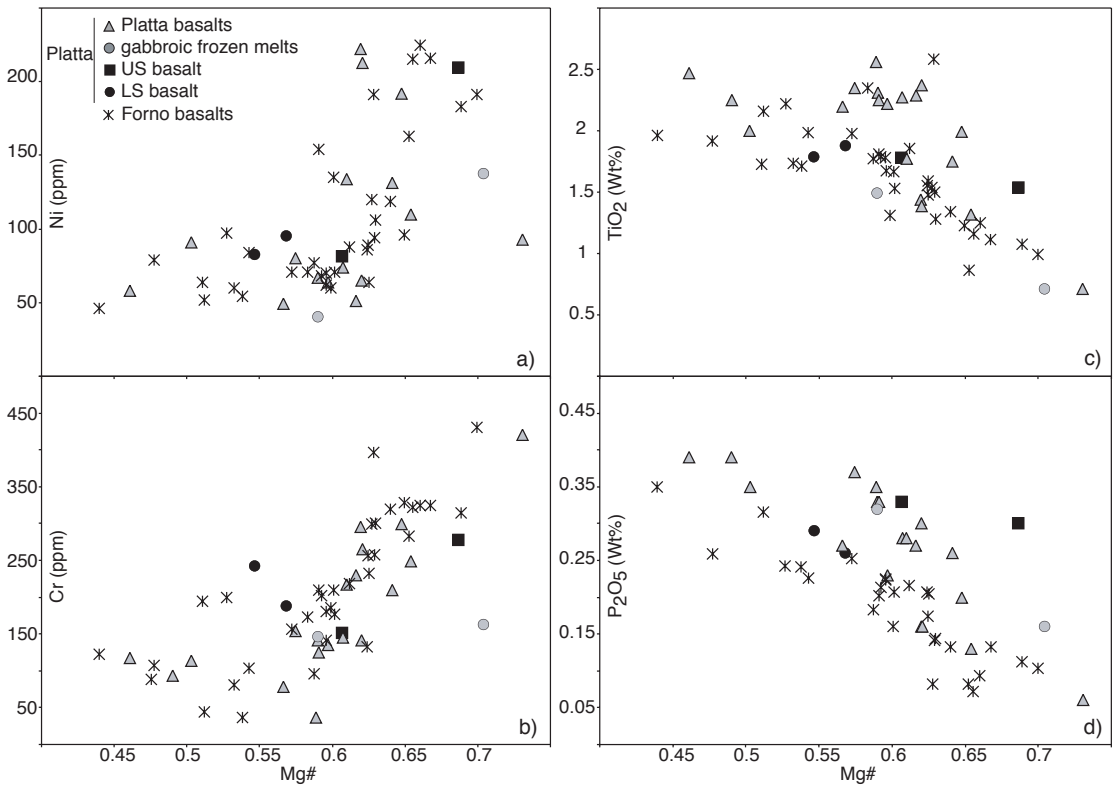

Figure 5-7: Variation of compatible and incompatible elements of the Platta basalts with Mg#. a). Ni vs. Mg#; b). Cr vs. Mg#; c). TiO_2 vs. Mg# and d). P_2O_5 vs. Mg#. The compatible elements Cr and Ni continuously decrease and the incompatible elements Ti and P increase with decreasing Mg#. Forno basalts form Puschnig (2000), Platta basalts from Frisch et al. (1994). US: upper serpentinite unit; LS: lower serpentinite unit of the Platta nappe.

The trace element compositions of the primitive liquids consisting of a basalt from the upper serpentinite unit (FAB1), one gabbroic frozen melt from the lower serpentinite unit (P6) and one basalt from the adjacent Forno unit (C14, Puschnig 2000) are represented in a chondrite normalized trace element diagram (Fig. 5-9a). These liquids show distinct patterns. The primitive basalt from the upper serpentinite (FAB1) is enriched in LREE, and other incompatible elements (Ta, Nb) compared to

the MREE and HREE and is characterized by a $(La/Sm)_N>1$ similar to T-MORB, and by a positive Zr anomaly. The primitive gabbroic frozen liquid (P6) from the lower serpentinite unit is depleted in incompatible elements relative to LREE, shows no Zr anomaly and HREE typical of N-MORB. The large differences in REE and other incompatible elements among the primitive liquids (Mg# 0.7 to 0.73, Ni: 2500 to 3500 ppm) can not be explained by fractional crystallization nor by possible effects of trapped liquids but rather reflect heterogeneity in the mantle source (see below). Indeed, simple modeling of low-pressure fractional crystallization (see below) led to an overall enrichment of the incompatible elements, but not to a strong fractionation between the HREE and the LREE considering liquids with $(La/Sm)_N>1$ (Fig. 5-9b) or liquids with $(La/Sm)_N<1$ (Fig. 5-9c), respectively. Another interesting observation regarding figure 5-10 is that most samples show a positive Zr anomaly with respect to the neighboring REE. Such a trace element pattern is not uncommon in basalts and is a characteristic feature of low-degree melts generated in the spinel peridotite field (e.g. Casey 1997).

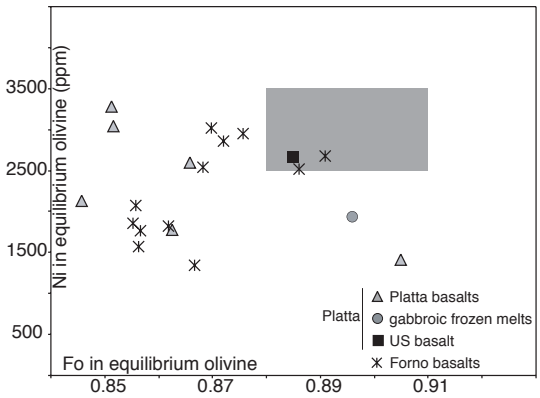

Figure 5-8: Ni and forsterite content of the calculated olivine in equilibrium with Platta and Forno basalts with MgO > 8wt%. Forsterite content calculated using a K_d FeO*/MgO of 0.3 (Roeder and Emslie 1970, Ulmer 1989), Ni content calculated using the equations of Kinzler et al. (1990) and $Fe^{3+}/SFe = 0.05$ (Christie et al. 1986). Grey square: Field of composition of olivine from abyssal peridotites (see text for discussion).

Gabbroic rocks: frozen liquids versus crystal fractionation

Field relations and whole rock chemistry of the gabbros show unambiguously that each individual gabbro occurrence represents a single batch of melt emplaced within the serpentinites. These batches underwent different magmatic evolutions at different places.

The gabbros of the Fuorcla da Faller area show a continuous evolution from olivine-bearing Mg-gabbro to highly differentiated diorite and Fe-Ti-P-gabbros. This evolution is well imaged by the increase in accessory minerals and the continuous decrease of the Mg# that correlate with the increase of the bulk REE without drastic changes in the modal abundance of plagioclase and clinopyroxene. Fractional or in situ crystallization (e.g. Langmuir 1989) is most probably the dominant process (see also modeling of crystal fractionation below). The strong enrichment of bulk Ti and Fe of sample MS3 is most probably derived from iron- and titanium-rich late magmatic liquids expelled by compaction from deeper-seated olivine gabbro cumulates (open system crystallization).

Gabbros in Val da Natons show a crystallization history different from that of Fuorcla da Faller in that their REE content does not correlate with the Mg# of the whole rock. Two samples (NAG3 and P6) have REE patterns close to a crystallized liquid. The

sample NAG9 shows also a very small degree of differentiation, but is enriched in HREE, U, Th and Zr. The liquids producing such a signature are most likely those of zircon-rich diorites, which occur as small veins within this particular outcrop. Despite the evidence of the infiltration of dioritic liquids, this sample has clinopyroxene with Mg# of 0.86, a LREE-depleted pattern and no Eu anomaly (Desmurs and Müntener, unpublished data) indicating that the cumulus clinopyroxene crystallized from fairly primitive liquids.

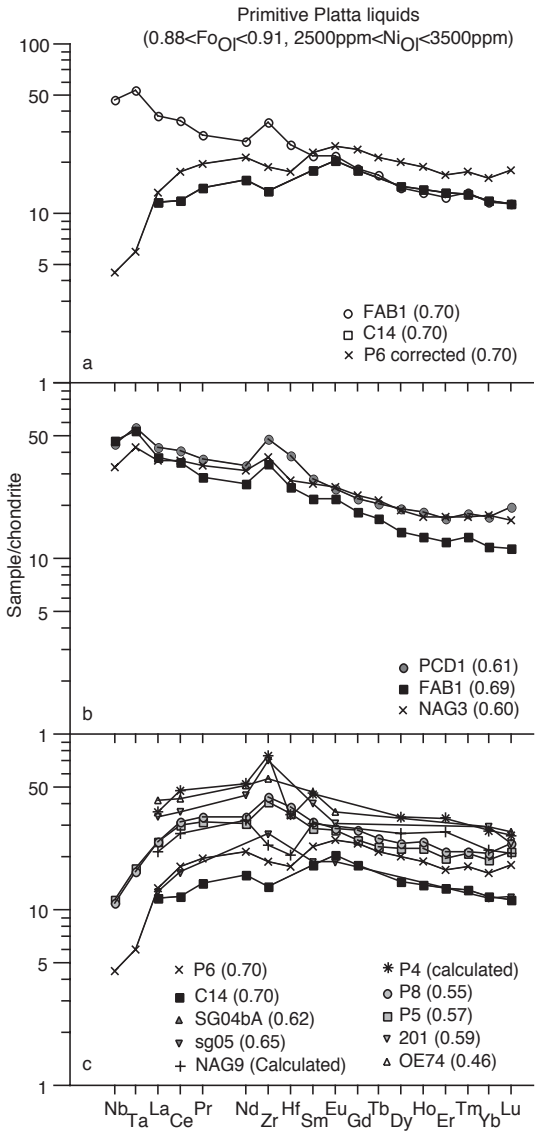

Figure 5-9: a) Trace element compositions of the most primitive basaltic liquids of the Platta nappe. b) Trace element composition of T-MORB and c) N-MORB of the Platta nappe. Crosses represent gabbroic parental melts. Sample NAG 9 and P4 are calculated from their clinopyroxene composition (Desmurs and Müntener, unpublished data) using the partition coefficient of Hart and Dunn (1993). Composition of sample C14 from Puschnig (2000), samples SG04a, SG05, OE74 and 201 from Frisch et al. (1994). Normalization to C1 chondrite (Sun and McDonough 1989).

Parental melts of the gabbros

The parental melts of the gabbros can be calculated by dividing the most primitive clinopyroxene compositions by crystal-liquid distribution coefficients. This procedure assumes that the clinopyroxenes retained the composition of crystals in

equilibrium with a liquid. Calculated liquid compositions from the most primitive samples (P4, NAG9) are strikingly similar to the measured composition of some gabbros that represent a frozen liquid (P6), and are relatively primitive N-MORB (sample P6, Mg#=0.70). Parental melts of Jurassic gabbros from the internal Ligurides calculated from the composition of clinopyroxene from olivine-gabbros show N-MORB affinities too (Tiepolo et al. 1997; Tribuzio et al. 1999). One notable exception is sample NAG 3, which has a different trace element signature (Fig. 5-9b) similar to that of T-MOR basalts.

Modeling crystal fractionation

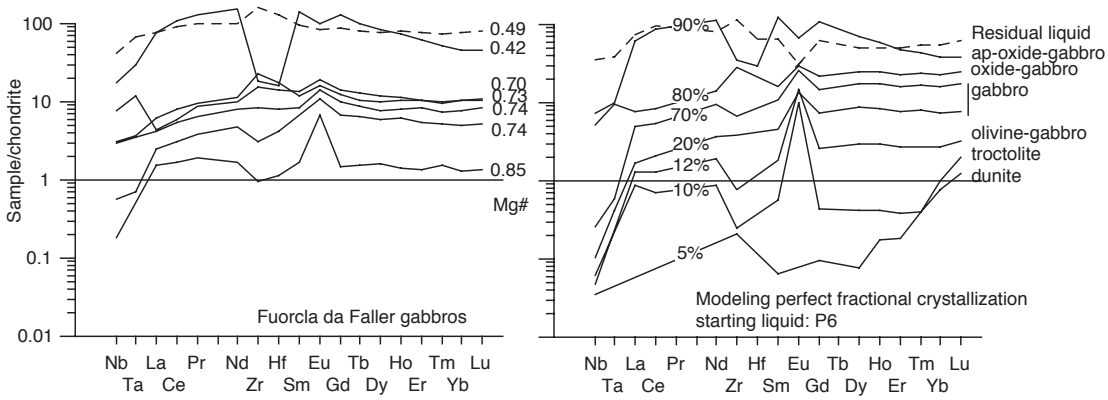

Figure 5-10: Comparison of the trace element patterns of the Fuorcla da Faller gabbro (left side) with the results of modeled fractional crystallization of a melt with a P6 composition (right side; MIXNFRAC software, Nielsen). Numbers indicate the percentage of solid phases. Dasched lines represent the composition of the diorite of the Fuorcla da Faller gabbro (left side) and of the calculated composition of residual liquid after 90% of crystallization (right side). Normalization to C1 chondrite (Sun and McDonough 1989).

Simple modeling of closed-system fractional crystallization of a liquid with a P6 composition using the MIXNFRAC software written by Roger Nielsen (http://EarthRef.org/GERM/bottom.htm) successfully matches the mineralogy and trace element composition of the Fuorcla da Faller 'cumulates'. As an initial liquid for modeling, we have chosen sample P6, which is close to a near-primary liquid (Fig. 5-9a). Modeling shows that olivine-gabbros formed after 10% of crystallization of olivine cumulates and troctolites. Between 15 % and 70 % of crystallization, clinopyroxene-plagioclase gabbros with less than 5% olivine are formed. Above ca. 75% crystallization, the model predicts the occurrence of a Fe-Ti oxide within the cumulate pile, and apatite appears after about 85% of crystallization. This crystallization sequence is consistent with the one found in the field. Furthermore, the model predicts no crystallization of orthopyroxene, which is also consistent with observations in the Fuorcla da Faller gabbro. The trace element patterns of the cumulate predicted by the model agree reasonably well with the ones observed (Fig. 5-10). It shows that the most primitive olivine-gabbro formed after about 12% of fractional crystallization. The REE pattern of the Mg-gabbros of the Fuorcla da Faller match the one predicted by the model between 20 and 70% of fractional crystallization. The predicted composition of the cumulate after 90% crystallization closely mimics the one of the Fe-Ti-P-gabbro, and the composition of the residual liquid matches the one of the diorite (Fig. 5-10). If the mineralogy and the trace elements of the gabbros are well simulated by the model, this is not the case for the

major elements especially for the most differentiated rock types. Indeed, the model predicts much more fractionated compositions in terms of Mg# numbers, than the ones observed in the most differentiated rocks. This is probably due to the presence of small quantities of interstitial liquids within the gabbro cumulates that equilibrated with the cumulus phases and which are not simulated by the model. Despite these shortcomings, the similarity between the modeled and measured compositions indicates that fractional crystallization was the dominant process in forming the Fuorcla da Faller gabbros.

Variation of degree and sources of melting

The volume of the mafic rocks is much bigger in the lower and originally oceanward serpentinite unit than in the upper unit (Fig. 5-1). Furthermore, their chemistry is different, as in the upper serpentinite unit they show predominantly T-MORB affinities and are dominated by N-MORB chemistry in the lower one. The two groups of basalts show different ratios of incompatible elements such as Nb/Zr and Th/Hf suggesting that they originated from different sources. In figure 5-11a, the Nb_n/Zr_n and the Ce_n/Sm_n ratios of the Platta basalts are plotted and compared to basalts from other Liguria-Piedmont ophiolites. The Platta T-MORBs are characterized by high ratios of Nb_n/Zr_n and Ce_n/Sm_n similar to the basalts from the Gets nappe which are associated with continental fragments and are characterized by low $\varepsilon Nd_{(166)}$ (4.5-5.9) (Bill et al. 2000). The Platta N-MORBs have ratios similar to the basalts from the Ligurides and Corsica and are characterized by variable ratios of Ce_n/Sm_n but low Nb_n/Zr_n, respectively. Both Platta N-MORBs and basalts form the Ligurides have high $\varepsilon Nd_{(160)}$ (+7.8-9.8) indicating an asthenospheric mantle source (Stille et al. 1989; Rampone et al. 1998; Schaltegger et al. Subm). The basalts from Liguria-Piedmont ophiolites show a positive anomaly in Zr (Fig. 5-11b) which indicates a low degree of melting in the spinel field (Casey 1997). The Zr anomaly is positive for the Platta basalts (1.1-1.5) and does not change from T- to N-MORB indicating that both groups represent relatively low degrees of melting. In contrast, the Zr* decreases from T- to N-Morb in Corsica and in the Ligurides indicating that they are the products of variable degrees of partial melting (higher for the N-MORBs than the T-MORBs). These data support the idea that the basalts from the Liguria-Piedmont ophiolites record two processes: first a shift from a slightly enriched (lithospheric) mantle, to a depleted (asthenospheric) mantle source, and second an increasing degree of melting in the latter source, which seems to correlate with the paleotectonic position of the respective unit.

Implications for magmatism in ocean-continent transitions

The occurrence of small and isolated gabbro bodies as well as the regional variability of volumes of basaltic rocks indicates that magmatism within the Platta ocean-continent transition is quite different from that at a slow spreading ridge as for example the Southwest Indian ridge (ODP Site 735b) (Dick et al. 2000) or the MARK area (Karson and Lawrence 1997). Indeed, even the most amagmatic segments of slow-spreading ridges such as the MARK area (Karson and Lawrence 1997) contain kilometer-sized gabbroic intrusions which can not be compared with the small volume of plutonic mafic rocks occurring along an ocean-continent transition. Similarly, magmatic rocks of slow spreading ridges are the result of higher degrees of melting than the ones occurring along ocean-continent transitions. Such isolated, small-scale

occurrences of igneous rocks could be an explanation for the weak magnetic anomalies found within the ocean continent transition of the Iberian margin (Whitmarsh et al. 2001).

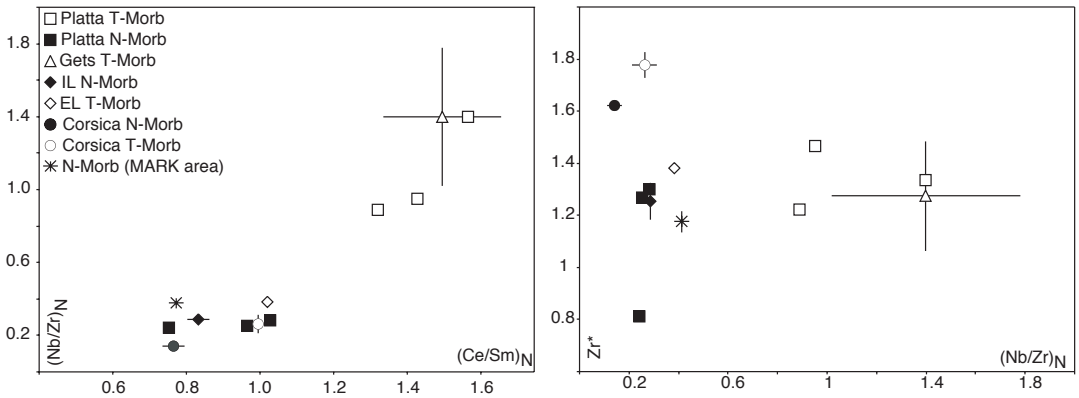

Figure 5-11: a) Incompatible ratio plots for T- and N-Morb of the Platta nappe and comparison with basalts from other Liguria- Piedmont ophiolites. High Nb_n/Zr_n values for nappe des Gets samples and Platta T-MORB indicates an enriched mantle source for these units whereas the lower values for the Platta N-MORBs, Liguride and Corsica basalts are similar to those of present-day N-MORBs. b) Zr* ($Zr_n/((Sm_n+Nd_n)/2)$) vs. Nb_n/Zr_n plot. Zr* is sensitive to changes in the degree of partial melting producing the basalts whereas Nb_n/Zr_n is characteristic of the source of melting (see text for discussion). Nappe des Gets from Bill et al. (2000), internal and external Ligurides from Rampone et al. (1998), and Corsica form Saccani et al. (2000). Average N-Morb of the MARK area from Meurer et al. (2001).

Jurassic Alpine ophiolites have often been compared with slow spreading ridges (e.g. Lagabrielle and Lemoine 1997), but the occurrence of isolated magmatic rocks and the sub-continental origin of the ultramafic basement rather points to an ocean-continent transition than to a slow spreading ridge. Like in the Platta ocean-continent transition, basalts from other Alpine units once close to the rifted continental crust show T-MORB affinities (Gets nappe (Bill et al. 2000), external Ligurides (Vannucci et al. 1993), Balagne nappe (Venturelli et al. 1981)), whereas more distal units contain N-MORB type magmatic rocks (internal Ligurides (Venturelli et al. 1981; Vannucci et al. 1993; Rampone et al. 1998), Montgenèvre ophiolite (Venturelli et al. 1981), Inzecca (Venturelli et al. 1981)). Isotopic data and geochemical modeling show that T-MORBs can be produced either by low degrees of melting of a depleted mantle source (external Liguride, (Vannucci et al. 1993; Rampone et al. 1998) or by melting of a slightly enriched mantle probably of sub-continental origin (Bill et al. 2000). N-MORB shows limited compositional variation and is the product of moderate degrees of partial melting (< 10%) of a depleted mantle source (e. g. Vannucci et al. 1993). Our data show that magmatic rock from the Platta ocean-continent transition record increasing degrees of melting and decreasing contamination of their source by an enriched component as they crystallized oceanward. This process is probably related to the continuous thinning of the sub-continental mantle and the associated uplift of the underlying asthenosphere during progressive rifting and exhumation of subcontinental mantle between crustal and lithospheric break-up.

Conclusions

Within the Platta ocean-continent transition, the volume of mafic rocks, expressed by gabbros and basalts, increases oceanward as most of the mafic rocks occur in the lower serpentinite unit.

The petrology and geochemistry of the gabbros shows that each continuous outcrop represents a different batch of melt that intruded the already exhumed and serpentinized mantle 161 Ma ago (Desmurs et al. 2001, Schaltegger et al. 2001). Each intrusion records different magmatic processes ranging from predominantly fractional crystallization to solidification without fractionation. The composition of the frozen melts as well as liquids calculated from the chemistry of the most primitive clinopyroxene cumulate indicates that the parental melt of the gabbros has the same range of composition as the overlying basalts.

Most of the basalts and the gabbro parental melts are already fractionated liquids in equilibrium with olivine cumulate and troctolite. These rock types were not found in the Platta nappe, which implies the occurrence of deeper cumulate gabbros that can not be observed today.

The chemistry of the mafic liquids (basalts and parental melts of the gabbros) changes from T-MORB to N-MORB composition as they crystallized away from the continent. These rocks are the result of low-degrees of melting of two distinct sources, a depleted (asthenospheric) mantle source for the N-MORBS and an 'enriched' mantle for T-MORBs, which is probably the sub-continental mantle. We interpret the increasing degree of melting as the result of the upwelling asthenosphere after continental break-up during a transitional stage before the establishment of a slow-spreading system.

Our work is part of the research project "Comparative anatomy of passive continental margins: Iberia and Eastern Alps" supported by the Swiss National Science Foundation, projects 21-049117.96/1 and 20-55284.98. We thank U. Schaltegger, D.Bernoulli, Y. Lagabrielle, and F. Chalot-Prat for stimulating discussions and helpful suggestions. We are grateful to E. Reusser for technical assistance with the electron microprobe at the ETH-Zurich and to F. Chalot-Prat for help with the ICP-MS trace element analysis performed at the CRPG, Nancy.

References

Bill M, Nägler TF, Masson H (2000) Geochemistry, Sm-Nd and Sr isotopes of mafic rocks from the earliest oceanic crust of Alpine Tethys. Schweiz Mineral Petrogr Mitt 80: 131-145.

Boillot G, Recq M, Winterer EL, Meyer AW, Applegate J, Baltuck M, Bergen JA, Comas MC, Davies TA, Dunham K, Evans CA, Girardeau J, Goldberg G, Haggerty J, Jansa LF, Johnson JA, Loreau J, Kasahara JP, Luna-Sierra E, Moullade M, Ogg J, Sarti M, Thurow J, Williamson M (1987) Tectonic denudation of the upper mantle along passive margin: a model based on drilling results (ODP Leg 103, Western Galicia Margin, Spain). Tectonophysics 132:334-342.

Casey JF (1997) Comparison of major- and trace-element geochemistry of abyssal peridotites and mafic plutonic rocks with basalts from the MARK region of the Mid-Atlantic Ridge. Proc Ocean Drill Prog Sci Res 153: 181-241.

Charpentier S, Kornprobst J, Chazot G, Cornen G, Boillot G (1998) Interaction entre lithosphère et asthenosphère au cours de l'ouverture océanique: données isotopiques préliminaires sur la Marge passive de Galice (Atlantique-Nord). C R Acad Sci Paris 326: 757-762.

Christie DM, Carmichael ISE, Langmuir CH (1986) Oxidation states of mid-ocean ridge basalt glasses. Earth Planet Sci Lett 79: 397-411.

Cornelius HP (1932) Geologische Karte der Err-Julier Gruppe 1:25'000. Schweizerische Geologische Kommission Spezialkarte Nr. 115A.

Cornen G, Girardeau J, Monnier C (1999) Basalts, underplated gabbros and pyroxenites record the rifting process of the West Iberian margin. Mineral Petrol 67: 111-142.

Desmurs L, Manatschal G, Bernoulli D (In press) The Steinmann trinity revisited: mantle exhumation and magmatism along an ocean-continent transition: the Platta nappe, eastern Switzerland. In: Wilson RCL, Whitmarsh RB, Taylor B, Froitzheim N (Eds) Non-volcanic Rifting of Continental Margins: a Comparison of Evidence from Land and Sea. Geol Soc London Spec Publ

Dick HJB, Natland JH, Alt JC, et al. (2000) A long in situ section of the lower ocean crust: results of ODP Leg 176 drilling at the Southwest Indian Ridge. Earth Planet Sci Lett 179: 31-51.

Dietrich V (1969) Die Ophiolithe des Oberhalbsteins (Graubünden) und das Ophiolithmaterial der ostschweizerischen Molasseablagerungen, ein petrographischer Vergleich. Verlag Herbert Lang & Cie, Bern, 179 pp.

Ferreiro-Mählmann R (1995) Das Diagenese-Metamorphose-Muster von Vitrinit-Reflexion und Illit-"Kristallinität" in Mittelbünden und im Oberhalbstein, Teil 1: Bezüge zur Stockwerktektonik. Schweiz Mineral Petrogr Mitt 75: 85-122.

Frisch W, Ring U, Dürr S, Borchert S, Biehler D (1994) The Arosa zone and Platta nappe ophiolites (Eastern Swiss Alps): Geochemical characteristics and their meaning for the evolution of the Penninic Ocean. Jahrb Geol Bundesanst (Wien) 137: 19-33.

Froitzheim N. Eberli GP (1990) Extensional detachment faulting in the evolution of a Tethys passive continental margin (Eastern Alps, Switzerland). Geol Soc Amer Bull 102: 1297-1308.

Froitzheim N, Schmid SM, Conti P (1994) Repeated change from crustal shortening to orogen-parallel extension in the Austroalpine units of Graubünden. Eclogae Geol Helv 87: 559-612.

Froitzheim N, Manatschal G (1996) Kinematics of Jurassic rifting, mantle exhumation, and passive-margin formation in the Austroalpine and Penninic nappes (eastern Switzerland). Geol Soc Amer Bull 108: 1120-1133.

Froitzheim N, Schmid SM, Frey M (1996) Mesozoic paleogeography and the timing of eclogite-facies metamorphism in the Alps: A working hypothesis. Eclogae Geol Helv 89: 81-110.

Grove TL, Kinzler RJ, Brian WB (1992) Fractionation of mid-ocean ridge basalts (MORB). In: Morgan JP et al. (Eds.) Mantle Flow and Melt Generation at Mid-Ocean Ridges. Geophys Monogr Ser, AGU, Washington DC, pp. 281-310.

Hart SR, Dunn T (1993) Experimental Cpx/melt partitioning of 24 trace elements. Contrib Mineral Petrol 113: 1-8.

Karson JA, Lawrence RM (1997) Tectonic window into gabbroic rocks of the middle oceanic crust in the MARK area near site 921-924. Proc Ocean Drill Prog Sci Res 153: 181-241.

Kinzler RJ, Grove TL, Recca SI (1990) An experimental study of temperature and melt composition on the partitioning of nickel between olivine and silicate melt. Geochim Cosmochim Acta 54: 1255-1265.

Lagabrielle Y, Lemoine M Alpine (1997) Corsican and Apennine ophiolites: the slow-spreading ridge model. C R Acad Sci Paris 325: 909-920.

Langmuir CH (1989) Geochemical consequences of in situ crystallization. Nature 340: 199-205.

Lemoine M, Tricart P, Boillot G (1987) Ultramafic and gabbroic ocean floor of the Ligurian Tethys (Alps, Corsica, Apennines): In search of a genetic model. Geology 15: 622-625.

Manatschal G, Nievergelt P (1997) A continent-ocean transition recorded in the Err and Platta nappes (Eastern Switzerland), Eclogae Geol Helv 90: 3-27.

Meurer WP, Sturm MA, Klein EM, Karson JA (2001) Basalt compositions from the Mid-Atlantic ridge at the SMARK area (22°30' to 22°50') - implications for parental liquid variability at isotopically homogeneous spreading centers. Earth Planet Sci Lett 186: 451-469.

Müntener O, Hermann J (In press) The role of lower crust and continental upper mantle during formation of nonvolcanic passive continental margins: evidence from the Alps. In: Wilson RCL, Whitmarsh RB, Taylor B, Froitzheim N (Eds) Non-volcanic Rifting of Continental Margins: a Comparison of Evidence from Land and Sea. Geol Soc London Spec Publ

Müntener O, Hermann J, Trommsdorff V (2000) Cooling history and exhumation of lower-crustal granulite and upper mantle (Malenco, Central Alps). J Petrol 41: 1-25.

Piccardo GB, Rampone E, Vannucci R (1990) Upper mantle evolution during continental rifting and ocean formation; evidences from peridotite bodies of the Western Alpine-Northern Apennine system. In: Roure, F., Heitzmann, P. & Polino, R. (Eds). Deep Structure of the Alps, Mém Soc Géol Fr: 156: 323-333.

Puschnig AR (2000) The oceanic Forno Unit (Rhetic Alps). Eclogae Geol Helv 93: 103-124.

Rampone E, Hofmann AW, Piccardo GB, Vannucci R, Bottazzi P, Ottolini L (1995) Petrology, mineral and isotope geochemistry of the external Liguride peridotites (Northern Apennines, Italy). J Petrol 36: 81-105.

Rampone E, Hofmann AW, Raczek (1998) I Isotopic contrast within the Internal Liguride Ophiolite (N. Italy): the lack of a genetic mantle-crust link. Earth Planet Sci Lett 163 :175-189.

Roeder PL, Emslie RF (1970) Olivine-liquid equilibrium. Contrib Mineral Petrol 29: 275-289.

Rubatto D, Gebauer D, Fanning M (1998) Jurassic formation and Eocene subduction of the Zermatt-Saas Fee ophiolites: implications for the geodynamic evolution of the Central and Western Alps. Contrib Mineral Petrol 132: 269-287.

Saccani E, Padoa E, Tassinari R (2000) Preliminary data on the Pineto gabbroic massif and Nebbio basalts: Progress toward the geochemical characterization of Alpine Corsica ophiolites. Ofioliti 25: 75-85.

Schaltegger U, Desmurs L, Manatschal G, Müntener O, Meier M, Bernoulli D (submitted) Transition from a rifted continental margin to a slow spreading system: field and isotopic constraints from a Tethyan ophiolite. Terra Nova.

Schärer U, Kornprobst J, Beslier MO, Boillot G, Girardeau J (1995) Gabbro and related rock emplacement beneath rifting continental crust: U-Pb geochronological and geochemical constraints for the Galicia passive margin (Spain). Earth Planet Sci Lett 130: 187-200.

Schärer U, Girardeau J, Cornen G, Boillot G (2000) 138-121 Ma asthenospheric magmatism prior to continental break-up in the North Atlantic and geodynamic implications. Earth Planet Sci Lett 181: 555-572

Stille P, Clauer N, Abrecht J (1989) Nd isotopic composition of Jurassic seawater and the genesis of Alpine Mn deposits: evidence from Sr-Nd isotope data. Geochim Cosmochim Acta 53: 1095-1099.

Sun SS, McDonough WF (1989) Chemical and isotopic systematics of oceanic basalts: implication for mantle composition and processes. In: Saunders AD, Norry MJ (Eds), Magmatism in the Ocean Basins, Geol. Soc. London Spec. Publ. 42: 313-345.

Tiepolo M, Tribuzio R, Vannucci R (1997) Mg- and Fe-gabbroids from Northern Apennine ophiolites: Parental liquids and differentiation process. Ofioliti 22: 57-69.

Tribuzio R, Tiepolo M, Vannucci R, Bottazzi P (1999) Trace element distribution within olivine-bearing gabbros from the Northern Apennine ophiolites (Italy): evidence for post-cumulus crystallization in MOR-type gabbroic rocks. Contrib Mineral Petrol 134: 123-133.

Trommsdorff V, Evans B (1974) Alpine metamorphism of peridotitic rocks. Schweiz Mineral Petrogr Mitt 54: 333-352.

Trommsdorff V (1983) Metamorphose magnesiumreicher Gesteine: Kritischer Vergleich von Natur, Experiment und thermodynamischer Datenbasis. Fortschr Mineral 61: 283-308.

Trommsdorff V, Piccardo GB, Montrasio A (1993) From magmatism through metamorphism to sea floor emplacement of subcontinental Adria during pre-Alpine rifting (Malenco, Italy). Schweiz Mineral Petrogr Mitt 73: 191-203.

Ulmer P (1989) The dependence of the Fe^{2+}-Mg cation-partitioning between olivine and basaltic liquid on pressure, temperature and composition; an experimental study to 30 kbars. Contrib Mineral Petrol 101: 261-273.

Vannucci R, Rampone E, Piccardo GB, Ottolini L, Bottazzi P (1993) Ophiolitic magmatism in the Ligurian Tethys; an ion microprobe study of basaltic clinopyroxenes. Contrib Mineral Petrol 115: 123-137.

Venturelli G, Thorpe RS, Potts PJ (1981) Rare earth and trace element characteristics of ophiolitic metabasalts from the Alpine-Apennine belt. Earth Planet Sci Lett 53: 109-123.

Whitmarsh RB, Minshull TA, Russel SM, Dean SM, Louden KE, Chian D (in press) The role of syn-rift magmatism in the rift-to-drift evolution of the west Iberia margin: geophysical observations. In: Wilson RCL, Whitmarsh RB, Taylor B, Froitzheim N (Eds) Non-volcanic Rifting of Continental Margins: a Comparison of Evidence from Land and Sea. Geol Soc London Spec Publ

Chapter 6: Tectonic and magmatic evolution of the Jurassic Platta ocean-continent transition: Summary and a conceptual model.

1. Introduction

The study of the Platta nappe showed that this ophiolite bears many similarities with modern ocean-continent transitions (OCT) imaged by geophysical methods and sampled by deep-sea drilling such as the present-day magma-poor Iberian passive margin. Like this modern analogue, the Platta OCT consists mainly of serpentinite, intruded by few gabbroic bodies and overlain by basaltic rocks, continent-derived extensional allochthons and breccias, and pelagic sediments. Mapping in the Err and Platta nappes allowed to trace tectonic and stratigraphic elements from the continental Err nappe into the ophiolitic Platta nappe and, combined with a structural analysis, permitted to propose a kinematic inversion of these nappes resulting in a palinspastic reconstruction of the former OCT. A major result of the thesis is that, based on fieldwork, it is possible to distinguish between two major serpentinite units or thrust sheets: an upper serpentinite unit in an originally more continentward position and a lower serpentinite unit in an originally more oceanward position (Fig. 6-1). This discovery allows for the first time to track lithological and chemical changes of mantle and magmatic rocks along a profile from the distal margin towards the ocean and to describe the structural evolution of the OCT as a part of the evolution of the whole margin.

In the following section, I first present the spatial distribution of rock types and structures in the reconstructed Platta OCT. Based on this reconstruction and using analytical results and kinematic data, I discuss, going back in time, how mantle rocks evolved during rifting paying particular attention to the relationship between deformation and magmatism and the exhumation history of the two different mantle units. The new data allow to test and refine a conceptual model proposed recently by Whitmarsh et al. (2001) and to discuss the evolution of deeper lithospheric levels occurring simultaneously with events at the surface and recorded in the sediments.

2. Lithologies and structures in the Platta OCT

2.1 Mantle rocks in the Platta OCT.

Study of the mantle rocks forming the upper and lower serpentinite units indicates that they are different in respect with their composition, structure, and temperature of equilibration.

The mantle rocks of the upper serpentinite unit are characterized by the association of relatively fertile spinel-lherzolite and numerous garnet-pyroxenite and by pressure and temperature of equilibration calculated as 7-12 kbars / ≈ 800°C indicating that the rocks equilibrated at a shallow sub-continental level. In contrast, the mantle rocks of the lower serpentinite unit are pyroxenite-free and consist of fertile lherzolite with subordinate depleted-lherzolite and harzburgite. They show higher temperatures of equilibration (≥1000°C) than the mantle rocks of the upper serpentinite unit, probably in the plagioclase stability field. A geochemical investigation indicates that the plagioclase crystallized by melt-rock reaction from MORB-type melt impregnating the mantle rocks of the lower serpentinite unit. Permian Sm/Nd model ages obtained

from clinopyroxene separates of the mantle rocks of the lower serpentinite unit suggest that these mantle rocks were in a deep level of the subcontinental mantle lithosphere before Mesozoic rifting started.
These results show that the mantle rocks in the more oceanward lower serpentinite unit represent a deeper pre-rift mantle than those exposed in the upper serpentinite unit. Moreover, a magmatic overprint, most likely associated with rifting, is only observed in the more oceanward lower serpentinite unit. Thus, the mantle rocks in the two units are different in respect with their pre-rift position as well as to their relation to rift-magmatism.
Thus, depending on their relative position in respect to the distal margin in the OCT, mantle rocks show a contrasting evolution during their exhumation on the sea floor. Mantle rocks in the upper serpentinite unit, i.e. exhumed close to the distal margin will simply record cooling and hydration whereas mantle rocks in the lower serpentinite unit, i.e. exhumed further oceanwards record impregnation by syn-rift melt and high-temperatures of equilibration during their exhumation before subsequent cooling and hydration (Fig. 6-1a).

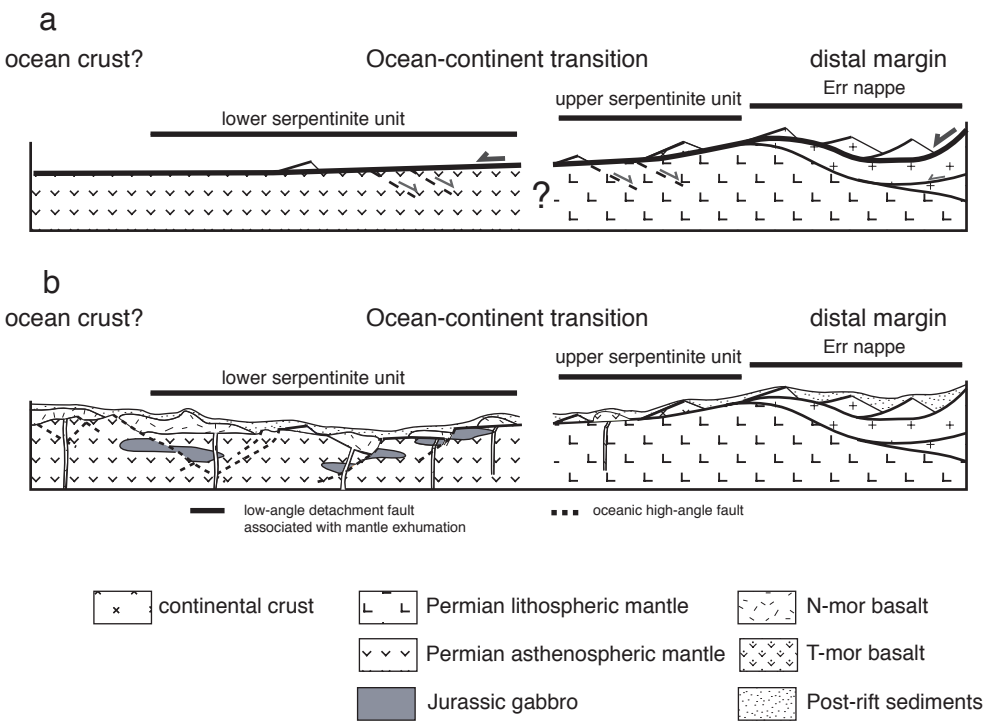

Figure 6-1: Reconstruction of the Platta OCT showing the distribution of the mantle a) and magmatic rocks b).

2.2. Chemistry, isotopes and age of the magmatic rocks in the Platta OCT.

Magmatic rocks occur as basalts and dolerite within the upper and lower serpentinite unit and as gabbros intruding the serpentinized lherzolite of the lower serpentinite unit. Mapping indicates that the volume of mafic rocks increases oceanward. The chemistry of the mafic liquids (basalts and parental melts of the gabbros) changes from T-MORB to N-MORB composition as they crystallized away from the continent. Trace element and isotopic chemistry suggest that these rocks are the result of low-degrees of melting of two distinct sources, a depleted (asthenospheric) mantle source for the N-MORBs and an 'enriched' mantle for T-

MORBs, which is probably the sub-continental mantle. As gabbros and basalts share similar parental melts, they probably belong to the same magmatic cycle, which can be dated by the age of crystallization of the gabbros (161±1 Ma; Schaltegger et al. subm). Our data show that magmatic rock from the Platta OCT record increasing degrees of melting and decreasing contamination of their source by an enriched component as they crystallized oceanward (Fig. 6-1b).
This chemical evolution of the mafic rocks is compatible with a continuous uplift of the asthenosphere after the break-up of the continental crust during a transitional stage leading to the establishment of a slow-spreading system.

2.3. Extensional structure within the Platta Ocean-continent transition.

Pre-Alpine structures are in many places preserved and observed in the Platta nappe. The structures preserved in the mantle rocks in the upper serpentinite unit and in the mantle and intrusive gabbros in the lower serpentinite unit are different concerning their high-temperature evolution but show the same low-temperature hydrous evolution. Anhydrous (granulite facies) shear-zones occur mostly in the upper serpentinite unit and show a top-to-the continent sense of shear. Such shear zones are associated with decompression and cooling recorded by the mantle rocks of the upper serpentinite unit to pressure between 7 and 12 kbars. Although such shear zones were active under retrograde metamorphic conditions, the lack of absolute time constraints do not permit to relate it unambiguously to Mesozoic rifting.
Hydrous shear-zones active under greenschist facies and lower grade conditions are found throughout the Platta OCT. Such shear zones bear several similarities with the Middle-Jurassic low-angle detachment structures documented in the overlying Err nappe (Froitzheim & Eberli 1990, Froitzheim & Manatschal 1996, Manatschal & Nievergelt 1997). Both show the same top-to-the ocean sense of shear and are characterized by the presence of cataclasites and gouges indicating low-grade metamorphic conditions during their activity, and both are overlain by extensional allochthons composed of upper continental crust and pre-rift sediments. Therefore, and supported by observations in the Tasna nappe, where similar faults can be followed from the crust to exhumed mantle (Florineth and Froitzheim 1994), Manatschal and Nievergelt (1997) suggested that the detachment system described in the Err nappe can be traced within the Platta nappe. Such detachments affected post-Variscan granites in the Err nappe and mantle rocks in the Platta nappe (Manatschal & Nievergelt 1997). However, no lower crustal rocks were found along these faults indicating that detachment faults are rather late in the rift evolution of the margin and had to postdate an earlier event during which the continental crust has been thinned leading locally to the juxtaposition of upper crust and upper mantle. The hydrous shear zones in the mantle rocks are cut or cut across by basaltic dykes suggesting that they were active during magmatic activity which has been dated by U/Pb on zircon at 161±1 Ma. Deformation under retrograde metamorphic conditions is also documented by the gabbros, which record deformation under granulite and greenschist-facies conditions. Their occurrence as clasts within sedimentary and basaltic breccias, overlain stratigraphically by Upper Jurassic radiolarian cherts, indicates that these gabbros had been exhumed at the sea floor shortly after their emplacement. The structures associated with their exhumation could be either the low-angle shear zones affecting the mantle rocks or high-angle normal faults, as has been documented along mid-ocean ridges, or a combination of both.

3. Tectonic model of Jurassic rifting

3.1. Introduction

In the past two decades, several rift models have been proposed for the evolution of the Liguria-Piedmond basin. In order to explain the asymmetry of the conjugate margins and the exhumation of mantle at the seafloor, Lemoine et al. (1987) proposed a simple shear model. The discovery of a detachment system within the Err nappe (Froitzheim and Eberli 1990, Manatschal and Nievergelt 1997) supported the importance of detachment faulting, but, based on sedimentological and structural arguments Froitzheim and Manatschal (1996) suggested that an initial stage of rifting was symmetric, an idea which is also supported by data obtained from the Iberian margin and its conjugate, the Newfoundland margin (Manatschal and Bernoulli 1998, 1999, Whitmarsh et al. 2001). The principal arguments for these authors to suggest a transition from initial symmetric pure-shear to late asymmetric simple-shear rifting are based on the observed changes in the temporal and spatial evolution of syn-rift sedimentation (e.g. Wilson et al. 2001), the contrasting isostatic evolution of the conjugate margins during latest rifting (Lemoine et al. 1987) and the observation of detachment faults restricted to the distal margin and leading to mantle exhumation post-dating initial, widely distributed, listric faulting within the proximal margins (Manatschal and Bernoulli 1999).
Simultaneously with the increasing knowledge of the evolution of the rifting at shallow levels, recorded in the sediments and by structures in the upper crust, investigations of the lower crust and upper mantle led to a new perspective of the rift-evolution. Handy and Zingg (1991) proposed the occurrence of a continent-ward dipping shear zone, the Pogallo line, active at mid-crustal level simultaneously with the evolution of the first rift basins within the proximal margin (see Fig. 11b in Handy and Zingg 1991). Trommsdorff et al. (1993) and Müntener and Hermann (2001) proposed a similar situation based on data from the Malenco area (see Fig. 4 in Trommsdorff et al. 1993). Hermann et al. (1997) demonstrated the occurrence of a fossil crust-mantle boundary in the Val Malenco area, which was welded by a Permian gabbro and exhumed during rifting at the seafloor. Müntener et al. (2000) described the P-T-t path of this crust-mantle boundary from Permian time to its exhumation at the seafloor during late Middle Jurassic time. This work allowed to quantify for the first time the P-T conditions at the crust-mantle boundary at the onset of rifting as well as to describe the early exhumation history of the mantle to the seafloor. However, due to the relatively strong Alpine tectonic and metamorphic overprint in the Malenco area, little was known concerning the mantle evolution during latest exhumation and its emplacement at the seafloor and the relation to the first magma associated with the rifting event. The data obtained from the Platta nappe and presented in this thesis can consequently fill this gap and allow to test and refine a conceptual model proposed recently by Whitmarsh et al. (2001).

3.2. A conceptual model for the transition from rifting to seafloor spreading

Recently Whitmarsh et al. (2001) proposed a conceptual model explaining the formation of magma-poor passive margin from initial rifting to onset of sea-floor spreading based on data from the passive margin reconstructed in the Alps and from the present-day Iberian margin. These authors assumed an initially equilibrated lithosphere with a four-layer rheology and a crust locally thickened by pre-rift

underplated gabbro. In this model, a first symmetric rifting phase is characterized by the necking of the upper mantle, the strongest part of the lithosphere, beneath the gabbros where it was weakest, allowing the asthenosphere to rise. Elsewhere, ductile flow of the lower crust determined where rift basins formed at the surface. Relatively little crustal thinning and subsidence occurred above the necked region, whereas the adjacent areas were strongly thinned during this first phase. Later, the thermal structure and gravitational response associated with the rising asthenosphere started to influence the rifting. In a later phase, rifting was localized within the previously only slightly extended crust and led to an important thinning of the lower crust. Using data from the Iberia Abyssal Plain, Manatschal et al. (2001) inferred that this late rifting phase is characterized by a change from initial listric, upward concave faults to one or more concave-downward faults reflected most likely a change in the distribution of weak layers. Whereas listric faults sole out in horizontal weak layers, concave-downward faults might be favoured by sub-vertical weak zones generated by the rise of the asthenosphere and the presence of melts in the latest stage of rifting. Top-to-the ocean downward concave faults may explain the exhumation of deeper mantle layers going oceanwards in the OCT. Eventually, increasing melt production led to the creation of `continuous' oceanic crust and the asthenosphere spawned oceanic upper mantle, which characterized the onset of sea-floor spreading.
In the following sections I will discuss the exhumation and deformation history of the mantle rocks and their relationship to magmatism and will show how these events may be correlated with events occurring at the surface and recorded in the sediments.

3.3. From mantle exhumation to seafloor spreading

As demonstrated above (Fig. 6-1), the reconstruction of the Platta nappe allows to identify a spatial transition from a cold to a hotter subcontinental mantle going oceanwards as well as an increase in the volume and intensity of magmatism in the same direction. To what extent this spatial transition represents also a temporal evolution is difficult to estimate because neither age data nor stratigraphic relationships allow to distinguish a temporal evolution in the Platta OCT. This is also one of the arguments, beside evidence from analogue presently active tectonic settings (e.g. Woodlark basin, Tregoning et al. 1998), suggesting that detachment faulting and consequently the exhumation of mantle and the transition to seafloor spreading is a rather fast process (in the order of cm/yr).
In the model (Fig. 6-2b) it is assumed that exhumation of a mantle which was already in a shallow level, occurred along top-to-the ocean downward concave faults, leading to the exhumation of increasing deeper mantle portions at the seafloor. The observation that fault zones showing a top to the ocean sense of shear are restricted to upper greenschist facies conditions and overprint an older lower amphibolite facies static hydration event suggests that the mantle was already exhumed to shallower levels, hydrated and most importantly, that the two serpentine units were already juxtaposed when the detachment faults became active. This is indicated by the same exhumation history found in both units from greenschist facies down to seafloor conditions, and by the occurrences of extensional allochthons derived from the distal margin in both units.
Although the increasing equilibration temperatures observed in the mantle going oceanwards is compatible with the exhumation of an increasing deeper lithospheric mantle as expected by the model, geochemical investigation of the mantle rocks of the lower serpentinite unit suggests that the impregnation of the mantle by MORB-type

melt led to the high-temperature equilibration of the mantle rocks in the plagioclase stability field. Although, this impregnation event is not directly dated, it has to be older that the intrusion of the gabbro and the extrusion of the basalts the former dated at 161 ±1 Ma. On the other hand, it should happen after Permian times as this time correspond to the accretion of the mantle rocks onto the subcontinental lithosphere where they equilibrated in the spinel stability field. As no major magmatic activity is recorded in this area during Triassic times, I infer that impregnation occurred during Mesozoic rifting. The low-grade shear-zones overprint the high-temperature assemblage indicating that the mantle rocks were already at a shallow depth before the top-to-the-ocean shear zones became active (Fig. 6-2b). This suggests that the onset of melting of the rising asthenosphere and the melt impregnation of the overlying mantle could be responsible for a change of the rheology of the lithosphere inducing vertical weaknesses within the mantle rocks. Indeed, the presence of ascending melts within the mantle rocks may produce a localization of the deformation along their pathways (Fig. 6-2a) leading to a concave downwards geometry of the faults.
The volume and the MORB character of the magmatic rocks increase as they crystallized oceanward, indicating increasing degrees of melting and decreasing contamination of their source by an enriched component. This observation can be related to the coeval thinning of the subcontinental mantle and rising of the asthenosphere, which will ultimately lead to the establishment of a spreading ridge system (Fig. 6-2a).

3.4. Mantle exhumation during rifting

The common low-temperature exhumation history observed in the mantle rocks of the upper and lower serpentinite units contrasts with their very different high-temperature evolution. The mantle rocks of the upper serpentinites unit are characterized by a subsolidus temperature of equilibration at relatively low-pressure and show many similarities with the Malenco ultramafics suggesting a position immediately beneath continental crust at the onset of rifting (Hermann *et al.* 1997, Müntener *et al.* 2000). The chemical evolution of the lherzolites of the lower serpentinite unit documents a polyphase magmatic evolution. During an early phase, the mantle rocks underwent partial melting that probably started within the garnet stability field. This melting event was followed first by localized "alkaline" metasomatism and then by impregnation of the mantle rocks by tholeiitic melts. Subsequently the mantle rocks equilibrated at high temperature (≈1000°C) in presence of plagioclase. Sm/Nd model ages performed on the clinopyroxene of the mantle rocks of the lower serpentinite unit yield Permian ages indicating that these mantle rocks accreted the mantle lithosphere at that time. However, the spinel foliation they probably acquire at that time suggest pressure of equilibration less than 20 kbars (Carrol-Webb and Wood 1986). These differences suggest that the mantle rocks of the upper and lower serpentinite unit have been juxtaposed before they have been exhumed at the seafloor along oceanward dipping detachment faults. Indeed, no major tectonic activity has been documented so far in the Adriatic domains during the period between the Permian extension and the Mesozoic rifting suggesting that the relative position of the mantle rocks after the Permian remained the same until the onset of rifting. If this is true, then the mantle rocks of the two units must have been juxtaposed during an earlier rifting phase.

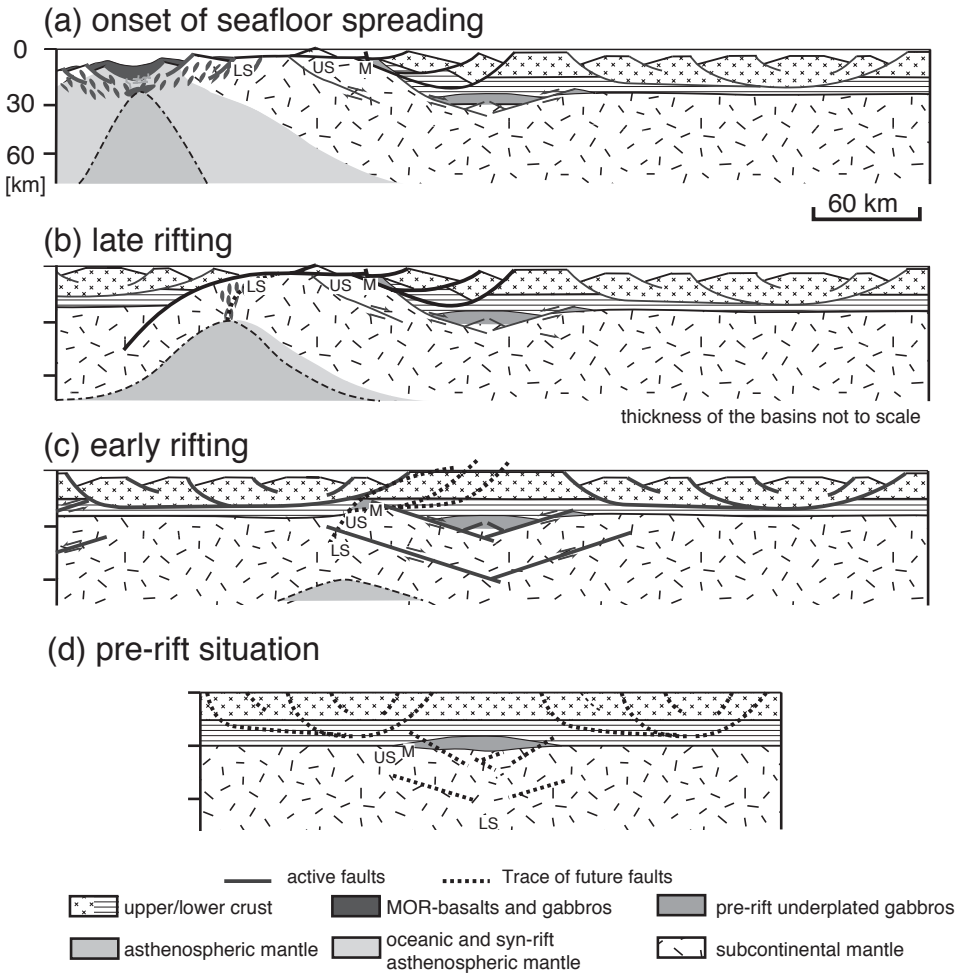

Figure 6-2: Lithospheric model of the formation of the Adriatic margin. a) Situation at the onset of sea floor spreading indicating the relative positions of the units recognized in Graubünden (M: Malenco, US: upper serpentinite unit, LS: lower serpentinite unit). This onset is due to the coeval thinning of the subcontinental mantle and uplift of the asthenosphere during the late phase of asymmetric rifting b). During this phase, the different units are already juxtaposed and exhumed along concave-downward normal faults, which localized along melt pathways. Initiation of this asymmetric extension might be related to the onset of melting of a rising asthenosphere. c) The rise of the asthenosphere might happen at the end of an early symmetric rifting characterized by the development of basins in the proximal part of the margin. Extension is accommodated by listric normal faults in the upper crust and by conjugate normal shear-zones at depth. Both structures soled out at mid-crustal level. This phase is responsible for the juxtaposition of different level of the subcontinental mantle rocks such as the originally shallow mantle rocks of the upper serpentinite unit and the deeper mantle rocks of the lower serpentinite unit d). (Modified from Whitmarsh et al. 2001).

In the Alpine realm, an earlier extensional phase occurred during the latest Triassic affecting a 30 km thick and equilibrated crust. This assumption is based on the shallow-water carbonate sedimentation prevailing along the evolving conjugate margins of the Liguria-Piedmont ocean and on P-T-t data obtained from a Permian gabbro and lower crustal rocks of the Malenco complex indicating that the crust-mantle boundary recorded temperature less than 650° at a pressure of 9-10 kbars before the onset of rifting (Müntener et al. 2000). This extension phase is documented by the formation of fault-bounded rift basins from latest Trassic to early Jurassic onwards which are localized in the proximal parts of the margin (e.g. Lombardian basins (Bertotti et al. 1993), Central Austroalpine (Eberli 1988), Dauphiné (Lemoine et al. 1986) (Fig 6-2c). In the Southern Alps, Bertotti (1991) showed that the faults

delimiting such basins had a listric geometry, which soled out at mid-crustal level. During that time, hemipelagic limestones were deposited in the future distal Adriatic margin (Err domain). These Middle Liassic sediments show a constant thickness and no indication of syn-sedimentary faulting indicating that, at shallow crustal levels, the distal margin was not much affected by this rifting phase. However, the entire margin was subsiding at that time (e.g. Manatschal and Bernoulli 1999).
Müntener and Hermann (2001) showed that, at depth within distal parts of the margin, extension was controlled by the formation of localized mylonitic hydrous shear zones within the lower crust and the upper mantle. These localized shear zones, such as the Margna normal faults could eventually accommodate substantial displacement during early rifting (Hermann and Müntener 1996). Hermann and Müntener (1996) showed that the Margna shear zone indicates a top-to-the Adriatic continent sense of shear and was largely responsible for the uplift of lower crust and upper mantle to a depth of less than 15 km (Hermann and Müntener 1996). The overall symmetrical geometry recorded by the conjugate margins during this early stage of rifting shows, however, that conjugated faults had to occur also beneath the conjugate European margin (Fig. 6-2c).
To explain how the two serpentinite units observed within the Platta nappe were juxtaposed before the oceanward-dipping detachment faults became active, we infer that shear zones similar to the Margna fault propagated at depth uplifting deeper levels of the subcontinental mantle. Although, similar continent-dipping retrograde shear zones are observed within the mantle rocks of the Platta nappe, which may suggest that they were kinematically linked, the lack of time constraints does not allow to clearly relate these high-temperature, anhydrous shear zones to this extensional system, active during an early stage of rifting.

4 Conclusions

During this work, a fossil ocean-continent transition, preserved in the Platta nappe has been reconstructed. This ophiolite consists of two large serpentinite units, the upper and lower serpentinite units. Kinematic inversion of the alpine deformation shows that the upper serpentinite unit was close to the continental margin whereas the lower serpentinite unit occurred in a more oceanward position. Field relationships indicate that the Platta nappe bears many similarities with modern OCT of magma-poor passive margin such as the Iberian margin. This ophiolite is characterized by the predominance of a serpentinite basement locally intruded by gabbroic rocks and overlain by basalts, continental-derived extensional allochthons and breccias, and pelagic sediments. A relative sequence of the emplacement of the different rock type can be determined from the field relationships, which indicate that gabbros and dolerites were emplaced in an already cool and serpentinized mantle. This magmatic activity overlaps in time with the activity of low-grade shear-zones exhuming the mantle rocks and emplacing extensional allochthons derived from the continental distal margin on top of the mantle rocks. All these lithologies are overlain by the same radiolarian cherts, which represent the first post-rift sediments.
Study of the mantle rocks indicates that they represent former sub-continental mantle. Although the low-temperature (amphibolite to greenschist and lower grade facies) evolution of the mantle rocks of the upper and lower serpentinite unit is similar they show a contrasting high-temperature (granulite facies) evolution. Petrologic and chemical study of the mantle rocks of the upper serpentinite unit show that they represent shallow level of the pre-rift subcontinental mantle as testified by their

subsolidus temperature of equilibration and their relatively low-pressure of equilibration (7-12 kbars). In contrast, the mantle rocks of the lower serpentinite unit may represent deeper levels of the subcontinental mantle as they accreted the mantle lithosphere in Permian times. The mantle rocks of these two units show also a contrasting evolution during the Mesozoic rifting. The mantle rocks of the upper serpentinite, which are exhumed close to the distal margin, records simply cooling and hydration during their exhumation at the sea floor. In contrast, those of the lower serpentinite unit, which are exhumed nearer to the ocean, were equilibrated at high-temperature (1000°C) in the plagioclase stability field and were additionally impregnated by MORB-type melts during their exhumation. Two types of possible rift-related structures have been found within the mantle rocks. The first are continent dipping anhydrous shear-zones characterized by a granulite-facies assemblage. This type of shear zones is pervasive in the mantle rocks of the upper serpentinite unit and localized and mylonitic in the lower serpentinite unit. Although, Jurassic shear-zones with a similar dip and sense of shear have been documented to be active during a first rifting phase in the lower continental crust (Handy and Zingg 1991; Müntener and Hermann 2001), the lack of time constraints do not allow to relate unambiguously the high-temperature shear zones in the mantle to Mesozoic rifting. In contrast, the low-grade hydrous shear zones characterized by greenschist facies and lower grade assemblages belong to the rifting event. They are similar in both units and can be related to a detachment system described in the distal margin (Froitzheim and Manatschal 1996; Manatschal and Nievergelt 1997), which led to the final exhumation of the mantle rock at the sea floor. However, this detachment phase has to be preceded by an earlier extension event juxtaposing the upper crustal rocks of the distal margin with the upper mantle rocks of the upper serpentinite unit and those with the deep subcontinental mantle rocks of the lower serpentinite unit.
Magmatic rocks within the Platta nappe occurs as basalts and dolerite dykes in both serpentinite units, gabbros occurrences being restricted to the lower serpentinite unit. Mapping of the magmatic rocks indicates that they are more numerous in the lower serpentinite unit than in the upper one. Dating of the gabbros by U/Pb on zircons yield a Jurassic age of 161±1 Ma. Although field relationships indicate that, locally, extrusion of basalts may be younger than the intrusion of the gabbros, trace element chemistry indicates that they share similar parental melts and that they represent the intrusive and extrusive terms of the same magmatic event. Trace element and isotope chemistry of the basalts and gabbros indicate that their parental melts are produced by low-degree of melting of a depleted-mantle source similar to those of N-MORB. In contrast, the trace element composition of the basalts and dolerites of the upper serpentinite unit indicates an enriched component in their source similar to T-MORB.

This work showed that the transition towards the oceanic lithosphere in the OCT is gradual and is characterized by the exhumation of originally deeper and deeper level of the subcontinental mantle towards the ocean. Magmatic rocks within the OCT are characterized by a lack of genetic link with the surrounding mantle rocks. They have an increasing N-MORB character towards the ocean. This coeval thinning of the subcontinental mantle lithosphere and uplift of the asthenosphere will ultimately lead to the establishment of an oceanic spreading system. Extension during this transitional phase toward a spreading system is accommodated by detachment faulting, which appears to overlap in time with magmatism. This transient and asymmetric phase appears to be fast as the same post-rift sediments overlie all his characteristic structural and lithological elements. The importance of magmatism during this phase contrast with the earlier symmetric phase of rifting, which seems largely amagmatic.

During this first phase, extension is accommodated by listric faults in the upper crust and by conjugate continent-dipping shear-zones at depth. I suggest that the onset of melting within an ascending and narrowing asthenosphere and the coeval melt-impregnation of the overlying mantle rocks change the rheology of the extended lithosphere. The onset of such vertical weaknesses might lead to the observed changes in the geometry of the extensional system.

References

BERTOTTI G. 1991. Early Mesozoic estension and Alpine shortening in the western southern Alps: the geology of the area between Lugano and menaggio (Lombardy, northern Italy) Mem. Soc. Geol. Padova, **43**, 17-123.

BERTOTTI G., PICOTTI V., BERNOULLI D. & CASTELLARIN A. 1993. From rifting to drifting; tectonic evolution of the South-Alpine upper crust from the Triassic to the Early Cretaceous. Sediment. Geol., **86**, 53-76.

CARROL-WEBB S. A. & WOOD B. J. 1986. Spinel-pyroxene-garnet relationships and their dependance on Cr/Al ratio, Contrib. Mineral. Petrol., **92**, 471-480.

EBERLI G.P. 1988. The evolution of the southern continental margin of the Jurassic tethys ocean as recorded in the Allgäu Formation of the Austroalpine nappes of Graubünden (Switzerland), Eclogae Geol. Helv., **81**, 175-224.

FLORINETH D. & FROITZHEIM N. 1994. Transition from continental to oceanic basement in the Tasna nappe (Engadine window, Graubünden, Switzerland): Evidence for the Cretaceous opening of the Valais ocean. Schweiz. Mineral. Petrogr. Mitt., **74**, 437-448.

FROITZHEIM N. & EBERLI G.P. 1990. Extensional detachment faulting in the evolution of a Tethys passive continental margin (Eastern Alps, Switzerland), Geolog. Soc. Am. Bull., **102**, 1297-1308.

FROITZHEIM N. & MANATSCHAL G. 1996. Kinematics of Jurassic rifting, mantle exhumation, and passive-margin formation in the Austroalpine and Penninic nappes (eastern Switzerland). Geolog. Soc. Am. Bull., **108**, 1120-1133.

HANDY M. & ZINGG A. 1991. The tectonic and rheological evolution of an attenuated cross section of the continental crust; Ivrea crustal section, southern Alps, northwestern Italy and southern Switzerland. Geol. Soc. Am. Bull., **103**; 236-253.

HERMANN J. & MÜNTENER O 1996. Extension-related structures in the Malenco-Margna system: Implication for paleogeography and consequences for rifting and Alpine tectonics, Schweiz. Mitt. Petrogr. Mitt., **76**, 501-519.

HERMANN J., MÜNTENER O., TROMMSDORFF V., HANSMANN W. & PICCARDO G. B. 1997. Fossil crust-to-mantle transition, Val Malenco (Italian Alps), J. Geophys. Res., **102**, B9, 20123-20132.

LEMOINE M., BAS T., ARNAUD-VANNEAU A., ARNAUD H., DUMONT T., GIDON M., BOURBON M., DE GRACIANSKY P.C., RUDKIEWICZ J.L., MEGARD GALLI J., & TRICART P. 1986. The continental margin of the mesozoic tethys in the Western Alps. Marine Petrol. Geol.,**3**,179-199.

LEMOINE M., TRICART P. & BOILLOT G. 1987. Ultramafic and gabbroic ocean floor of the Ligurian Tethys (Alps, Corsica, Apennines): In search of a genetic model. Geology, **15**, 622-625.

MANATSCHAL G. & BERNOULLI D. 1998. Rifting and early evolution of ancient ocean basins: the record of the Mesozoic Tethys and of the Galicia-Newfoundland margins, Marine Geophy. Res., **20**, 371-381.

MANATSCHAL G. & BERNOULLI D. 1999. Architecture and tectonic evolution of non-volcanic margins: present-day Galicia and ancient Adria, Tectonics, **18**, 1099-1119.

MANATSCHAL G. & NIEVERGELT P. 1997. A continent-ocean transition recorded in the Err and Platta nappes (Eastern Switzerland), Eclogae Geol. Helv., **90**, 3-27.

MANATSCHAL G., FROITZHEIM N., RUBENACH M. J. & TURRIN B. 2001. The role of detachment faulting in the formation of an ocean-continent transition: insights from the Iberia Abyssal Plain, in: R.C.L. Wilson, R.B. Whitmarsh, B. Taylor & N. Froitzheim (Eds): Non-volcanic Rifting of Continental Margins: a Comparison of Evidence from Land and Sea, Geol. Soc. London. Spec. Publ. (in press).

MÜNTENER O. & HERMANN J. 2001. The role of lower crust and continental upper mantle during formation of non volcanic passive continental margins: evidence from the Alps, in: R.C.L. Wilson, R.B. Whitmarsh, B. Taylor & N. Froitzheim (Eds): Non-volcanic Rifting of Continental Margins: a Comparison of Evidence from Land and Sea, Geol. Soc. London Spec. Publ. (in press).

MÜNTENER O., HERMANN J. & TROMMSDORFF V. 2000. Cooling history and exhumation of lower-crustal granulite and upper mantle (Malenco, Central Alps), J. Petrol., **41**, 1-25.

TREGONING P., LAMBECK K., STOLZ A., MORGAN P., MCCLUSKY S. C., VAN DER BEEK-P., MCQUEEN H., JACKSON R. J., LITTLE R.P., LAING A. & MURPHY B. 1998. Estimation of current plate motions in Papua New Guinea from Global Positioning System. J. Geophys. Res., **103**, 12,181-12,12,203.

TROMMSDORFF V., PICCARDO G.B. & MONTRASIO A. 1993. From magmatism through metamorphism to sea floor emplacement of subcontinental Adria during pre-Alpine rifting (Malenco, Italy), Schweiz. Mineral. Petrogr. Mitt., **73**, 191-203.

WHITMARSCH, R. B, MANATSCHAL G & MINSHULL T. A. 2001. Evolution of magma-poor continental margins from rifting to seafloor spreading. Nature, **413**, 150-154.

WILSON R.C.L., MANATSCHAL G. & WISE S. 2001. Rifting along non-volcanic passive margins: stratigraphic and seismic evidence from the Mesozoic succession of the Alps and western Iberia. In: Non-volcanic rifting of continental margins: evidence from land and sea. Wilson R.C.L., Whitmarsh R.B., Taylor B. and Froitzheim N.(eds). Geol. Soc. London, Spec.Publ., in press.

Appendix 1- Sample location

Sample		location	applied method
Lower serpentinite unit			
MSP1	serpentinized lherzolite	764'750/147'175	EMP, E-ICP, ICP-MS
CRP3	serpentinized lherzolite	767'750/147'250	EMP, E-ICP, ICP-MS
CRP1	serpentinite	767'750/147'250	E-ICP, ICP-MS
SUP2	serpentinized lherzolite	769'200/153'750	EMP, E-ICP, ICP-MS
SUP3	serpentinized lherzolite	769'200/153'750	EMP, E-ICP, ICP-MS
SUP4	serpentinized lherzolite	769'200/153'750	E-MS, ICP-MS
SUP5	serpentinized lherzolite	768'000/155'175	E-MS, ICP-MS
SUP6	serpentinized lherzolite	768'000/155'175	EMP
NAP1	serpentinized lherzolite	769'650/152'500	EMP
NAP2	serpentinized lherzolite	769'650/152'500	EMP, E-ICP, ICP-MS
NAP3	serpentinite	769'650/152'500	E-ICP, ICP-MS
NAP4	serpentinite	769'925/153'005	
NAP5	serpentinized lherzolite	769'925/153'005	
NAP6	serpentinized lherzolite	769'500/153'005	EMP
NAP7	serpentinized lherzolite	769'500/153'005	EMP, E-ICP, ICP-MS
LAP1	serpentinized lherzolite	769'125/152'005	EMP, E-ICP, ICP-MS
STP1	serpentinized lherzolite	767'500/152'155	EMP, E-ICP, ICP-MS
STP2	serpentinized lherzolite	766'875/151'900	EMP, E-ICP, ICP-MS
STP3	serpentinized lherzolite	766'875/151'900	E-ICP, ICP-MS
STP4	serpentinized lherzolite	766'900/151'750	EMP
STP5	serpentinized lherzolite	766'350/151'125	EMP
stp5-2	serpentinized lherzolite	766'400/151'125	EMP
stp11	serpentinized lherzolite	766'400/151'125	EMP
VSP1	serpentinized lherzolite	770'175/153'600	
VSP2	serpentinized lherzolite	770'175/153'600	
VSP3	serpentinized lherzolite	770'125/153'125	
VSP4	serpentinized lherzolite	770'125/153'125	
VSP5	serpentinized lherzolite	770'125/153'125	
VSP6	serpentinized lherzolite	770'125/153'125	
P4	Mg-gabbro	765'225/147'375	EMP, E-ICP, ICP-MS, Nd-Sr
MS15	Mg-gabbro	765'300/147'425	EMP, E-ICP, ICP-MS
MS9	Mg-gabbro	765'300/147'425	EMP, E-ICP, ICP-MS
MS8	Mg-gabbro	765'300/147'425	EMP, E-ICP, ICP-MS
MS13	Mg-gabbro	765'300/147'425	EMP, E-ICP, ICP-MS
MS7	Fe-gabbro	765'300/147'425	EMP
MS3	Fe-gabbro	765'300/147'425	EMP, Nd-Sr, U-Pb, Hf
11 (P2)	Fe-Ti gabbro	765'300/147'425	EMP, E-ICP, ICP-MS, U-Pb,Hf
MS11 (P9)	Fe-Ti gabbro	765'300/147'425	EMP, E-ICP, ICP-MS, Nd-Sr
MS10 (P1)	diorite	765'300/147'425	EMP, E-ICP, ICP-MS, U-Pb
MSG-1	Mg-gabbro	765'300/147'425	EMP
MSG-3	Fe/Diorite	765'300/147'425	EMP
MSG-2	diorite	765'300/147'425	EMP
MSG	dyke	765'250/147'250	EMP
NAG1	Fe-gabbro	771'250/152'400	E-ICP, ICP-MS
NAG5	Fe-gabbro	771'250/152'400	EMP
P6	Mg-gabbro	769'575/151'375	EMP, E-ICP, ICP-MS, Nd-Sr, U-Pb, Hf
NAG3	Mg-gabbro	770'000/152'325	EMP, E-ICP, ICP-MS
NAG9	Mg-gabbro	770'690/152'200	EMP, E-ICP, ICP-MS
NAG7	Fe-Ti-gabbro	770'325/151'675	EMP, E-ICP, ICP-MS
P7	diorite	769'575/151'375	EMP, E-ICP, ICP-MS
SC5	Mg-gabbro	766'350/151'125	EMP, E-ICP, ICP-MS
P3	dolerite	765'875/146'675	E-ICP, ICP-MS, Nd, Sr
STG4	dolerite	766'900/151'750	E-ICP, ICP-MS

STG1	dolerite	766'350/151'125	E-ICP, ICP-MS
P8	basalt	769'000/150'750	E-ICP, ICP-MS, Nd, Sr
P5	basalt	765'875/146'675	E-ICP, ICP-MS, Nd, Sr
MSP56	albitite		Nd-Sr, U-Pb, Hf
	Upper serpentinite unit		
VEP1	serpentinized lhezolite	772'800/159'800	
VEP2	serpentinized lhezolite	772'800/159'800	E-ICP, ICP-MS
VEP3	serpentinized lhezolite	772'800/159'800	EMP
VEP5	serpentinized lhezolite	771'900/159'775	
VEP6	serpentinized lhezolite	771'900/159'775	
VEP7	serpentinized lhezolite	772'625/159675	EMP, E-ICP, ICP-MS
VEP8	serpentinized lhezolite	772'625/159675	EMP, E-ICP, ICP-MS
VEP11	serpentinized lhezolite	772'625/159675	EMP
FAP1	serpentinite	771'325/157'650	
FAP3	serpentinite	771'325/157'650	E-ICP, ICP-MS
FAP4	serpentinized lhezolite	771'325/157'650	EMP, E-ICP, ICP-MS
FAP6	serpentinized lhezolite	771'325/157'750	EMP
FAP9	serpentinized lhezolite	771'325/157'750	
CUP1	serpentinized lhezolite	770'925/155'850	EMP
CUP2	serpentinized lhezolite	770'925/155'850	EMP
CUP3	serpentinized lhezolite	770'925/155'850	EMP
PCD1	basalt	771'600/153'000	E-ICP, ICP-MS
FAB1	basalt	771'750/157'650	E-ICP, ICP-MS

Appendix 2- Whole rock chemistry

	Upper serpentinite unit							Lower serpentinite unit		
	Ultramafic rocks (UM)					Basalts		UM		
sample	VEP2	VEP7	VEP8	FAP3	FAP4	PCD1	FAB1	NAP7	NAP3	LAP1
SiO_2	40.72	41.87	39.17	37.05	39.24	49.49	47.35	39.26	38.16	38.53
TiO_2	3.11	5.57	2.51	4.01	4.23	1.72	1.46	3.74	1.84	3.44
Al_2O_3	8.14	7.1	8.19	8.9	8.99	17.01	15.67	8.47	8.25	9.97
Fe_2O_3	0.14	0.13	0.11	0.12	0.12	8	8.83	0.12	0.08	0.16
MnO	31.59	30.49	35.84	37.03	32.63	0.11	0.13	33.5	38.6	34.1
MgO	4.4	5.62	1.82	< d.l.	3.48	6.23	9.76	3.08	< d.l.	2.11
CaO	0.1	0.15	0.07	< d.l.	0.1	8.58	8.11	< d.l.	< d.l.	< d.l.
Na_2O	< d.l.	< d.l.	< d.l.	< d.l.	< d.l.	5.02	2.86	< d.l.	< d.l.	< d.l.
K_2O	0.08	0.17	0.08	0.14	0.22	0.06	0.12	0.17	< d.l.	0.14
P_2O_5	0.13	0.11	0.08	0.11	0.1	0.32	0.28	0.12	0.08	0.09
L.O.I.	11.68	8.56	12.35	12.82	10.98	3.28	5.27	11.37	13.06	11.73
Total	100.11	99.77	100.22	100.27	100.09	99.82	99.84	99.85	100.11	100.28
As	< d.l.	1.126	< d.l.	< d.l.	< d.l.	< d.l.	1.897	< d.l.	0.535	< d.l.
Ba	5.173	3.346	< d.l.	< d.l.	< d.l.	44.022	37.740	< d.l.	< d.l.	< d.l.
Be	< d.l.	< d.l.	< d.l.	< d.l.	< d.l.	1.3604	< d.l.	< d.l.	< d.l.	< d.l.
Ce	0.191	0.860	0.303	0.713	0.653	25.137	21.472	0.675	0.176	0.736
Co	105	76	100	103	102	30	46	101	109	102
Cr	2904	3104	2663	2773	2697	151	278	2764	2734	2773
Cs	4.452	1.810	0.992	0.292	0.749	< d.l.	< d.l.	< d.l.	< d.l.	0.276
Cu	20.17	74.53	20.64	22.01	40.32	50.70	52.53	14.62	16.40	28.09
Dy	0.371	0.586	0.266	0.677	1.120	4.845	3.621	0.718	0.092	0.528
Er	0.237	0.296	0.145	0.436	0.698	2.767	2.047	0.388	0.076	0.340
Eu	0.078	0.195	0.062	0.061	0.200	1.437	1.260	0.199	0.054	0.108
Ga	2.606	4.772	2.647	2.938	4.416	17.541	16.411	3.085	1.834	3.136
Gd	0.211	0.411	0.194	0.570	0.800	4.522	3.766	0.587	0.040	0.381
Ge	0.774	1.296	0.978	0.990	1.139	1.403	1.537	1.063	1.212	0.900
Hf	0.068	0.141	0.082	0.192	0.261	4.113	2.720	0.212	< d.l.	0.205
Ho	0.089	0.119	0.055	0.158	0.245	1.041	0.764	0.138	0.026	0.125
In	< d.l.	< d.l.	< d.l.	< d.l.	< d.l.	< d.l.	< d.l.	< d.l.	< d.l.	< d.l.
La	0.033	0.264	0.058	0.191	0.131	10.180	8.954	0.197	0.078	0.188
Lu	0.043	0.061	0.025	0.071	0.110	0.491	0.284	0.070	0.019	0.061
Mo	0.265	0.254	0.248	0.340	0.273	< d.l.	2.178	0.251	0.341	0.201
Nb	0.022	0.082	0.022	0.083	0.048	10.937	11.533	0.027	0.060	0.054
Nd	0.344	0.963	0.305	0.979	0.935	15.674	12.382	0.951	0.094	0.830
Ni	1996	1572	1904	1859	1877	81	210	1896	2044	1961
Pb	< d.l.	< d.l.	< d.l.	< d.l.	< d.l.	0.622	2.656	< d.l.	< d.l.	< d.l.
Pr	0.049	0.164	0.072	0.151	0.168	3.491	2.772	0.158	0.024	0.132
Rb	1.022	< d.l.	< d.l.	< d.l.	< d.l.	< d.l.	4.103	< d.l.	< d.l.	< d.l.
Sb	< d.l.	< d.l.	< d.l.	< d.l.	< d.l.	< d.l.	< d.l.	< d.l.	< d.l.	< d.l.
Sm	0.172	0.365	0.152	0.382	0.460	4.295	3.349	0.281	0.025	0.252
Sn	< d.l.	< d.l.	< d.l.	< d.l.	< d.l.	1.827	1.413	< d.l.	< d.l.	< d.l.
Sr	24.97	11.41	9.29	< d.l.	8.33	211.88	175.11	< d.l.	< d.l.	< d.l.
Ta	0.001	0.008	0.002	0.009	0.007	0.774	0.751	0.004	0.004	0.006
Tb	0.047	0.0787	0.0286	0.106	0.1481	0.7585	0.6199	0.09	0.010	0.079
Th	<d.l.	0.0079	0.0012	0.0066	0.0045	0.7176	0.7033	0.0016	0.0021	0.0043
Tm	0.037	0.057	0.0261	0.0619	0.1374	0.448	0.3341	0.0581	0.014	0.0602
U	0.1159	0.0046	0.0036	0.0043	0.0083	0.2719	0.2312	<d.l.	<d.l.	0.0054
V	68.07	143.02	64.65	92.13	121.46	201.89	170.38	87.73	52.07	78.97
W	< d.l.	< d.l.	< d.l.	< d.l.	< d.l.	0.2267	0.2584	0.1909	0.1116	< d.l.
Y	2.630	3.203	1.576	4.525	7.548	29.394	22.867	4.094	0.737	3.628
Yb	0.266	0.385	0.150	0.442	0.903	2.936	2.000	0.432	0.111	0.349
Zn	59.37	45.91	66.28	36.70	72.63	72.93	74.07	53.90	30.23	49.72
Zr	2.834	5.549	2.242	6.043	7.517	184.332	132.067	8.567	< d.l.	7.360

	Lower serpentinite unit (continued)									
	UM									
sample	NAP99-	SUP2	SUP3	SUP4	SUP5	STP1	STP2	STP3	MSP1	CRP1
SiO_2	39.62	40.13	39.31	39.3	39.43	39.24	39.56	39.14	39.57	41.01
TiO_2	3.42	3.5	3.2	3.45	3.51	3.35	2.11	2.67	3.11	1.1
Al_2O_3	8.74	8.23	8.37	8.51	8.7	8.93	7.95	9.39	8.67	7.79
Fe_2O_3	0.14	0.12	0.13	0.11	0.11	0.17	0.14	0.15	0.11	0.07
MnO	33.51	34.56	34.6	34.75	34.27	33.89	36.27	35.21	35.16	37.8
MgO	3.23	2.35	1.83	1.88	2.32	2.73	2	1.31	2.71	< d.l.
CaO	< d.l.	< d.l.	< d.l.	< d.l.	0.06	< d.l.	< d.l.	< d.l.	< d.l.	< d.l.
Na_2O	< d.l.	< d.l.	< d.l.	< d.l.	< d.l.	< d.l.	< d.l.	< d.l.	< d.l.	< d.l.
K_2O	0.12	0.13	0.1	0.13	0.14	0.15	< d.l.	0.08	0.08	< d.l.
P_2O_5	0.1	0.1	0.11	0.09	0.11	0.12	0.1	0.08	0.1	0.08
L.O.I.	11.21	11.37	12.41	11.85	11.32	11.67	12.25	12.1	10.94	12.31
Total	100.09	100.5	100.08	100.09	99.97	100.28	100.43	100.13	100.45	100.18
As	< d.l.	< d.l.	< d.l.	< d.l.	< d.l.	< d.l.	< d.l.	0.684	4.799	2.275
Ba	< d.l.	< d.l.	< d.l.	< d.l.	< d.l.	< d.l.	< d.l.	< d.l.	< d.l.	< d.l.
Be	< d.l.	< d.l.	< d.l.	< d.l.	< d.l.	< d.l.	< d.l.	< d.l.	< d.l.	< d.l.
Ce	0.545	0.523	0.507	0.550	0.809	0.659	0.102	0.376	0.266	0.023
Co	101	97	99	104	104	105	111	91	96	114
Cr	2537	2491	2650	2660	2866	2970	2985	2890	2288	3317
Cs	1.235	1.163	0.292	1.312	0.779	0.256	< d.l.	1.422	0.233	0.208
Cu	25.49	20.75	26.49	24.30	14.54	17.54	5.76	15.03	8.25	< d.l.
Dy	0.490	0.475	0.458	0.499	0.505	0.636	0.186	0.352	0.280	0.014
Er	0.311	0.314	0.268	0.342	0.308	0.393	0.136	0.253	0.188	0.015
Eu	0.115	0.131	0.113	0.133	0.124	0.109	0.018	0.093	0.055	0.003
Ga	3.038	3.556	2.756	2.961	3.096	2.804	1.834	2.504	2.430	1.016
Gd	0.462	0.407	0.361	0.387	0.424	0.480	0.075	0.255	0.209	0.071
Ge	0.978	0.902	0.941	0.944	1.010	0.797	0.854	0.960	0.820	0.972
Hf	0.174	0.202	0.152	0.168	0.199	0.228	< d.l.	0.118	0.051	< d.l.
Ho	0.112	0.105	0.106	0.115	0.115	0.125	0.050	0.089	0.061	0.004
In	< d.l.	< d.l.	< d.l.	< d.l.	< d.l.	< d.l.	< d.l.	< d.l.	< d.l.	< d.l.
La	0.144	0.151	0.234	0.128	0.179	0.164	0.050	0.093	0.060	0.020
Lu	0.051	0.063	0.057	0.067	0.051	0.062	0.029	0.043	0.028	0.005
Mo	0.270	0.209	0.333	0.228	0.258	0.205	0.229	0.238	0.242	0.260
Nb	0.028	0.038	0.049	0.014	0.053	0.055	0.033	0.040	0.012	0.007
Nd	0.545	0.625	0.587	0.618	0.778	0.802	0.063	0.401	0.246	0.025
Ni	1910	1797	1878	2009	1940	1995	2154	2056	1708	2295
Pb	< d.l.	< d.l.	< d.l.	< d.l.	< d.l.	0.763	< d.l.	< d.l.	< d.l.	0.747
Pr	0.125	0.108	0.103	0.102	0.134	0.123	0.013	0.071	0.046	0.004
Rb	< d.l.	1.122	1.104	< d.l.	< d.l.	< d.l.	< d.l.	1.042	< d.l.	< d.l.
Sb	< d.l.	< d.l.	< d.l.	< d.l.	0.137	< d.l.	< d.l.	0.151	0.782	0.150
Sm	0.298	0.263	0.234	0.234	0.232	0.359	0.040	0.167	0.123	0.008
Sn	< d.l.	< d.l.	< d.l.	< d.l.	< d.l.	< d.l.	< d.l.	< d.l.	< d.l.	< d.l.
Sr	4.55	9.44	5.98	4.85	5.89	< d.l.	< d.l.	8.22	< d.l.	< d.l.
Ta	0.004	0.006	0.010	0.002	0.007	0.004	0.002	0.005	0.003	0.001
Tb	0.0639	0.0683	0.0643	0.0683	0.0779	0.0723	0.020	0.0468	0.0322	0.002
Th	0.0028	0.0031	0.0153	0.0012	0.0050	0.0077	0.0069	0.0111	0.0066	<d.l.
Tm	0.0508	0.054	0.049	0.0576	0.0538	0.0677	0.023	0.0407	0.0283	0.003
U	<d.l.	0.0028	0.0105	0.0011	<d.l.	0.0083	0.0056	0.0082	0.0071	0.0524
V	74.48	74.25	71.95	75.07	76.56	84.21	70.61	65.54	76.32	36.41
W	< d.l.	< d.l.	0.1013	0.1252	< d.l.	< d.l.	< d.l.	0.145	0.5226	< d.l.
Y	3.210	3.309	2.968	3.135	3.314	3.793	1.386	2.424	1.728	0.126
Yb	0.309	0.325	0.300	0.356	0.369	0.422	0.176	0.283	0.160	0.025
Zn	52.82	48.62	94.06	53.71	49.12	106.72	47.60	69.92	30.69	58.53
Zr	5.963	6.694	4.842	5.992	6.555	7.156	< d.l.	3.725	2.001	< d.l.

	Lower serpentinite unit									
	UM	Mg-gabbro								Fe-gabbro
sample	CRP3	P6	NAG3	NAG9	P4	MS15	MS9	MS13	SC5	NAG1
SiO_2	40.26	49.55	51.87	52.75	46.95	48.59	49.79	49.92	46.79	43.3
TiO_2	4	13.97	17.04	13.96	23.19	16.75	16.28	15.77	17.58	12.81
Al_2O_3	7.84	7.68	6.93	4.18	2.61	5.7	6.21	5.48	4.72	15.47
Fe_2O_3	0.12	0.13	0.14	0.07	0.05	0.1	0.1	0.1	0.08	0.19
MnO	32.21	9.51	5.17	9.55	7.42	8.34	8.43	7.96	9.2	5.97
MgO	4.49	11.78	7.96	10.17	8.59	12.28	10.91	13.36	13.66	10.1
CaO	0.05	3.43	5.51	4.74	2.91	3.24	3.81	3.4	2.55	3.26
Na_2O	< d.l.	0.15	0.91	0.29	2.6	0.69	0.46	0.29	0.45	0.13
K_2O	0.15	0.71	1.49	0.23	0.11	0.47	0.6	0.37	0.31	6.4
P_2O_5	0.1	0.16	0.32	0.09	0.08	0.09	0.09	0.08	0.08	0.14
L.O.I.	10.43	2.75	2.51	3.82	5.38	3.61	3.14	3.08	4.43	2.22
Total	99.65	99.82	99.85	99.85	99.89	99.86	99.82	99.81	99.85	99.99
As	5.267	< d.l.	1.009	< d.l.	< d.l.	< d.l.	< d.l.	< d.l.	0.521	2.131
Ba	< d.l.	3.327	249.174	25.471	191.789	38.813	7.013	15.869	26.625	41.839
Be	< d.l.	1.414	1.1724	1.1438	< d.l.	< d.l.	< d.l.	< d.l.	< d.l.	< d.l.
Ce	0.634	10.811	22.064	5.309	1.049	3.331	5.014	1.908	1.915	3.398
Co	93	55	24	30	25	35	34	33	18	53
Cr	2849	163	146	365	1031	51	84	136	1004	45
Cs	2.424	< d.l.	10.386	< d.l.	0.696	0.223	< d.l.	< d.l.	0.258	0.212
Cu	37.14	105.76	81.41	47.64	21.75	47.71	27.24	46.03	22.20	70.63
Dy	0.574	5.071	4.728	1.969	0.406	1.994	2.530	1.522	1.305	2.743
Er	0.396	2.823	2.843	1.365	0.229	1.408	1.702	0.909	0.796	1.612
Eu	0.144	1.436	1.465	0.445	0.391	0.831	0.938	0.640	0.547	0.829
Ga	3.537	17.911	15.282	11.248	11.125	15.704	14.859	12.808	14.837	16.847
Gd	0.456	4.917	4.703	1.385	0.307	2.021	2.515	1.423	1.251	2.682
Ge	0.874	1.917	1.675	1.291	1.316	1.914	1.572	1.634	1.836	1.656
Hf	0.215	1.893	2.976	1.639	0.121	0.846	1.917	0.442	0.356	1.790
Ho	0.144	1.063	0.989	0.426	0.079	0.459	0.587	0.351	0.323	0.582
In	< d.l.	< d.l.	< d.l.	< d.l.	< d.l.	< d.l.	< d.l.	< d.l.	< d.l.	0.107
La	0.151	3.167	8.560	1.720	0.364	1.009	1.455	0.578	0.565	0.940
Lu	0.063	0.446	0.413	0.366	0.034	0.213	0.268	0.129	0.115	0.239
Mo	< d.l.	0.356	0.170	< d.l.	< d.l.	1.196	0.282	0.472	0.161	1.179
Nb	0.011	1.106	8.053	7.450	< d.l.	0.740	0.751	0.139	< d.l.	2.547
Nd	0.831	9.932	14.715	3.458	0.801	3.712	5.369	2.217	2.103	4.068
Ni	1713	138	41	216	352	82	101	83	177	77
Pb	< d.l.	< d.l.	0.743	1.046	0.976	1.057	< d.l.	1.555	2.521	1.203
Pr	0.136	1.876	3.214	0.715	0.180	0.617	0.905	0.369	0.355	0.676
Rb	2.704	2.269	23.169	5.129	45.212	11.045	4.515	5.342	15.507	5.386
Sb	0.253	< d.l.	0.158	< d.l.	< d.l.	< d.l.	< d.l.	< d.l.	< d.l.	0.323
Sm	0.291	3.502	4.074	1.016	0.258	1.312	1.794	1.023	0.823	1.914
Sn	< d.l.	0.910	1.307	2.198	< d.l.	< d.l.	0.635	< d.l.	0.536	0.979
Sr	7.81	92.86	272.08	526.57	81.99	844.53	326.11	363.38	49.21	1270.90
Ta	0.003	0.082	0.604	0.858	< d.l.	0.048	0.052	0.010	< d.l.	0.228
Tb	0.0837	0.7952	0.7982	0.2965	0.0563	0.329	0.3867	0.2362	0.202	0.417
Th	0.0011	0.0499	0.6360	0.6036	0.0145	0.0779	0.0330	0.1019	0.0071	0.0275
Tm	0.0686	0.4382	0.4336	0.2724	0.0379	0.1833	0.2419	0.1317	0.1264	0.2544
U	<d.l.	0.0221	0.2270	0.2643	0.0049	0.0336	0.0161	0.0164	0.0138	0.0348
V	90.03	265.09	201.69	87.62	38.53	198.67	179.69	169.55	136.80	869.71
W	0.1033	0.5029	0.3071	< d.l.	< d.l.	< d.l.	< d.l.	< d.l.	0.1933	0.1938
Y	4.162	32.363	28.733	13.951	2.333	14.112	18.612	9.273	8.744	17.638
Yb	0.433	2.760	3.009	2.180	0.223	1.322	1.795	0.830	0.860	1.660
Zn	38.74	71.66	58.81	20.68	15.39	30.10	38.56	25.50	42.71	111.02
Zr	6.968	73.309	145.074	26.600	3.663	32.516	86.895	11.724	9.178	72.587

	Lower serpentinite unit									
	Fe-gabbro	Fe-Ti-gabbro		diorite		dolerite			Basalts	
sample	MS3	NAG7	P9	MS10	P7	P3	STG4	STG1	P8	P5
SiO_2	44.13	39.76	34.5	52.23	55.12	46.53	42.41	40.63	47.19	48.17
TiO_2	10.55	12.38	9.98	17.56	18.82	0.89	0.56	0.97	1.69	1.82
Al_2O_3	11.47	17.18	22.44	6.33	4.77	20.84	20.67	17.14	14.99	15.88
Fe_2O_3	0.2	0.29	0.32	0.07	0.07	6.47	5.16	7.49	9.11	9.91
MnO	13.58	6.54	8.29	3.03	3.28	0.1	0.06	0.11	0.15	0.16
MgO	9.26	11.95	10.2	11.71	9.72	6.19	7.34	7.52	5.54	6.58
CaO	2.25	2.44	1.97	5.57	5.99	9.89	16.12	20.86	10.5	9.78
Na_2O	0	0	0	0	0.11	3.96	1.92	0.33	4.36	4.3
K_2O	3.88	3.86	5.27	1.01	0.38	0.27	0	0	0.76	0
P_2O_5	0.12	1.9	2.58	0.28	0.1	0.14	0.11	0.16	0.27	0.25
L.O.I.	4.39	3.2	3.45	2.09	1.5	4.55	5.47	4.61	5.27	2.98
Total	99.83	99.51	99.04	99.9	99.86	99.83	99.82	99.82	99.83	99.83
As	< d.l.	< d.l.	0.593	< d.l.	< d.l.	< d.l.	< d.l.	< d.l.	< d.l.	3.044
Ba	5.113	9.885	3.556	8.286	3.379	24.061	8.729	4.488	28.840	7.542
Be	< d.l.	< d.l.	< d.l.	1.4291	5.2734	< d.l.	< d.l.	< d.l.	< d.l.	< d.l.
Ce	3.706	66.841	68.001	55.728	58.863	9.471	5.951	9.398	19.249	18.524
Co	40	17	48	13	18	30	33	40	34	32
Cr	80	24	7	0	132	268	344	279	242	188
Cs	< d.l.	< d.l.	0.250	< d.l.	< d.l.	< d.l.	< d.l.	< d.l.	0.202	< d.l.
Cu	38.52	30.25	31.12	22.01	8.30	57.48	29.83	53.07	60.48	39.30
Dy	3.075	19.639	21.262	19.246	9.765	2.538	1.816	2.909	6.114	5.635
Er	1.728	10.466	10.442	13.035	7.076	1.467	0.920	1.756	3.521	3.282
Eu	1.103	5.651	5.879	4.805	1.954	0.952	0.576	0.900	1.696	1.661
Ga	12.769	23.829	19.145	39.400	34.619	13.175	12.881	14.238	16.257	17.912
Gd	2.858	24.429	26.670	17.941	7.549	2.435	1.553	2.717	5.895	5.165
Ge	1.603	2.133	1.482	1.787	2.870	1.123	0.783	1.429	1.201	1.489
Hf	1.497	2.435	1.743	14.168	7.388	1.683	0.962	1.867	4.138	3.780
Ho	0.638	4.149	4.184	4.606	2.307	0.596	0.400	0.657	1.374	1.268
In	< d.l.	0.131	0.124	0.193	< d.l.	< d.l.	< d.l.	< d.l.	< d.l.	< d.l.
La	1.035	19.226	18.652	17.953	22.947	3.269	2.050	2.975	5.835	5.730
Lu	0.257	1.168	1.137	1.979	1.526	0.268	0.162	0.286	0.600	0.535
Mo	0.234	0.461	0.304	< d.l.	0.754	0.230	< d.l.	< d.l.	0.365	0.316
Nb	1.861	4.310	4.401	10.118	14.467	2.215	1.185	1.715	2.655	2.799
Nd	4.640	65.260	72.042	47.585	28.761	6.904	4.221	6.627	15.736	14.460
Ni	88	24	39	15	42	126	230	190	83	95
Pb	2.775	1.462	0.971	< d.l.	0.696	0.734	< d.l.	< d.l.	0.701	1.373
Pr	0.820	11.309	12.416	9.331	6.925	1.431	0.887	1.411	3.195	3.033
Rb	< d.l.	< d.l.	< d.l.	< d.l.	1.557	4.181	< d.l.	< d.l.	17.920	< d.l.
Sb	< d.l.	< d.l.	< d.l.	< d.l.	< d.l.	< d.l.	< d.l.	< d.l.	< d.l.	< d.l.
Sm	2.107	20.719	21.959	14.858	7.256	2.014	1.311	2.088	4.859	4.392
Sn	0.754	0.891	0.725	7.182	5.932	0.625	< d.l.	0.650	1.421	1.482
Sr	218.05	794.41	116.25	829.52	780.20	149.86	155.14	42.45	81.75	94.34
Ta	0.170	0.403	0.410	0.953	1.552	0.178	0.086	0.140	0.230	0.241
Tb	0.4704	3.5715	3.7685	2.964	1.4125	0.3875	0.2509	0.4692	0.9401	0.8377
Th	0.0178	0.1124	0.0890	1.0098	1.5700	0.1815	0.0954	0.1320	0.1887	0.1760
Tm	0.247	1.3911	1.3249	1.847	1.3154	0.2371	0.1464	0.2759	0.5371	0.5246
U	0.0117	0.0707	0.0582	0.4567	0.8932	0.0609	0.0337	0.0435	0.1156	0.0745
V	532.15	290.70	398.93	77.56	117.02	120.45	85.43	154.50	245.53	259.66
W	< d.l.	0.2584	< d.l.	0.1626	0.2428	0.1019	< d.l.	0.1591	0.1083	< d.l.
Y	19.313	115.313	124.771	120.851	81.240	16.068	11.422	19.246	38.866	36.431
Yb	1.787	7.918	7.713	13.252	9.954	1.475	0.998	1.900	3.565	3.294
Zn	76.60	156.43	125.34	32.19	34.07	42.17	34.49	49.19	84.74	77.98
Zr	59.899	91.057	70.105	621.559	238.948	72.109	48.197	81.917	169.439	158.525

Appendix 3-Curriculum Vitae of Laurent Desmurs

Personal

Name and Given name:	Desmurs, Laurent
Date and Place of birth:	1. November 1973, Lyon, France
Citizenship:	French
Civil status:	single

Education

1988 - 1991	High School in Lyon (Lycée Edouart Herriot)
1991-1994	Full time student of “Sciences des structures de la matière” at the Université Claude Bernard (Lyon I)
1994 - 1997	Full time student of Geology at the Université Claude Bernard (Lyon I). Master thesis: " Etude pétrologique et géochronologique de la croûte continentale de Galice ". Supervisor: V. Gardien
1997 - 2001	Ph.D. student at "Geologisches Institute", ETH Zürich. PhD thesis: “Mantle evolution and magmatism along an evolving ocean-continent transition: The Platta nappe, eastern Swtitzerland.” Advisors: Prof. D. Bernoulli, Prof. Dr. U. Schaltegger, Dr. G. Manatschal, Dr. O. Muentener,